BIOMASS GASIFICATION IN A CIRCULATING FLUIDIZED BED

By

Xuantian Li

B. A. Sc. Zhejiang University, Hangzhou, China, 1986
M. A. Sc. Zhejiang University, Hangzhou, China, 1989
D. Eng. Zhejiang University, Hangzhou, China, 1992

A THESIS SUBMITTED IN PARTIAL FULFILMENT OF
THE REQUIREMENTS FOR THE DEGREE OF
DOCTOR OF PHILOSOPHY

in

THE FACULTY OF GRADUATE STUDIES
DEPARTMENT OF CHEMICAL AND BIOLOGICAL ENGINEERING

We accept this thesis as conforming
to the required standard

THE UNIVERSITY OF BRITISH COLUMBIA

September 2002

In presenting this thesis in partial fulfillment of the requirements for an advanced degree at the University of British Columbia, I agree that the Library shall make it freely available for reference and study. I further agree that permission for extensive copying of this thesis for scholarly purpose may be granted by the head of my department or by his or her representatives. It is understood that copying or publication of this thesis for financial gain shall not be allowed without my written permission.

Department of Chemical and Biological Engineering
The University of British Columbia
Vancouver, Canada

Date: Oct. 3, 2002

ABSTRACT

This work is devoted to the experimental study of biomass gasification in a pilot-scale circulating fluidized bed, and development of an equilibrium model of the process based on Gibbs free-energy minimization. Biomass gasification has considerable potential for reducing greenhouse gas emissions. In the present study, six types of sawdust were gasified in a pilot-scale air-blown circulating fluidized bed gasifier to produce low-calorific-value gases.

The pilot gasifier employs a riser 6.5 m high and 0.1 m in diameter, a high-temperature cyclone for solids recycle and a ceramic fibre filter unit for gas cleaning. The riser temperature was maintained at 970-1120 K (700-850°C), while the sawdust feed rate varied from 16-45 kg/h, corresponding to a superficial gas velocity of 4-10 m/s. It was found that gas composition and heating value depended heavily on the air or O/C ratio, and to a lesser extent on operating temperature. The higher heating value of the product gas decreased from 5.6 to 2.1 MJ/Nm^3 as the stoichiometric air ratio increased from 0.22 to 0.54. The gas heating value was increased by increasing the overall suspension density in the riser. Fly ash re-injection and steam injection led to increases in gas heating value for the same O/C molar ratio.

Tar yield from biomass gasification was found to decrease drastically from 15 to 0.54 g/Nm^3 as the average suspension temperature increased from 970 to 1090 K. Elevating the operating temperature provides the simplest solution for tar removal in the absence of any catalyst. Secondary air had only a very limited effect on tar removal with the total air ratio maintained constant. A nickel-based catalyst proved to be effective in reducing the tar yield and in adjusting the gas composition.

The cold gas efficiency decreased with increasing air ratio (or O/C molar ratio), though the carbon conversion increased. The cold gas efficiency provides a better criterion for evaluating the gasification process than the carbon conversion. Experimental data showed that the gasification efficiency can be maximized within an optimum range of air ratio (a = 0.30-0.35, or O/C = 1.5-1.7), while keeping the tar yield acceptably low.

A non-stoichiometric equilibrium model based on Gibbs free energy minimization was developed for biomass gasification. Five elements (C, H, O, N and S) and 44 species were considered in the model. Both pure equilibrium and situations where kinetic factors cause a partial approach to equilibrium are considered. The equilibrium model predicts that the product gas composition from gasification of woody biomass (e.g. sawdust) depends primarily on the air ratio. An air ratio of 0.2-0.3 is predicted to be most favourable for producing CO-rich gas, while temperatures of 1200-1400 K and an air ratio of 0.15-0.25 are predicted to be optimum for H_2 production. The predicted cold gas efficiency reached a maximum at an air ratio of about 0.25. The model successfully predicts the onset of carbon formation in a C-H-O-dominated system when the relative abundance of carbon exceeds a certain level. When a system is C-saturated, the gas composition is insensitive to the elemental abundance of carbon in the total feed streams.

The equilibrium model successfully predicts the limiting behaviour of the system with changes in different operating parameters and provides an in-depth understanding of the underlying thermodynamic principles governing biomass gasification. The model was modified to take non-equilibrium factors into account. The modified model successfully predicts product gas compositions, heating value, gas yield and cold gas efficiency in good qualitative agreement with the experimental data.

TABLE OF CONTENTS

LIST OF TABLES

LIST OF FIGURES

ACKNOWLEDGMENT

I am most grateful to my supervisors, Drs. John R. Grace, C. Jim Lim and A. Paul Watkinson. This thesis would have been inconceivable without their support, guidance and encouragement. They have helped in every possible way: lecturing my courses, leading group discussion, participating in pilot plant tests, writing control programs, proofreading the thesis and improving its quality both scientifically and editorially, and offering financial support.

Many thanks are given to Drs. Chad P. J. Bennington and Peter V. Barr for kindly being members of my supervising committee.

My gratitude is also due Dr. Hanping Chen, Dr. Jung-Rae Kim, Mr. Milaim Dervishaj and Dr. Yonghua Li for their assistance in the pilot experiments, to Drs. Ali Ergüdenler and Jim Lucas for constructive suggestions with respect to the experimental work and equilibrium model. Dr. Harrie Knoef at the Twente University, the Netherlands, kindly gave me advice in our communications with his rich expertise in tar sampling.

Special thanks are given to Mr. Horace Lam and Mrs. Chee Chen in the store for helping me with all kinds of procurement, and to Mr. Peter Roberts, Mr. Robert Carrasco, Mr. Graham Liebelt, and Mr. Alex Thng in the workshop for making a number of components and control panels. My former and present officemates and fellow graduate students have made my program a completely pleasant experience.

I would also like to thank Sunrise Manufacturing and Allied Blowers for fabricating and installing the feed system and horizontal gas bypass. Thanks, also, to Jan Barynin of Dynamotive Inc. for generously providing mixed sawdust for use in the experimental study.

Finally, I am deeply indebted to my wife Keke for her consistent backing and encouragement, which have been a steady source of peace, pleasure and inspiration.

CHAPTER 1. INTRODUCTION

1.1 Biomass Gasification: Concept and Significance

The biomass share in current world energy consumption is 14%, with 4% in North America, 38% on average in developing countries, and 85% in the least developed ones (Hall and Rosillo-Calle, 1998). In the developed world, biomass energy is utilized with modern technologies in a more or less centralized manner, while in the developing countries, traditional energy options still dominate the end user pattern. Industrialization will result in a decreasing share of biomass energy in the developing countries from the current figure to about 15% in the decades to come. On the other hand, the developed world is trying to increase the biomass share in their energy mix to 12-15% projected by 2010. Overall, the biomass share in world energy mix is expected to stay near 15% in the foreseeable future.

The underlying reason for the rising profile of biomass in world energy affairs is the global warming issue. The International Panel for Climate Change (IPCC) estimates that the global mean temperature of the earth's surface has increased by 0.3-0.6 ^{o}C over the past 100 years due to the rising atmospheric concentrations of greenhouse gases, mainly carbon dioxide, methane and nitrous oxide (IPCC, 2000). CO_2 accounts for 65% of the greenhouse effect. There is widespread consensus on the need to reduce CO_2 emissions. As a major step in this direction, the EU White Paper on energy proposed to double the contribution of renewable energy sources to 12% of the overall energy consumption by the year 2010 from 5.7% in 1998 (Maniatis and Millich, 1998). In North America, the United States had installed more than 8000 MWe biomass-based power generating capacity by 1990 as a result of the Public Utility Regulatory Policies Act of 1978 (Williams and Larson, 1996). Canada is committed to lower greenhouse gas emissions

by 6% by 2012 from those of the baseline year of 1990, under the Kyoto Protocol. One recent study (Granatstein *et al.*, 2001) suggested that the coal-fired power generation must be reduced by 38%. The goal can also be achieved through a shift to natural gas, biomass and hydropower.

However, a major shift from coal to natural gas in North America has already brought about unwanted consequences, including gas supply shortages and ballooning gas prices. Hydropower, on the other hand, has strong geographical limitations and is much more capital-intensive than fossil fuel-based power generation. Therefore, it is widely accepted that biomass has to play a major role in finding a practical solution to the global warming problem. World renewable energy sources should increase from an estimated 800 Mtoe (million ton oil equivalent) to more than 1340 Mtoe in 2020 (Maniatis and Millich, 1998).

Biomass energy is the energy contained in plants and non-fossil organic matter. It has a great variety in form. Biomass energy sources include wood, wood wastes (e.g., sawdust and hog fuel), short rotation energy woods and crops (e.g., willow and switchgrass), agricultural crops and their residues (e.g., corn stover, sugar cane bagasse), some municipal solid wastes, animal manure, wastes from food processing, waste sludge from pulp and paper industry (black liquor), and aquatic plants and algae. Wood and wood wastes account for more than 60% of the total. A typical empirical molecular formula for woody biomass derived from the ultimate analysis of the species can be represented by $C_{3.3\text{-}4.9}H_{5.1\text{-}7.2}O_{2.0\text{-}3.1}$, assuming a molecular weight of 100, when only three major elements are considered (Tillman, 1991). The sawdust used in our present study suggest an average molecular formula of $C_{4.25}H_{6.25}N_{0.05}O_{2.56}S_{0.01}$ when five elements are considered.

Biomass is neutral in greenhouse gas circulation in the earth's biosphere because the amount of greenhouse gas it consumes through photosynthesis is the same as that gives off by combustion. As a renewable energy source, biomass is particularly suitable for countries with

few fossil energy sources. Biomass cultivation and processing is a job-intensive industry, suitable for industrial and developing countries alike. Energy crops have the additional advantage that they can be grown on marginal lands (Nieminen and Kivela, 1998).

Gasification is one of the most promising clean energy options to utilize biomass. A definition of biomass gasification can be proposed based on the EPA definition of gasification: a process technology that is designed and operated for the purpose of producing synthesis or fuel gas through the chemical conversion of biomass, usually involving partial oxidation of the feedstock in a reducing atmosphere in the presence of air and/or steam. A simplified mechanism for biomass gasification (Probstein and Hicks, 1982; Schuster *et al.*, 2001) can be represented as follows, consisting of four overlapping aspects:

(1) Pyrolysis:

$$\text{Biomass} \rightarrow \text{Char}, H_2, CO, CO_2, H_2O, CH_4, C_nH_m, \text{tars}, \ldots \quad (1\text{-}1)$$

(2) Tar cracking:

$$\text{Tar} \rightarrow H_2 + CO + CO_2 + \ldots \quad (1\text{-}2)$$

(3) Heterogeneous reactions:

$$C + 1/2\ O_2 = CO \quad (1\text{-}3)$$

$$C + O2 = CO_2 \quad (1\text{-}4)$$

$$C + CO_2 = 2\ CO \quad (1\text{-}5)$$

$$C + H_2O = CO + H_2 \quad (1\text{-}6)$$

$$C + 2\ H_2 \Leftrightarrow CH_4 \quad (1\text{-}7)$$

(4) Homogeneous reactions:

$$CO + \tfrac{1}{2}\ O_2 = CO_2 \quad \text{(combustion)} \quad (1\text{-}8)$$

$$H_2 + \tfrac{1}{2}\ O_2 = H_2O \quad (1\text{-}9)$$

$$CO + H_2O \Leftrightarrow CO_2 + H_2 \quad \text{(water-gas shift)} \quad (1\text{-}10)$$

$$CH_4 + H_2O \Leftrightarrow CO + 3\ H_2 \quad \text{(methane reforming)} \qquad (1\text{-}11)$$

The typical dry synthesis gas from air-blown biomass gasification contains about 6% H_2, 19% CO, 14% CO_2, 3% CH_4 and 58% N_2, with a higher heating value (HHV) of 4.3 MJ/Nm^3 when only a third of the air required for stoichiometric combustion is supplied. Gas composition varies with air supply and suspension temperature and other operating parameters.

In addition to its advantage in emissions reduction, biomass gasification enjoys higher power generating efficiency than combustion-based power generation if the gasifier is coupled with a gas turbine in a combined cycle. However, certain drawbacks remain in modern biomass gasification technologies:

(1) High tar and particulate concentrations in the product gas must be reduced before entering the gas turbine.

(2) Limited land area is available for cultivation of productive biomass species. The land area needed to sustain feedstock supply for every 100 MW_{th} of biomass energy is about 1500-7500 km^2 (Nieminen and Kivela, 1998).

(3) Due to the low bulk density and energy density (typically 2.5 GJ/m^3 compared to 30 GJ/m^3 for coal), the economical transport distance for biomass is only 30-80 km, beyond which transport of biomass is not economically attractive (Nieminen and Kivela, 1998).

Despite these drawbacks, biomass energy is enjoying rapid worldwide progress in research, development and commercialization. Among the various technical options, biomass gasification is especially promising owing to its high efficiency and flexibility.

1.2 Scope of This Study

This work has two primary objectives: to investigate a process for biomass gasification in a circulating fluidized bed, and to develop an equilibrium model of the process based on free-energy minimization. The scope of the present work is outlined below.

Chapter 2 provides an overview of current research efforts as well as a critical review of biomass gasification. The technology is broken down into process concepts, laboratory-scale experimental study, reaction mechanism and kinetics, pilot and demonstration project, and modeling efforts, with emphasis on technical comparison between representative biomass gasification processes under development or available in different parts of the world. This background knowledge helps provide an understanding of why biomass gasification, combined with a circulating fluidized bed (CFB) reactor, is promising for biomass energy use. This leads to a statement of the objectives of this thesis.

The second part of the thesis presents pilot study of biomass gasification in a CFB gasifier. In Chapter 3, we first introduce the experimental system, fuel and bed materials. Then a brief outline of experimental methods and procedure is given. Chapter 4 reports the experimental results from the pilot study, while Chapter 5 provides an overall mass and energy balance and recommends measures for improving carbon conversion.

Following the experimental study, an equilibrium model of biomass gasification is presented in Chapter 6, based on minimization of the Gibbs free energy of the reaction system at chemical equilibrium. This approach is suitable for predicting equilibrium contents of different species in a complex reaction system with multiple material and energy streams, yet no clearly defined reaction mechanism. Kinetic modification is made to account for unconverted solid carbon and methane, and predictions are compared with experimental data. Finally, a brief summary of conclusions is given together with recommendations for future work.

CHAPTER 2. BACKGROUND

2.1 Gasification for Energy Use of Biomass

Gasification is a thermochemical process where less than the stoichiometric amount of oxygen is supplied to convert carbonaceous materials into gaseous fuels using media such as air, oxygen and steam. Biomass can be pyrolysed or gasified for many energy uses, such as producing synthesis gas, hydrogen, methanol, bio-oil, fuel-cell applications, as well as for making raw fuel gas for combustion in process applications or for combined cycle power generation.

Because of the relatively small size of biomass gasifiers compared to coal units, it is rarely economically justified to build an oxygen plant to supply pure oxygen for gasification. Instead, air-blown biomass gasifiers can be used to produce low-calorific value gases with higher heating values of typically 3-7 MJ/Nm^3. Such low-quality gases cannot maintain high enough temperature to maintain combustion in a furnace cooled with membrane walls when fired independently. Instead, the gas can be co-fired in a PC boiler to partially displace coal, as in the Lahti project (Babu, 1995). Another reason for co-combustion is that the process requires virtually no gas cleaning since the gas is directly fired. In addition, little integration is needed. In co-combustion, the gasifier is integrated into the steam cycle instead of a gas turbine cycle, greatly reducing the maintenance and service cost. If the gasifier is shut down, the rest of the plant can continue to operate without being much affected.

Alternatively, biomass fuel gas can be used in a combined cycle power plant with a gas turbine, as in the biomass integrated gasifier/gas turbine (BIG/GT) system. A recent study (Williams and Larson, 1996) shows that a biomass integrated gasifier/steam injected gas turbine (BIG/SIGT) and its modified version, the biomass integrated gasifier/intercooled steam-injected

gas turbine (BIG/ISIGT), both enjoy major cost reductions compared with the double extraction/condensing steam turbine (CEST) system. The viability of this highly integrated configuration depends on a number of factors, the most important being removal of tars and alkali metals from the gasifier product. The tolerable tar and alkali loading for today's gas turbine usually do not exceed 100 ppb and 250 ppb, respectively (Williams and Larson, 1996; Babu, 1995).

Over the past century, many processes have been developed for gasifying different feedstocks from coal, biomass and municipal wastes. Because of the common fundamental principles, processes for biomass gasification are closely related to coal-based processes, but with some distinct characteristics. These processes can be classified in a number of ways.

There are high-temperature processes operating at 1120-1470 K (850-1200 °C) discharging ash as smelt, and low-temperature processes at 870-1120 K (600-850 °C) discharging solid ash, depending on the fuel and process employed. Since the ash content of biomass is very low (< 3% for most woody biomass), ash discharge is hardly needed. However, biomass gasification generally involves particulate materials like sand and dolomite, either as the bed material or as catalyst or sorbent. Depending on the working pressure, gasification processes can be classified as atmospheric, as most biomass gasifiers are, and pressurized (Kurkela and Stahlberg, 1992; Knight, 2000).

Depending on the hydrodynamic properties of reactors, gasifiers can be fixed or moving beds, bubbling or circulating fluidized beds, spouted beds, rotary kilns, or some combination of these types. Gasifiers may be directly heated (most gasifiers), or indirectly heated, usually employing molten salt designs (Pletka *et al.*, 2001).

A number of gasifying agents can be used. While air, oxygen and steam are most common, some gasifiers employ hydrogen, carbon dioxide or mixtures of these gases (Hebden and Stroud,

1981; Garcia *et al.*, 1999). Other possible gasifying agents include molten salt ballast (Ido *et al.*, 1999; Pletka *et al.*, 2001) and supercritical water (Xu and Antal, 1998; Antal *et al.*, 2000; Schmieder and Abeln, 1999). Air-blown processes produce low-quality gases with a higher heating value (HHV) in the range of typically 3-7 MJ/Nm^3, while oxygen- and steam-blown processes provide gases with HHV of 10-18 MJ/Nm^3 (Schuster *et al.*, 2001). Oxygen, however, adds considerably to the production cost, and makes the process more complex.

2.2 Existing Commercial Processes

According to an online survey (Knoef, 2002a), there have been 57 manufacturers reporting nearly 100 operations or on-going biomass installations in Europe and North America. The largest is the 14 MW_e Bioelettica Energy Farm demonstration project at Cascina, Italy to be completed in 2002. This employs a Lurgi atmospheric circulating fluidized bed gasifier plus a Nouvo Pignone gas turbine configuration for biomass integrated gasification / gas turbine (BIG/GT) power generation.

2.2.1 Fixed- and moving-bed gasifiers

Fixed bed gasifiers constitutes the first generation of commercial gasifiers, with Lurgi, Riley-Morgan, Kellogg, and Woodall Duckham coal gasifiers of this type are prominent suppliers (Hebden and Stroud, 1981). Lurgi is still an active player in world biomass gasification market. A Wellman updraft gasifier was demonstrated near Birmingham in the UK (Babu, 1995).

In his excellent review, Beenackers (1999) outlined the advantages and problems of many fixed and moving-bed designs. Updraft gasification is the oldest and simplest gasification process. It employs a counter-current fixed-bed contact process between the biomass and the gasifying agent. The fuel is fed from the top, successively passing through a drying zone, pyrolysis zone, reduction zone and hearth zone, and the ash is removed from the bottom of the

gasifier, from where sub-stoichiometric air is supplied. The major advantages are simplicity, high carbon conversion, low gas exit temperature, and the ability to handle a variety of feedstocks. However, gas channeling is a major drawback, which can lead to oxygen breakthrough and dangerous, explosive situations (FAO, 1986). In addition, because the tars produced in the pyrolysis zone do not pass through a high-temperature thermal cracking zone before leaving the gasifier, a high tar yield is a critical drawback for the updraft gasifier.

Though most moving-bed gasifiers adopt updraft, there are a number of downdraft designs, also called co-current gasifiers since the feed moves in the same direction as the gasifying agent. The solids pass through the same zones as for an updraft gasifier. Air is supplied at the interface between the pyrolysis zone in which feed particles undergo pyrolysis under oxygen-free conditions and the zone in which char gasification takes place. This design is claimed to enable tar-free gas production. However, it suffers from weak fuel flexibility and flow problems. The inability to maintain uniform radial temperature profiles and local slagging problems make moving beds unsuitable for large installations.

Nevertheless, due to its low tar yield, downdraft designs are still being developed, e.g. by the Energy Centre of the Netherlands (ECN) (Schenk *et al.*, 1997) and several other institutions (Chern *et al.*, 1991; De Bari *et al.*, 2000; Warnacker, 2000; Susanto and Beenakers, 1996). Newly developed processes have reported capacities up to 5 MW_{th}, corresponding to ~1 MW_e for downdraft gasifiers (Schenk *et al.*, 1997). When fully developed, fixed bed biomass gasifier is suitable for a capacity range of 3-5 MW_e, with a throughput of typically 0.5 kg/m^2-s.

2.2.2 Fluidized bed gasifiers

Fluidized bed processes have the advantages of excellent gas-solid mixing and the uniform temperature within the bed. The presence of a dense suspension provides a large thermal inventory required for flash pyrolysis of solid fuel particles. However, due to the non-uniformity

of particle residence times in the fluidized bed as well as solids entrainment, a single fluidized bed cannot achieve high carbon conversion.

To improve carbon conversion and reduce tar yields, most bubbling fluidized beds are equipped with internal or external separators to capture entrained particles and return them to the bed. Secondary air is introduced to form a high-temperature zone in the freeboard for thermal cracking of tar.

The Hygas, Winkler, Westinghouse and U-gas processes are well-known examples of fluidized bed coal gasifiers (Hebden and Stroud, 1981), and these have also been marketed for gasifying biomass. In the last decade, institutions in many countries have been involved in research and development on fluidized bed biomass gasification (e.g. Ergudenler and Ghaly, 1992; Jiang and Morey, 1992; Gudenau *et al.*, 1993; Caballero *et al.*, 1997; Corella *et al.*, 1998; Collot *et al.*, 1999; Pan *et al.*, 2000; Liu *et al.*, 2000).

The circulating fluidized bed (CFB) is a natural extension of the bubbling bed concept, in which cyclones or other types of separators are employed for solids capture and recycle in order to extend the solids residence time in the reaction zone. Unlike bubbling fluidized beds, CFB gasifiers operate in either the turbulent fluidization or fast fluidization regime. CFB biomass gasification is now undergoing rapid commercialization. Fundamental and pilot studies are, nevertheless, required for scale-up, as well as to fill knowledge gaps in understanding the underlying principles.

2.2.3 Other types of biomass gasifiers

A two-vessel process has been proposed for biomass gasification (Latif *et al.*, 1999) with slight modification from its coal-based prototype. The general principle of a two-vessel design is that gasification and combustion occur in two separate vessels. Fresh biomass particles are fed to the gasifier, where they undergo pyrolysis. The char particles are then carried into the combustor

and burn there. Particles heated in the combustor act in turn as heat carriers, providing heat for the endothermic gasification reactions in the gasifier. Since this design separates gasification product and flue gas streams, it can produce gases with higher heating value without using oxygen. However, the process is very prone to operating problems or even shutdown due to possible malfunction of the solids circulation. Secondly, the temperature in the gasifier is always lower than in the combustor, leading to lower reaction rates in the former, though high reaction rates are crucial for both char gasification and tar cracking. Therefore, this design usually suffers from higher tar yields.

Several other biomass gasification processes have been reported, employing radically different concepts. The molten salt gasifier has two options, directly- and indirectly-heated, both operating at temperatures between 970 and 1170 K. The directly-heated option usually employs molten carbonate salts. Operating data are so far unavailable for this type of gasifier. Anaerobic biomass gasification was popular in China until the early 1990s, but more recent research is focused on fluidized bed processes (Xu, 1997).

2.3 Overview of Recent Research Activities

Research and development activities in 17 countries over the past decade are summarized below. The survey is by no means exhaustive. Almost all the processes employed for coal gasification have been utilized for biomass applications.

2.3.1 North America

As coal-based power plants are reaching their efficiency limits, due to the problems in marketing pressurized fluidized bed combustion (PFBC) technology and the perception that coal is a dirty and outmoded fuel, the general situation in recent years in North America seems to favour development of biomass alternatives.

More than a third of biomass literature has been generated in the US. The National Renewable Energy Laboratory (NREL) conducted a number of scale-up and site-specific commercial feasibility studies in a 400 kg/h pilot fluidized bed gasifier. Other research areas of NREL include hot gas cleanup, catalytic conditioning of synthesis gas and longevity of catalysts (Bain, 1993; Ratcliff *et al.*, 1995; Gebhard *et al.*, 1993; Jacoby *et al.*, 1995; Garcia *et al.*, 2000). The Institute of Gas Technology (IGT) has been a leading technology vendor in gasification. Its RENUGAS process is the biomass version of its coal-based U-GAS process. The Hawaii National Energy Institute of the University of Hawaii at Manoa has played an active role in researching steam gasification and wet biomass gasification in supercritical water (Aihara *et al.*, 1993; Antal *et al.*, 2000), indirectly heated FB gasification (Wang and Kinoshita, 1992) and release of nitrogen and inorganic matter in gasification (Zhou *et al.*, 2000; Turn *et al.*, 1998). The University of Hawaii also played a role in the Hawaii Project, an IEA sponsored demonstration project to gasify bagasse with the IGT-developed RENUGAS process (Lau, 1998). Larson and coworkers at Princeton University proposed a biomass-integrated gasifier/gas turbine (BIG/GT) process for combined cycle power generation (Larson and Williams, 1990; Williams and Larson, 1996; Larson *et al.*, 1999). The Brookhaven National Laboratory (BNL) proposed the Hynol process, which employs hydrogasification of biomass, as an economical option for methanol and alcohol production (Steinberg *et al.*, 1993; Dong and Steinberg, 1997). Iowa State University also runs an 800 kW_{th} FB gasifying livestock manure and crop residues (Brown *et al.*, 2000). American industry is also actively marketing biomass gasifiers. Battelle provided its high throughput Multisolids gasifier for the Vermont biomass power program (Paisley and Anson, 1998) sponsored by US DOE. Foster Wheeler is developing a ceramic filter for gas cleaning for IGCC applications (Engstrom 1998).

Canada enjoys the third largest share (6%) of the world's forest resource (FAO, 2001). Government agencies such as Environment Canada, Natural Resources Canada and CANMET are active coordinators of biomass-related investigations. Ghaly and co-workers at Dalhousie University conducted a wheat-straw gasification project in a dual-distributor fluidized bed, and developed a mathematical model of the gasifier (Ergüdenler and Ghaly, 1992; Ergüdenler *et al.*, 1997a, 1997b). Their more recent efforts include a TGA/DTG kinetic study and a pilot test of the thermal degradation and gasification of rice husks in a fluidized bed (Mansaray and Ghaly, 1999a, 1999b; Mansaray *et al.*, 1999). The University of British Columbia started a project on the gasification of coal, biomass and black liquor in 1996. Data on high-temperature gas filtration and on coal and biomass gasification have been reported by Ergüdenler *et al.* (1997c) and by Li *et al.* (2001).

2.3.2 Europe

Efforts of European countries to commercialize biomass gasification through the Joule and Thermie Programmes have been very fruitful in two major aspects: system integration, and gas cleaning, most noteworthy with catalytic gas conditioning and tar reduction. The success of the Lahti project provides a practical, short-term option for promoting biomass energy with relatively low cost and technical complexity. Pressurized entrained bed and downdraft moving bed gasifiers, originally developed for coal gasification, are examples of 'European' technologies. Because of their small capacity range, downdraft gasifiers provide a compromise between capacity and the decentralized nature of biomass energy.

Spain has made significant progress in biomass gasification over the past decade. Much of the research has been completed at the University of Saragossa. Early studies were focused on scale-up of downdraft moving-bed gasifiers (Garciabacaicoa *et al.*, 1994), but followed by catalytic gasification in a 150 mm ID, 3.2 m high fluidized bed gasifier, operating in conjunction

with a downstream catalytic reactor for tar removal and gas conditioning (Degaldo *et al.*, 1996; Aznar *et al.*, 1998; Gil *et al.*, 1997; Corella *et al.*, 1999). Catalysts included naturally occurring minerals like dolomite, magnesite and calcite (Olivares *et al.*, 1997), as well as several commercial steam-reforming catalysts for methane and naphthas, like the BASF G1-50, ICI 46-1 and Topsoe R-67. These catalysts were tested in a reactor (Caballero *et al.*, 1997) downstream of a steam- and oxygen-blown fluidized bed gasifier, operating at relatively low temperature (970 K). They found that dolomite gave slightly better performance when fed in a second bed instead of in the main fluidized bed. Tar content in the gas leaving the catalyst reactor was reportedly as low as 10 mg/Nm^3 (Caballero *et al.*, 2000). Some kinetic data were reported regarding catalytic gas conditioning (Narvaez *et al.*, 1997). Researchers at the University of Complutense at Madrid conducted experimental studies in a pilot-scale air-blown atmospheric fluidized bed (AFB) gasifier (Narvaez *et al.*, 1996). A few other Spanish universities have also been involved in biomass gasification projects.

Italy's early activities in biomass gasification were reviewed by Brunetti (1989). Di Blasi and coworkers (1999) at the University of Naples studied counter-current (updraft) and co-current (downdraft) fixed bed gasification. However, inadequate mixing, partial ash sintering and flow channeling remain problems with moving-bed gasifiers. Rapagna *et al.* (2000) of the University of Aquila carried out fluidized-bed steam gasification of biomass using olivine as the bed material and catalyst. They found the optimum temperature for olivine to be about 1070 K.

The Energy Centre of Netherlands (ECN), the Netherlands operates bench-scale fluidized-bed and entrained-bed gasifiers, a 300 kWth downdraft moving bed pilot unit, and a 500 kWth BIVKIN circulating fluidized bed gasifier. Their on-going activities are focused on biomass as an alternative fuel for power production to displace fossil fuels, development of integrated

biomass gasification processes and advanced poly-generation processes (Schenk *et al.*, 1997; ECN, 2001).

Since the early 1990s, the University of Lund, Sweden, has been active in studying tar removal, ammonia and hydrogen sulfide reduction in biomass gasification in a 90 kW fluidized bed (Gustavsson, 1994; Wang *et al.*, 1999, 2000; Padban *et al.*, 2000). Researchers at the University of Gothenburg studied alkali metal emissions (Olsson *et al.*, 1998). Research efforts in Finland were described in a review paper by Kurkela *et al.* (1989), focused on peat and biomass gasification. VTT is a leading institution in tar sampling as well as other emissions and tar-related research (Hepola *et al.*, 1994; Simell *et al.*, 1997, 2000). Hepola *et al.* (1994) reported that the sulfur content in the gas was a more serious cause of catalyst deactivation with ammonia decomposition than with tar cracking. More recently, the Technical University of Denmark proposed a two-stage downdraft gasifier for biomass, but little is known about their experimental results (Hindsgaul *et al.*, 2000).

The German contribution in developing gasification technology has already been mentioned. Lurgi has been especially active, and was a partner in proposing the 1998 version of the tar sampling protocol. In addition to these technology-directed investigations, fundamental research has been conducted at German institutions (Diener *et al.*, 1990; Plzak and Wendt, 1992). In England, the University of Aston made some early efforts in studying biomass-based IGCC. Bridgwater (1995) recommended a demonstration project to prove the IGCC concept in order to obtain reliable performance data. He argued that the areas of uncertainty in turbine development, gas cleaning and tar removal will not be resolved unless a large integrated plant is built. France has also contributed to biomass gasification. Courson *et al.* (2000a, b) studied biomass gasification in the presence of olivine-supported catalysts featuring high attrition resistance and activity for tar cracking.

2.3.3 Asia

Biomass gasification in Asia has largely been focused on decentralized applications, especially in India and China. Updraft moving bed gasifiers are still being developed owing to their easy operation and low power consumption (Krishnamoorthy *et al.*, 1991; Ravindranath, 1993). However, newer processes are also being studied for large-scale commercialization of biomass energy in the future.

An early review of Chinese efforts on biomass gasification was carried out by Sheng (1989). There were 52 million anaerobic biogas digesters operating in China's rural areas in 1993, but the number was rapidly decreasing with rural electrification (Xu, 1997; Li *et al.*, 1997). The process operates unattended at room temperature in a manner suitable for decentralized rural installations. This anaerobic process can be revived once it is combined with advanced biological reactors and enzyme technology in order to elevate its productivity. Studies of fluidized bed biomass gasification at Tsinghua University (Guo *et al.*, 2001) and a few other universities represent another direction of Chinese research on biomass gasification. A catalytic pyrolysis process for sawdust was proposed using Ni-based and nickel-aluminate co-precipitation catalysts, operating at 920-970 K for producing CO-rich gas (Guo *et al.*, 2002).

Research on biomass gasification has been reported by Japanese institutions, including the kinetic and pilot studies in a FB gasifier at the Seikei University (Kojima *et al.*, 1993), and fundamental research at the University of Tokyo (Sakaki and Yamada, 1997). More recently, the University of Tsukuba developed a catalytic cellulose gasification processes that operates at very low temperatures (720-820 K) with Rh-based catalysts supported on CeO_2, ZrO_2 and a few other metal oxides, but only CeO_2 showed excellent catalytic performance at higher temperatures (Asadullah *et al.*, 2001). This low temperature process is particularly promising in reducing gaseous emissions.

2.4 Demonstration Projects

Because of the large cost involved, international collaboration is a striking feature in developing and commercializing biomass gasification technologies. The IEA Biomass Thermal Gasification Activity, in connection with the Institute of Gas Technology (IGT), completed in 1994, recruited experts from Canada, Denmark, Finland, the Netherlands, Norway, Sweden, Switzerland, UK and US (Babu, 1995). A 15 MW_{th} pressurized air-blown pilot plant based on the IGT U-Gas process was built in Tampere, Finland. About 650 hours of pilot operation with 98% carbon conversion and low tar yield was reported. While there was considerable progress in these demonstration projects, feeding was problematic with some biomass species.

The European Community launched a series of demonstration projects under the Thermie-Joule Program, initiated in 1990. The goal of the program was to introduce IGCC power plants in the 8-15 MW_e range by the late 1990's, 20-30 MW_e range by 2000, and 50-80 MW_e by 2005 (Babu, 1995).

Table 2.1 summarizes the most influential demonstration projects in Europe and North America in the past ten years. These demonstration projects employ diversified technologies to prove different concepts.

Table 2.1 Major biomass gasification demonstration projects

Project name, location and capacity	Fuel and gasifying agent	Design parameters	Status and comments	Source
Amer [1] CFB gasifier 20 MW_e (Geertruidenberg, Netherlands)	Demolition wood; air-blown; gas cleaned with a scrubber	Lurgi atmospheric CFB gasifier. Energy input = 85 MW_{th}	Gasifier installed in 2000. Results unknown.	Willeboer (1998) Knoef (2002a)
ARBRE [1] CFB gasifier 8 MW_e (Eggborough, UK)	2800 ha of short-rotation forest (SRF) plantation supplies the wood fuel; dolomite for tar removal	TPS gasification process coupled with Siemens steam turbine and EGT/Typhoon gas turbine; water scrubbing for gas cleaning. Plant electrical efficiency = 30.6%	Gasifier installed in 1999.	Babu (1995) Pitcher *et al.* (1998)
BIG/GT project [2] ACFB gasifier 30 MW_e (Brazil)	Wood chips from a eucalyptus plantation; air-blown; methane reforming catalyst for tar removal	TPS gasification process. Operating data unavailable. Design electrical efficiency = 37%.	Project initiated in 1992. Contracted to Hydroelectric Co. of Sao Francisco. Construction started in 1996.	Babu (1995) Waldheim and Carpentieri (2001)
BioCoComb [1] CFB gasifier, 3.5 MW_e (10 MW_{th}) (Zeltweg, Austria)	Wet wood chips, bark and sawdust with moisture up to 70%; air-blown; no need for tar removal since gas is co-fired	Babcock Borsig Power and Austrian Energy's CFB gasifier, gas co-fired with a PC boiler. Operating temperature = 1120 K (850 °C). Gas HHV = 2.5-5 MJ/Nm^3. Unconverted carbon in char = 10%. Particle size entering boiler = 200 μm.	Project initiated in 1993; construction started in 1997; gasifier installed in 1998. Contracted to Draukraft. Now in operation.	Mory and Zotter (1998) Knoef (2002a)
Biocycle [1] pressurized FB gasifier 7.2 MW_e and 6.78 MW_{th} (Denmark)	1325 ha of short-rotation forest supplies wood fuel; air-blown; dolomite for tar removal	U-GAS / RENUGAS pressurized FB gasifier from Enviropower, coupled with EGT/Typhoon gas turbine. Ceramic candle filter for gas cleaning. Design electrical efficiency = 39.8%.	Status unknown.	Babu (1995)

Bioelettrica Energy Farm [1] CFB gasifier 14.1 MW_e + 41 MW_{th} (Cascina, Italy)	3680 ha of land supplies SRF wood, agricultural residues, sawdust; water scrubbing for tar removal	Lurgi atmospheric CFB gasifier, Nuovo Pignone for gas turbine in an IGCC configuration. Wet scrubber and filter for gas cleaning. Bag filter for gas cleaning. Designed electrical efficiency = 33%.	Installation scheduled in 2002.	Babu (1995) Knoef (2002a)
Hawaii BGF project [2], pressurized FB gasifier, 5 MW_e (Hawaii, USA)	Gasifying 100 t/d of bagasse in the first stage; oxygen/air and steam blown.	IGT RENUGAS process. Operating pressure = 0.6-2.14 MPa. Temperature = 1020-1250 K (750-980 °C). Designed plant efficiency = 30-35%.	Had to operate at reduced capacity and pressure. Feed system did not perform consistently. Fuel handling and lockhopper feed system modified.	Lau (1998)
KARA-SGI Downdraft moving bed, 0.15 MW_e +0.25 MW_{th} (Almelo, Netherlands)	Gasifying demolition wood, waste wood; air-blown.	KARA/BGT gasification process. Gas cleaning with cyclones and fabric filter.	Gasifier installed in 2000. Commercial operation started in 2000.	Knoef (2002a)
Lahti project [1] CFB gasifier 70 MW_{th} (Lahti, Finland)	Using wet wood chips and recycled refuse fuels, with 20-60% moisture, fed with a screw feeder; air-blown; produce gas co-fired with a PC boiler.	Foster Wheeler technology. Operating at 1070-1270 K (800-1000 °C), atmospheric pressure. Gas HHV = 1.6-2.4 MJ/Nm^3. Gas composition (v. % wet): H_2 = 5.9, N_2 = 40.2, CO = 4.6, C_xH_y = 3.4, CO_2 = 12.9, H_2O = 33.0. Emissions: NH_3 = 800-1000 mg/Nm^3, HCN = 23-45 mg/Nm^3, HCl = 30-90 ppmv, H_2S = 50-80 ppmv, tars = 7-12 g/Nm^3 (dry), carbon content in bottom ash is less than 0.5%.	Project initiated in 1996. Gasifier started commercial operation in 1998. Excellent performance reported, with 4730 h operation in 1998. The syngas provides 15-30% energy input to a PC boiler. HCl emission increased when shredded tires and/or refuse-derived fuels were fired. Bird's nests formed by tire wires. Gas burner required special design to suit the low-Btu gas.	Nieminen and Kivela (1998)
SAFI-Greve [1] demonstration project, 6.7 MW_e (Testi, Italy)	Gasifying wood chips, air-blown; cyclones for gas cleaning.	TPS atmospheric CFB process. Gas produced for co-combustion.	Contractor unknown. Project now operational.	Knoef (2002a)
Tampere pilot plant pressurized CFB gasifier, 15 MW_{th} (Tampere, Finland)	Dry waste wood chips; air and steam blown	IGT pressurized CFB gasifier.	Gasifier installed in 1991. Operating status unknown.	Knoef (2002a)

Varnamo BIG/GT [1] PCFB gasification pilot plant, 6 MW_e +9 MW_{th} (Varnamo, Sweden)	Gasifying wood chips, forest residues, sawdust and bark pellets, willow, straw and refuse-derived fuel (RDF); air-blown	Foster Wheeler technology. Design capacity: 6 MWe and 9 MWth district heating. 32% net electrical efficiency achieved.	Gasifier installed in 1996. Contracted to Sydkraft AB. Plant shut-down in Oct. 1999.	Knoef (2002a)
Vermont FERCO [2] atmospheric MSFB gasifier (s. 1995), 12 MWe (Burlington, VT, USA)	Gasifying 180 dry t/d of wood; steam and air blown; dolomite for tar removal	T = 1250-1310 K (980-1040 °C), atmospheric pressure. Gas HHV = 11-14 MJ/Nm^3. Biomass throughput = 14.6 t/h-m^2. Plant electrical efficiency = 30-35%.	Battelle/FERCO technology. Medium Btu gas is produced by two-bed design. Technology complexity and high sand and biomass flow rates caused operating problems.	Babu (1995) Paisley and Anson (1998)

Notes:
[1] Demonstration project supported by European Union (EU) Joule-Thermie Programme (1994-1998).
[2] IEA demonstration plants.
[3] All projects listed in the table are demonstration projects unless otherwise specified.

2.5 Thematic Outline of the Technology

2.5.1 Mechanism and kinetics of biomass gasification

The history of a single biomass particle injected into a high-temperature gasification reactor starts with rapid evaporation of moisture. Following this stage the temperature of the particle soars quickly while the particle undergoes rapid pyrolysis, releasing volatiles and generating a solid char. The volatiles evolved by pyrolysis may undergo intra-particle tar cracking or other complex homogeneous reactions. Subsequently, the char undergoes a prolonged gasification stage, which usually determines the overall carbon conversion.

Pyrolysis

In this stage, organics in the fuel evolve as small molecules and tars by cracking of larger molecules. The mechanism of pyrolysis has been extensively studied for coal and biomass: (1) Pyrolysis increases the porosity and specific surface area of the solid phase while forming chars (Raveendran and Ganesh, 1998). Instead of being controlled by intrinsic kinetics, the rate of pyrolysis is usually determined by heat and mass transfer limitations. Vacuum enhances pyrolysis (Roy *et al.*, 1994). (2) The product of pyrolysis varies with temperature, pressure, heating rate and surrounding gas composition. Pyrolysis conditions under which char is produced strongly influence the char reactivity in subsequent gasification or combustion stages. Chars reactivity increases with increasing heating rate and decreasing pressure (Di Blasi, 1993; Wanzl, 1994; Raveendran *et al.*, 1995; Demirbas, 2001; Henrich *et al.*, 1999). (3) Pyrolysis conditions determine how much of the alkali and other metals remains in the char, and how much evolves into the gas phase (French and Milne, 1994; Jensen *et al.*, 2000).

Little is known about intraparticle heat mass transfer in biomass pyrolysis. There has been a paucity of intrinsic kinetic data. The product gas contains a spectrum of species from tar to CH_4 and H_2, depending on the degree of cracking, which in turn is a function of the distribution of

apparent activation energies. The high methane content in the tarry pyrolysis gas suggests that pyrolysis usually cannot achieve equilibrium in laboratory facilities. This statement applies to both coal and biomass pyrolysis (Coates *et al.*, 1974; Depner and Jess, 1999). Further study is required to reveal the effect of intraparticle heat and mass transfer in pyrolysis, the distribution of apparent activation energy, and the effect of the heating rate and pressure on pyrolysis gas composition.

Char gasification

Although char gasification is almost always considered separately from pyrolysis, they overlap in time and space. The gas phase reactions, e.g. Reactions (1-8) through (1-11), are generally considered to reach equilibrium. Char gasification is, however, largely controlled by kinetic factors. A close look at the heterogeneous reaction mechanism and kinetics is crucial to the understanding of gasification.

The two step mechanism of carbon-gas reaction, first proposed in the 1960s with evolved gas analysis and later confirmed with thermogravimetric analysis (TGA) methods, is widely adopted for the C-CO_2 reaction (Johnson, 1981):

Step 1. $C_f + CO_2 \xleftrightarrow{k_1, k_1'} C(O) + CO$ (oxygen exchange) (2-1)

Step 2. $C + C(O) \xleftrightarrow{k_3, k_3''} CO + C_f$ (gasification) (2-2)

C_f denotes a free active site on the carbon surface, and C(O) is the carbon-oxygen complex, or a site occupied by a chemisorbed oxygen atom. The rate of carbon consumption can be described in Langmuir-Hinshelwood form:

$$r = \frac{1}{m}\frac{dm}{dt} = \frac{k_1 P_{CO_2}}{1 + \frac{k_1'}{k_3} P_{CO} + \frac{k_1}{k_3} P_{CO_2}}, \qquad (2\text{-}3)$$

where k_1, k_1' and k_3 are kinetic parameters that depend on temperature and the nature of the char. P is the partial pressure of a species present in the reaction system.

When the partial pressure of CO is such that $(k_1'/k_3)P_{CO} << 1$, the kinetics of the reaction can be either first order or zero order in the CO_2 concentration depending on whether $(k_1/k_3)P_{CO_2}$ is very much less than or very much greater than unity. If experimental conditions are such that none of the terms can be neglected, a fractional order with respect to CO_2 may be expected.

Analogously, a rate equation of the same form has been proposed (Kapteijn and Moulijn, 1985) for the non-catalytic C-H_2O reaction, also based on a two-step mechanism:

Step 1. $$C_f + H_2O \xleftrightarrow{k_1,k_1'} C(O) + H_2 \qquad (2\text{-}4)$$

Step 2. $$C + C(O) \xleftrightarrow{k_3,k_3''} CO + C_f \qquad (2\text{-}5)$$

The concept of active surface area (ASA) was introduced (Walker *et al.*, 1953; Laine *et al.*, 1963) for studying carbon-gas reactions. The total surface area (TSA) of carbonaceous materials can be categorized into two parts, i.e. basal plane surface and edge plane surface. The edge surface, found at the edges of the carbon basal planes, is chemically much more active than the basal surface. The instantaneous reaction rate based on ASA was found essentially constant, while that based on TSA varied with unreacted carbon. The ASA concept was soon widely accepted (Radivic *et al.*, 1983; Li, 1999). The standard method for measuring ASA is by oxygen chemisorption at 573 K under an initial oxygen pressure of 70 Pa for 24 hours. However, problems arose in later studies with amorphous carbons (Walker *et al.*, 1991; Radovic *et al.*, 1991) when the area actually occupied by oxygen exceeded those occupied by oxygen in low-temperature chemisorption. At higher carbon conversions, the actual area occupied by oxygen even exceeded the TSA. To explain new experimental findings, Lizzio *et al.* (1990) proposed the

concept of reactive surface area (RSA), which is the concentration of carbon atoms on which the carbon oxygen surface intermediates form and decompose to gaseous products. Thus the ASA is further divided into RSA and the area occupied by stable surface complexes. A reactive surface complex is given the name 'surface intermediate'. The RSA is normally determined with transient kinetic techniques under the reaction conditions. The reaction constants based on RSA were found to be constant over a wide range of conversions (Lizzio *et al.*, 1990). The concept of active sites and their differentiations are essential in understanding carbon reactivity.

Though chars are chemically derived from volatile-containing carbonaceous materials, char gasification is usually examined separately from pyrolysis. Reference to the pyrolysis conditions (temperature, pressure, heating rate and gas atmosphere) is crucial to understand char reaction data, often fitted to a Langmuir-Hinshelwood form. The rate constant k is expressed in Arrhenius form:

$$k = k_0 \exp(-E / RT) \tag{2-6}$$

A compensation effect is usually found between the activation energy, E, and the frequency factor, k_0, for varying reference temperatures.

$$\ln k_0 = cE + c_0 \tag{2-7}$$

However, biomass gasification can be catalyzed by catalysts and, as in pulp and paper applications, by the alkali content in the feed (Kapteijn and Moulijn, 1985). The effects of the catalyst can be threefold: it lowers the activation energy, increases the number of active sites, and provides an alternative reaction pathway if the catalyst loading is high enough to change the reaction mechanism. The catalyst must therefore be considered in kinetic modeling.

Nine major reactions which can be involved in biomass gasification are outlined in Table 2-2, with kinetic and thermodynamic parameters. The kinetic parameters listed assume first order with respect to partial pressure of gas reactants and zero-th order with respect to carbon for

carbon-gas reactions. Data are summarized from different sources, using different units and rate definitions. This makes them incomparable in some cases.

Table 2-2. Major reactions involved in gasification

Reaction	Frequency factor, k_0 (see notes for units)	Activation energy, E (kJ/mol)	Heat of reaction at 1000 K, ΔH (kJ/mol)	Equil. const. at 1000 K, log$K$ (-) [c]
$C + ½ O_2 = CO$	6.47×10^3 [a]	167 [a]	-112 [b]	10.5
$C + O_2 = CO_2$	7.58×10^4-0.045 [a]	9.6-113 [a]	-395 [b]	20.7
$C + CO_2 = 2\ CO$	0.0732 [e]	113 [e]	171 [b]	0.241
$C + H_2O = CO + H_2$	0.0782 [e]	115 [e]	136 [b]	0.400
$C + 2\ H_2 = CH_4$	2.78×10^{-4} [f]	150-213 [f]	74.9 [b]	-1.02
$CO + H_2O = CO_2 + H_2$	-	-	-34.7 [b]	0.159
$H_2 + ½ O_2 = H_2O$	3.09×10^{11} [a]	99.8 [a]	-242 [d]	10.1
$CO + ½ O_2 = CO_2$	8.83×10^{11} [a]	99.8 [a]	-283 [d]	10.2
$CH_4 + H_2O = CO + 3\ H_2$	-	-	206 [b]	1.42

Notes:

(a) Frequency factor in s^{-1} atm^{-1} for heterogeneous reactions, and m^3 mol^{-1} s^{-1} for homogeneous reactions. Data from Kim *et al.* (2000).
(b) Kapteijn and Moulijn (1985).
(c) All data in this column from our own work calculated from JANAF thermodynamic data.
(d) Hamel and Krumm (2001).
(e) Units in kg $Pa^{-0.5}$ s^{-1} m^{-2}, from Chen *et al.*, (2000).
(f) Frequency factor in s^{-1}, based on current carbon mass. Data from Tomita *et al.* (1977).

2.5.2 Carbon conversion and coke formation

Since gasification is a process to convert biomass from the solid state into gas phase products, there is a fractional conversion for each of the elements present in the feed. Hydrogen is a volatile element in all biomass, as well as fossil fuels. It is believed that, if allocated appropriately to the carbon, even the amount of hydrogen in coal would be sufficient to permit nearly complete volatilization of all rich elements in the coal (Howard 1981). Though some researchers (Middleton *et al.*, 1997) have suggested correlating the release of nitrogen and sulfur with the overall conversion, common elements forming biomass, i.e. H, O, N and even S, would

almost all evolve as gaseous species during pyrolysis if no carbon were present. However, the chars remain after pyrolysis, typically 15-20% of the initial dry mass, due to the presence of carbon.

The conversion of carbon is difficult to predict using any equilibrium model because the actual conversion depends on kinetic factors. Experimental evidence shows that carbon conversion in biomass gasification increases with increasing air or O/C ratio, temperature, and solids residence time, since it involves slow heterogeneous reactions that usually do not approach equilibrium in real processes. Equilibrium conversion provides an upper bound on the conversion efficiency practically achievable in a gasifier. On the other hand, the validity of equilibrium models largely rests upon the assumption that all reactions reach chemical equilibrium.

In practice, all carbon that does not evolve as gaseous pyrolysis products is assumed to occur as char in a gasification environment. Some processes may encounter reverse reactions that produce carbon, i.e. coking. Previous studies show that a clear demarcation exists between regimes with and without carbon formation. This demarcation can be called the carbon formation boundary, though the term carbon may refer to practically all amorphous carbons, such as carbon black, chars, coke, soot, and Dent carbon (Dent *et al.*, 1945). The mechanism of carbon formation in high-temperature processes is still not well understood. Nevertheless, the nature of the phenomenon can be adequately explained by saturation of solid carbon in the bulk gas phase serving as a solvent, as suggested in our previous work (Li *et al.*, 2001).

The significance of the carbon formation boundary is twofold. It shows, on a thermodynamic basis, whether complete carbon conversion is possible in a particular system or process. Secondly, by examining how far the system is from the boundary, one can estimate the

margin of parameter change in the system under consideration to achieve maximum carbon conversion without forming carbon black.

Gasification systems are usually treated as C-H-O systems since nitrogen and sulfur are small in amount or largely inert. The carbon formation boundaries predicted from early thermodynamic modeling were plotted in different diagrams, such as the ternary diagram of White *et al.* (1975), the plot in Cartesian coordinates of Gruber (1975), and the carbon formation envelope of Probstein and Hicks (1982). These diagrams correctly predicted the onset of carbon formation as the molar fraction of carbon increases to a certain level determined by thermodynamic constraints. Unfortunately, they were not accurate enough for more complex systems such as gasifiers because they were all derived based on simplified reaction mechanisms and a stoichiometric approach to equilibrium modeling. Therefore, they all failed to predict bends in the carbon formation boundaries due to a shift in the carbon oxidation mechanism at lower temperatures as the O/C molar ratio increased. The former involved two steps and forms CO as intermediate product, while the latter features direct oxidation to produce CO_2.

In Chapter 6 we show that more complex systems can only be tackled by a non-stoichiometric approach which is independent of reaction mechanism. In the initial work, we proposed a carbon formation boundary predicted by a non-stoichiometric equilibrium model. The results not only apply to gasification processes (Li *et al.*, 2001), but also to more generalized C-H-O systems such as steam methane reforming reactors (Grace *et al.*, 2001).

2.5.3 Fuel and feeding

The possible fuels for biomass gasification include wood-based (sawdust, hog fuel, demolition wood, short-rotation plants), herbaceous or straw-based (energy crops, agricultural residues, bagasse), animal residues and manure, municipal solid wastes (MSW), and pulp and paper wastes. One of the important implications of the Lahti demonstration project is the

importance of fuel handling in biomass energy, including production/harvesting, transportation, storage, size reduction, drying, and feeding. As stated previously, due to the low bulk density, an economical transport distance for biomass fuels is typically only 30-80 km. This means that the capacity of the biomass gasifier is limited by the amount of biomass available within this range (Nieminen and Kivela, 1998; Granatstein *et al.*, 2001).

The way biomass fuels are fed depends primarily on the type of gasifier, size requirement, and the working pressure. Evaluation of alternative feeders started about ten years ago as one of the technical tasks of the IEA Biomass Thermal Gasification Activity, with the participation of nine countries (Babu, 1995). All the feeders tested have had problems handling certain types of feedstock or operating in conjunction with a pressurized system, or both. In his end-of-task report, Babu also addressed the problem of size reduction. He estimated that the energy consumption for size reduction from 2 to 0.5 mm mean particle diameter/length ranges from 200 to 1500 kJ/kg. He warned of the dust explosion hazard with decreasing particle size due to spontaneous ignition of dust in the feed system.

Moisture content between 12 and 20% is considered suitable in most cases, though lower moisture is achievable with drying. However, in the Lahti project, the moisture content of the feedstock was as high as 55% without any drying. High moisture content causes operational problems. While fuel moisture content is believed to aid the carbon-steam reaction, its chemical reaction effectiveness has not been examined and compared with steam injection.

2.5.4 Tars: definition and sampling

Since tars can cause operational problems, it is imperative to reduce the tar loading of gasification product gas to levels acceptable for downstream combustion equipment. This figure is currently about 100 mg/Nm^3 for typical gas turbines (Hasler and Nussbaumer, 2000). However, what constitutes tar has been subject to on-going discussion for many years. There are different

tar definitions and more than a dozen sampling methods in use, causing data from different sources to be hardly comparable in many cases.

At a tar sampling meeting in Brussels in 1998, jointly steered by the IEA, the Directorate General of the European Commission (DG XV11) and the US DOE, it was agreed that a tar protocol would fulfil the need for a standard method of determining the concentrations of particulates and heavy hydrocarbon impurities in the fuel gas. It was decided to define tars as hydrocarbons with molecular weight higher than benzene (Maniatis and Beenackers, 2000; Abatzoglou *et al.*, 2000). This controversial definition received reactions from "irrelevant" to "gladly we finally have a common definition". Nevertheless, alternative definitions are still in use. Moersch *et al.* (2000) found that it would be reasonable to define tars, or condensable organic compounds, as species having molecular weights from 78 (benzene) to 300. Another classification proposed by Hasler and Nussbaumer (2000) states that tars consist of four parts: (a) heavy tars including all high molecular organic compounds with boiling point higher than 473 K (200°C), (b) Polyaromatic hydrocarbons (PAH) including naphthalene and phenanthrene, (c) phenols, and (d) water-soluble organic residues.

A provisional version of the Tar Protocol is now available, and a newer version will appear soon. Though sampling principles are largely decided, selection of the tar solvents/temperature combination remains an area of uncertainty (Maniatis and Beenackers, 2000). The 1998 provisional protocol recommended three solvents, i.e. dichloromethane (DCM), acetone and isopropyl glycol, for tar sampling. Moreover, sampling procedure, including the condensation temperature, sampling duration, sampling flow rate, maintaining isokinetic conditions and the need to include particulates determination, were areas in which work should be continued to improve the protocols.

A quasi-continuous on-line tar sampling method developed by Moersch *et al.* (2000) employs a flame ionization detector (FID), a tar filter at 273-363 K (0-90°C) and temperatures below the dew point. The tar concentration is determined by difference between total and non-condensable hydrocarbons. The method assumes that all condensable tars condense and can be captured by a single tar filter. However, this is very unlikely to be achievable in practice.

2.5.5 Tar reduction and catalytic gasification

Tars can be reduced by either *in situ* or post-gasification cracking, or a combination. The final target of tar reduction is a tar loading of 100 mg/Nm^3 or less if it is to be fired in a gas turbine (Hasler and Nussbaumer, 2000). Fundamental and pilot studies indicate that the most effective and economic way to reduce tar yield is by increasing operating temperature in the gasifier without a catalyst. Establishment of a local high-temperature zone by introducing secondary air was also found effective in reducing tar yield as well as in adjusting gas composition (Pan *et al.*, 1999), though often at the expense of lowered gas heating value.

Tar reduction is often achieved simultaneously with catalytic gasification because of their similar mechanisms and catalyst types. The overall equation of steam reforming of hydrocarbons can be written as (Sutton *et al.*, 2001):

$$C_nH_m + nH_2O \Leftrightarrow nCO + (n+m/2)\,H_2 \qquad (2\text{-}8)$$

The first comprehensive review of catalytic carbon-gas reactions was by Walker *et al.* (1968). More recently, Sutton *et al.* (2001) evaluated three groups of catalysts: naturally occurring carbonates (dolomite, magnesite and calcite), alkali metals and nickel. The criteria for ideal catalysts are as follows:

(1) The catalyst must be effective in removal of tars.

(2) If the desired product is syngas, the catalyst must be capable of reforming methane, thus providing a suitable syngas ratio for the intended process.

(3) The catalyst should be resistant to deactivation as a result of carbon fouling and sintering.

(4) The catalyst should be easily regenerated, mechanically strong, and inexpensive.

Based on these criteria, naturally occurring carbonates, such as dolomite, have been found to be suitable catalysts for removal of hydrocarbons. Dolomites are most active at temperatures above 800 °C. With suitable ratios of biomass feed to oxidant, almost 100% elimination of tars can be achieved (Olivares *et al.*, 1997; Sutton *et al.*, 2001). A comparison between different dolomites (Orio *et al.*, 1997) indicated that those with higher Fe_2O_3 and larger pore diameter had higher activity. It was also found that the order of activity was dolomite > magnesite > calcite (Degaldo *et al.*, 1997). But one problem with dolomite, and perhaps also with calcite, is its relatively low mechanical strength that often causes undesired attrition and catalyst losses from the fluidized bed, while increasing particulate loading to the gas cleaning equipment (Degaldo *et al.*, 1997).

In general, alkali metals (Li, Na, K, Rb and Cs) are all good catalysts for the C-CO_2 reaction, while alkaline earth metals (Ca, Sr, Ba) catalyse the C-H_2O reaction. Kapteijn and Moulijn (1985) estimated that alkali metals could lower the apparent activation energy for carbon-gas reactions by 20-60 kJ/mol. These catalysts also reduce tar yield and methane content in the gas, though their hydrocarbon conversion efficiency rarely exceeds 80%. Moreover, they are difficult to recover due to high-temperature evaporation, and cause agglomeration and possible defluidization in moving- and fluidized-bed gasifiers (Sutton *et al.*, 2001).

Nickel-based commercial catalysts are highly effective in tar removal and adjustment of gas composition. Sutton *et al.* (2001) commented that such catalysts acted best as secondary catalyst located in a downstream reactor for gas conditioning, operated under different conditions than those of the gasifier. Properly operated to prevent deactivation by carbon deposition, this group of catalysts was found to be most active with long lifetimes at 1050 K in a fluidized bed.

2.5.6 Particulates and gas clean-up

The recommended concentration of particulates in producer gas for combustion in a gas turbine is below 50 mg/Nm^3. However, the concentration in raw gas produced by gasifiers varies from 5 to 30 g/Nm^3 (Babu, 1995; Hasler and Nussbaumer, 2000; Coll *et al.*, 2001). This necessitates high-efficiency gas clean-up and particulate removal to prevent damage to the gas turbine in IGCC and fuel cell applications. Although wet scrubbers can be used to removal particulates and soluble gases such as hydrogen sulfide, they cause a significant efficiency loss that reduces back the efficiency gain of combined cycle systems. Hence dry hot gas clean-up technology is most suitable for combined cycle technology.

The most efficient ways of removing particulates from raw gases at elevated temperature is to use various types of ceramic filters, e.g. as ceramic composite, ceramic fabric and ceramic (e.g. silicon carbide) candles (Newby and Bannister, 1994; Ergüdenler *et al.*, 1997c; Engstrom, 1998). The IEA Thermal Gasification Activity evaluated three types of hot gas filtration equipment (Babu, 1995). The Schumacher ceramic filter elements installed at the VTT pilot gasifier could be used up to 1000°C in reducing atmosphere, with a pressure drop of 5500 Pa after 20000 cycles. The Lurgi Lentjes Babcock ceramic candle filters were tested up to 540 K (265°C) and 25 bar pressure. The third type tested was the WEC candle filters, tested up to 770 K (500°C) and 24 bar owing to a proprietary seal design. Other manufacturers of filter elements include 3M, Coors and DuPont. Ergüdenler *et al.* (1997c) reported results from investigation of the performance of two 3M ceramic fabric filters. The filter bags demonstrated 99.95-99.99% filtration efficiency with the face velocity maintained in the range of 12-24 mm/s. Filter bags can be used at temperatures up to 820 K (550°C) under gasification conditions and 1020 K (750°C) under combustion conditions.

One challenge to all types of filter elements is to keep them clean. Particulate deposition on the external surface of the filter elements can result in a high rate of increase in pressure drop and even failure (Cahill *et al.*, 1993). Filter lifetime is significantly affected by particulate properties, as well as by the temperature and atmosphere of the gas clean-up unit (Alvin, 1998). Recent integration of particulate removal with tar removal with nickel-activated ceramic filters (Zhao *et al.*, 2000a, b) appears to be promising.

2.5.7 Minerals in biomass gasification

Biomass ash is rich in minerals, including alkali metals. The alkali of primary concern is potassium, present at levels usually below 5% of dry mass (Turn *et al.*, 1998). Other principal inorganic elements are silica, calcium, chlorine and sodium, their relative proportions depending on biomass species and mode of transportation, handling and processing. Since CaO, K_2O and SiO_2 are the three dominant species of biomass ash, a ternary diagram can be employed for characterization of the ash composition in terms of their relative abundance (Zevenhoven-Onderwater *et al.*, 2001a). The fusion temperature of biomass ash under reducing (gasification) conditions varies from 1070-1190 K, the range of operation for most gasifiers (Ergüdenler and Ghaly, 1992).

Though biomass has much lower ash content than coals, the minerals still pose threats to operation. Metal oxides in ash are responsible for fouling, corrosion, sintering and agglomeration in combustion and gasification equipment. Alkali vapor deposition is the major cause of fouling and metal corrosion in IGCC power systems. However, Raveendran *et al.* (1995) reported that metals also influence pyrolysis and gasification mechanism. Alkali metals are good catalysts for carbon-gas reactions. A number of experimental and modeling studies have been conducted to observe and predict ash behaviour in gasification systems (Zevenhoven-Onderwater *et al.*, 2001a,b). It was found that the order of retention in the bed for different elements is Ca > K >

Mg > P (Arvelakis *et al.*, 1999). However, the closure of the element balance remains a problem for many trace elements.

There are four general ways to deal with alkali-induced problems (Turn *et al.*, 1998). First, metals can be removed from biomass feedstock prior to gasification by mechanical dewatering and leaching (Jenkins *et al.*, 1996; Turn *et al.*, 1997). However, such treatment is only applicable to small systems because of the danger of water pollution. The second method is to use limestone, dolomite or other metal oxides with high melting point (e.g. TiO_2) as bed material to raise the fusion temperature of ash, thus preventing sintering and slagging in the bed. This method is well established in coal gasification, and is also recommended for biomass gasification, even for feedstocks like black liquor solids that contains more than 20% alkalis (Pels *et al.*, 1997; Zeng and van Heiningen, 1997). The third method is by gas clean-up with a wet scrubber or a "gettering" bed. Finally, metals will not be a problem to downstream equipment if they are not released during gasification. New processes that operate at lower temperatures should help to solve this problem. Notwithstanding findings with coal ash behaviour, there has still been a dearth of literature with respect to the fate of minerals in biomass gasification.

2.5.8 Modeling of biomass gasification

Models of biomass gasification largely fall into two groups: kinetic and equilibrium. Kinetic models deal with the mechanism, rates and the resulting species concentration at any point in time and space within the system, while equilibrium models predict the maximum achievable conversion and the distribution of each species in the product streams subject to thermodynamic and mass transfer constraints. Kinetic models are in general process specific; they provide valuable insights to reaction mechanism and ways to increase rate of a given reaction or process. Equilibrium models claim no geometric dimensionality and do not predict the time needed to reach equilibrium.

Typical kinetic models include those of Vamvuka *et al.* (1995) and Chen *et al.* (2000) for entrained flow gasifiers, and those of Yan and Zhang (2000) and Hamel and Krumm (2001) for fluidized beds. Kim *et al.* (2000) developed a kinetic model for an internally circulating fluidized bed gasifier. The above models all consider the whole reactor. A one-dimensional, two-phase kinetic model was proposed by Fiaschi and Michelini (2001) for a fluidized bed biomass gasifier. Unlike most other models that usually under-predict methane content, this kinetic model makes reasonable predictions for methane, but overestimates hydrogen, and needs to be further modified. Borelli *et al.* (1996) proposed a single particle model that considered progress of carbon-gas reaction with percolative fragmentation. Such single-particle models, assisted by progress in kinetic data, especially with respect to the heterogeneous reactions, are now sophisticated enough to predict product composition with reasonable precision for a wide range of applications, though adjustible model parameters are still unavoidable in many cases.

There are two approaches to equilibrium modeling of complex chemical reaction systems. The stoichiometric approach is based on a well-defined mechanism and initial chemical compositions, while the non-stoichiometric approach, though equivalent in essence, does not differentiate between chemical compositions of feed streams so long as the input elemental abundance is the same. Generally speaking, equilibrium models developed for coal combustion or gasification apply well to biomass with little modification. Examples of stoichiometric equilibrium models are those of Chern *et al.* (1991), Watkinson *et al.*, (1991) for coal gasification, the recent work of Zainal *et al.* (2001) for downdraft biomass gasifiers, and that of Schuster *et al.* (2000) for steam gasification of biomass. Backman and Hupa (1990) developed a non-stoichiometric equilibrium model for pressurized gasification of black liquor. More recently, Ruggiero and Manfrida (1999) proposed a simplified one for a biomass gasifier, but the predictions do not compare well with measured data because of the inability of the model to

consider slow reactions that affect the final gas composition. The challenge to equilibrium models lies in the incomplete conversion of carbon and cracking of tars and methane due to kinetic reasons. Such non-equilibrium uncertainties require more detailed future work.

2.6 Summary and Objectives for This Project

In this chapter we reviewed the state of the art of biomass gasification and research activities around the world. Different types of gasifiers are introduced and their advantages and problems discussed. Major topics of biomass gasification are outlined in order to identify opportunities and potential challenges facing biomass gasification. The feasibility of biomass gasification has been strongly supported by a number of demonstration projects in Europe. The technology seems particularly suitable for Canada, a major pulp and paper producer in the world. Pulp mills are ideal sites for biomass gasification plants due to availability of fuel (e.g. sawdust, hog fuel), electricity, oxygen and steam, and end user for the product gas.

What kind of gasifier should be developed for biomass gasification? The following criteria can be proposed:

(1) A process for medium or large-capacity should employ a reactor with excellent gas-solid mixing to enable large throughput within a small volume, while preventing gas channeling and short-cutting due to hydrodynamic non-uniformity across the reactor.

(2) The process must be able to achieve high carbon conversion by providing adequate residence time for both the solids particle and gas.

(3) The process should have means to reduce tar loading in the product gas and to adjust the gas composition to suit the particular downstream application.

(4) The process should be flexible to changes in fuel type, feed rate, particle size and moisture content.

The circulating fluidized bed gasifier satisfies all of these criteria, at least in principle, owing to excellent mixing and heat transfer conditions, effective solids recycle and an inherent flexibility with fuel type and load turndown. Naturally occurring minerals and commercial catalysts can be added to the bed for effective tar reduction and hydrocarbon reforming.

What factors and effects should be examined in the pilot study? The objectives of the present work are to answer, both experimentally and by mathematical modeling, the following essential questions with respect to the pilot gasifier:

(1) How gas composition and heating value from the pilot gasifier vary with operating parameters, e.g. air or O/C ratio, operating temperature, suspension density, secondary air and fly ash re-injection, and how gas composition varies with spatial position in the gasifier;

(2) How carbon conversion, gas yield, gasification efficiency and tar yield vary with operating conditions;

(3) How fuel moisture behaves in gasification and how to evaluate its role;

(4) In mathematical modelling, how to evaluate and account for the degree of the system's deviation from chemical equilibrium;

(5) How to predict and prevent the onset of carbon/coke formation.

The remaining chapters of the thesis report experimental and modeling results in an effort to clarify essential aspects of these questions.

CHAPTER 3. PILOT STUDY OF BIOMASS GASIFICATION: EXPERIMENTAL SETUP

This chapter introduces the CFB gasifier, the fuel, bed materials and catalyst, the sampling method and the operating procedure for our pilot study. The gasifier was first built in 1997. Adaptations were made to facilitate feeding of sawdust and to by-pass a damaged secondary cyclone. An operating procedure was tested and followed to ensure safe start-up, operation and shutdown. A tar sampling method was developed based on the recommendations of the 1998 provisional tar protocol, but with modifications to avoid freezing of water vapour in the sampling train.

3.1 Gasifier

A schematic diagram of the experimental system appears in Figure 3-1. The pilot gasifier employs a riser which is 6590 mm high and 100 mm ID (4"). It is also equipped with a high-temperature cyclone for solids recycle and a ceramic fibre high-temperature filter unit for gas cleaning. Engineering and fabrication of the gasifier were completed by Axton Manufacturing, Ltd. The riser and cyclone were fabricated from heat-resistant Incoloy alloy (800HT, SB-407-N08810) and hydro-tested in compliance with the ASME code to allow continuous operation to 1145 K temperature and 8.3 bar pressure (1500°F, 125 psi). The high-temperature parts are insulated with 90 mm thick high-density ceramic fibre blanket covered by a 38 mm thick layer of ceramic wool, and wrapped with a 0.5 mm thick aluminum jacket or a ceramic cloth jacket. This reduces surface heat losses to about 3-5% of the total energy input. The sensible heat of the hot gas and hot water is not recovered because there is no end user.

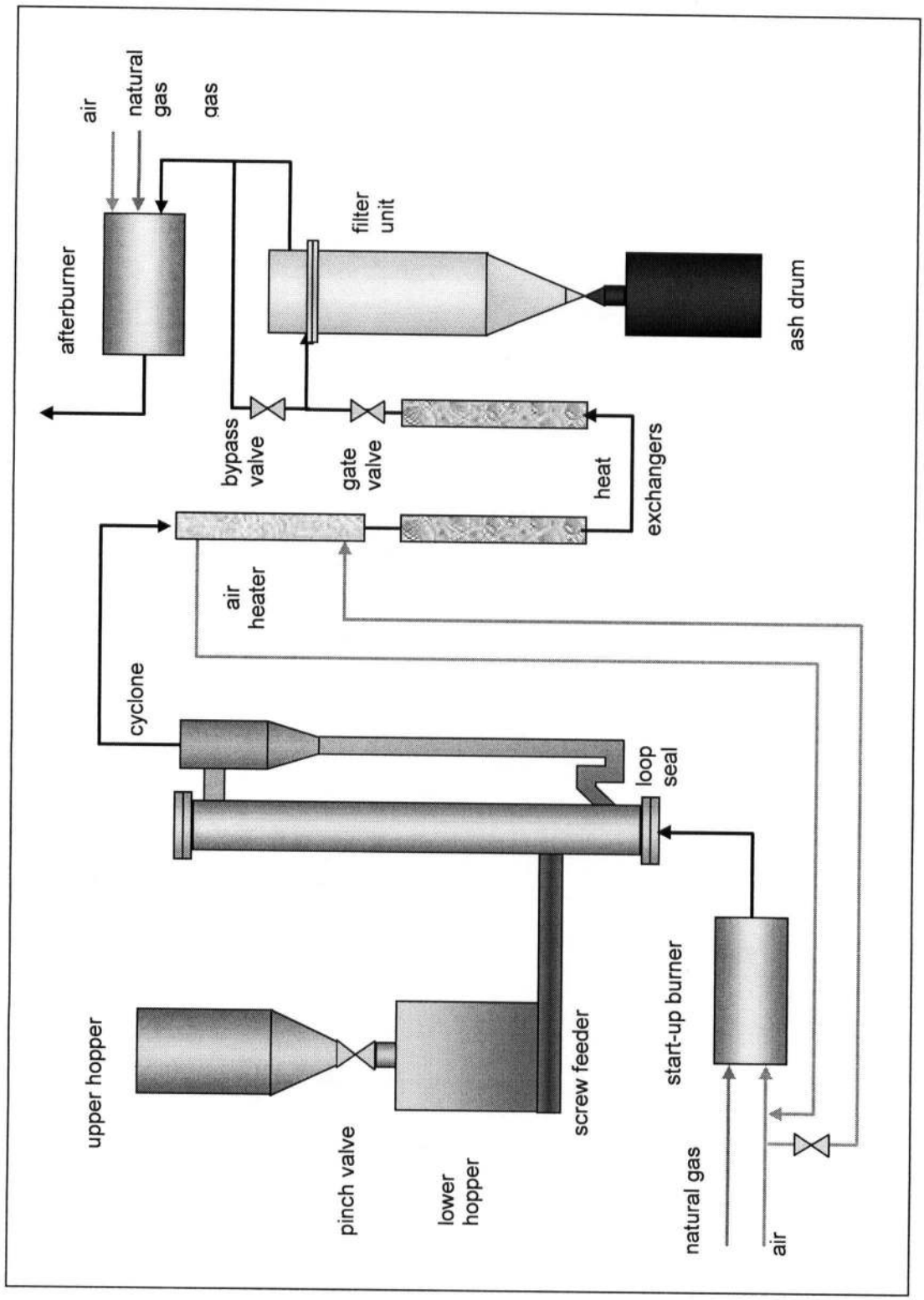

Figure 3-1. Schematic diagram of CFB gasifier.

To prevent back propagation of a flame, the rooftop burner which treats the product gas is equipped with an Enardo Series 7 Model 71006/C-C4R 100 mm (4") flame arrestor, capable of working at pressures up to 10.5 bar (150 psi). The geometry of the bottom of the riser, loop seal and feed ports appears in Figure 3-2. Note that the CFB gasifier does not have an air distributor commonly found at the bottom of CFB risers. Instead, a 230 mm high conical expansion is used, as shown in Figure 3-2.

Only part of the air for complete combustion is supplied as oxidant and fluidizing agent after passing through a natural gas-fired start-up burner installed near the bottom of the gasifier. Primary air is supplied from the bottom of the riser, while secondary air, which can account for up to 20% of the total air, is injected from two facing 32 mm ID (1 ½") ports, centred 2294 mm above the axis of the primary air inlet. Cold air pressure is first reduced to 3.0 bar (29 psig), then further regulated to 1.07-1.35 bar for nearly atmospheric operations. The burner is furnished with a Tervcon 5602 flame safeguard control and two Honeywell gas pressure switches to ensure that the gauge pressure at the burner inlet is in the range 15-45 kPa (2-6 psig). A 120V / 6000V ignition transformer is used together with an Auburn I-2 spark ignitor and an Auburn FRS-2 resistance flame detector. Hot gas leaving the burner and pre-heated air are mixed to preheat the bed and, if needed, to maintain the suspension temperature at the desired level. Temperatures of both the primary and secondary air can be tuned by adjusting the total air supply and the fraction of each stream.

The start-up burner heats the gasifier up to 670-820 K (400-550°C) before coal or biomass fuel can be fed to the riser in order to further raise the temperature to a desired level. Then the system is switched to the gasification mode. Since the natural gas pressure is only 1.35 bar (5 psig), the burner can only be used for atmospheric operation, or before pressurizing the system. The pressure of the CFB system can be adjusted by opening or closing a Kitz 300SCLS 60 mm

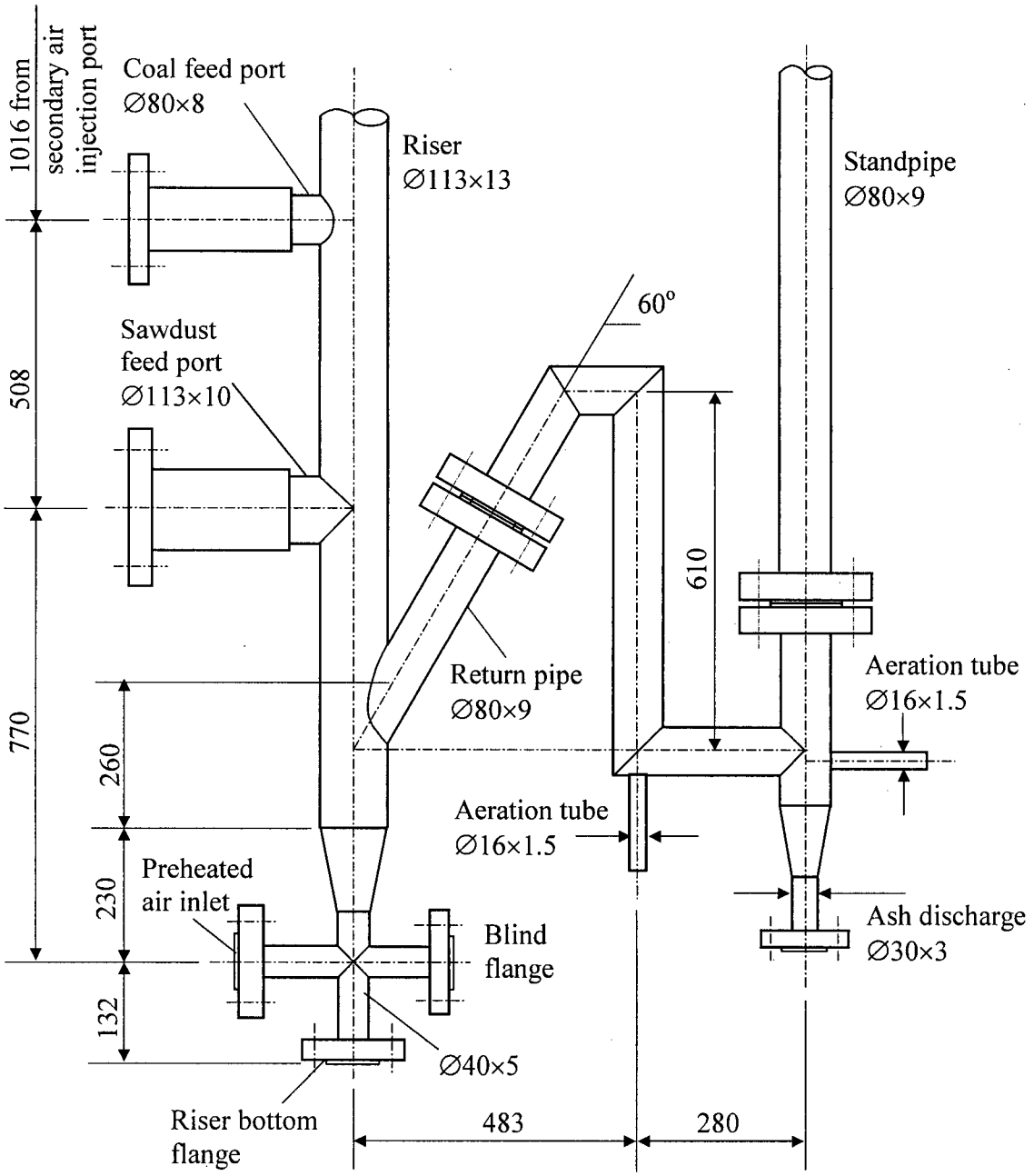

Figure 3-2. Geometry of bottom of riser and loop seal. All dimensions are given in mm, outer diameter and wall thickness are used to specify tubing and pipe sizes.

ID (2 ½") steel gate valve, located between the heat exchangers and the ceramic fabric filter, as shown in Figure 3-1.

During start-up, the gas temperature at the exit of the heat exchangers is not high enough to prevent vapor condensation inside the filter unit. Therefore, the filter bags could become wet, causing the pressure drop to increase very much until the gas temperature exceeds the gas dewpoint. To protect the filter bags from possible moisture-induced aging, the filter bypass line can be opened. This, however, risks blocking the flame arrestor on the rooftop by particulates. Thus it is not recommended unless an alternative gas cleaning system is installed on the bypass line.

When the overall system operates in the gasification mode, feed particles undergo moisture evaporation, pyrolysis and char gasification primarily in the riser. The fast fluidization regime is maintained at the operating temperature, with a typical superficial velocity between 4 and 10 m/s, corresponding to an air flow of 40-65 Nm^3/h. The solids feed rate is 25-45 kg/h (corresponding to a flux 0.7-2.0 kg/m^2s) for typical sawdust. Coarser particles in the hot gas are captured by a high-temperature cyclone immediately downstream of the riser.

The top of riser and the cyclone are shown in Figure 3-3. The blunt-turning exit of the riser is expected to increase the solids density at the top of riser by establishing a C-shaped solids density profile along the height of riser. The cyclone has a 187 mm ID (8 5/8" OD x 5/8" thick wall), 463 mm high cylindrical stage and a 305 mm high conical base. The dimension of the tangential inlet of the cyclone is 76 mm x 38 mm, measured on the inner surface. Because of its excellent mixing, high temperature and considerable residence time, the cyclone provides an extended reaction zone for both homogeneous and heterogeneous reactions such as methane reforming and thermal cracking of tar. The solids captured in the cyclone are returned to the bottom of the riser through an air-driven loop seal. Hot gas leaving the cyclone at a temperature

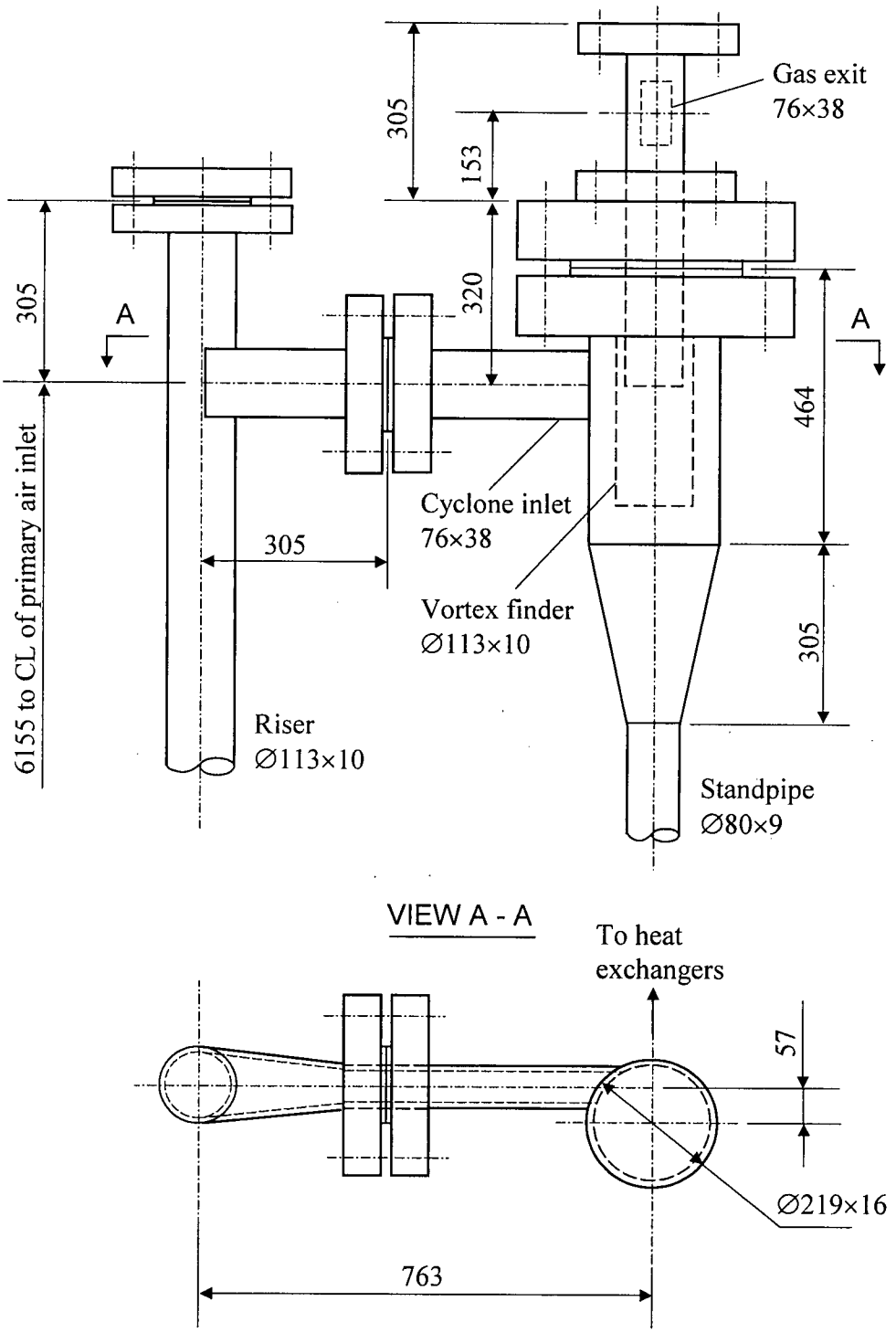

Figure 3-3. Geometry of top of riser and cyclone. All dimensions are given in mm, outer diameter and wall thickness are used to specify tubing and pipe sizes.

of 600-800°C is cooled by a two-stage water-jacket heat exchanger and a single-stage air preheater before entering the filter unit. The cyclone exit duct from the vortex finder has the same dimensions as, but perpendicular to, the cyclone inlet duct. Connected to the bottom of the cyclone is a half-supported, half suspended 4086 mm high and 65 mm ID (3") standpipe, linked with a 305 mm long expansion joint in the middle position. The loop seal has a 610 mm high vertical pipe and a return pipe at an angle of 30° to the vertical. Solids are returned 622 mm above the riser bottom flange, about 490 mm above the primary air inlet.

Connected via a transition to the rectangular cyclone exit duct a horizontal 100 mm ID (4") SS 312L pipe is located between the cyclone and the first heat exchanger. Inside the horizontal pass is a water-cooling coil, protecting the pipe itself. The coil is 890 mm in length, shaped from 10 mm (3/8") SS316 stainless steel tubing. Three heat exchangers are employed for further cooling of the gas. The first stage has a 2450 mm long, 60 mm ID (2 ½") SA 312TP inner pipe, cooled by an air-jacket made from a 2150 mm long, 100 mm OD copper tube. Air preheated in this stage is returned to the bottom of riser to mix with primary air. The second and third stages are water-cooled, having the same structure as the first stage except for its length. Each of these two stages is 3100 mm long, with a 2800 mm long water-cooled section. Cooling water inlets are located at the bottom of the cooling jacket, while the outlets are at the top. Gate valves are installed next to the cooling water outlets in order to establish an overflow height inside the cooling jacket, protecting the welds from possible overheating and failure.

The gasifier is equipped with high-efficiency ceramic fabric filter bags for gas cleaning. The filter vessel is comprised of a 260 mm high top cover, a 620 mm OD and 910 mm long cylinder, and an 800 mm high cone, all fabricated from 6.4 mm thick carbon steel plate. Inside the filter unit there are 12 filter elements sewn from 3M™ FB-900 ceramic fibre cloth, designed for continuous operation at up to 1020 K and 820 K under oxidizing and reducing conditions,

respectively. Each of the filter bags is 100 mm in dia. and 914 mm long, supported from inside by a stainless steel cage, and secured at the top with a spring collar for easy maintenance and replacement. The total filtration area is 3.43 m^2. The measured capture efficiency of this type of filter material is above 99.95% at a face velocity of 14-24 mm/s for the Highvale coal ash and 3M char of mass mean diameter 8.5 and 12.8 μm, respectively (Ergüdenler *et al.*, 1997c). For both materials tested, more than 50% by number of the ash particle particles were smaller than 2 μm. A 152 mm OD pipe and a knife plate valve are used for discharging fly ash.

The filter unit is equipped with a nitrogen purge system located at the top of the vessel to prevent build-up of pressure drop across the filter bags as well as to inhibit undesired temperature rise inside the filter. Nitrogen is first filled into a 300 mm ID and 1000 m tall buffer cylinder, purging the filter at 1-3 bar (15-45 psig) pressure, depending on the condition of the filter bags. Higher purge pressure can be used for newly installed bags. The purge system has four 25 mm (1") main entries, each branched into three 15 mm OD (5/8") purging jets, inserted a few millimetres into the inlets of the Venturi nozzles installed at the top of the filter bags.

The gasifier employs two independent feed systems, one for the main fuel (biomass) and the other for auxiliary fuel (coal), used during start-up. The biomass feed system consists of two sealed hoppers, each of volume 0.30 m^3, a screw feeder driven by a 0.5 kW Balder CDP 3440 variable-speed DC motor, and a gearbox which reduce the rotation speed from 1750 rpm to less than 60 rpm. The screw is designed with a tapered pitch and sleeve diameter to allow compaction of the sawdust volume by approximately 10% to facilitate feeding and gas sealing. The upper hopper can be refilled while the lower hopper is in service. A 191 mm ID (8") rubber pinch valve isolates the upper hopper from the working pressure in the riser, thus allowing safe "lock-hopper" refilling of the solid fuel without interrupting the operation of the CFB reactor. The coal feed system employs a 320 mm ID hopper, with a 2500 mm high cylindrical stage and a 500 mm

high conical base, the total volume of which is 0.23 m^3. At the bottom of the coal hopper, there is a DC-motor-driven rotary valve feeding coal with a water-cooled injector 1278 mm above the primary air inlet through a 16 mm dia. (5/8") pneumatic conveying line. Each of the two feed ports has a cooling water jacket.

3.2 Fuel, Bed Materials and Catalyst

Six sawdust species were used; their ultimate analyses and other relevant properties appear in Table 3-1. Four of these - cypress, hemlock, spruce-pine-fir mixture (SPF), cedar, - are coastal species purchased from the Dunbar Transport sawmill. The other two - pine bark-spruce whitewood (PS) and a mixed sawdust, its exact composition unknown - were produced by an inland sawmill and provided by the Dynamotive company. The mixed sawdust can also be received as 5 mm dia. pellets with a length of typically 10-20 mm, and can easily be converted into loose sawdust by spraying with water. The sawdust produced in this manner contains up to 70% of moisture and therefore needs to be dried before it is used for gasification tests. Air-drying takes about a week to lower the moisture content to 10-15%, while indirect steam drying takes about four days to achieve the same moisture content if the sawdust is blended once a day.

The ultimate analyses of the first four sawdust species were determined in collaboration with Hyundai Heavy Industry, Korea, while those for the PS and mixed sawdust were performed by the Huazhong University of Science and Technology (HUST), China, all samples were provided by the author. The standard methods used in both countries for fuel ultimate analysis are identical to, or derived from, well-accepted international standards, e.g. ISO 625-1975 (E) / ASTM D3178M / GB476-91 (Liebig high-temperature combustion method) for determining carbon and hydrogen content, ISO 333-1983 (E) / ASTM 3179M / GB476-91 (semimicro

Kjeldahl method) for determining nitrogen, and ISO 334 / ASTM D3177M / GB/T 214-1996 (Eschka fusion method) for total sulfur. The ash content was determined by ISO 1171M / ASTM D3174M (high-temperature ashing method). Oxygen was obtained by difference. Fuel calorific value was measured in compliance with ISO 1928 M / ASTM 2015M / GB 213-1996 using the calorimetric bomb method. The moisture contents were obtained from the weight losses after drying the sawdust samples at 378 K (105°C) for 5 hours. The bulk densities were determined using the dried samples by weighing a known volume (litres) of sawdust. The mixed sawdust and PS had much higher bulk densities than the other four species because they had been pelletized during processing, and still maintained a degree of compaction after spraying with water.

Table 3-1. Ultimate analyses of test fuels [1]

Fuel type		Sawdust species						Highvale
		Cypress	Hemlock	SPF [2]	Cedar	PS [3]	Mixed	Coal
Carbon	wt. %	51.6	51.8	50.4	52.3	49.1	48.9	62.9
Hydrogen	wt. %	6.20	6.20	6.25	6.11	7.26	7.86	3.63
Oxygen	wt. %	40.4	40.6	41.6	39.9	39.5	40.3	17.8
Nitrogen	wt. %	0.65	0.60	0.62	0.52	0.25	0.21	0.22
Sulfur	wt. %	0.46	0.38	0.34	0.39	0.50	0.07	0.77
Ash	wt. %	0.70	0.40	0.70	0.79	3.34	2.69	14.7
Higher heating value	MJ/kg	20.3	20.3	19.8	20.4	21.1	21.7	23.8
Higher heating value	kcal/kg	4840	4850	4720	4880	5030	5170	5560
Stoichiometric air	Nm^3/kg	5.36	5.36	5.20	5.40	5.46	5.56	6.52
Bulk density (air-dried)	kg/m^3	140	130	120	150	350	460	815
Mean particle diameter	mm	1.49	0.92	0.82	0.67	0.38	0.43	0.56

Notes:
1. All ultimate analyses, heating values and stoichiometric air volumes are on a dry basis.
2. SPF = spruce, pine and fir mixed sawdust.
3. PS = 50 wt.% pine bark / 50 wt.% spruce whitewood mix.

The Highvale coal is a sub-bituminous coal from Alberta used in many previous UBC studies, especially as a convenient start-up fuel to conserve the sawdust. The ultimate analysis of the coal is repeated from a previous gasification study (Ergüdenler, 1998) for the same coal. For the pilot tests in this work, coal was crushed to less than 6 mm, while sawdust was screened to less than 13 mm. Size distribution data for the sawdust, coal, silica sand, bed ash and fly ash are given in Appendix I. In some runs fly ash was pneumatically re-injected into the riser. The carbon contents of the bed materials and the re-injected fly ash were accounted for in the overall mass and energy balances. Bed ash collected from a previous run was used as the starting bed material, with silica sand used to make up the solids loss.

The Sauter mean diameter is obtained from the sieving data to characterize the particles (Cheremisinoff and Cheremisinoff, 1985):

$$\bar{d} = \frac{1}{\sum_i \frac{f_i}{d_i}}, \tag{3-1}$$

where f_i is the mass fraction of particles with a nominal diameter d_i, in mm.

In the last two runs, a catalyst was used to test for simultaneous tar removal and methane reforming. The nickel-based catalyst, C11-9 LDP, is a product of Süd-Chemie used for steam methane reforming. It contains 70-90% aluminum oxide as a carrier and 10-30% nickel oxide as the active component. The particle density is 2820 kg/m^3. In each of these runs, about 11-14 kg of catalyst, crushed and screened to 0.25-1.7 mm in diameter, was added to the riser by pneumatic conveying immediately prior to switching the system to the gasification mode.

3.3 Instrumentation

The flows of all air streams (including primary air, secondary air, loop seal vertical and horizontal aeration, coal feeding air, sawdust hopper purge air, pressure tap purge air) were measured by rotameters located on the front panel. Rotameter calibration data are listed as a concordance table between rotameter readings and air flow rates in Appendix II. The natural gas flow was indicated by a rotameter of the same type as the secondary air rotameter. The natural gas flow was manually adjusted based on the gas temperature at the exit of the start-up burner. Cooling water flows were measured by rotameters. Each cooling water stream was maintained above 80 kg/h to ensure that no evaporation occurred inside the cooling system, based on a worst-case estimation.

The steam injection system supplied 5 bar saturated steam. The steam flow rate was measured by an in-line steam meter and calibrated by weighing condensate water over a known time interval. The coal feeder was calibrated for the Highvale coal. Sawdust and coal feeders were calibrated for cypress sawdust, but the data were converted to volumetric flow rates so that the results could be extrapolated to other species by comparing their bulk density. A concordance table similar to that for air rotameters is provided in Appendix III, together with calibration curves for the steam meter.

The gas sampling port is located near the inlet of the heat exchanger. The gas sampling system, shown in Figure 3-4, consists of a heated sampling tube, a 38 mm dia., 230 mm long sintered stainless steel candle filter (or alternatively a 50 mm ID, 250 mm long glass fibre filter filled with 200 g of silica gel) for particulate removal, a 50 mm dia. 300 mm long moisture trap filled with 200 g of silica gel or magnesium perchlorate, and an on-off valve. The ceramic candle filter in Figure 3-4(a) was frequently blocked by condensate and particles deposited on the

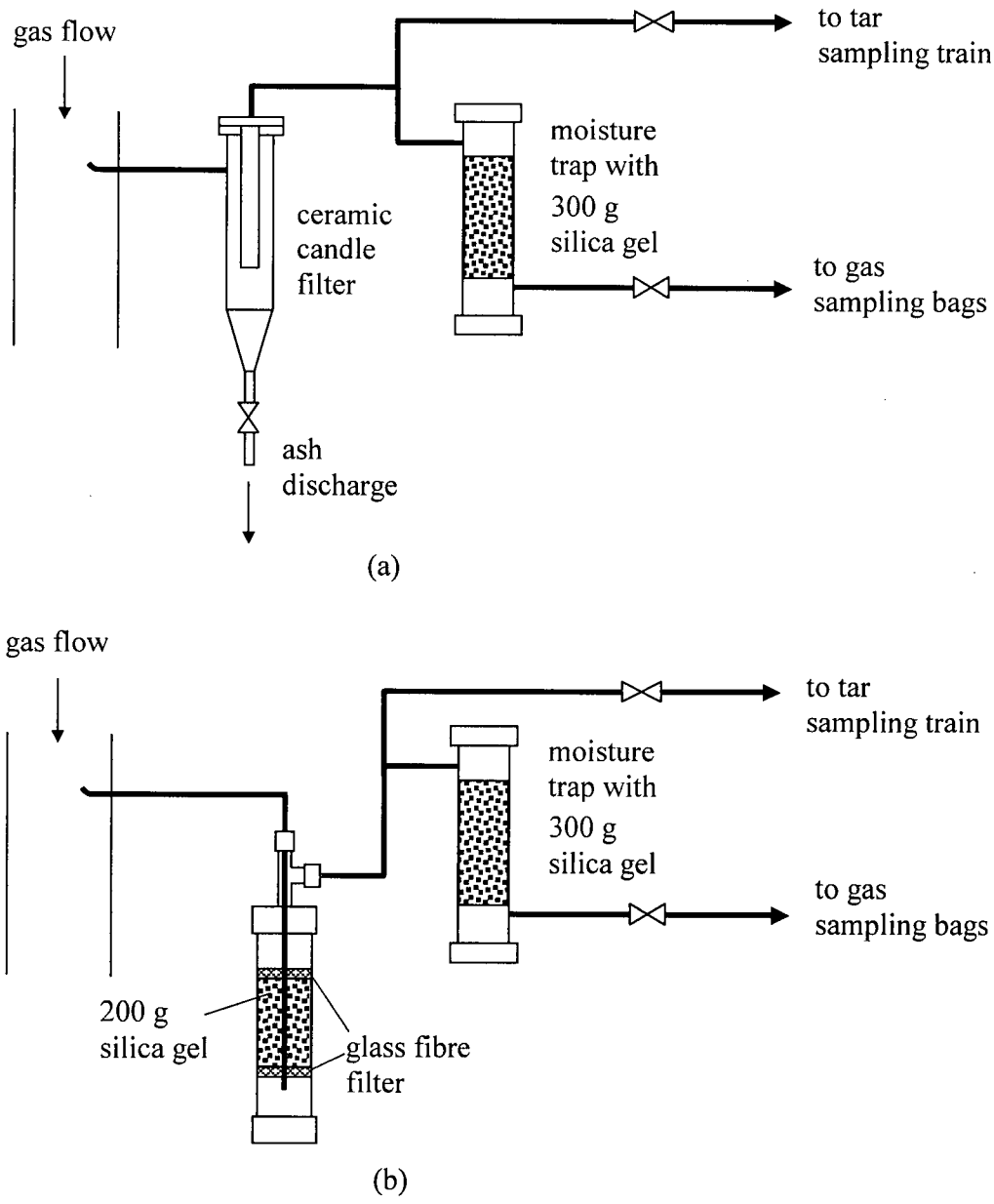

Figure 3-4. Schematic of gas sampling device: (a) with ceramic candle filter; (b) with glass fibre filter. Rotameter is located after the tar sampling train.

outside of the ceramic candle element. The glass fibre alternative provided a satisfactory solution to this problem and was used from Run 4 on. A heated bypass line was connected to the tar sampling train. Gas samples were taken with SKC 232-01 sampling bags, each of 1 litre volume, with an additional cooled condensate catchpot, working at 270 to 273 K (–3 to 0°C), for further moisture removal. A movable gas sampling device, used for measuring the axial and radial gas composition profiles, is shown in Figure 3-5. It consists of a glass fibre filter exactly the same as that shown in Figure 3-4(b), and a 6.5 mm OD, 350 mm long (1/4" tubing x 14") scaled tube to be inserted into the high-temperature reaction zone from the thermocouple sockets. However, the movable sampling device does not have the second-stage moisture trap. The gas sampling flow was monitored for tar sampling but not for GC sampling. The gas flow was maintained at 0.09-0.12 m^3/h (1.5-2.0 L/min) for tar sampling.

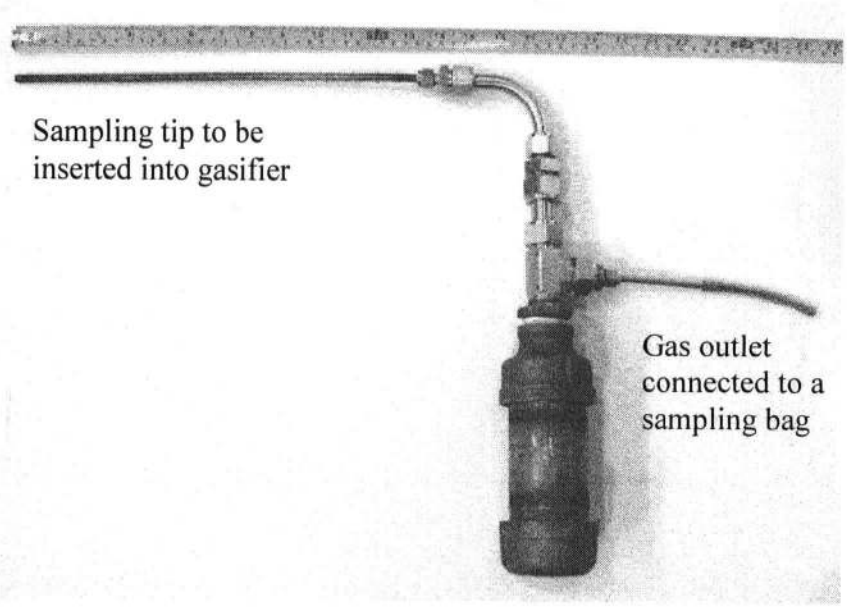

Figure 3-5. Movable gas sampling device.

Gas samples were taken every 20 minutes on average and analyzed for H_2, CO, CO_2, CH_4, N_2 and O_2 by a Shimadzu GC-8A gas chromatograph with a 3.2 mm OD and 4570 mm long (15 ft x 1/8") 60/80 mesh Supelco Carboxen-1000 molecular sieve column (Column 1 in the GC) and a

TCD (thermal conductivity detector), together with a Chromatopac data processor. Argon gas, with its pressure regulated to 5.0 bar, was used as the carrier gas for the GC. The detector heating current was set at 60 mA, the oven temperature at 373 K (100°C), and the detector temperature at 110°C. For each injection, about 1 ml of gas sample was extracted from a sample bag with a 1.0 ml syringe, and then 100 µl of the gas sample was injected into the GC column. Both instantaneous and time-averaged data are reported in Chapter 4.

Process data such as temperature and pressure were logged into a PC data acquisition system. In total 23 thermocouples and 10 pressure transducers were placed at the key points along the gas, air and water flow paths for instantaneous monitoring of the system temperature and pressure. The thermocouples used for probing high temperatures were of K type, while those for monitoring water or air temperature were E type. The locations and numbering of the thermocouples are indicated in Figure 3-6. The tips of thermocouples along the riser and standpipe are were flush with the wall for protection against erosion by the solids stream. Therefore, the temperature readings are slightly (about 20 K) lower than in the core of the reactor. Two absolute pressure transducers and eight differential transducers were employed to monitor the system pressure. The locations and numbering of these thermocouples and transducers are indicated in Figure 3-6. More details are provided in Appendix IV.

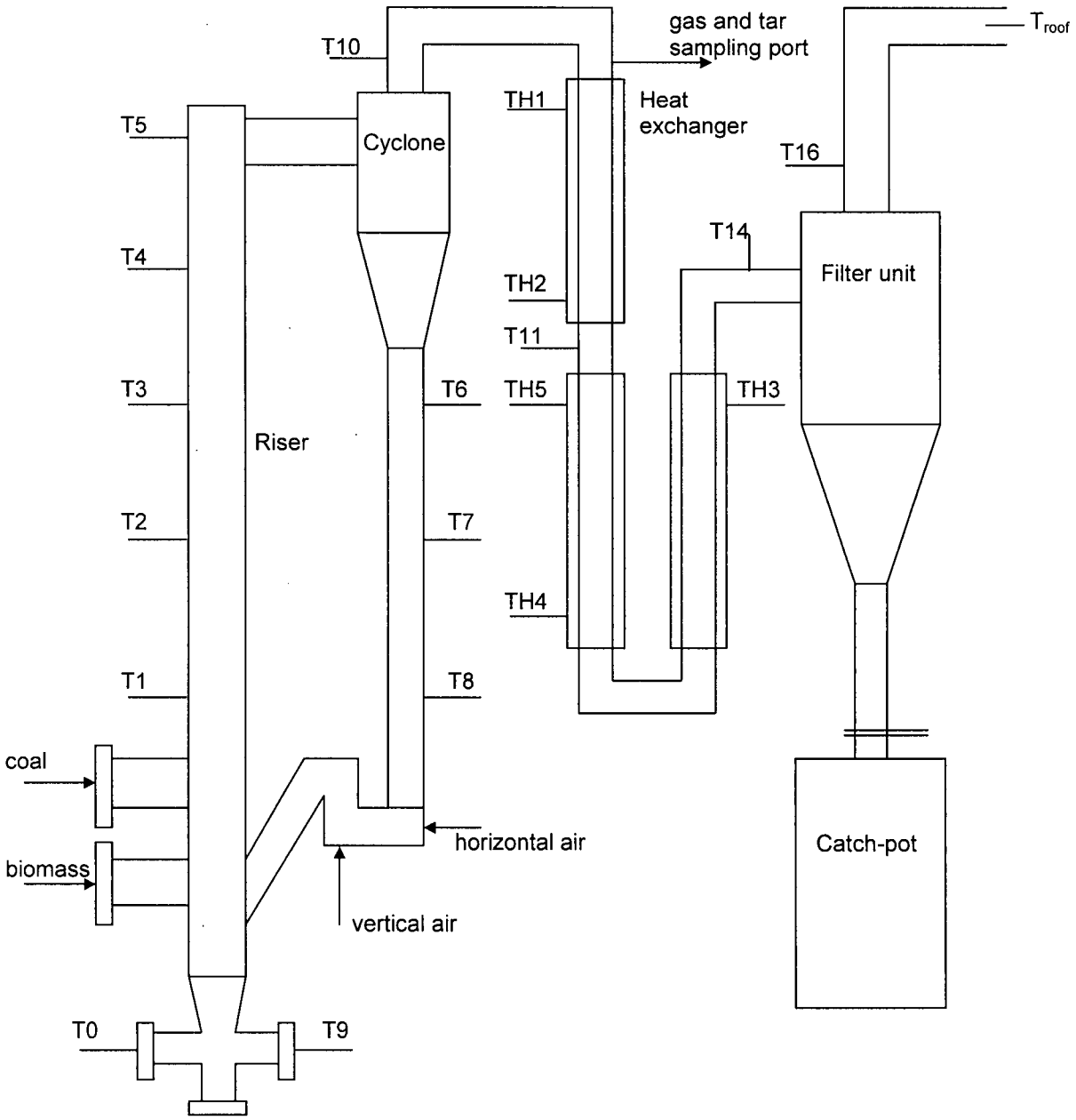

Figure 3-6. Distribution of thermocouples, pressure transducers and sampling port.

3.4 Methodology: Typical Start-up, Operating and Shutdown Curves

An operating procedure (Appendix V) was developed for sawdust. To illustrate the procedure, a test run is divided into start-up, test operation and shutdown stages. Each stage is shown by means of a group of temperature curves at different spatial locations in the primary loop of the CFB. These temperature curves are important for both operating control and interpretation of test conditions since they provide evidence regarding operation of the whole system.

3.4.1 Start-up

A typical start-up stage appears in Figure 3-7. Prior to each run, 30-35 kg of bed material was fed to the riser by pneumatic conveying. The gasifier was first run in a cold state for about 10-20 minutes in the fast fluidization mode to establish solids recycle, as well as to redistribute the pressure drop in the system so that the pressure at the bottom of the riser was less than 1.3 bar absolute (5 psig). The cooling water supply must be verified before the natural-gas-fired start-up burner can be turned on to heat up the contents of the riser. The gas temperature at the exit of the burner should be maintained between 1200-1240 K (930 and 970°C) in order to maximize the heating rate while protecting the burner and riser from overheating and possible materials failure. This was accomplished by supplying excess air to the burner to absorb heat, so that the flue gas left the burner chamber at the desired temperature. The riser was quickly heated up to 520-570 K (250-300°C) in the first hour, but it usually took twice as much time to raise the temperature (with T3 assumed to demarcate average temperature) to 670-720 K (400-450°C) before coal ignition could be initiated. Numbers assigned to the various thermocouples are given in Figure 3-6.

The coal feed rate was increased progressively to aid heat-up of the riser. At the same time, air flow rates were adjusted to provide adequate combustion air for both the natural gas and coal. When the system temperature reached 800°C, sawdust was added to displace coal as the start-up

fuel. This was done in order to eliminate, or at least reduce, the coal "memory" in the gasification period following the start-up stage.

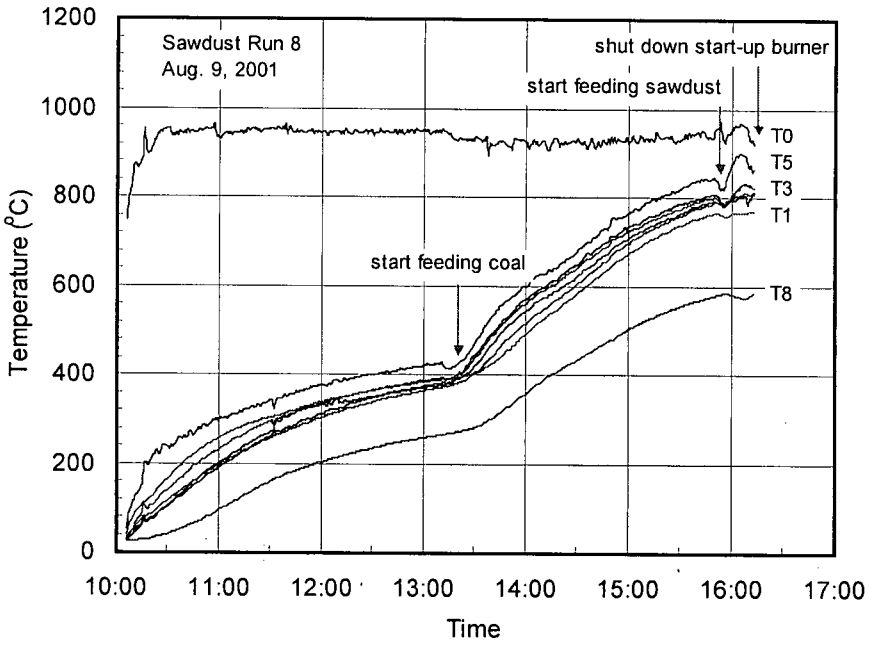

Figure 3-7. Typical temperature vs. time curves during start-up stage.

3.4.2 Operation in gasification mode

Typical air flow distribution and fuel feed rates during start-up and operation stages are listed in Table 3-2. Data in this table are for Run 8, gasifying SPF/cypress mixture.

Typical temperature traces during the operating (gasification) stages are shown in Figure 3-8, respectively. The transition from combustion to gasification starts when the air flow is reduced to about 60% of that required for stoichiometric combustion, based on a preliminary estimate of the sawdust feed rate and air flow. A final adjustment to the target air ratio is made after one gas sample is taken and analysed to verify that the system is operating properly. Accompanying this transition there is usually a rapid temperature decrease in the temperature of the whole system due to reduced heat release until a new balance is reached. Then the test period begins.

Table 3-2. Typical control panel settings during start-up and gasification stages.

Parameter	Control panel setting	Value	Percentage of total air (%)
Start-up stage			
Pressure at exit of rotameters (bar)	1.19	1.19	
Primary air 1 (P1) (Nm^3/h)	150	30.20	41.67
Primary air 2 (P2) (Nm^3/h)	38	19.13	26.40
Secondary air (S) (Nm^3/h)	15	1.27	1.75
Loop seal horizontal aeration (H) (Nm^3/h)	0.5	2.22	3.06
Loop seal vertical aeration (V) (Nm^3/h)	110	4.90	6.76
Pneumatic conveying air* (PC) (Nm^3/h)	40	11.01	16.29
Lower hopper purge air (LHP) (Nm^3/h)	10	2.96	4.07
Total air (Nm^3/h)	-	72.46	100
Coal feed rate (kg/h-wet)	2	10.65	
Sawdust feed rate (kg/h-wet)	0	0	
Natural gas flow (m^3/h)	0.1	-	
Gasification stage			
Pressure at exit of rotameters (bar)	1.19	1.19	
Primary air 1 (P1) (Nm^3/h)	120	24.16	46.30
Primary air 2 (P2) (Nm^3/h)	30	15.10	28.95
Secondary air (S) (Nm^3/h)	18	1.52	2.92
Loop seal horizontal aeration (H) (Nm^3/h)	0.4	1.77	3.40
Loop seal vertical aeration (V) (Nm^3/h)	110	4.90	9.39
Pneumatic conveying air (PC) (Nm^3/h)	0	0	0
Lower hopper purge air (LHP) (Nm^3/h)	16	4.72	9.05
Total air (Nm^3/h)	-	52.18	100
Coal feed rate (kg/h-wet)	0	0	
Sawdust feed rate (kg/h-wet)	7	33.73	
Natural gas flow (m^3/h)	0	0	

Note: * Pneumatic conveying air was used for feeding of coal or for re-injecting fly ash.

Because each hopper can only contain about 35 kg of sawdust in each batch, each must be refilled every hour or so. By examining the short temperature surges at the control point (T14, slightly prior to the filter unit) as exhibited in Figure 3-9, one can easily reconstruct the exact time of refilling in post-test data processing.

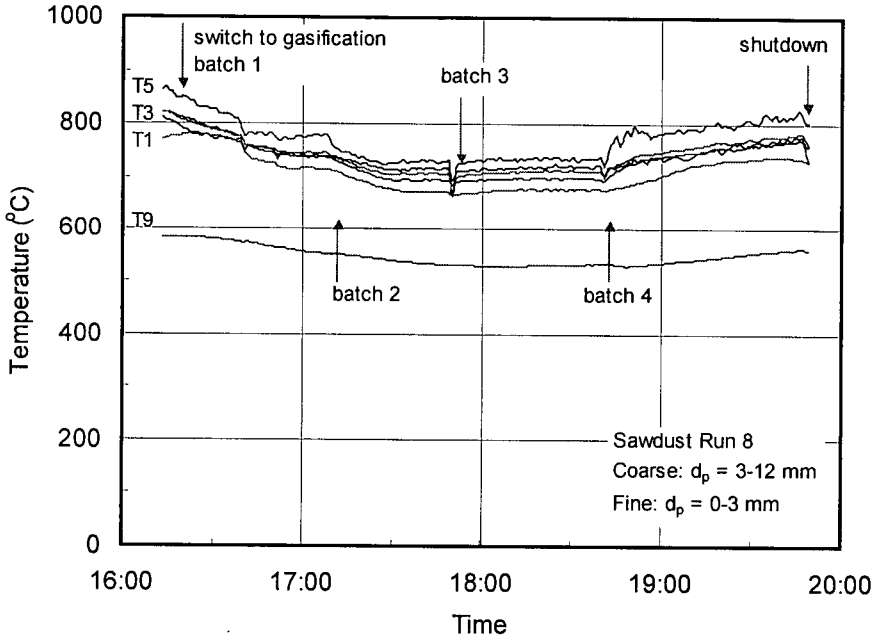

Figure 3-8. Typical temperature vs. time curves for operation stage.

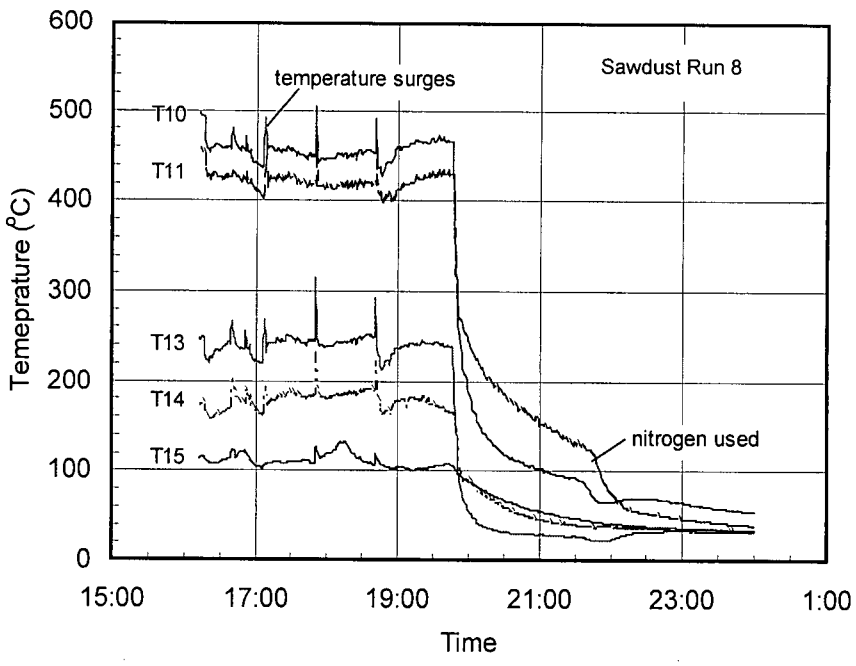

Figure 3-9. Typical temperature curves in the vicinity of filter unit.

3.4.3 Shutdown

Safe shutdown is as important as safe start-up and operation. Reburning of fly ash in the cyclone and filter unit during shutdown must be strictly avoided to protect the system. To do this, all air streams supplied to the gasifier must be cut off immediately after stopping the main fuel supply. Continuing the air supply could result in a high-temperature emergency. From Run 6 on, nitrogen was introduced during the shutdown from the bottom of bed to flush any remaining oxygen from the whole system. Smooth shutdown was achieved in this manner for all runs. Figure 3-9 shows some typical temperature vs. time traces during shutdown in the vicinity of the filter unit. The operators ensured that cooling water continued to flow overnight for at least 24 hours. All the ash samples were taken after the system was completely cooled down.

3.4.4 Purging of filter unit

The variation of pressure drop across the ceramic fabric filter is shown in Figure 3-10, again taking Run 8 as example. The curve is typical for newly-cleaned filter bags. Since the gas contained sulfur dioxide, its dewpoint was higher than 100°C. During the start-up period, the pressure drop increased from the baseline value of 0.8 kPa to about 3 kPa due to accumulation of fly ash, as well as gradual wetting of the filter bags by condensate water. Thus, the pressure drop kept on increasing until it stabilized at around 3.7 kPa. Nitrogen purge was manually activated to reduce the pressure drop to about 2.5 kPa, but it soon returned to the same level as before the purge. Controlled by four solenoid valves and solid-state relays, the nitrogen purge worked in a cyclic manner from the first cluster of 3 bags to the fourth group, purging three bags at a time. The nitrogen purge is activated when the gas temperature inside the filter rises to 250°C, or when the pressure drop across the filter unit is greater than a set value, typically 5-6 kPa. Each purge lasted 3 s, followed by a time delay of 12 s before the next group of three bags was purged. After completion of each cycle, all twelve filter bags had been purged. Since the inner ash layer on the

outside of the bags was quite wet, an immediate reduction in the pressure drop was not necessarily observed. In that case, the nitrogen purge cycle was repeated a number of times. The pressure drop returned to the baseline (0.7 kPa) when the system was shutdown.

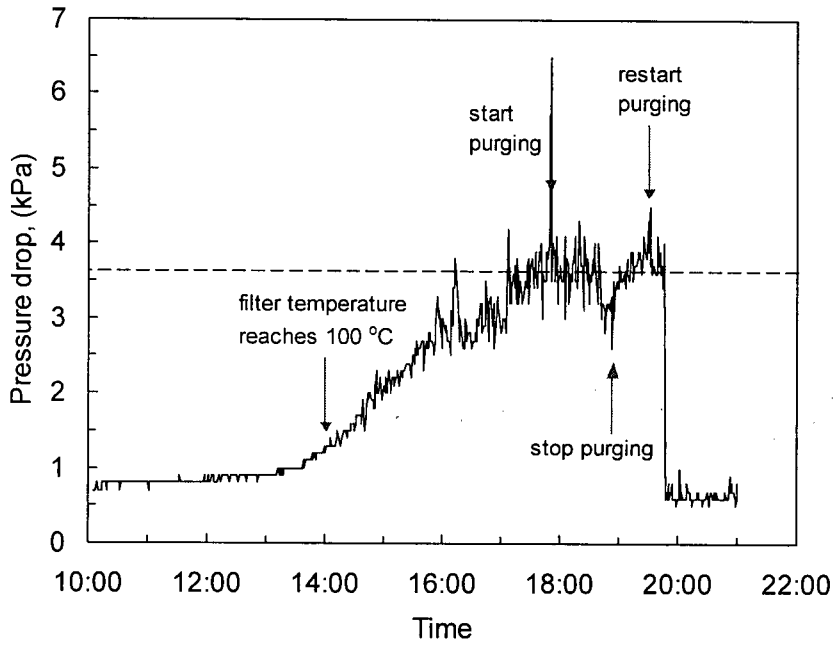

Figure 3-10. Variation of pressure drop across filter unit.

3.5 Tars: Definition and Sampling Procedure

In this study, we adopted the tar definition proposed in the provisional Tar Protocol (Maniatis and Beenackers, 2000; Abatzoglou *et al.*, 2000), i.e. tars from biomass gasification are all organic compounds with a molecular weight greater than that of benzene (78 Daltons). The upper limit for the species molecular weight is taken as 300 Daltons, above which the melting point of a species usually exceeds 520 K (250°C), and it is then no longer considered a component of tar. This definition is practical and simple, but even within this range, hundreds of chemical species have been identified as constituents of tars (Hasler and Nussbaumer, 2000).

Thus, it is practically impossible, as well as unnecessary, to know the mass fraction of each particular species in the tars. Note that the molecular weight upper limit is only a guideline, since the tar sampling protocol does not ensure that species with molecular weights above 300 are not collected during tar sampling. Similarly, the distinction between heavy and light tars by their boiling point, as proposed by Hasler and Nussbaumer (2000), is optional. However, particulates and water collected together with tars must be separated when determining the tar yield.

A flow diagram of the tar sampling system appears in Figure 3-11. It is similar to the sampling train recommended in the provisional protocol. Two solvent-temperature combinations were tested: acetone at 194 K (–79°C), as recommended by the Protocol, and acetone at 270 K (–3°C). Dichloromethane (DCM) is another solvent recommended for tar sampling. Although DCM is even better in terms of its performance as tar solvent/absorber, it was not used in the present study because of its toxicity and high ozone depletion potential (Abatzoglou *et al.*, 2000).

The method recommended in the Protocol led to some problems during the first few trials in our experimental study. First, the inlet tubes of the impingers were easily blocked by ice formed at very low temperature after one or two hours of sampling. This happened even with two moisture traps in line. Another problem was that dense tar fog formed inside the impingers due to carryover because acetone is highly volatile. This tar fog greatly reduced the absorption efficiency, while causing contamination and blockage of the tubing and rotameter downstream of the impingers. In the first three trials, the tar sampling efficiency over a two-hour sampling period was estimated to be only about 70% based on the amount of tars collected from the stack. To prevent tar fog carryover, Knoef (2002b) used a modified sampling procedure that employed five impingers. The first impinger was at 313 K (40°C), the second at 263 K (–10°C), the third at 313 K, while the final two were at 263 K. By heating the first impinger to 313 K, larger aerosol droplets formed which were easier to intercept in the next impinger. This procedure also

eliminates ice formation in the tubes. A new tar protocol will soon be released on the tar website (Knoef, 2002b).

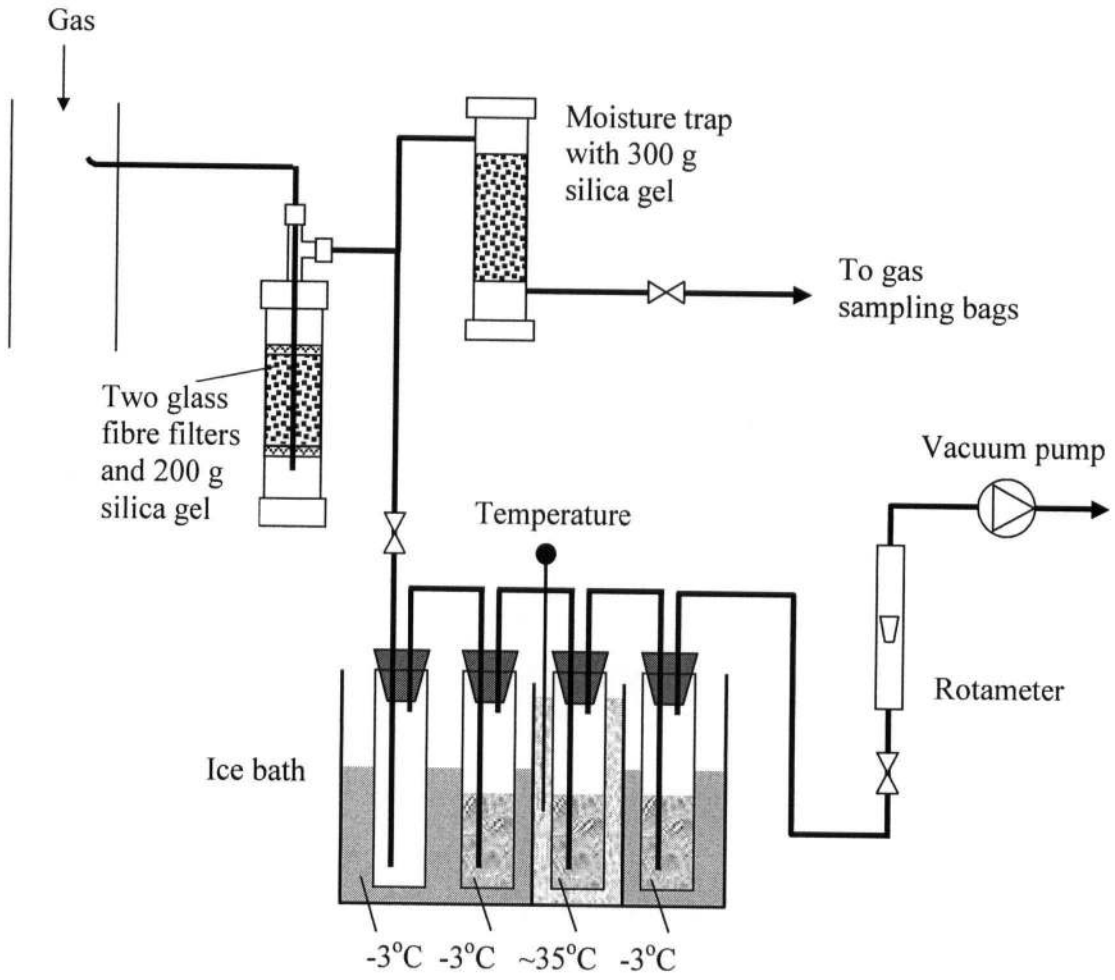

Figure 3-11. Tar sampling train: First, empty bottle acts as a condenser. The three filled ones are tar impingers, with acetone as solvent. Temperature varies from 270 K to about 308 K.

In view of the above, our revised sampling train used four 250 ml impingers as shown in Figure 3-11, using acetone as the solvent, working alternatively at 270 K and room temperature (about 305-310 K in the sampling area) in order to reduce tar fog by forming larger droplets at room temperature that are easier to capture in the next impinger. The vacuum pump was optional since a stable positive pressure could be maintained at the sampling port. The advantage of

positive-pressure sampling is that it can prevent errors caused by air infiltration that is difficult to eliminate in vacuum sampling systems. The disadvantage is that the working pressure inside the filter unit fluctuates due to ash deposition on the filter bags. To maintain the sampling flow as stable as possible, the system pressure was maintained at 7.5-15.0 kPa above atmospheric (1-2 psig), about three times higher than the pressure inside the filter unit. The sampling flow rate was maintained at 0.09-0.12 Nm^3/h (1.5-2.0 litres/min), corrected to 273 K and 1.013 bar, corresponding to an actual gas velocity of 1.7-2.6 m/s in the gas pipe at the inlet of the first heat exchanger. Larger sampling flows are not recommended since they increase sampling losses due to solvent carryover or tar fog. Since the temperature at the sampling port was in excess of 570 K, tars were in the vapour state. Therefore, isokinetic sampling was not a requirement for sampling gas and tar, though it was absolutely necessary for particulates. One or two more impingers could be added to further increase tar absorption efficiency, though this may increase the overall pressure drop.

The detailed sampling and post-sampling and calculating procedure is provided in Appendix VI. Each sampling usually lasted 2-3 hours; tars were determined gravimetrically after separating particles and water. In the post-sampling procedure, water was separated by simple extraction with the organic solvent, e.g. acetone or DCM, while particulates in the tar-solvent-water-particles mixture were removed by filtration using analytical grade filter paper and flushing with the solvent. However, water extraction was not always successful if the amount of water was small in the samples collected. Tars were also collected by scraping from the inside of the stack after each run for comparison with the sampling results. A later tar audit showed that the difference between the impinger-sampled tar yields and estimates based on the stack-collected tars was less than 10%.

However, a few uncertainties remained, one being the error due to residual moisture and water-soluble organic species in tars, which were lost when water was separated from the insolubles. In an alternative post-sampling procedure, water was not extracted before solvent evaporation at 323 K (50°C). Therefore, these water-soluble organic species were not lost, but the dissolved alkalis, e.g. Na_2O and K_2O, were not removed either. In biomass gasification, the total amount of the vapor-phase alkalis (Na + K) measured after the cyclone, before the gas cooler, has been in the 1-10 ppm range (Salo and Mojitahedi, 1998). Based on this value, the error caused by dissolved alkali (converted to K_2O equivalent) in tar sampling is estimated to be 0.004-0.04 g/Nm^3, two orders of magnitude less than the experimental tar yield from biomass gasification. This indicates that water extraction is not necessary prior to solvent evaporation.

CHAPTER 4. PILOT STUDY: EXPERIMENTAL RESULTS

This chapter presents results from the pilot study of biomass gasification. The effects of various parameters on product gas composition and heating value are examined. Fifteen test runs were conducted on the CFB gasifier. Each run was performed to satisfy particular objectives, contributing to a detailed parametric study of the effects of operating temperature, air ratio, suspension density, steam injection, fly ash re-injection, secondary air rate and catalyst addition. The operating pressure in the system was maintained at 1.05-1.20 bar at the bottom of the riser, slightly above atmospheric, except for the first run, where the pressure was 1.65 bar. A complete set of gas composition data measured by gas chromatography during the pilot plant tests is provided in Appendix VII. Operating conditions, gas yields, efficiencies and carbon conversion data are listed in Table 5-1. The influences of the biomass species and moisture content were examined by comparing results from different fuels with different moisture contents. Tar yield was measured by in-line tar sampling using the sampling train described in Chapter 3, together with post-test direct tar collection from the stack.

4.1 Parameters That Define the Biomass Gasification Process

Biomass gasification can be characterized by a number of operating parameters and variables representing the feedstock, process, and products. The air ratio, a, is defined as the ratio of the actual air supply to the stoichiometric air requirement for complete combustion. The moles of oxygen required for stoichiometric combustion of 1 kg sawdust (dry basis) is determined from fuel ultimate analysis, assuming that CO_2, H_2O and SO_2 are the sole combustion products:

$$n_0 = 10 \times \left(\frac{C}{12.011} + \frac{H}{4 \times 1.008} + \frac{S}{32.066} - \frac{O}{2 \times 15.999} \right), \quad \text{(mol)} \qquad (4\text{-}1)$$

where C, H, S and O represent the carbon, hydrogen, sulfur and oxygen contents of the fuel (wt.%, dry basis), respectively. The fuel-bound oxygen is considered in determining the external oxygen requirement. Assuming ideal-gas behaviour for air and using the North American standard air composition (Lide, 1994), the stoichiometric air requirement can be calculated by

$$V_0 = \frac{n_0 R T_{\text{ref}}}{0.209476 \times P_{\text{ref}}}. \qquad (4\text{-}2)$$

Here V_0, in Nm^3/kg-fuel, corresponds to the reference state of $T_{\text{ref}} = 298$ K and $P_{\text{ref}} = 1.013$ bar. R is the ideal-gas constant, i.e. $R = 8.31448$ J/mol-K.

Likewise, the equivalence ratio (ER) is defined as the ratio of moles of oxygen actually supplied to the gasifier to that required for stoichiometric combustion. We also use the O/C molar ratio where steam addition or ash re-injection is involved. Since sawdust has a high oxygen content, the minimum O/C molar ratio is about 0.6, corresponding to air-free pyrolysis conditions. The air ratio or O/C molar ratio can be easily extended to an equivalence ratio for oxygen-blown processes.

Two other ratios have been proposed by Gil et al (1999) to specify the chemical composition of the feed streams. These are the steam-to-biomass ratio (S/B), defined as the mass flow rate of steam to the mass feed rate of biomass, for steam gasification, and the gasifying-agent-to-biomass ratio (GR), for processes employing a steam-oxygen mixture as the gasifying agent. Usually, the dry-ash-free (daf) basis is used when calculating the S/B ratio and the GR of biomass feedstock. However, for the equilibrium model in Chapter 6, the most important parameters that define the feed streams are the molar composition of all the elements involved. This elemental composition can be fully represented by an elemental abundance vector. In typical biomass gasification processes, e.g. for coal gasification, three elements, i.e. carbon,

hydrogen and oxygen, dominate the elemental composition of the feedstock. The molar ratios of the three elements can therefore be conveniently illustrated in a ternary diagram.

A number of parameters are used to characterize the product streams in addition to the commonly used gas composition, in which the volume (i.e. molar) percentages of all species are listed. The gas heating value is usually given as the higher heating value (HHV) of the dry product gas, in MJ/Nm^3, corresponding to a standard state. Three molar ratios are defined to highlight the progress of major gasification reactions. The CO/CO_2 molar ratio provides a measure of the relative importance of the $C\text{-}O_2$ gasification and combustion reactions, one producing CO and the other CO_2. The ratio also allows one to identify the approach to equilibrium for the $C\text{-}CO_2$ reaction. The H_2/CO ratio gives some sense of how the $C\text{-}H_2O$ and shift reactions are proceeding, while the CH_4/H_2 ratio indicates the relative contribution of pyrolysis and gasification in determining the final gas composition, as well as the extent of hydrocarbons cracking.

The tar yield is usually given as the mass of tar present in unit volume of raw gas, in g/Nm^3, but an alternative is available, which defines tar yield as the mass of tar produced per unit weight of biomass feed, such as in Gil et al (1999). In this thesis, the former is used to specify the tar yield, as practised by most other researchers.

The main process parameters include the operating temperature, pressure, suspension density, primary-to-secondary air ratio or the fraction or percentage of secondary air, and the superficial gas velocity, which is closely related to the air ratio for a given gasifier. A number of other parameters for special purposes are also used where necessary.

Presently, the widely accepted standard state is the thermodynamic standard state, (298 K, 1 bar). For example, this is employed in the latest version of JANAF thermodynamic data. However, a few alternatives are still in use, such as the (273 K, 1.013 bar) standard state adopted

in some earlier data collections, and the (288 K, 1.013 bar) standard state proposed by the American Gas Society for calculating natural and syngas heating value. Care must be taken when comparing data from sources adopting different standard states since this may cause a difference in the gas heating value of up to 7%. In the present work, we normally use (273 K, 1.013 bar) as the standard state for our experimental study because almost all heating values, stoichiometric air requirement available are based on this standard state. However, in the equilibrium model (Chapter 6), we adopt (298 K, 1 bar) as the standard state because all the JANAF thermodynamic data are given at this standard state. The difference is in practice only significant for enthalpies, heating values and free energies. Other properties such as heat capacities are nearly identical at the two temperatures given the experimental precision. The slight difference, where applicable, is handled directly in the program code individually depending on the nature of the variables concerned.

Since all the process parameters and gas composition data recorded by the data acquisition system or obtained from GC analysis represent instantaneous values, averaging over the gasification period was therefore required to obtain time-mean values. The mean value, $\bar{x}$, of a series of instantaneous variables x_i is calculated from the following generic equation:

$$\bar{x} = \frac{\sum_i x_i \Delta t_i}{\sum_i \Delta t_i}, \qquad (i = 1, 2. \ldots) \tag{4-3}$$

where Δt_i is the time interval over which x_i was measured.

4.2 Temperature Profiles

A brief look at the temperature profile helps reveal some aspects of the hydrodynamic, mixing and heat transfer properties in the riser, though the objectives of the present work did not include a study of the hydrodynamics of a CFB riser. Figures 4-1 and 4-2 show measured axial and radial temperature distributions in the riser, respectively. To facilitate discussion, the temperature T_3, measured at the T3 level (3946 mm above the primary air inlet) is used as the representative temperature of the riser.

The first measurement (Run 11) of the radial profile indicated that there could be as much as a 45 K difference between the core and wall region of the riser. While the far side (right-hand side in the Figures) showed quite a flat temperature profile, the near side from which the thermocouple was inserted exhibited a deviation from symmetry due to wall contact heat transfer as well as local hydrodynamic disturbances. A later measurement made in Run 12 from the opposite side, with the thermocouple tip withdrawn 2 mm from the wall showed improved symmetry and less than a 15 K centre-to-wall gradient. The radial temperature uniformity indicates that there was extensive radial mixing and radial heat transfer in the riser, facilitating both homogeneous and heterogeneous reactions.

The temperature was measured along the whole height of the riser. The increase of suspension temperature over the riser height was explained by presence of endothermic processes such as evaporation of fuel moisture and pyrolysis in the lower part, and slight oxidation of product gas above the secondary air level. While the temperature difference across most of the riser height was less than 100 K, consistent with normal CFB reactors, a temperature increment as large was detected between the air inlet and the solids recycle port due to the absence of an air distributor in the gasifier concerned. Measured temperature at the bottom of the riser is 870-970 K for all test runs. The coarser particles settled in the bottom and cooled there. However, intense solids recycle generally helped maintain a small temperature gradient.

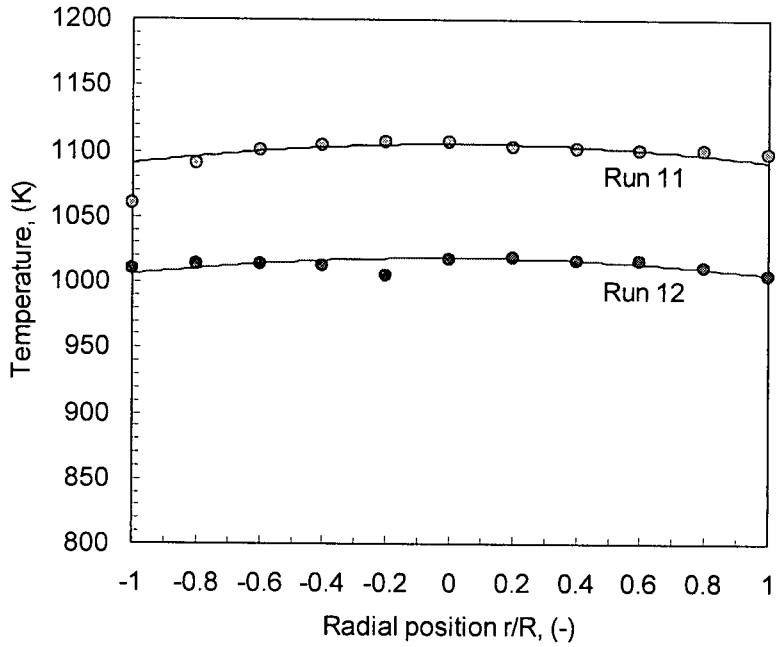

Figure 4-1. Measured radial temperature profile in the CFB gasifier: ○ - Run 11, hemlock sawdust, air ratio a = 0.325, T_3 = 1062 K, P = 1.1 bar; ●- Run 12, 50% pine + 50% spruce mixed sawdust, a = 0.23, T_3 = 974 K, P = 1.1 bar.

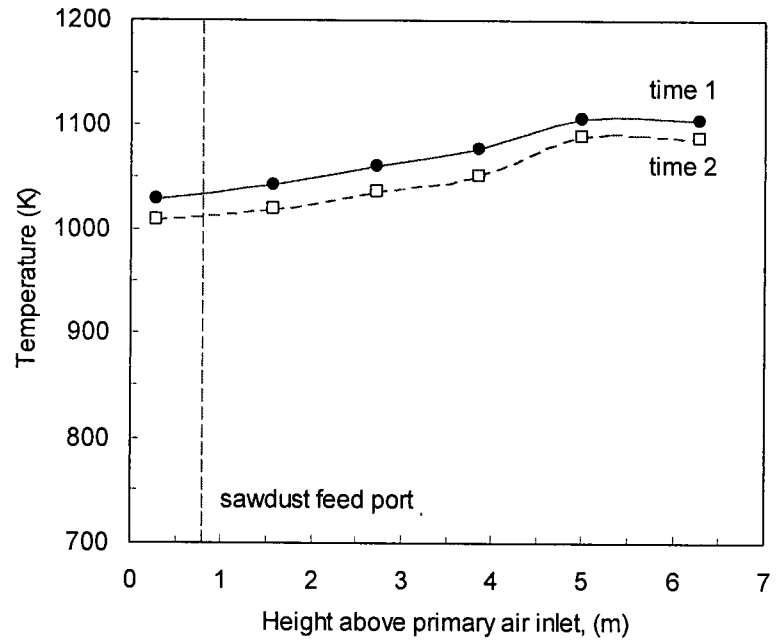

Figure 4-2. Measured axial temperature profile in the CFB gasifier. Data from Run 11, gasifying hemlock sawdust. Air ratio a = 0.325, T_3 = 1062 K, P = 1.1 bar. Measured twice at the wall zone, at 18:00 (time 1) and 19:00 (time 2), respectively.

4.3 Gas Composition Profiles

The core-annulus model of CFB, together with the temperature profiles, suggests that there must be non-uniform radial and axial profiles in gas composition in the riser. It is well accepted that the annulus region in a circulating fluidized bed operating in the fast fluidization flow regime is much denser than the core region. Particles tend to migrate toward the wall, driven by fluid-particle interactions and boundary effect, and descend along the wall, while bulk upflow is maintained in the core region (Brereton, 1987; Brereton *et al.*, 1988; Berruti and Kalogerakis, 1989). As a result, a considerable portion of the pyrolysis reactions take place in the thin wall region, forming a reducing region there, as indicated by the rising CH_4, H_2 and CO concentrations towards the wall, shown in Figure 4-3.

The axial gas composition profile is plotted in Figure 4-4. The lower part of the riser was mainly used for pyrolysis of returning particles and evaporation of moisture from fresh particles. Char gasification took place in the upper part of the riser, consuming a considerable fraction of the CO_2 produced in the pyrolysis and oxidation reactions. The N_2 content decreased monotonically along the riser height, indicating increasing conversion of carbonaceous species. A major rise in the CO_2 content is observed over the 0.9-2.0 m height interval (T1 to T2 level), where the CO-shift reaction and oxidation of pyrolysis products also resulted in a simultaneous decrease in the concentrations of CO and other combustible species. CO_2-gasification of char continued along the remainder of the riser, raising the CO level again, while the C-H_2O reaction increased the H_2 content. The concentration of CH_4, another major pyrolysis product, should be viewed separately. It is believed that this species almost never approaches its equilibrium level in small units due to the limited gas residence time in the riser (Coates *et al.*, 1974). Although a crossover of CO and CO_2 contents occurred in Run 3, this crossover was not repeated for the higher air ratio employed in Run 15.

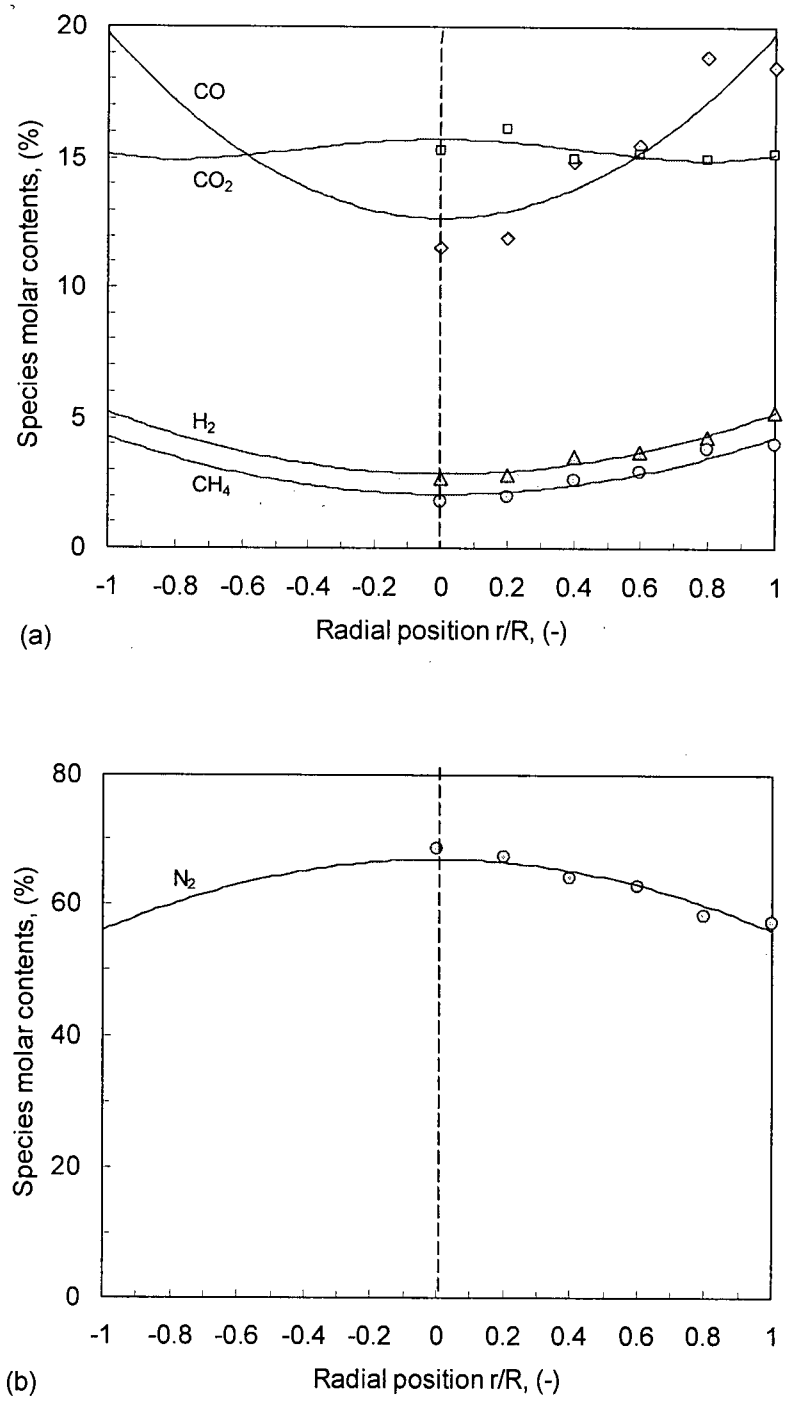

Figure 4-3. Radial gas composition profile: (a) H_2, CO, CO_2 and CH_4; (b) N_2. Data from Run 7, gasifying hemlock sawdust, T_3 = 1088 K, a = 0.45. Gas samples taken at T4 level (5089 mm above the primary air inlet).

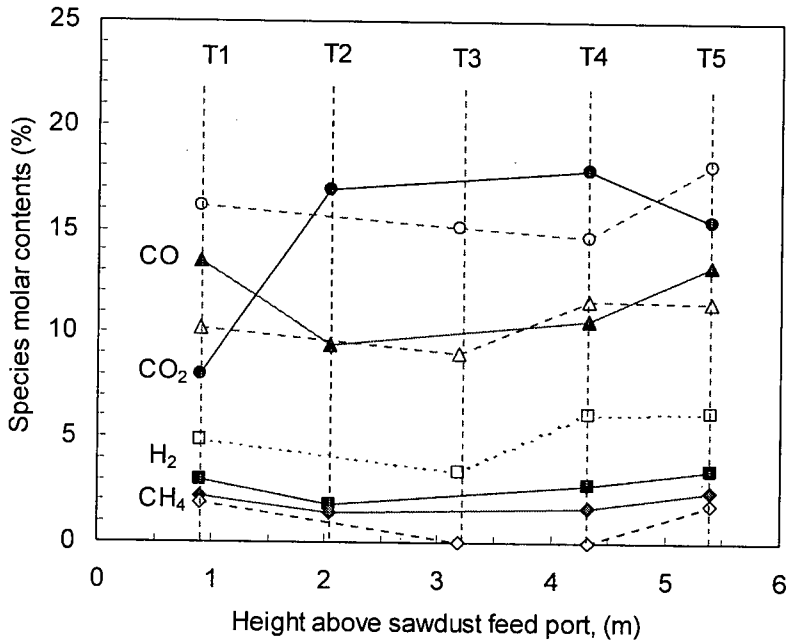

Figure 4-4. Axial gas composition profiles. (a) Solid lines and closed points: Run 3, gasifying spruce, pine and fir mixed sawdust, a = 0.38, T_3 = 1020 K, M = 10.5%; (b) Dashed lines and open points: Run 15, gasifying mixed sawdust, a = 0.46, T_3 = 1080 K, M = 4.2%. Gas samples taken from the wall zone.

4.4 Effects of Air Ratio, O/C Molar Ratio and Feed Rate

The air ratio represents the degree of oxidation in broad terms. It is therefore natural to find from the gas chromatography data that the concentration of CO_2 increases with air ratio, while reducing species such as CO, H_2 and CH_4 decrease. For the same reason, the moisture content of the wet gas also increases with increasing air ratio. Figure 4-5 portrays clear trends of the changes in the concentrations of different species vs. air ratio. The short straight lines suggest more the general trend than true linear relationships. These lines, as shown below, only apply over narrow ranges of air ratio, providing only a local approximation to the more complex relationships which apply over the entire range tested. Notwithstanding the improved carbon conversion at higher air ratios as more biomass is converted to gaseous species, the total fractions

of both the oxidizing and reducing species decrease with increasing air ratio, while the inert nitrogen content grows with increasing air ratio, since the increase in nitrogen far exceeds the gains in wood-borne species.

Dry gas heating value can be estimated from the gas composition by

$$HHV = (12.75[H_2] + 12.63[CO] + 39.82[CH_4] + 63.43[C_2H_4] + \cdots)/100, \qquad (4\text{-}4)$$

where the species contents are given in mol %, and their heats of combustion, in MJ/Nm^3. This equation is derived from the heats of combustion data (Lide, 1994), assuming ideal-gas behaviour for the gaseous species. The higher heating value HHV is in MJ/Nm^3, corresponding to the standard state of 1.013 bar and 273 K.

Figure 4-6 shows how the dry gas heating value varies with air ratio over the entire range tested. The mean values are determined using Eq. (4-3). An exponential relationship is observed between the gas heating value and the air ratio:

$$HHV = 9.78\exp(-2.86a). \qquad (0.22 \le a < 0.54) \qquad (4\text{-}5)$$

The correlation factor for this relationship is $R^2 = 0.91$. The standard error (SE) of the gas heating value is given as error bars in the figure, suggesting 7-8% of the mean value. Extrapolation of the fitted correlation for the mean gas heating value to $a = 1$ suggests a residual heating value even for stoichiometric combustion. The correlation implies a maximum heating value under pyrolysis condition ($a = 0$), with the exponential part showing the sensitivity of the gas heating value to the air ratio. Different ranges of feedrate are denoted by different legends in Figure 4-6 for comparison. It appears that feed rate has no significant influence on the trend of gas heating value over the feedrate range tested. However, there are signs that the gasifier approached its throughput limit as the sawdust feedrate increased. For example, the methane content in the final gas composition was high (> 5%) when the feedrate exceeded 40 kg/h, suggesting inadequate gas residence time for effective cracking of hydrocarbons.

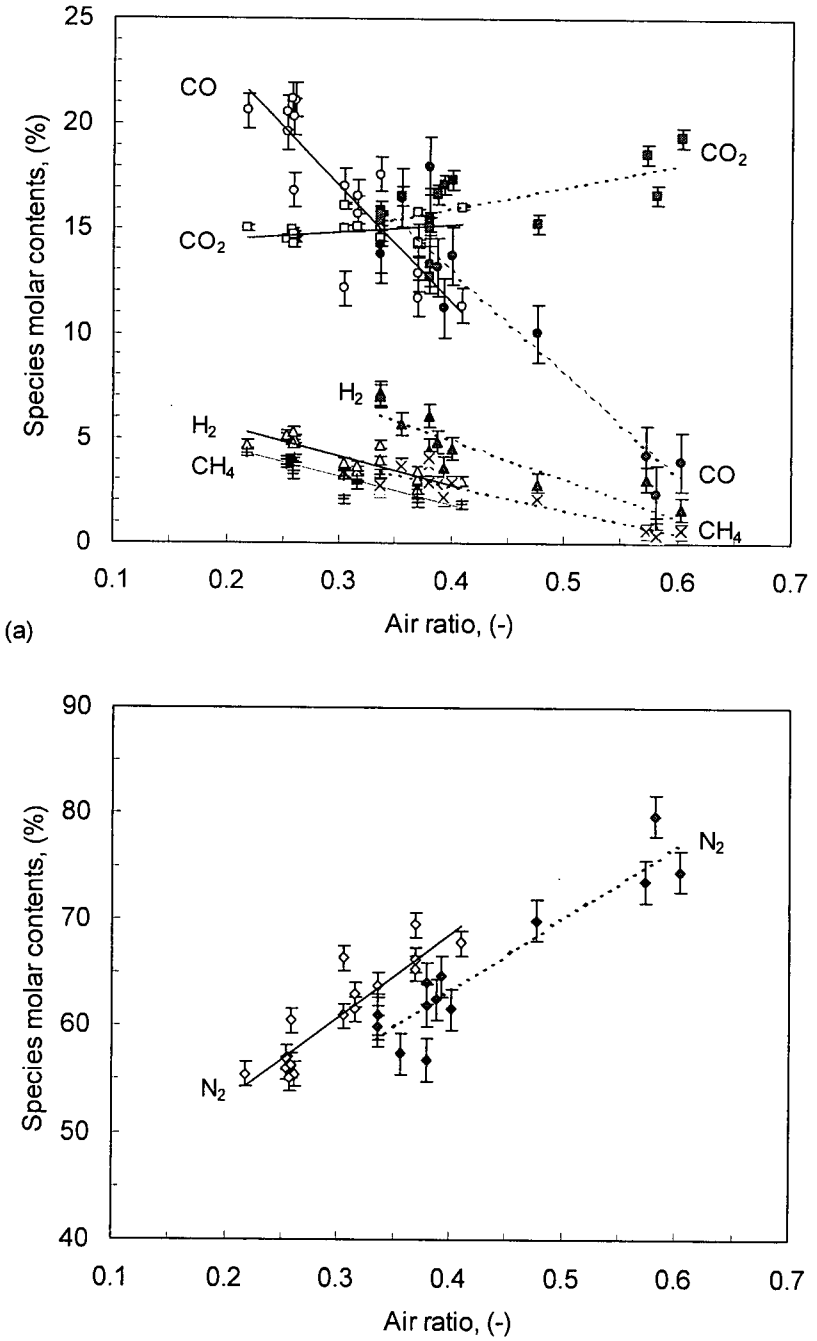

Figure 4-5. Effect of air ratio on instantaneous values of gas composition: Fuel moisture M = 6.6-22.0%. Solid lines for riser temperatures T_3 = 970 ± 10 K, dashed lines for T_3 = 1090 ± 10 K. Symbols: + / × = CH_4, Δ / ▲ = H_2, ○ / ● - CO, □ / ■ – CO_2, ◊ / ♦ - N_2. Data taken from various times.

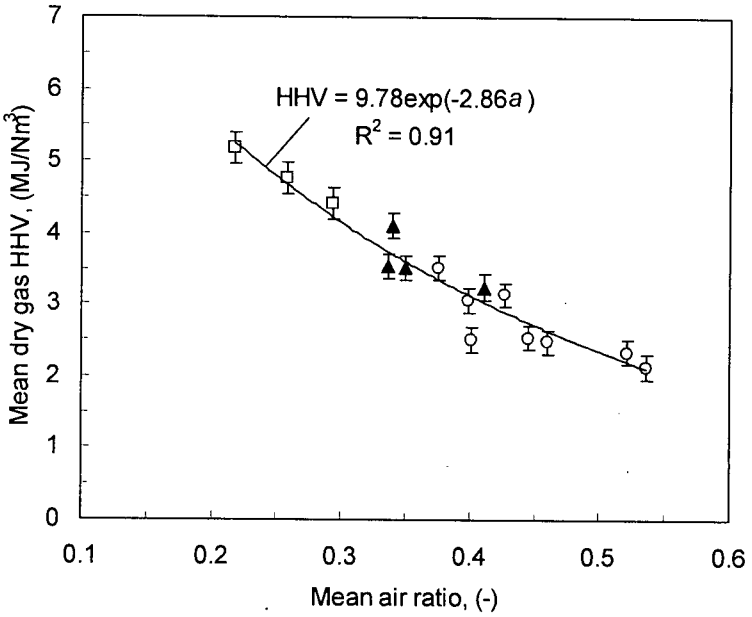

Figure 4-6. Effect of air ratio and feed rate on mean dry gas heating value: T = 970-1120 K, M = 6.6-15.0 %. Data from test runs using six sawdust species; feed rates: ○ – 16-27 kg/h; ▲ – 31-35 kg/h; □ – 40-49 kg/h.

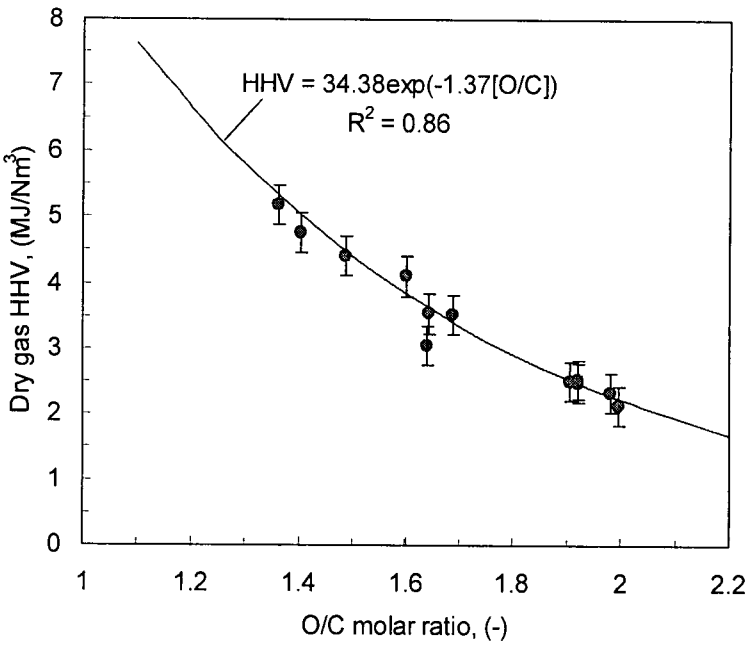

Figure 4-7. Effect of O/C molar ratio on dry gas heating value. Data from twelve runs without steam injection or fly ash re-injection, using six sawdust species; M = 4.2-15.0%.

Another way to correlate gas quality with the degree of oxidation is by using the O/C molar ratio, as shown in Figure 4-7. The use of the O/C molar ratio is of compelling importance with steam- or CO_2-blown processes. In view of this, an alternative correlation for the dry gas heating value in terms of the O/C ratio was obtained from the data:

$$HHV = 34.38\exp(-1.37[O/C]), \qquad (1.1 \le O/C < 2.1) \qquad (4\text{-}6)$$

where the higher heating value (HHV at 273 K) is in MJ/Nm^3. The correlation factor of this equation is $R^2 = 0.86$. This equation could be equally represented by correlating gas heating value versus the O/[C+H] or O/[C+H/4] molar ratio where the molar abundance of hydrogen in the system is comparable with that of carbon.

Three molar ratios are commonly used to characterize gas composition: CO/CO_2, H_2/CO and CH_4/H_2. As more oxygen is supplied, more carbon is oxidized to CO_2 instead of forming CO, causing a decrease in CO/CO_2 ratio, as shown in Figure 4-8. The O/C molar ratio varies between 1.1 and 2.1 for most cases tested.

Figure 4-9 shows the influence of the O/C ratio on the H_2/CO and CH_4/H_2 molar ratios. Since H_2 content in the raw gas is mainly determined by the CO-shift reaction, it is less sensitive to the change in O/C ratio than CH_4. The H_2/CO molar ratio increases slightly with O/C while the CH_4/H_2 molar ratio decreases more sharply. Air- or oxygen-blown gasification of biomass usually gives a H_2/CO molar ratio less than 1, as observed from this work and a recent study (van der Drift *et al.*, 2001) carried out in a bubbling fluidized bed gasifier. Injection of steam as gasifying agent increases the H_2/CO molar ratio because moisture promotes both the steam gasification and CO-shift reactions. The endothermic C-H_2O reaction produces more H_2 as operating temperatures increases. CO_2, N_2 and CH_4 contents are similar for the two studies, but almost all tests in our work led to higher CO content, but lower H_2 values in the product gas. Thus, van der Drift *et al.* (2001) reported a higher H_2/CO ratio than ours. This is probably due to

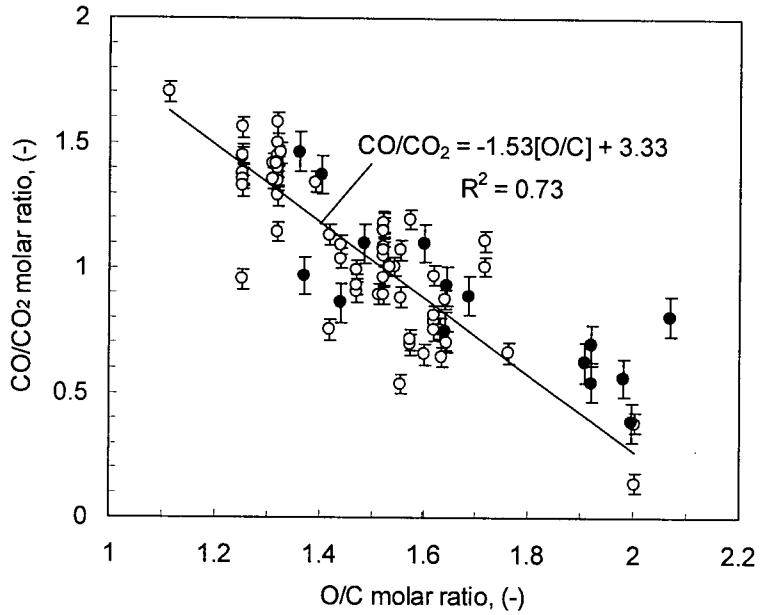

Figure 4-8. Effect of O/C ratio on the CO/CO_2 molar ratio in the off-gas. T_3 = 970-1120 K, M = 6.6-15.0 %. Open points denote instantaneous values obtained from runs with no steam injection or fly ash re-injection; solid points are time-averaged values for all runs.

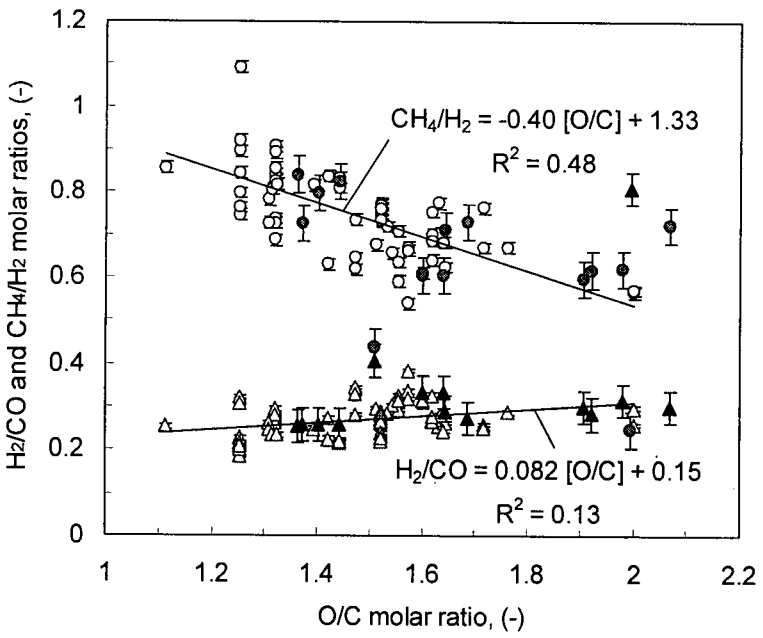

Figure 4-9. Effect of O/C ratio on instantaneous H_2/CO and CH_4/H_2 molar ratios in the off-gas. T_3 = 970-1120 K, M = 6.6-15.0 %. Open points represent instantaneous values obtained from runs with no steam injection or fly ash re-injection; solid points are time-averaged values.

different operating temperatures altering the equilibrium constants. Good surface insulation and air preheating helps elevate the operating temperature. Even an increase of 50 K in the riser temperature may have a significant effect on the final gas composition.

A high CH_4/H_2 ratio implies a dominant role of pyrolysis in determining the final gas composition for pressurized and atmospheric gasification processes alike. Our recent modeling work (Li *et al.*, 2001) (see also Chapter 6) shows that the equilibrium methane concentration in the fuel gas is less than 0.1% for the temperature and pressure ranges tested. This suggests that the high CH_4/H_2 ratio of the product gas (0.6-0.8) is not due to methanation. Instead, it results from incomplete thermal cracking of pyrolysis products and incomplete reforming reactions. Hemicellulose is the most reactive wood substance, being decomposed slightly more rapidly than cellulose (Probstein and Hicks, 1982). Cellulose, however, produces most gaseous products and the least char, while lignin, which decomposes slowly, produces the most char and is also responsible for the aromatic content of the liquid product (Probstein and Hicks, 1982). During flash pyrolysis of cellulose and hemicellulose, methane is produced either as a direct product or from cracking of higher paraffins (e.g. *n*-butane) with high selectivity, while ethylene is produced from cracking of higher olefins. Consideration of these product ratios gives some insight into the contribution of char gasification relative to that of the pyrolysis stage.

4.5 Effect of Operating Temperature

Operating temperature plays an important role in biomass gasification. While the gas heating value decreases with increasing air ratio, it increases slightly with temperature for a given air ratio because of improved carbon conversion at a higher temperature. As shown in Figure 4-10, gas HHV increases by 10% for an increase in temperature from 970 to 1070 K, again taking T_3 as the temperature representing the whole riser. At lower air ratios, the gain in gas heating value with increasing temperature is larger than predicted by an equilibrium model, which suggests an increase of only about 10% over the temperature range 600-1600 K. This reveals that the actual process is only partially governed by chemical equilibrium, so that there is a margin for a larger increase in the gas heating value with improved kinetics.

Slight increases in the H_2, CO and CH_4 contents were found to account for most of the increase in dry gas heating value, as shown in Figure 4-11. In doing mass balances, all the hydrocarbons were represented as a CH_4-equivalent because methane was the dominant species in the hydrocarbons detected by GC analysis. The concentration of ethylene in the gas was typically less than 30% of the methane concentration, and the concentrations of higher hydrocarbon species were all very small and undetected. The ethylene peak in the GC histogram happened to overlap with the H_2O peak. It was thus difficult to identify whether a small peak was due to ethylene or water vapour. The CO_2 concentration also increased slightly, while the balance, N_2, showed a corresponding decrease, again indicating that carbon conversion, methane reforming and tar cracking improved with increasing temperature, resulting in more moles of gas. The increase of gas heating value with increasing temperature indicates that the gasification reactor can benefit from better thermal insulation and air preheating to utilize the enthalpy of the product gas. Therefore, it is always recommended to preheat as much air as possible during the test runs.

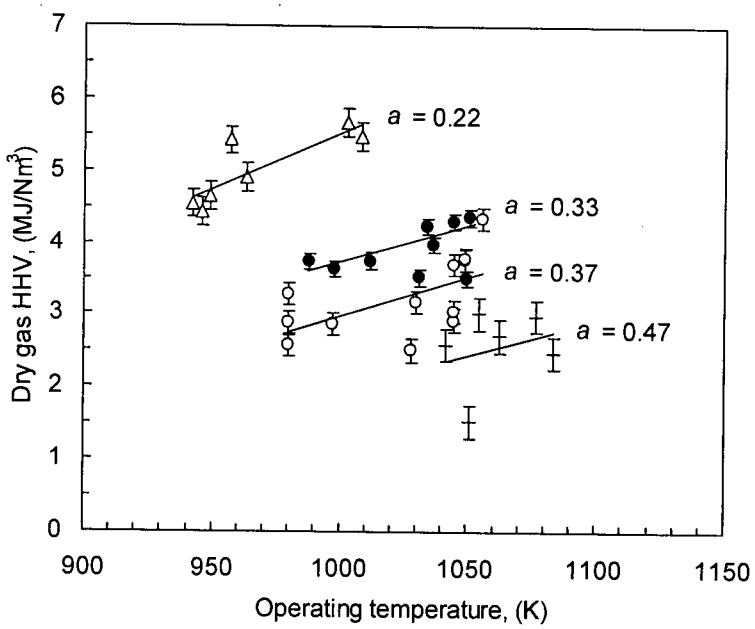

Figure 4-10. Effect of operating temperature on dry gas heating value. T_3 = 940-1080 K; M = 6.6-15.0 %. Air ratios for each group of data points are given, within ±0.005 uncertainty.

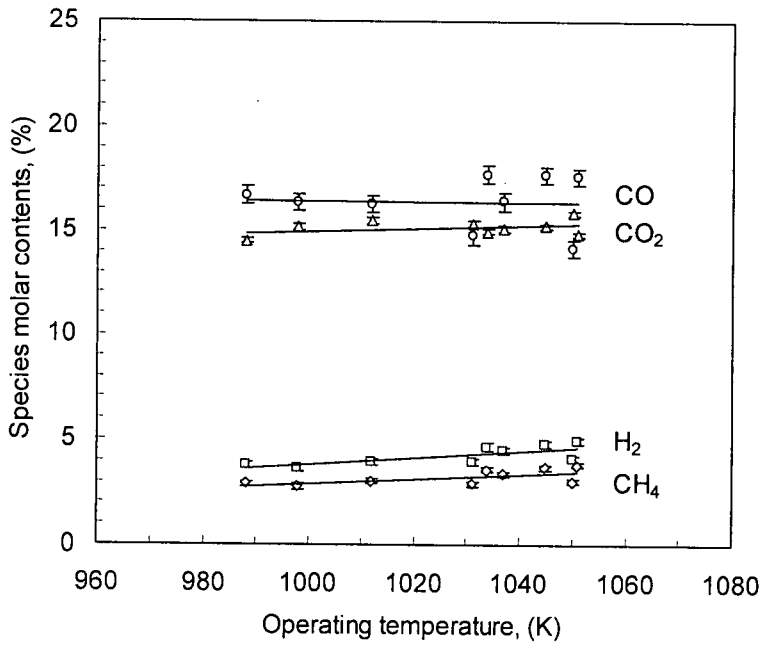

Figure 4-11. Effect of operating temperature on measured species contents. Data from Run 11, using hemlock sawdust; a = 0.33.

4.6 Effect of Secondary Air

Secondary air was found to have only a small effect on the gas composition. A previous study (Pan *et al.*, 1999) showed that it also contributed to tar removal, but at the expense of lowering the gas heating value, a 14% decrease in the gas heating value as the secondary air fraction increased from zero to 20%. The proposed mechanism for tar removal by secondary air is the formation of local high temperature zones where thermal cracking of tar is promoted. Since the degree of tar reduction depends heavily on the local temperature in this zone, the authors recommended that oxygen be used instead of air for more effective partial oxidation. However, this is economically viable only in an oxygen-blown gasification plant. For a given overall air ratio, the local temperature rise caused by secondary air is not expected to persist along the height of the riser. Instead, because of rapid mixing, and the temperature in the upper part of the riser soon returns to a level dictated by the overall stoichiometry in the gasifier.

In this work, up to 14.3% of the total air was secondary air, while keeping the total air flow essentially constant, within ±0.02. As shown in Figure 4-12, all combustible species (H_2, CO and CH_4) showed a very slight decrease in concentration as the fraction of secondary air increased. The decrease was less pronounced than reported by Pan *et al* (1999). However, in that earlier work, there appeared to be an increase in total air supply as the secondary air level increased. Figure 4-12 indicates that the gas heating value dropped from an average of 4.20 MJ/Nm^3 for no secondary air to 4.02 MJ/Nm^3 for 14.3% secondary air, less than a 5% decrease. Secondary air clearly causes only a slight change in gas composition for the range of conditions investigated.

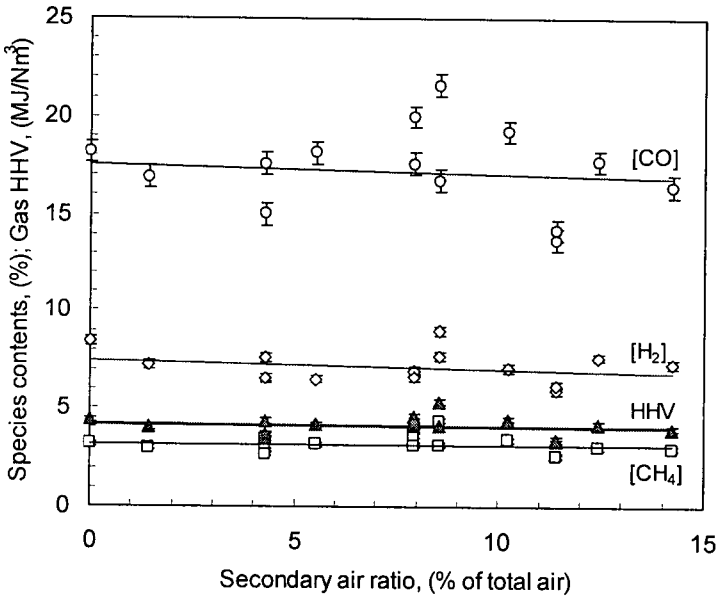

Figure 4-12. Effect of secondary air on gas composition and heating value, for mixed fine sawdust. Data from Run 14, $T = 1030 \pm 15$ K, $a = 0.30 \pm 0.02$, $M = 6.7\%$.

4.7 Effect of Suspension Density

The overall suspension density is closely related to the hydrodynamics, heat transfer, mixing and solids recycle in a circulating fluidized bed. It can be estimated from the pressure drop across the riser. The total pressure drop is caused by four terms, i.e. pressure drop induced by friction between the suspension and the riser wall, gas gravity, solids gravity, and solids acceleration. In most CFB systems the solids gravity term is an order of magnitude greater than the other three terms. The pressure drop can then be given by:

$$\Delta P = \rho_p g(1-\bar{\varepsilon})\Delta h \tag{4-7}$$

Hence, the suspension density can be estimated as

$$\rho_{susp} = \rho_p(1-\bar{\varepsilon}) = \Delta P / g\Delta h \tag{4-8}$$

The suspension density was adjusted by draining solids from the system with the air ratio maintained constant. However, the suspension density was not exactly proportional to bed inventory. Suspension densities below and above the secondary air injection level were measured. The overall suspension density in the riser is taken as the weighted average of the two on a height basis, i.e.

$$\rho_{susp} = \frac{H_1}{H}\rho_{susp1} + \frac{H_2}{H}\rho_{susp2}, \tag{4-9}$$

with $H = H_1 + H_2$ being the total height of the riser, divided into the lower part (H_1 = 1660 mm, from the bottom of riser to the T1 level,) and the upper part (H_2 = 4496 mm, from the T1 level to the top of riser). ρ_{susp1} and ρ_{susp2} represent the suspension densities, in kg/m^3, in the lower and upper parts of the riser, respectively.

Figure 4-13 shows the effect of the overall suspension density on the gas heating value. The suspension density at the bottom of the riser was between 100-140 kg/m^3. The data show that for the three runs at lower air ratios (Runs 11 to 13), the product-gas heating value increased from

3.5 to 4.7 MJ/Nm^3 as the overall suspension density increased from 42 to 93 kg/m^3 for air ratios from 0.22 to 0.33 and operating temperatures from 950 to 1050 K. The solid line is the best fit for all data points, correlation factor R^2 = 0.72. The positive influence of suspension density on gas quality is likely due to an increase in solid reactants concentration, together with enhanced solids mixing.

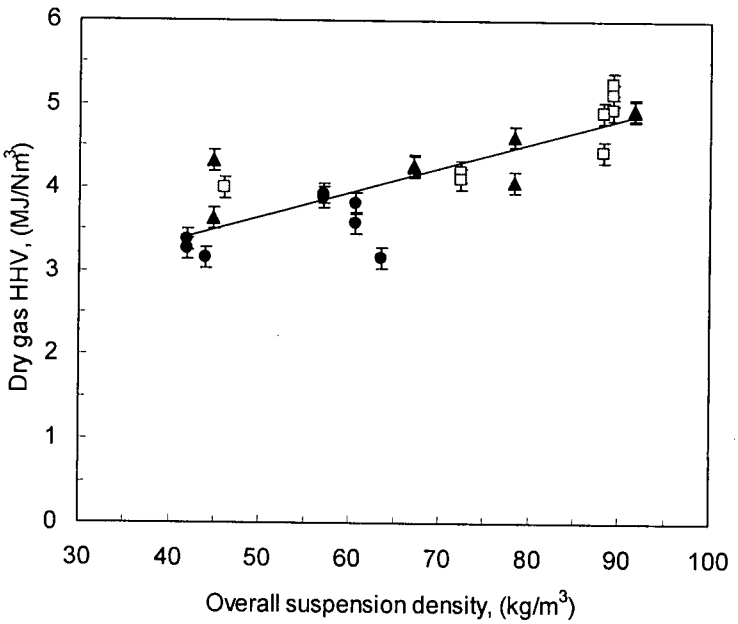

Figure 4-13. Effect of suspension density on gas heating value: ● – Hemlock sawdust, a = 0.337, T = 990-1050 K, M = 14.7%; □ – Pine and spruce mix, a = 0.218, T = 950-1010 K, M = 10.1%; ▲ – Mixed sawdust, a = 0.258, T = 980-1040 K, M = 6.6%.

4.8 Effect of Fly Ash Re-injection

Since fly ash re-injection can increase suspension density as well as the carbon concentration in the riser, it should have a similar effect to raising the suspension density on gas quality and carbon conversion. To facilitate discussion, we first define

$$F = \frac{\dot{m}_{fa} C_{fa}}{\dot{m}_f C_f}. \qquad (4\text{-}10)$$

F is the ratio of the carbon in re-injected fly ash to the carbon introduced with the fuel, where $\dot{m}$ denotes feed rate, in kg/h dry mass and C is the fractional carbon content. Subscripts *fa* and *f* refer to fly ash and fuel, respectively. The carbon content in the bed ash was less than 2% for all runs, while it varied from 12.4 to 63.3% in the fly ash, whose surface-mean diameter (Eq. 3-1) was about 60 μm. This makes fly ash a major source of carbon loss if it is not recycled. Table 4-1 lists the test conditions for the fly ash re-injection trials.

Table 4-1. Detailed test conditions for fly ash re-injection.

Run #	air ratio	T_b	HHV_{far}	HHV_0	$\dot{m}_{fa}$	$\dot{m}_f$	C_{fa}	F	HHV_{far}/HHV_0
-	(-)	(K)	(MJ/Nm^3)	(MJ/Nm^3)	(kg/h)	(kg/h dry)	(%)	(-)	(-)
8	0.410	995	2.86	2.46	12.32	30.04	45.9	0.37	1.16
8	0.410	1013	2.83	2.46	12.32	30.04	45.9	0.37	1.15
8	0.443	1043	3.35	2.15	32.69	25.46	45.9	1.16	1.56
8	0.443	1060	3.12	2.15	32.69	25.46	45.9	1.16	1.45
9	0.415	1008	2.83	2.41	12.49	27.41	42.5	0.34	1.17
9	0.348	1002	4.22	3.15	12.49	27.41	37.5	0.34	1.34
9	0.430	1004	3.38	2.27	16.70	27.41	37.5	0.45	1.49
10	0.424	1090	2.65	2.32	5.73	24.88	41.6	0.18	1.14
10	0.424	1087	2.47	2.32	5.73	24.88	41.6	0.18	1.06

A simple, empirical correlation (with the line plotted in Figure 4-14) for the species and parameter range tested is

$$HHV_{far} / HHV_0 = 1 + 0.6[1 - \exp(-F / 0.7)]. \quad (4\text{-}11)$$

Here the subscripts *far* and 0 stand for cases with and without fly ash re-injection, respectively. The correlation factor is $R^2 = 0.74$. The effect of ash re-injection diminishes as F decreases to zero. The benefit of carbon re-injection reaches a limit due to the kinetic limitations at a given temperature and solids residence time. It is expected that the effect of fly ash re-injection can be

further enhanced by raising the operating temperature. Confirming this would require future experimentation.

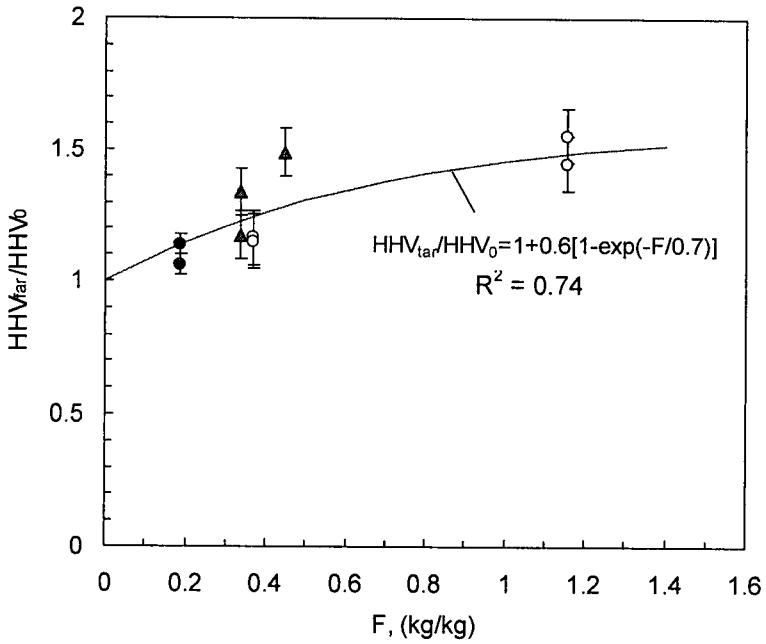

Figure 4-14. Effect of fly ash re-injection on gas heating value: ○ – SPF/cypress mix, a = 0.35, T_3 = 970-1010 K, M = 11.3 %; (b) ▲ – SPF/cypress sawdust, a = 0.41, T_3 = 990-1030 K, M = 15.0 %; and (c) ● – Cedar/hemlock mix, a = 0.40, T_3 = 1070-1100 K, M = 12.6 %.

A closer look at the results shows that fly ash re-injection has little effect on the product H_2/CO and CH_4/H_2 ratios, as seen from the experimental data in Figure 4-15. Since the fly ash mainly contains fixed carbon and minerals, with less than 8% volatiles as reported by van der Drift *et al.* (2001), it has little impact on the hydrogen balance assuming that no steam reacts with it. However, measured gas compositions indicate that the fly ash does affect the CO/CO_2 ratio. Figure 4-16 shows that, at a given total oxygen / total carbon ratio, the CO/CO_2 ratio increased with increasing re-injection rate. However, due to the scatter, more experimental data are required to draw any quantitative conclusion.

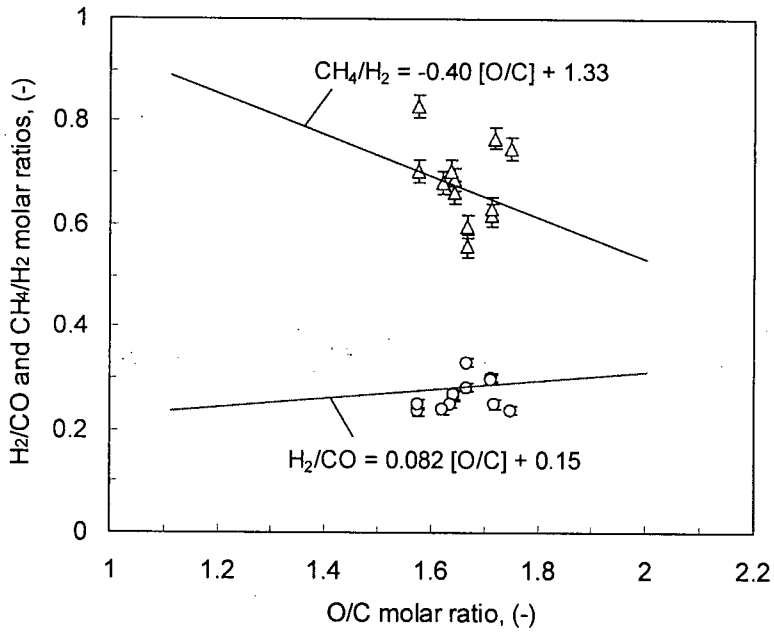

Figure 4-15. Effect of fly ash re-injection on the H_2/CO and CH_4/H_2 molar ratios in product gas. T = 1000-1090 K, a = 0.35-0.41, M = 11.3-15.0%. Solid lines represent fit line for zero ash re-injection. Open triangles and circles represent instantaneous values with fly ash re-injection.

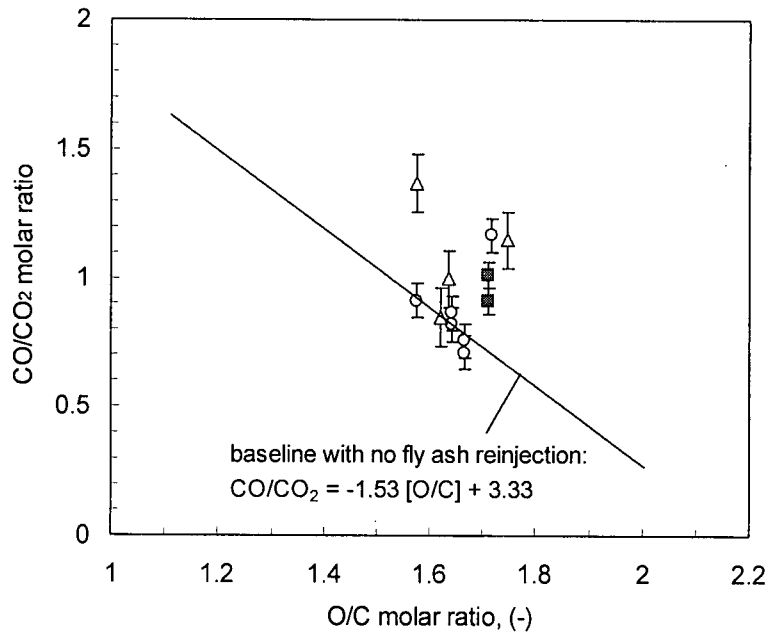

Figure 4-16. Effect of fly ash re-injection on the CO/CO_2 molar ratio in product gas. T = 1000-1090 K, a = 0.35-0.41, M = 11.3-15.0%. Solid lines represent equation for zero ash re-injection. Experimental data: ○ – $F < 0.4$; Δ - F = 0.4-0.8; ■ – $F > 0.8$. See Eq. (4-10) for F ratio.

4.9 Effect of Fuel-Bound Moisture and Steam Injection

Figure 4-17 shows that steam injection can significantly improve gas quality at a given O/C molar ratio. When steam is introduced, CO and H_2 are formed as products of the endothermic steam-char reaction. For this reason, steam injection makes the gas heating value higher than for purely air-blown processes having the same O/C ratios. This effect can also be seen from the product molar ratios, reflecting progress of the shift reactions.

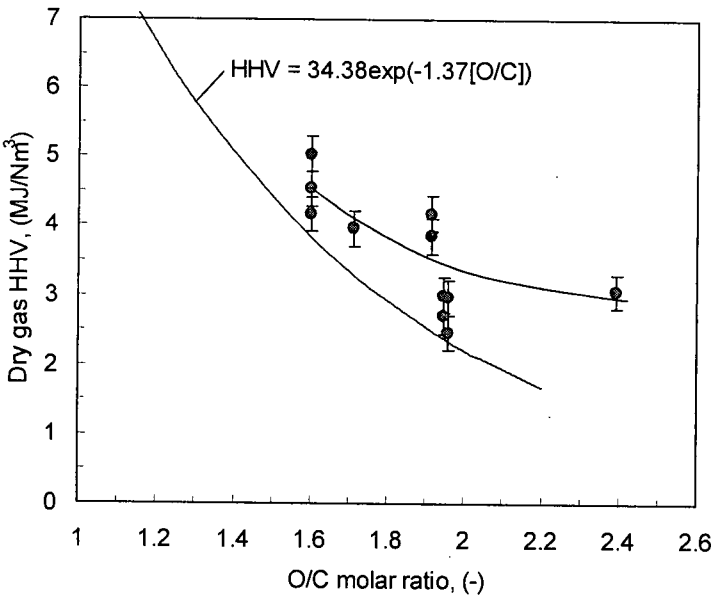

Figure 4-17. Effect of steam injection rate on instantaneous dry gas heating values for hemlock sawdust. T_3 = 1020-1070 K, a = 0.38-0.43, M = 8.8-9.2 %. Solid line: best-fit for no steam injection; solid points: with steam injection.

Despite the fact that steam injection provides another way to improve the carbon conversion, it differs in many ways from increasing the air supply. Figures 4-18 and 4-19 show how the product molar ratios CO/CO_2, H_2/CO and CH_4/H_2 vary with increasing O/C ratio due to steam injection. A decrease in the operating temperature could be expected for very large steam injection rates since the heat consumed for raising the saturated steam to the riser temperature increases with increasing injection rate. However, no decrease in the operating temperature was observed during the steam injection tests for the injection rates tested. In Run 5, there was even a

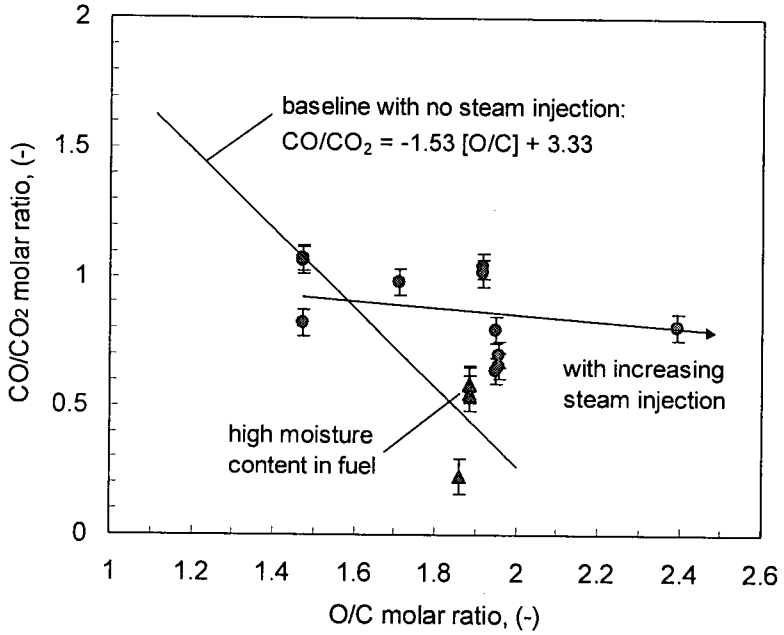

Figure 4-18. Effect of steam injection on the CO/CO_2 molar ratio. Data from Runs 1, 5 and 6, gasifying hemlock. Solid line represents cases without steam injection; ● – with steam injection; ▲ – with high moisture content in fuel (22.0%).

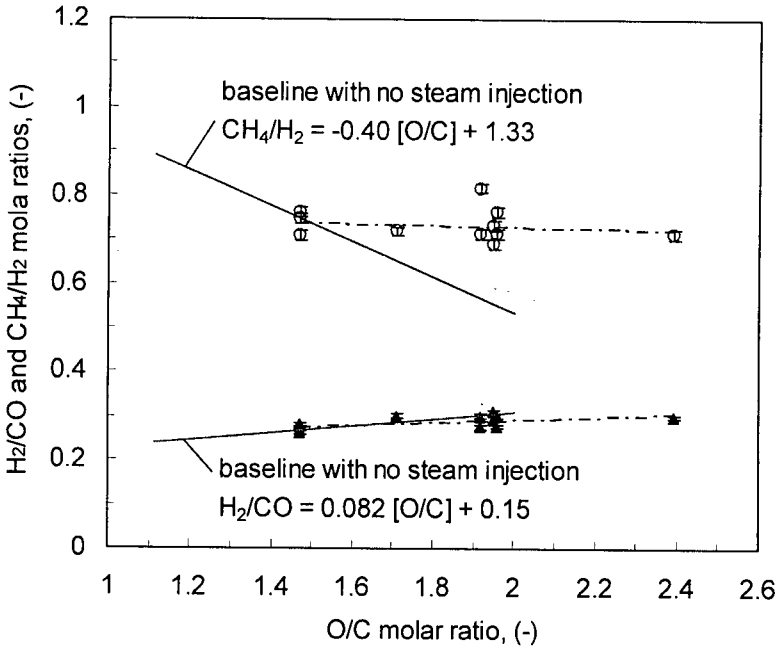

Figure 4-19. Effect of steam injection on the H_2/CO and CH_4/H_2 molar ratios. Data from runs 5 and 6, gasifying hemlock. Open points represent cases without steam injection; solid points represent cases with steam injection.

10-20 K increase in upper riser temperature. First, the addition of steam to the gasifier drastically changed the trend of the CO/CO_2 versus O/C line; it helps maintain a better gas quality with a higher CO content than can be obtained by increasing the air ratio. Similarly, the hydrogen entering the system together with steam injection substantially nullifies the declining trend in the CH_4/H_2 vs. O/C trend lines, suggesting simultaneously increasing H_2 and CO contents in the gas as a result of the steam-carbon reaction.

Though chemically the same, the behaviour of fuel-bound moisture differs from that of moisture added as steam. A possible reason for this is that the fuel-bound moisture may require a prolonged evaporation time. This means that the position where a fresh sawdust particle starts to pyrolyse ascends toward the top of riser. This has two implications. First, fuel-bound moisture allows less time for methane and tar cracking, leading to higher methane and tar contents in the gas. Secondly, because much of the lower part of the riser is devoted to moisture evaporation instead of chemical reactions, it makes the system less effective in terms of throughput. Increasing the height of the riser helps improve moisture involvement in gasification reactions, but in real processes the height of the riser is usually restricted by many other factors, such as structural and fan power consumption considerations. Moisture in the fuel can also cause bridging in hoppers and feeders. High moisture content can cause other operating problems including blockage of the screw feeder. In the present study, the highest fuel moisture content tested was 22%, using cypress sawdust.

The above discussion raises the issue of the chemical reaction effectiveness of fuel moisture, particularly in small units with relatively short gas residence times. Pilot test results implied that fuel-bound moisture hardly participated in the chemical reactions before leaving the reaction zone with the bulk gas flow because of the very restricted residence time in a pilot unit. Figure 4-18 helps to clarify the point. We can see that, unlike the steam injected, the fuel moisture has

little effect on the CO/CO_2 molar ratio. The steam, although injected at a higher level, effected greater changes in the product ratios, and showed much better reactivity than fuel moisture. To produce hydrogen-rich gas from small units, it is desirable where feasible to employ steam injection. Pre-drying (e.g. utilizing the waste heat of gas) and feeding sawdust in the recycle leg may help improve the availability of moisture content to the chemical reactions.

4.10 Effect of Sawdust Species and Particle Size

The effect of wood species manifests itself in a number of ways. Notwithstanding differences in wood type and geographic source, different sawdust species show greater uniformity in chemical composition (Table 3-1) than coal and other solid fossil fuels. Six biomass species and seven combinations were tested in the present study. Species effects on gas heating value, and carbon conversion appeared to be insignificant, as shown in Figure 4-20.

However, the various sawdust species behaved differently during gasification due to differences in physical properties, e.g. fibre length, moisture, shape and particle size, caused by different methods of processing. For example, cedar hog fuel, because of its long fibre length, has a tendency to cause bridging in the feed hoppers. This tendency remained when the hog fuel was ground to less than 6 mm, the same size as the other species tested. Blending the ground cedar hog fuel with a more granular sawdust helped alleviate the bridging tendency. When up to 50% hemlock was added to the ground cedar hog fuel, the mixture was marginally viable for operation with the screw feeder. The hemlock and cypress sawdusts proved to be most suitable because of their size distribution, more or less granular shape, and their low bridging tendency, even at relatively elevated moisture contents. Over the limited range tested in this work, particle size effects on gas heating value and carbon conversion were negligible. However, tar yield appeared to decrease with increasing particle size because of the secondary cracking effect.

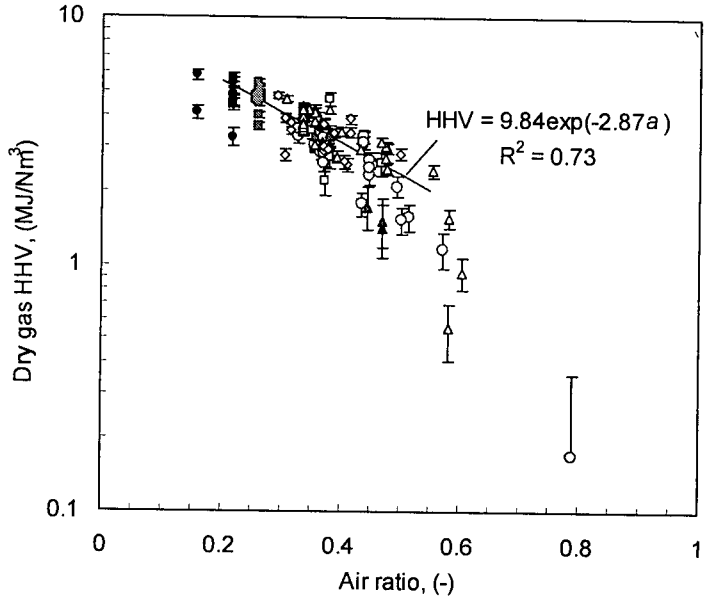

Figure 4-20. Comparison of different species in gasification. Data from Runs 1-13. Legends: ○ - cypress; ● - pine/spruce mixture; △ - hemlock; ▲ - spruce, pine and fir (SPF) mixture; ◇ - SPF/cypress mixture; □ - cedar/hemlock mixture; ■ - mixed sawdust.

4.11 Tar Yield from Pilot Study

Tars present the biggest threat to operation when gasification products are burnt in a gas turbine. Therefore, minimization of tar production is a major concern in biomass gasification. Tar sampling was conducted in all runs from Run 7 on. After three runs of experimentation and correcting problems, we have been able to determine tar yield with reasonable accuracy following the revised procedure described in Chapter 3, Section 3.5.

Shown in Figure 4-21 are results from Runs 10 to 15. The experimental data show that tar concentration is primarily dependent on the operating temperature. The measured tar yield dropped drastically from 15.2 g/Nm^3 at 970 K to 0.4 g/Nm^3 at 1090 K. This arises because the tar cracking rate increases exponentially with increasing temperature. The results are approximately linear on semi-log paper suggesting an exponential decay function. The results from this work are in qualitative agreement with previous studies (Moersch *et al*, 2000; Rapagna *et al*, 2000), as

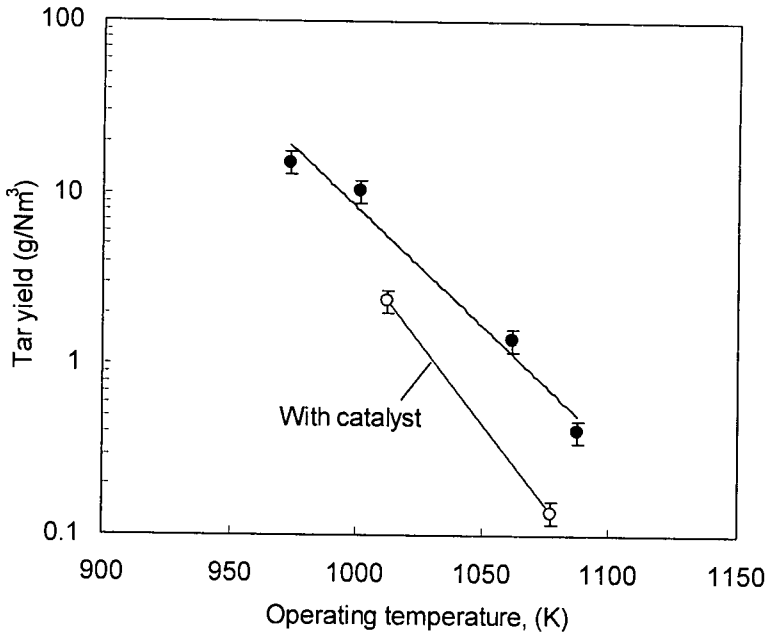

Figure 4-21. Temperature dependence of tar yield and effect of nickel-based catalyst: a = 0.21-0.46, T_3 = 970-1090 K, M = 4.18-14.7 %. ● – no catalyst; ○ – with catalyst.

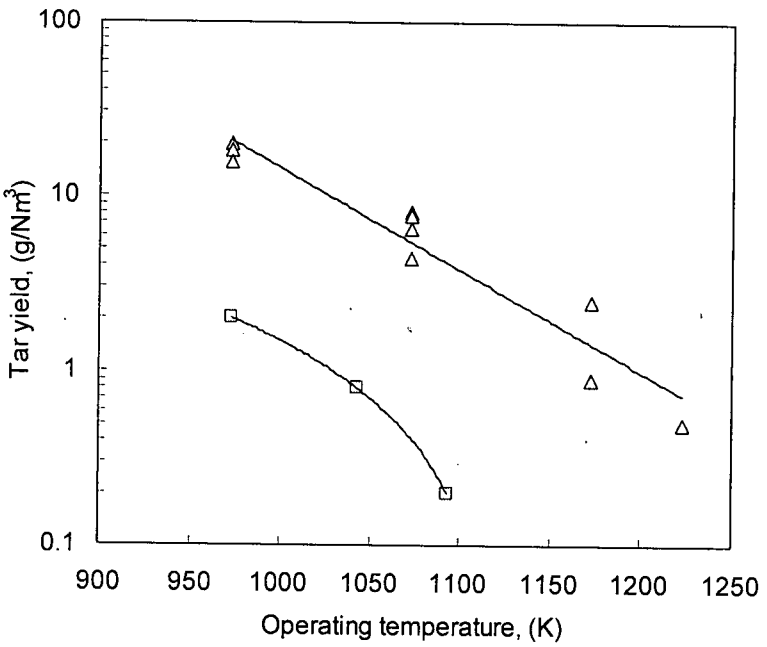

Figure 4-22. Temperature dependence of tar yield from previous studies: (a) Δ - Moersch *et al.* (2000), T = 970-1220 K, a = 0.15-0.25; (b) □ - Rapagna *et al.* (2000), T = 970-1090 K, steam/biomass ratio = 0.5-1.0.

shown in Figure 4-22. The slope of the trend in our study is similar to that of Rapagna *et al.* (2000), but greater than that of Moersch *et al.* (2000). Another set of measurement data by van der Drift *et al.* (2001), although it fits our trend line well at higher temperatures, shows considerable scatter, and these data are therefore excluded in Figure 4-22.

It should be noted that operating temperature is not completely independent of other parameters. Figure 4-23 plots the mean operating temperature for all the test runs versus the air ratio. Despite its generally weak dependence on the air ratio ($R^2 = 0.31$), the 100 K increase in the suspension temperature with increasing air ratio from 0.2-0.55 is large enough to make a substantial difference in the tar yield.

In addition to raising the operating temperature, it has been reported (Sutton *et al.*, 2001; Rapagna *et al.*, 2000) that further tar reduction can be achieved by using commercial or mineral catalysts. In one test run (Run 14), 62% tar removal was achieved at a reactor temperature of 1010 K by adding 30% Ni-based commercial steam-reforming catalyst (C11-9 LDP, Süd-Chemie). (See Appendix I, Table A-2 for size distribution). The catalytic gasification results are described in Section 4.12 in more detail.

Another factor that may affect tar yield is the fuel particle size. Particle size is important whenever diffusional processes are important. It is reported (Suuberg, 1977; Howard, 1981) that bigger particles tend to produce less tars in pyrolysis due to secondary tar cracking along the pores of particles. However, a recent TGA study (Seebauer *et al.*, 1997) shows a contradictory trend. Further data are needed before drawing any conclusion regarding the particle size effects on tar removal.

Tar composition has rarely been reported in the previous literature because of its extreme complexity in terms of molecular formula, and difficulty in quantitative determination of all the species identified in the tar. However, tar analysis is required in order to determine the overall

mass and heat balance of gasification. A much more convenient alternative is to determine the elemental composition of tar (as for coal), and estimate its heating value based on general equations derived for carbonaceous materials. Tar heating value can be estimated in this manner by the Dulong formula (Probstein and Hicks, 1982):

$$[HHV]_t = 33.83C + 144.3(H - O/8) + 9.42S, \quad \text{(MJ/kg)} \tag{4-12}$$

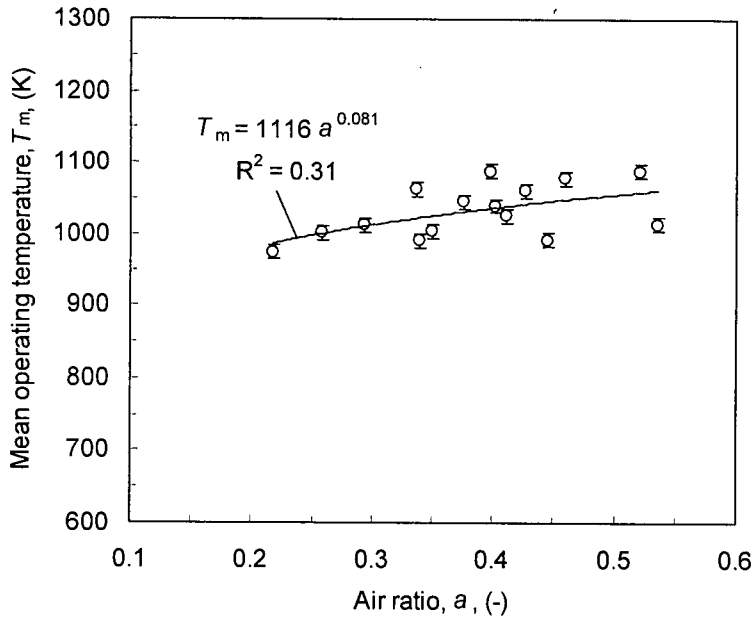

Figure 4-23. Mean operating temperature versus mean air ratio: Moisture content in sawdust varies between 6.5-22.0%.

Table 4-2 lists the analysis data of three tar samples from hot (T11) and cold (T16) positions. The first two were sampled at the inlet of the heat exchangers and mixed with that collected from the vertical stack pipe, while the third was collected from the rooftop horizontal pipe. The carbon content in the low-dewpoint (< 330 K) tar (Tar Rooftop) is considerably higher than that for the high-dewpoint (> 330 K) tars (Tar 10 and Tar 13), while there is little difference between the two samples from two different runs at the same position. The high-dewpoint tars contains more oxygen and hydrogen than the low-dewpoint tar, though they appear to be much denser and more

viscous. Also remarkable is the concentration of sulfur in the tars. Since the sulfur content in the sawdust is very low, the sulfur content in the tars may partly come from the start-up and transition stages when coal is fired. The major sulfur-containing species in combustion and gasification are SO_2 and H_2S, respectively, both extremely soluble in water. They may well first dissolve in the condensate water, accumulate in it, and eventually mix with the tars.

Table 4-2. Ultimate analysis of tars.

Tar sample		Tar 10	Tar 13	Tar Rooftop
Carbon	%	64.23	66.51	78.14
Hydrogen	%	6.56	6.40	5.90
Nitrogen	%	1.87	2.12	0.66
Oxygen	%	25.60	21.62	11.98
Sulfur	%	0.48	0.47	0.40
Others	%	1.26	2.88	2.92

4.12 Catalytic Gasification: Preliminary Results

Preliminary results are presented from two runs with catalyst addition to the reactor. However, catalytic gasification is a major area that requires much more detailed work to be well understood. Catalytic gasification involves at least two interacting mechanisms, i.e. increased rates of the carbon-gas reactions and enhanced cracking of higher hydrocarbons. The former is achieved by lowering the activation energy and increasing the active site density, while the latter facilitates such reactions as:

$$C_nH_m + nH_2O \Leftrightarrow nCO + (n+m/2)\,H_2 \qquad (4\text{-}13)$$

$$C_nH_m + nCO_2 \Leftrightarrow 2nCO + (m/2)\,H_2 \qquad (4\text{-}14)$$

Both reactions crack hydrocarbons to produce carbon monoxide and hydrogen. It can therefore be expected that the CO and H_2 contents of the product gas should increase with addition of a suitable catalyst, causing changes in the product molar ratios.

The Ni-based catalyst (C11-9-02, Süd-Chemie) was received as pellets 15 mm in diameter and 15 mm high. In the present study, the pellets were crushed and sieved before adding to the riser in Runs 14 and 15 prior to switching the system to gasification mode. Fine particles less than 0.21 mm in diameter were discarded since they tend to escape from the system, while coarse particles larger than 1.70 mm in diameter were returned to the mill for further crushing. Size distribution data of the crushed catalyst is provided in Appendix I, Table A-2.

Figure 4-24 shows the effect of catalyst addition on the CO/CO_2 ratio of the product gas. At first sight, one would judge that addition of catalyst did not cause much change in the CO/CO_2 molar ratio, but a close look suggests that the trend of the variation of CO/CO_2 ratio with O/C ratio has been completely reversed. Catalyst performance is much better at higher O/C ratios than with lower O/C ratios. Sutton *et al.* (2001) reviewed previous literature on catalyst performance in gasification and concluded that the effectiveness of catalytic gasification depends on

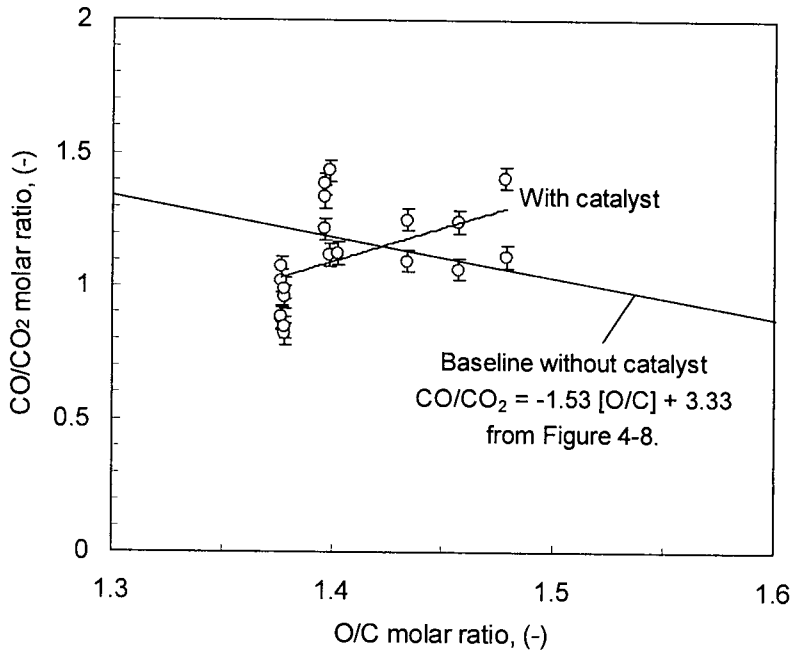

Figure 4-24. Effect of catalyst addition on the CO/CO_2 molar ratio. All points shown were from Runs 14 with Ni-based catalyst present. Points which led to the "baseline without catalyst" are given in Figure 4-8.

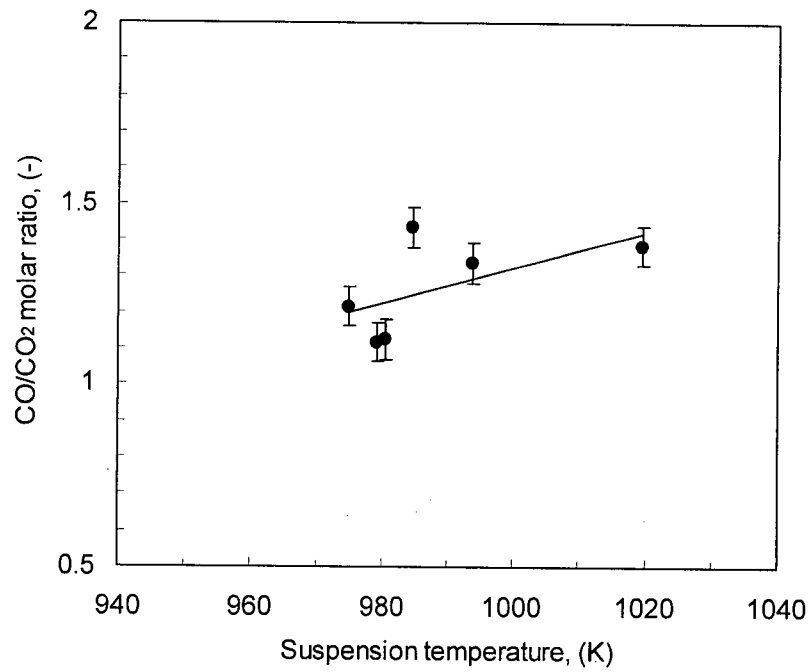

Figure 4-25. Effect of suspension temperature on CO/CO_2 molar ratio. Run 14, using mixed sawdust, O/C ratio fixed at 1.400 ± 0.004, T_3 = 970-1020 K, M = 6.7%.

temperature. The optimum temperature for Ni-based catalysts is above 1070 K. However, the bed temperature in our test was 960-1030 K, with the corresponding O/C ratio being 1.35-1.45. A strong interaction between suspension temperature and the air or O/C ratio is found, as shown in Figure 4-20. If we fix the O/C ratio at a given value and plot the CO/CO_2 ratio against suspension temperature, as in Figure 4-25, the catalyst effectiveness increased with increasing temperature for the range tested. However, more experimental evidence is needed to further validate the trend.

Figure 4-26 shows that catalyst addition substantially increases the H_2/CO ratio and decreases the CH_4/H_2 ratio, as a result of increased hydrogen content. The effect of catalyst addition on tar yield was shown in Figure 4-21, and is not repeated here. Since the total time of operation with catalyst was less than 10 hours, no conclusion can be drawn at this stage with respect to catalyst lifetime or deactivation due to carbon deposition and/or sulfur poisoning.

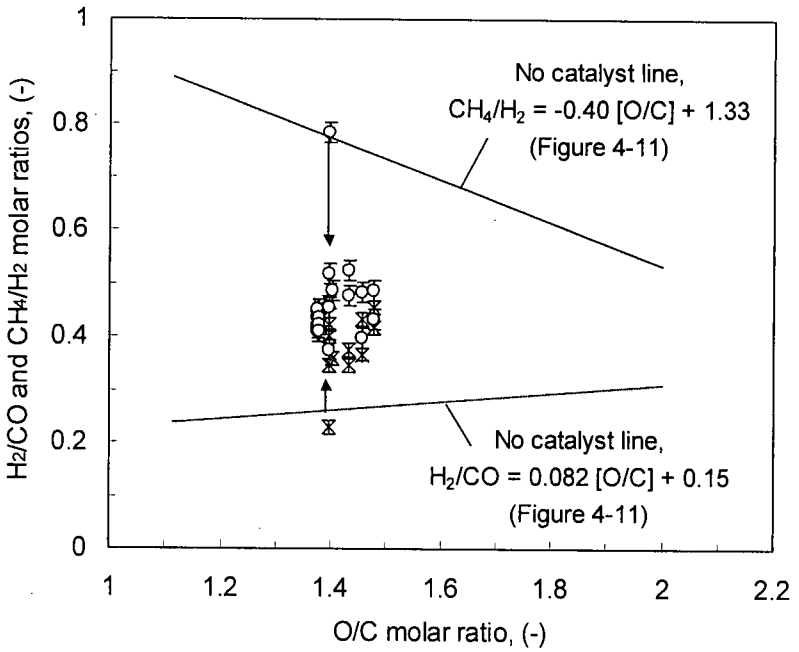

Figure 4-26. Effect of catalyst addition on H_2/CO and CH_4/H_2 molar ratios: Data from Run 14, using mixed sawdust, O/C ratio fixed at 1.400 ± 0.004, T_3 = 970-1020 K, M = 6.7%. Solid lines represent cases with no catalyst addition; data points: ∗ – H_2/CO ratio, ○ – CH_4/H_2 ratio.

Catalyst selection is an issue to be further studied. The nickel-based reforming catalyst left a high nickel content in the ash, leading to a special waste-handling problem. Naturally occurring catalysts (e.g. dolomite, olivine) are competitive alternatives despite an increase in the particulate loading in the raw gas due to their relatively low mechanic strength at high temperatures.

4.13 Other Operational Issues

The present pilot study has been completed successfully. Of all the formal trials, only two had to be abandoned, one due to a power failure, and the other due to agglomeration and termination of solids recycle when alkali had been intentionally sprayed to impregnate the fuel with catalyst (see below). Nevertheless, operational problems were encountered as summarized below.

4.13.1 Feeding disturbances

The smoothness of feeding is not solely a function of the species. Cedar has been proved difficult to feed with many feed systems, but even hemlock and cypress were subject to feeding disturbances. Since sawdust is a loose bulky material, with irregular and fibrous particle shapes, sieving is imperative before sawdust is loaded into feed hoppers. Both with a pneumatic conveying system and a screw feeder, it was found that the feed system must operate at the same pressure as the reactor. If the pressure in the hopper is lower than that of the reactor, the ensuing hot gas reflux could cause unwanted heating, ignition and even explosion of sawdust in the hopper that would endanger the whole system. One way to prevent this is to keep the feed system well sealed so that no stable gas flow can be established. Another measure is to maintain an appropriate moisture content in the sawdust. For the pilot CFB gasifier concerned, the optimum moisture content for a typical screw feeder system is 10-15%. Beyond this level, the surface

friction between the metal surface and the sawdust in the hoppers and auger will increase remarkably, causing bridging and blockage. If such disturbances cannot be controlled and feeding restored in a few minutes, the test must be terminated and air supply completely cut off so that the hot fine particles which had accumulated in the cyclone and filter unit would not reburn.

4.13.2 Agglomeration and malfunction of solids recycle

Alkalis are known to lower the ash fusion temperature and cause slagging and fouling in biomass energy applications (Miles *et al.,* 1993; McLaughlin *et al.*, 1996). Run 7 was scheduled for multiple objectives; 1 wt.% of sodium (2.54 wt.% NaCl) was sprayed onto the sawdust in order to examine the effect of alkali, in particular the possibility of agglomeration. The test lasted about 2.5 hours before an abnormal temperature rise occurred, as shown Figure 4-27. Biomass was fed to the reactor about an hour to displace coal before it was completely stopped. Bed temperatures in the upper part of riser rose, while temperatures at the bottom dropped, as a result of blockage of the recycle line. It was postulated that there might have been agglomeration due to the addition of alkali which was intentionally added to the fuel. Post-test evidence supported this postulate. Fragments of a loose, cylindrical agglomerate, about 50 mm in diameter and 40 mm long, were collected from directly above the aeration port at the base of the standpipe. These fragments displayed a low degree of sintering, and low mechanical strength. Though loose enough to be easily broken, these agglomerates were strong enough to withstand the impact of the downcoming solids stream and block solids recycle. A picture of the fragments appears in Figure 4-28. Because of possible damage to the gasifier, a planned second test scheduled with Na_2CO_3 addition was cancelled.

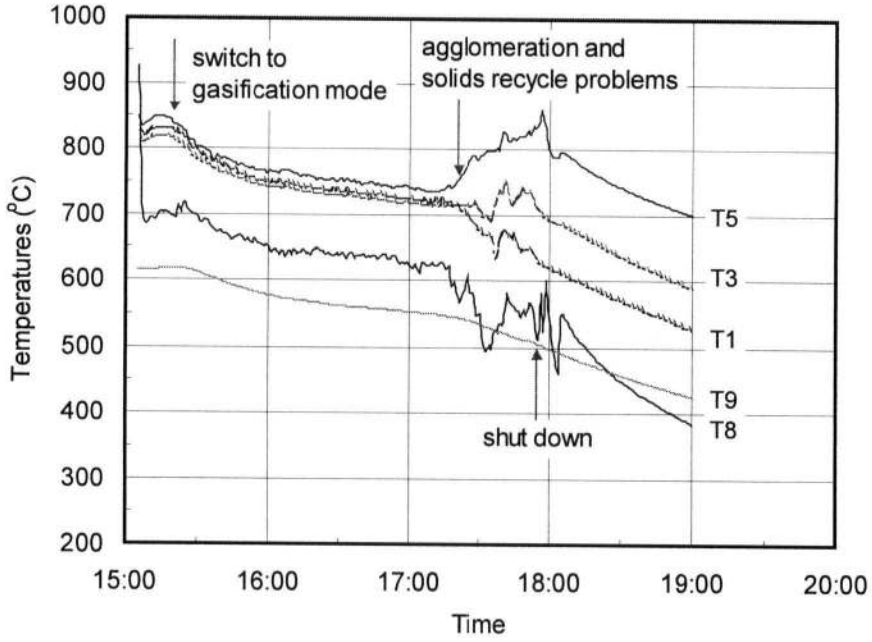

Figure 4-27. Agglomeration caused by alkali addition to the sawdust. Run 7, sawdust dosed with 1 wt.% NaCl. For location of thermocouples, see Figure 3-3 or Appendix IV.

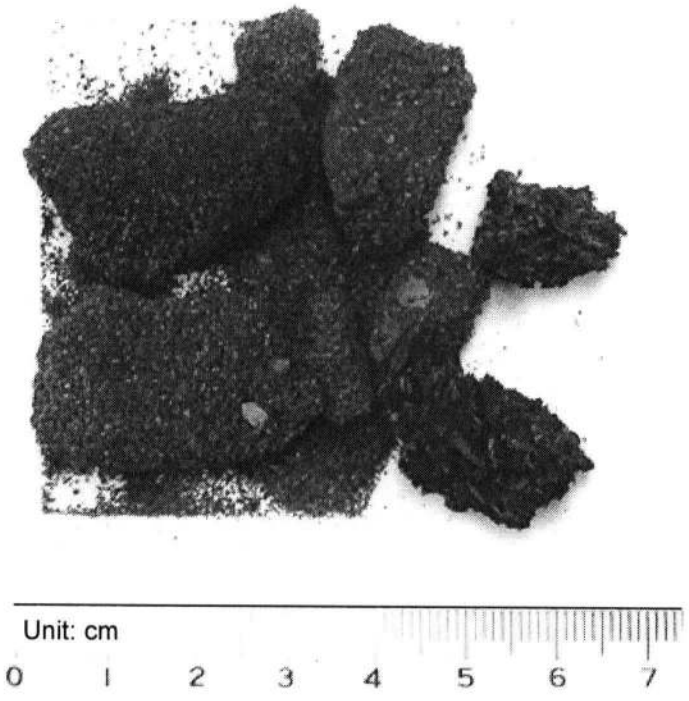

Figure 4-28. Agglomerates collected from the standpipe.

4.13.3 Abnormal temperature rise

The problems encountered with fine sawdust was increased carbon loss due to lowered cyclone efficiency. To compound the problem, a considerable fraction of the fine particles, already fully dried and reduced in size due to fragmentation and attrition, deposited in the piping downstream of the hot cyclone. Once the oxygen concentration in the system increased for a very short time due to air-aided fuel loading, or when the air ratio increased, they would burn, leading to high temperature (up to 1000 K) in the vicinity of the gas cleaning system.

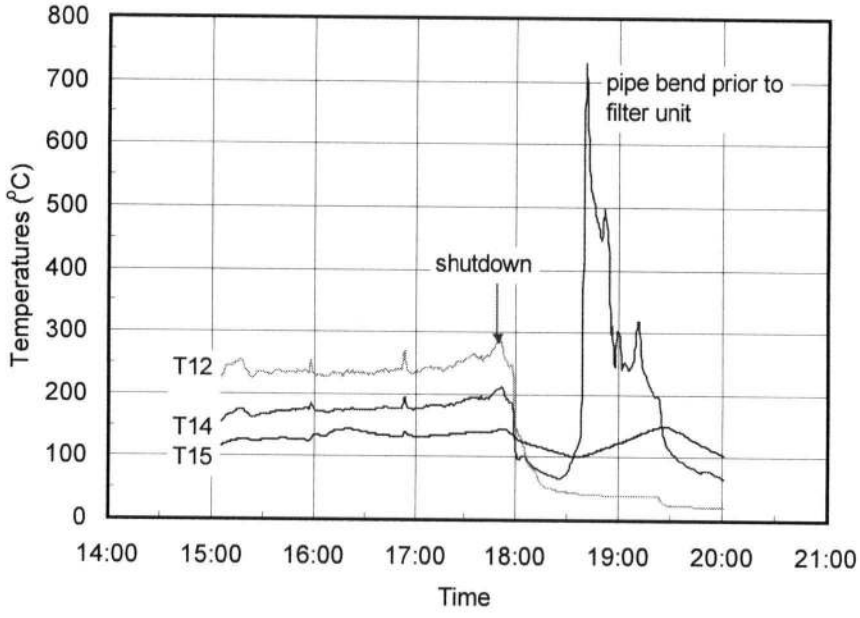

Figure 4-29. Abnormal temperature rise due to char reburning in pipe bend before filter unit. Data from Run 7. Thermocouples: T12 – Inlet of air preheater, T14 – Pipe bend prior to filter unit, T15 – Inside filter unit.

In one test run (Run 7), char burning was observed in the pipe bend prior to the filter unit. Temperature records in Figure 4-29 show that the temperature soared from 350 to 1000 K (80 to 730 °C) within five minutes. Nitrogen purge into the pipe bend and surface blowing with a fan were activated to cool the system immediately after the abnormal temperature rise was detected, but the temperature kept rising for a short while before falling. Fortunately, the local high

temperature caused oxygen depletion that actually protected the more delicate filter unit. A revised operating procedure was subsequently enforced to prevent char burning. However, the procedure cannot eliminate the possibility of combustion resulting from an extra large fines fraction in the feed.

4.13.4 Pressure drop build-up in filter unit

The pressure drop across the filter unit is usually 3-8 kPa, depending on the operating time, local temperature inside the filter and the moisture content in the gas. Ash cakes deposited on the outer surface of the ceramic fabric filter bags, layered by each run, are clearly discernible in Figure 4-30.

Figure 4-30. Ash deposition on the outside of the filter bags. Picture taken after two continuous runs without cleaning the filter unit. Two distinct layers can be identified.

Because of the fine particles produced, a filter cake of ash about 5 mm thick is deposited on the outside of the filter bags during each test run. For typical operating conditions, the pressure drop of the filter unit increases by typically 2-2.5 kPa during each run. Therefore, if the filter bags are not cleaned after three runs, the filter pressure drop can rise to 8-10 kPa. It is therefore

necessary to clean the filter bags after every two runs. Nitrogen Purge is activated, automatically or manually, when the pressure drop across the filter unit exceeds a set value between 3-6 kPa, or if the temperature inside the filter exceeds 530 K. Purge method and typical purge lines are given in Chapter 3, Section 3.4.

4.14 Data Quality and Sources of Error

The experimental data was observed to have considerable scatter throughout the pilot study, particularly in the instantaneous data points. The error bars in the figures suggest standard errors less than 10-15% of the mean values, depending on the nature of the parameters concerned. The scatter is believed to result from a number of factors, e.g. feeding disturbances, cyclic fluctuations in plant air pressure, systematic error in sampling, injection of gas samples into the gas chromatograph, and reading the gauges.

One of the biggest sources of scatter is disturbances and fluctuations in feeding that are impossible to eliminate when a screw feeder is used. The rotation speed of the screw was about 2-6 rpm. This subjects gas sampling to the influence of cyclic disturbances and fluctuations in feeding. Fixed bed gasifiers, such as downdraft gasifiers, are insensitive to small fluctuations in feeding because the feedstock is first preheated by the static bed for a long time before entering the hot reaction zone. Bubbling fluidized bed gasifiers with lower superficial gas velocities are also relatively tolerant to feeding disturbances, because the dense bed provides good initial mixing for fresh feed particles. However, in a CFB gasifier in which the turbulent or fast fluidization flow regime is maintained, the superficial gas velocity is so high that the fed sawdust particles are very unlikely to drop to the dense phase at the bottom of the riser before being carried upward by the gas-solid flow. Therefore, small disturbances in feeding are transmitted

along the riser height as the feed particles make their first flight through the riser. Solids dispersion and mixing in fast fluidization is generally less intensive than in a bubbling bed where rising bubbles create excellent mixing conditions for the solids.

Another reason for the considerable scatter due to feeding fluctuations lies in the strong dependence of species composition on the pyrolysis stage, while the char gasification stage only influences the final gas composition in a minor way. Since the gasifier operated at relatively low temperatures, the C-CO_2 and C-H_2O reactions were not fast enough to exert a decisive impact on the gas composition. This can also be seen from the high methane content of the product gas. Methane is a product of the pyrolysis and cracking of higher hydrocarbons instead of char-hydrogen methanation reaction. When the reactor operated at 1000 K, with an air ratio of 0.3, the predicted equilibrium concentration of CH_4 produced by methanation was below 0.01%, two orders of magnitude lower than the experimental data. The equilibrium constants of both C-H_2 and CO_2-H_2 methanation reactions are small ($\lg K < -1$) at 1000 K (Hougen *et al.*, 1964).

All the feeders and steam gauges were calibrated. However, the feeder rotation speeds and steam gauge readings were not accepted for overall mass balances. Instead, these readings were only used for operational reference. All solids feed streams and steam flows were gravimetrically re-evaluated by post-test mass audit and inline measurement of condensate water.

It is observed that the pressure of the building air varied between 6.1 and 8.2 bar (75 to 105 psig). Despite an inline pressure regulator, there were still fluctuations in the air pressure. When the secondary air pressure was 3 ± 0.1 bar (29 ± 1.5 psig), the corresponding variations in rotameter readings were ± 3-4 %, depending on the bed and filter pressure drops. To minimize this part of the error, a stable and relatively high overall pressure drop of the system, from the start-up burner to the rooftop burner, should be established and maintained. This baseline pressure drop can be adjusted by adjusting the inventory of bed material and the superficial

velocity. It is also influenced by the working conditions of the filter bags. Over the ranges tested, an overall pressure drop of 0.1-0.2 bar would be appropriate without substantial deviation from atmospheric pressure operations.

Despite many advantages of the CFB process, these two factors make a CFB biomass gasifier particularly sensitive to feeding fluctuations compared to bubbling bed and fixed bed ones. The typical gas sampling interval was about 20 minutes, but the time to collect each sample was only about 1 min. To reduce sampling errors, gas samples for each case or position were repeated at least once to ensure sampling consistency. If one sample for a given set of conditions differed significantly from the other, a third sample was taken in order to obtain a more representative average. Most samples were accepted. However, a few samples that were clearly wrong, containing mostly air, were rejected. Further extension of the gas sampling time could reduce, but cannot eliminate, such scatter. To counter the possible effect of feeding fluctuations on experimental results, gas sampling was repeated at least once for each set of operating conditions in the pilot study, thereby improving the statistical soundness of the data. Errors in solids sampling were related to closure of solids balance (63-111% for the fifteen test runs). Post-test mass balance was performed to obtain the mass of different solids streams, together with their carbon and moisture contents.

4.15 Summary

The following conclusions can be drawn from the pilot study:

(1) Gas composition and heating value depend heavily on the air or O/C ratio, and to a lesser extent on operating temperature. The high methane content of the product gas does not originate from methanation, but from pyrolysis.

(2) The gas heating value can be increased by increasing the overall suspension density in the riser. A high suspension density helps increase the carbon concentration in the reaction zone, while enhancing gas-solid mixing.

(3) Both fly ash re-injection and steam injection caused changes in the product molar ratios. Ash re-injection improved carbon conversion and promoted production of carbon monoxide, while having little effect on the hydrogen balance and hydrogen content of the product gas.

(4) Steam injection seems to be more effective than increasing fuel-bound moisture in promoting steam gasification of char. Since the total gas residence time in the reaction zone is less than 2 sec, it is desirable to maintain a relatively low moisture content (e.g. 8-15%) in the fuel while employing steam injection when there is a moisture demand.

(5) Tar yield from biomass gasification decreases exponentially with increasing operating temperature. Elevating operating temperature provides the simplest solution for tar removal in the absence of a catalyst. Secondary air has only a very limited effect on tar removal for a given total air ratio.

(6) Addition of a nickel-based catalyst significantly affected the product gas composition and species molar ratios as a result of increased hydrogen and carbon monoxide production due to reforming and cracking of higher hydrocarbons. The effectiveness of the catalyst depends on the operating temperature and the catalyst loading.

Further research is required to examine the effects of catalytic addition on tar removal and gas conditioning, the influence of fly ash steam injection on carbon conversion, and the role of carbon deposition on catalyst deactivation. The role of fuel-bound moisture also requires further study.

Since the experimental results are, for the most part, based on instantaneous values, time-mean values over each run need to be evaluated through overall mass and heat balance. Such values include the carbon conversion, thermal efficiencies, as well as a number of other process parameters. These factors are considered in the next Chapter.

CHAPTER 5. MASS AND ENERGY BALANCE

Mass and energy balances provide a solid basis for more in-depth evaluation of the time-mean quantities during the pilot tests. The direct objective of the mass and energy balance calculations is to determine the carbon conversion, the distribution of particular elements, and the efficiency of the gasification process. With the aid of these data, one can envisage possible ways to further improve the process.

5.1 Mass and Energy Balance for Pilot Runs

Post-test mass balances were performed to determine the carbon conversion and thermal efficiencies. A nitrogen balance was chosen as the primary basis for the mass balance for several reasons: (1) Nitrogen is the most abundant element in an air-blown gasification system. (2) It is relatively easy to determine accurately by experimental means and largely independent of other elements. (3) Fuel nitrogen is a volatile element that can be considered completely converted into the gas phase during biomass gasification, with little unconverted nitrogen remaining in the solid or liquid phase. Therefore, mass balances based on a nitrogen balance should result in minimum errors. A secondary auxiliary basis for the mass balance calculations is the oxygen balance, which helps diminish errors when the moisture content in the product gas is unknown, or cannot be measured accurately. Alternatively, a hydrogen balance can be used as a secondary basis (van der Drift *et al.*, 2001).

The basic step for the mass balance is doing the elemental balances. The feed streams are fuel (dry basis), auxiliary fuel, moisture content in fuel, injected steam, oxidant, and re-injected ash. The bed material is a mixture of fresh silica sand and bottom ash collected from the previous run,

sieved to the proper size range. It is also considered a feed stream since it contains up to 2% carbon. The product streams include product gas, ash, tar, and water. At steady state the total mass (or number of moles) of each element in the incoming feed streams must equal the total in the product streams, i.e.

$$\sum_{i}^{M} m_i x_{i,k} = \sum_{j}^{N} m_j x_{j,k} \qquad (i = 1, 2, \ldots, M; j = 1, 2, \ldots, N; k = 1, 2, \ldots, K) \tag{5-1}$$

subject to the overall mass balance constraint:

$$\sum_{i}^{M} m_i = \sum_{j}^{N} m_j \,. \qquad (i = 1, 2, \ldots, M; j = 1, 2, \ldots, N) \tag{5-2}$$

Here m_i and m_j denote mass of the i-th feed stream and j-th product stream, respectively, both in kg. Similarly, $x_{i,k}$ and $x_{j,k}$ represent the mass fraction of the k-th element in the i-th feed stream and j-th product stream, respectively, with $\sum_k x_{i,k} = \sum_k x_{j,k} \equiv 1$. M and N are the total numbers of feed and product streams, respectively. In the present study, $K = 5$, i.e. only five elements (C, H, O, N, and S) are considered in the mass balance. There are K+1 simultaneous linear equations in the mass balance formulation. Ash is accounted for in the mass balances as an inert solid stream. By doing mass balance, one examines how close the two sides of these equations approach each other, while also determining the performance parameters such as the carbon conversion.

A complete set of gas composition data is provided in Appendix VII, based on which the time-mean gas composition for each test run was obtained. The bed ash and fly ash were discharged from the system after each test run. Bed ash was sieved, and the portion with particle sizes under 710 microns was used as the bed material for the next run. About 10 kg of fresh silica sand were added together with the sieved bed ash prior to each test run to make up for the loss in the previous run. Although the carbon content in the bed ash was usually less than 2%, it was accounted for in the mass balance by adding the number of moles of carbon in the start-up

material to that fed. Tar was drained from the stack by gravity after each run to reduce tar accumulation in the product streams. Most of the tar produced was collected in the few minutes immediately after a test run, when the stack pipe was still hot. This step was very quick and effective since the drain pipe was flushed by the hot water accumulated in the condensate well, but the draining process could last a few days to ensure clean-up because the tar was highly viscous. The remnant tar in the horizontal stage of the stack pipe and flame arrestor was also collected (twice) while the researchers were cleaning the flame arrestor on the rooftop. The tar collected was weighed and allotted to previous runs based on their respective hours of gasification run, operating temperatures, and tar loadings determined by tar sampling. Therefore, mass balances were adjusted slightly once more tar collected from the stack. In this way, the error caused by the tar was greatly reduced.

For closure of these elemental balances, one needs to know the elemental (ultimate) analyses of all feed and product streams in the solid and liquid states. For the gas streams, the elemental compositions are obtained from gas chromatography on a moisture-free basis. Carbon and hydrogen balances can thus be fully determined. Because of the low sulfur content in the fuel, neglecting hydrogen sulfide would not cause a significant error in the hydrogen balance. Nevertheless, the H_2S concentration predicted by a non-stoichiometric equilibrium model developed in this work, described in Chapter 6, was used to correct for the hydrogen balance. Though small in amount, moisture and CO_2 in air were also considered in mass balance calculations by adding them to the numbers of moles of carbon, oxygen and hydrogen in the feed, as shown in Appendix VIII.

There are two ways to evaluate the carbon conversion. The forward balance approach considers carbon from the product side, i.e. by determining the mass (or moles) of carbon converted into gas-phase products. The reverse balance approach, on the contrary, examines the

fraction of carbon that remains in the ash (and probably tars) as unconverted carbon, and determines the carbon conversion by deduction. In the present study, the fractional carbon conversion to gas, C, is determined by forward balance:

$$C = \frac{M_C P V_g x_C}{RT \sum_i^M m_i y_{i,C}}, \tag{5-3}$$

where M_C is the atomic weight of carbon, M_C = 12.011 kg/kmol. The term PV_g/RT is the total number of moles of the product gas, assuming ideal gas behaviour, with P (Pa) and T (K) representing the pressure and temperature of a standard state, respectively. V_g denotes the total volume of the product gas, and R is the ideal gas constant, i.e. R = 8.31448 J/mol-K. The gas yield was determined based on nitrogen balance.

The fractional carbon content $y_{i,C}$ of the feed is obtained from the ultimate analysis of the feedstock. x_C is the total molar fraction of carbon in the product gas, which can be determined by summing the molar (volume) fractions of all carbon-containing species obtained from gas chromatography:

$$x_C = x_{CO} + x_{CO_2} + x_{CH_4} + 2x_{C_2H_4} + \ldots \tag{5-4}$$

The carbon conversion defined in Eq. (5-3) is the fraction of carbon in the feed converted to gaseous products. A modified carbon conversion, C^+, can be defined which also account for the contribution of tars. The results of mass balances and gasification efficiency calculations appear in Table 5-1. A detailed sample procedure for the mass balance calculations is provided in Appendix VIII. For all fifteen runs in the pilot plant, the overall mass balance gives 93.8-100.7% closure. Since the carbon balance is based on other elemental balances, it is difficult to achieve perfect closure. Therefore, there may be small differences between carbon conversions estimated

from a forward balance and those obtained from a reverse balance. The major sources of error are discussed in Chapter 4.

An energy balance is carried out in a similar, but simplified, manner. Since the primary objective of the pilot plant study is to demonstrate the effectiveness of the gasification process, a cold gas efficiency is defined to evaluate the gasification performance, while heat losses due to surface heat transfer and sensible heat of product gas are not accounted for. Results of gasification efficiency calculations are given in the last four rows of Table 5.1. Definitions of the cold gas efficiencies E_1 and E_2, excluding and including the contribution of tars, respectively, are provided in Section 5.4, together with more detailed results of energy balance. Results of mass balances for inert solids (ash and silica sand) appear in Table 5-2, giving 63.2-110.7% overall closure.

Table 5-1. Summary of mass balance and gasification efficiency calculations.

Run number		1	2	3	4	5	6	7	8	9	10	11	12	13	14	15
Sawdust species		cyp.	cyp.	SPF	hem.	hem.	hem	hem	SPF/C	hem.	c/h	hem.	PBS	mixed	mixed	mixed
Total gasification run time	h	3.80	4.53	3.00	4.23	4.10	4.27	2.62	3.57	3.62	3.58	3.80	2.42	3.07	3.98	3.55
Sawdust consumption	kg	91.0	103.8	80.7	110.6	118.6	108.2	88.1	126.3	112.3	95.4	120.8	117.3	140.0	164.8	55.2
Moisture content in sawdust	%	22.0	9.7	10.5	10.0	8.8	9.2	11.7	11.3	15.0	12.6	14.7	10.1	6.6	6.7	4.2
Throughput, dry basis	kg/s-m^2	0.87	0.97	1.13	1.10	1.23	1.08	1.39	1.47	1.23	1.09	1.27	2.04	1.99	1.81	0.70
Total air supplied	Nm^3	310	255	177	281	226	225	142	207	207	179	186	125	188	251	135
Fly ash re-injection	kg	0	0	0	0	0	0	0	16.8	20.0	5.2	0	0	0	0	0
Total steam injection	kg	0	0	0	0	2.86	24.17	0	0	0	0	0	0	0	0	0
Mean suspension temp. (T_3)	K	1013	991	1039	1088	1045	1060	991	1003	1025	1088	1062	974	1001	1012	1078
Primary air pressure	bar	1.65	1.19	1.19	1.19	1.19	1.19	1.19	1.19	1.19	1.19	1.19	1.19	1.19	1.19	1.19
Time-mean air ratio	-	0.536	0.445	0.402	0.522	0.376	0.427	0.340	0.350	0.411	0.399	0.337	0.218	0.258	0.294	0.460
Mean gas composition (dry basis)																
H_2	%	5.6	3.1	3.2	3.0	4.0	3.8	5.5	3.9	3.5	4.1	4.2	5.4	5.1	7.3	5.9
N_2	%	68.0	68.1	67.1	68.4	61.8	65.2	59.5	62.5	64.8	64.6	62.6	53.9	56.3	55.4	64.6
CO	%	6.9	11.0	10.7	9.6	14.7	12.6	16.6	15.1	13.4	12.3	14.6	21.4	19.9	17.9	10.0
CH_4	%	1.4	1.9	1.9	1.9	2.9	2.7	3.4	2.8	2.8	2.5	3.0	4.6	4.1	3.2	1.2
CO_2	%	18.1	15.9	17.1	17.1	16.5	15.7	15.0	15.6	15.6	16.5	15.7	14.7	14.5	16.3	18.3
Mean dry gas heating value	MJ/Nm^3	2.43	2.96	2.92	2.75	4.14	3.73	4.82	4.13	3.85	3.59	4.17	6.13	5.62	4.60	2.54
Gas yield	Nm^3/kg	3.30	2.92	2.48	3.10	2.59	2.75	2.34	2.27	2.46	2.51	2.13	1.72	2.06	2.35	3.24
Tar yield	g/Nm^3	n. a.	n. a.	n. a.	n. a.	n. a.	n. a.	n. a.	n. a.	n. a.	0.41	1.39	15.13	10.26	2.35	0.04
Overall mass balance closure	%	98.3	99.6	97.7	98.4	97.8	98.7	98.0	96.9	98.7	97.5	98.7	100.5	100.7	100.1	95.4
Carbon conversion, gas	%	97.7	102.0	92.9	99.2	98.6	93.0	91.9	85.8	91.1	87.6	81.9	81.6	89.8	94.9	98.3
Carbon conversion, gas + tar	%	n. a.	n. a.	n. a.	n. a.	n. a.	n. a.	n. a.	n. a.	n. a.	87.7	82.4	85.7	93.1	95.8	98.3
Cold-gas efficiency, E_1	%	53.2	51.8	44.8	52.2	64.3	60.3	71.4	51.0	50.8	53.6	58.7	63.3	64.7	60.5	44.2
Overall thermal efficiency, E_2	%	n. a.	n. a.	n. a.	n. a.	n. a.	n. a.	n. a.	n. a.	n. a.	53.8	59.3	67.9	68.2	61.5	44.2

Notes: cyp = cypress; SPF = spruce-pine-fir mix; hem = hemlock; SPF/C = spruce-pine-fir/cypress mix; c/h = cedar-hemlock mix; PBS = pine bark-spruce mix.

Table 5-2. Summary of mass balances for inert solids in pilot tests.

Run		1	2	3	4	5	6	7	8	9	10	11	12	13	14	15
1. Input																
Ash entering with sawdust	kg	0.65	0.80	0.74	0.45	0.44	0.44	0.44	0.72	0.40	0.57	0.41	4.20	4.44	4.51	2.30
Total coal consumption for start-up	kg	64.4	20.2	40.1	37.3	44.7	51.0	44.8	40.5	41.1	42.6	61.0	71.8	45.5	45.1	41.1
Ash entering with coal	kg	8.6	2.7	5.4	5.0	6.0	6.8	6.0	5.4	5.5	5.7	8.2	9.6	6.1	6.1	5.5
Total weight of initial bed material	kg	29.5	31.8	29.5	27.2	27.2	27.2	29.5	27.2	31.8	32.7	30.0	27.2	31.8	32.0	35.2
Bed ash re-used as initial bed material*	kg	0	23.6	25.0	23.2	18.6	18.6	21.6	21.8	21.8	32.7	18.6	23.7	19.3	22.0	19.3
Fresh silica sand in bed material	kg	29.5	8.2	4.58	4.1	8.6	8.6	7.9	5.4	10.0	0.0	11.4	3.5	12.5	10.0	15.9
Inert solids re-injected as fly ash**	kg	0	0	0	0	0	0	0	6.0	7.5	2.3	0	0	0	0	0
Total inert solids in feed	kg	38.8	35.3	35.5	32.6	33.6	34.5	35.9	33.0	37.6	38.8	38.4	40.9	42.1	42.2	42.7
Sawdust ash in feed	kg	0.7	0.8	0.7	0.5	0. 4	0.4	0.4	0.7	0.4	0.6	0.4	4.2	4.4	4.5	2.3
Coal ash in feed	kg	8.6	2.7	5.4	5.0	6.0	6.8	6.0	5.4	5.5	5.7	8.2	9.6	6.1	6.1	5.5
Silica sand in feed	kg	29.5	31.7	29.4	27.2	27.2	27.2	29.5	26.9	31.7	32.5	29.9	27.1	31.6	31.6	34.9
2. Output																
Total bed ash collected	kg	23.6	25.0	23.2	18.6	18.6	21.6	21.8	21.8	32.7	21.1	23.8	25.0	23.8	19.3	19.3
Total dry inert solids in bed ash	kg	23.6	24.9	23.1	18.5	18.6	21.5	21.4	21.7	32.5	21.0	23.7	24.7	23.4	19.0	19.3
Silica sand in bed ash	kg	21.2	22.4	20.8	16.7	16.7	19.4	19.3	19.6	29.3	18.9	21.3	22.3	21.1	17.1	17.3
Coal ash in bed ash	kg	2.4	2.5	2.3	1.9	1.9	2.2	2.1	2.2	3.3	2.1	2.4	2.5	2.3	1.9	1.9
Total fly ash collected	kg	8.3	8.8	8.2	7.7	8.2	13.2	12.3	23.6	24.1	20.0	24.5	29.1	29.5	34.1	12.5
Total dry inert solids in fly ash**	kg	5.4	7.4	5.0	5.6	5.1	5.8	4.5	8.4	9.1	8.8	9.2	14.7	10.9	16.4	7.7
Total inert solids in product	kg	28.9	32.3	28.1	24.1	23.7	27.3	25.9	30.2	41.7	29.8	32.8	39.4	34.3	35.4	26.9
Sawdust ash in product	kg	0.4	0.5	0.4	0.4	0.4	0.4	0.3	0.6	0.6	0.6	0.6	4.1	3.1	4.6	2.2
Coal ash in product	kg	5.6	6.9	5.3	5.2	4.9	5.6	4.8	7.2	8.7	7.4	7.9	9.8	7.8	10.1	5.8
Silica sand in product	kg	23.0	24.9	22.4	18.5	18.4	21.3	20.8	22.3	32.3	21.8	24.3	25.5	23.5	20.7	19.0
Closure of total inert solids balance	%	74.6	91.7	79.0	73.9	70.4	79.3	72.1	91.3	110.7	76.8	85.4	96.5	81.4	83.9	63.2

Notes: * It is assumed that inert bed ash composition = 90% silica sand + 10% coal ash.
** Type 1 fly ash dry inert solids composition is assumed to be 33% silica sand + 60% coal ash + 7% sawdust ash for Runs 1-11. Type 2 fly ash dry inert solids composition is assumed to be 22% silica sand + 50% coal ash + 28% sawdust ash for Runs 12-15.

5.2 Carbon Conversion

The bottom ash and fly ash collected after each test and their carbon contents are listed in Table 5-3. The moisture contents of the samples were determined by weight difference after drying at 378 K for 5 hours, while the residual carbon and volatiles were determined by ashing at 1173 K for 2 hours. The ash samples were first dried and then ashed. The total weight loss, therefore, was composed of three parts: moisture, residual carbon, and loss due to other elements (hydrogen, oxygen, alkalis, etc.). Therefore, the residual carbon content was determined on an empirical basis by splitting between residual carbon and other elements. Probstein and Hicks (1982) reported that the char remaining on pyrolysis of wood contains about 80% wt.% C, 3 wt.% H and 17 wt.% O. More recently, Van der Drift *et al.* (2001) reported that the burnt fraction of biomass ash contains 92 wt.% C, 1 wt.% H, 6.4 wt.% O and 0.6 wt.% N. Ash composition analysis in the present work suggested a higher proportion of non-carbon elements. The analysis data of four ash samples gave values of 8, 14.1, 13.3 and 6.9 wt.% for the sum of H+O+N, giving an average of 10.6 wt.% principal non-carbon elements in the sample weight, accounting for on average 23.6 wt.% of the total ashing loss. Therefore, in the present study when no ash composition data were available, 76 wt.% C, 4 wt.% H and 20 wt.% O were assumed as the typical C-H-O split in the burnt fraction of fly ash, while neglecting N and other elements.

Typical fly ash composition and leaching test data, including total ignition loss of combustibles, residual carbon and sulfur, 11 oxides and 43 other elements are listed in Appendix IX. The samples were all analyzed by the ISO9002-accredited Acme Analytical Laboratories, Ltd. The four samples prepared represent one base case run, one with steam injection, one with fly ash re-injection, and one with catalyst addition.

The sensitivity of the results to the bottom ash analysis is relatively small because silica sand accounted for the majority of the total weight of bottom ash, coal ash left over from the combustion stage contributed about 10%, while the total combustibles determined by ashing tests were always less than 2% of the sample weight. It was therefore assumed, without causing much error (< 0.05 % in overall mass balance), that all the weight losses during ashing of bottom ash samples were due to residual carbon only.

Table 5-3. Post-test ash collection and ashing loss data.

Run No.	Air ratio	T_3	Bottom ash wt.	Ashing wt. loss	Moisture	Fly ash wt.	Ashing wt. loss	Moisture
(-)	(-)	(K)	(kg)	(%)	(%)	(kg)	(%)	(%)
1	0.54	1012	23.6	0.2	0.1	8.2	28.4	4.3
2	0.45	991	25.0	0.4	0.1	8.9	12.4	4.3
3	0.40	1039	23.2	0.2	0.0	8.2	31.4	4.6
4	0.52	1088	18.6	0.4	0.1	7.7	20.2	4.3
5	0.38	1045	18.6	0.2	0.1	8.2	31.6	3.8
6	0.43	1060	21.6	0.2	0.1	13.2	47.2	16.4
7	0.34	991	21.8	1.6	0.2	12.3	62.4	3.5
8	0.35	1003	21.8	0.3	0.0	23.6	60.4	2.9
9	0.41	1025	32.7	0.6	0.1	24.1	49.4	1.9
10	0.40	1088	21.1	0.6	0.1	15.4	54.7	0.9
11	0.34	1062	23.8	0.7	0.2	24.5	38.3	16.8
12	0.22	974	25.0	1.0	0.2	29.1	40.9	5.5
13	0.26	1001	23.8	1.7	0.1	9.3	58.2	2.8
14	0.29	1012	19.3	1.7	0.6	32.0	49.7	4.2
15	0.46	1078	20.7	0.2	0.1	12.5	34.2	6.4

The carbon conversion is determined from the product gas composition and gas yield, and plotted in Figure 5-1 versus the air ratio. The air (or O/C) ratio is the primary factor influencing carbon conversion, while temperature and other factors had relatively little effect over the range tested. A simple correlation for the experimental carbon conversion vs. air ratio is:

$$C = 0.25 + 0.75[1 - \exp(-a/0.23)] \qquad (0.22 \le a < 0.54) \qquad (5\text{-}5)$$

The correlation coefficient (R^2) of Eq. (5-5) is 0.86. Temperature and residence time are not included in the equation because of their relatively weak influence, as well as the limited number of data points. The correlation coefficient (R^2) between the carbon conversion and the suspension temperature is estimated to be only 0.03, showing a statistically weak correlation. For our gasifier, the actual carbon conversion is much lower than the equilibrium upper bound. In a manner similar to the way the gasification efficiency is defined, tars can also be considered in a modified carbon conversion. Tar composition was analyzed and is provided in Table 4.3. The modified carbon conversions are listed in Table 5-1.

Experimental data from previous studies are shown in Figure 5-2. A comparison between our test results and those of the previous study (van der Drift *et al.*, 2001) shows substantial agreement in the trend, despite a difference of ~5% in the absolute carbon conversion. This difference may arise from the differences in the reactor configuration, cyclone efficiency, fuel moisture content in the fuel and operating temperatures, but it may also be partly due to the inclusion of about 0.09-0.26 v.% higher hydrocarbons (C_2H_6, benzene, toluene, xylene) and other reducing species (H_2S, NH_3 and HCl) in their gas analysis. However, the portion of heating value contributed by the major species (e.g. H_2, CO, CH_4) in our study is even higher than in that of van der Drift *et al.* (2001).

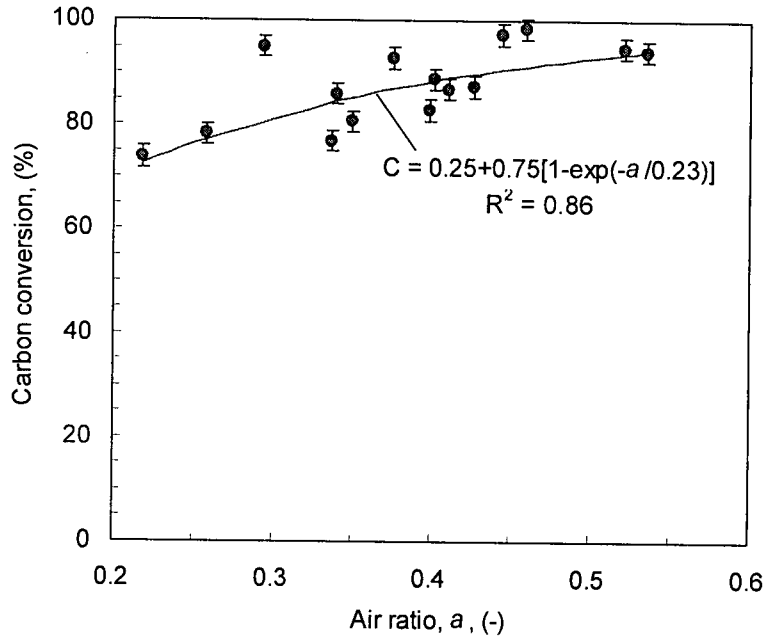

Figure 5-1. Effect of air ratio on carbon conversion to gas: Data from Runs 1-15, T_3 = 970-1090 K, a = 0.21-0.54, M = 4.2-22.0%.

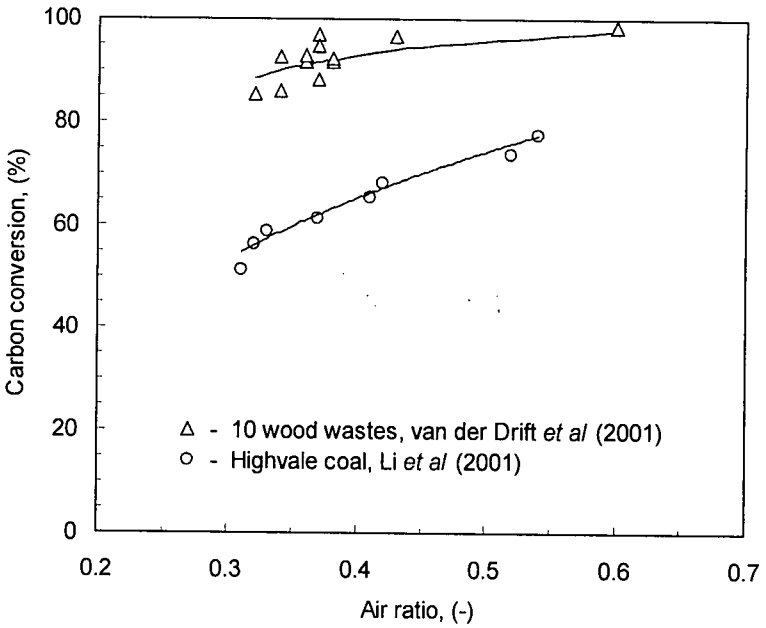

Figure 5-2. Carbon conversion vs. air ratio: previous work for comparison: ○ - Li *et al.*, 2001, T = 970-1150 K, a = 0.31-0.54, M = 9.0%; Δ - van der Drift et al (2001), T = 1070-1130 K, a = 0.32-0.60, M = 3.5-17.5%.

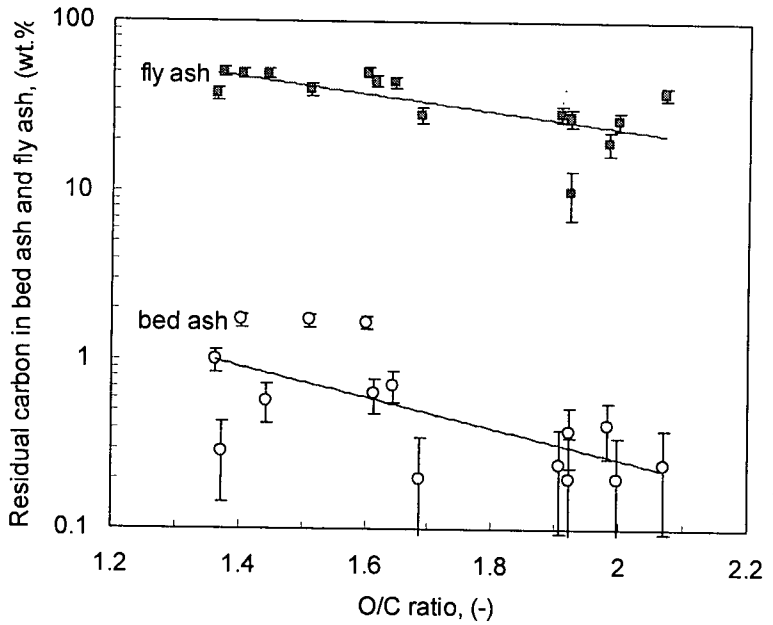

Figure 5-3. Effect of O/C ratio on residual carbon contents in the bed ash and fly ash. Data from Runs 1-15. Operating temperature T_3 varied between 970 and 1090 K.

Note that, sawdust shows a much higher carbon conversion and reactivity than the Highvale coal. Gasified in the same reactor and operating at a similar range of air ratio and slightly higher temperature (970-1150 K), the carbon conversion for the Highvale coal varies between 40-78%. This difference is partly attributed to the high ash content and low reactivity of the coal that increases the diffusion resistance for the gaseous reactants. Another difference is likely to relate to how carbon is bound chemically in the coal and in the biomass.

The residual carbon contents in the bed ash and fly ash are shown in Figure 5-3. Carbon content in the bed ash was always less than 2% for the parameter ranges tested, showing that the circulating fluidized bed offered sufficient residence time for the gasification of coarser char particles. However, the carbon content in the fine fly ash collected from the filter unit was as high as 15-65%, depending on the operating temperature and air ratio, representing a major part of the total carbon loss. One likely reason for the high residual carbon content in the fly ash is the insufficient separation efficiency of the high-temperature cyclone.

The boundary layer separation theory (Leith and Licht, 1972; Dirgo and Leith, 1986) indicates that the grade efficiency of a cyclone increases with increasing dimensionless particle size (d_p/d_{50}), i.e.

$$\eta_i = 1 - \exp\left[-a\left(\frac{d_p}{d_{50}}\right)^{1/(1+n)}\right] \tag{5-6}$$

with $a = 0.693$, and the cut size for 50% grade efficiency being

$$d_{50} = \sqrt{\frac{9\mu b}{2\pi N_c(\rho_p - \rho_g)U_i}} \tag{5-7}$$

where μ is the gas dynamic viscosity, N_c the number of revolutions traveled by a particle in the cyclone before leaving or captured by the boundary layer, $(\rho_p - \rho_g)$ is the difference in density between the particle and the gas (kg/m^3), and U_i is the inlet velocity of the particle-laden gas. The equations were derived for standard cyclone designs with inlet width being a quarter of the cyclone cylinder diameter.

Eq. (5-7) shows that the cut size is inversely proportional to the particle-gas density difference $(\rho_p - \rho_g)$ squared. Because the density of sawdust char particles is less than 100 kg/m^3, the centrifugal force exerted on a sawdust particle is an order of magnitude smaller than that exerted on a coal ash particle of the same diameter. Therefore, the cut size of the cyclone for sawdust char articles is ~3-4 times larger than for coal char particles.

The fly ash was found to contain mostly fine sawdust char and silica sand, with a small portion of coal ash produced during the start-up stage. The measured mean diameter of the fly ash collected by the filter unit was nearly 60 μm, much larger than for the coal, also causing considerable carbon loss. In Runs 8-10, these fine particles were re-injected into the bottom of the reactor. However, as in their first trip through the reaction zone, they also tend to escape

from the cyclone again. Thus, once-through fly ash re-injection cannot convert all the residual carbon.

5.3 Elemental Distributions

The time-mean species contents are plotted in Figure 5-4 against the O/C ratio. This figure shows substantial agreement with the instantaneous data in Figure 4-6. As expected, CO, H_2 and CH_4 decrease as O/C molar ratio increases, while CO_2 increases. Based on these mean species contents, we can determine the product distribution for each element present in the gasification system.

The distribution of carbon among four major product species is shown in Figure 5-5. As expected, the percentage of carbon that remains as unconverted solid carbon decreases with the O/C ratio. A similar decreasing trend is found with the CO portion. The portion accounted for by CH_4 is insensitive to air supply, which again suggests that CH_4 is primarily a product of pyrolysis. Only the CO_2 portion increases with the air ratio. For an O/C ratio of 1.6, about 45% of the total moles of carbon in the system is converted to CO_2, 39% to CO, 8% to leave the reaction zone as CH_4, and the remaining 8% as unconverted carbon. Tar only contributes to less than 0.5% in the carbon distribution.

Figure 5-6 shows the hydrogen distribution. H_2O is always the dominant carrier of hydrogen. The portions accounted for by combustible gas species (H_2 and CH_4) increase with decreasing O/C ratio. Since steam was injected in only two runs, the high content of the off-gas water suggests generally ineffective use of fuel-bound moisture content. Note, however, that the framed points indicate that reforming catalyst addition helps improve the water conversion.

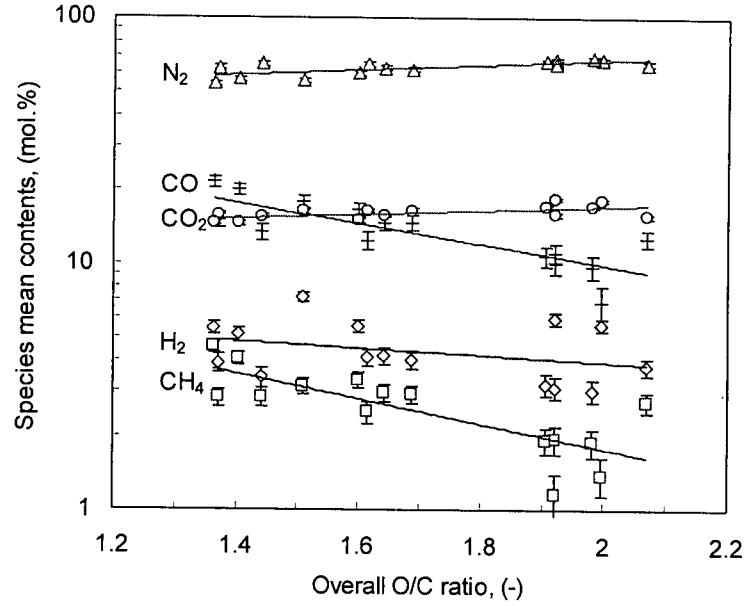

Figure 5-4. Effect of overall O/C molar ratio on mean gas composition. Data from Runs 1-15. a = 0.21-0.54, T_3 = 970-1090 K, M = 4.2-22.0%.

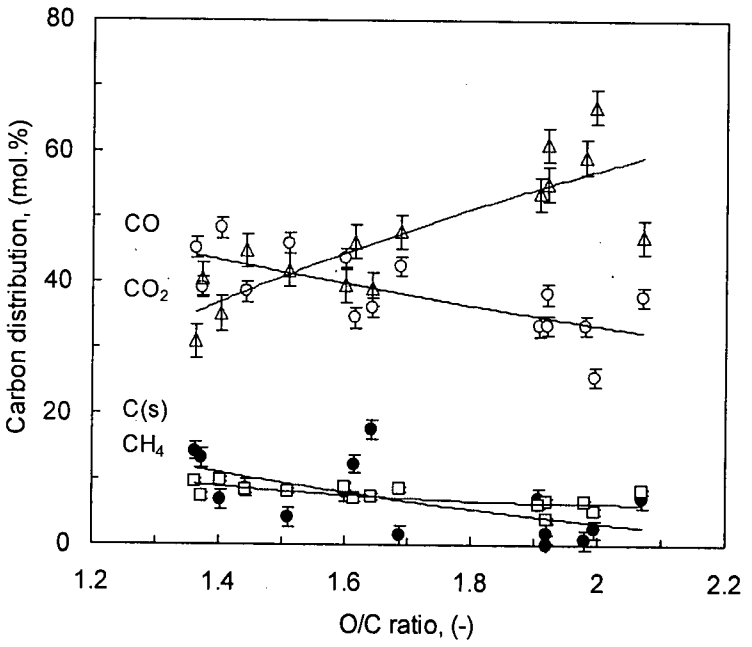

Figure 5-5. Variation of carbon distribution with O/C ratio: • – C(s) or unconverted carbon, □ – CH_4, ∗ – CO, Δ – CO_2. Data from Runs 1-15. a = 0.21-0.54, T_3 = 970-1090 K, M = 4.2-22.0%.

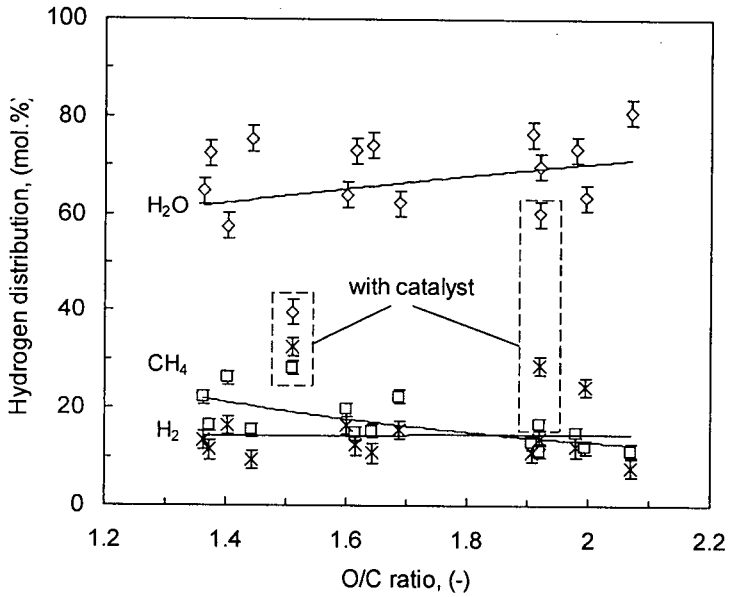

Figure 5-6. Variation of hydrogen distribution with O/C ratio: □ – CH_4, + – H_2, ◇– H_2O. Data from Runs 1-15. a = 0.21-0.54, T_3 = 970-1090 K, M = 4.2-22.0%.

Chapter 6 discusses the impact of unconverted carbon and methane on equilibrium model prediction of gas composition from a biomass gasifier. Figure 5-7 provides quantitative data, as well as simplified correlations for the methane impact on the carbon and hydrogen balance. It is found from our pilot plant study that methane accounts for about 12-18% of the total hydrogen and 5-9% of the total carbon present in the gasification system. If methane is assumed to result from pyrolysis, and kinetically controlled, this portion of hydrogen and carbon should also be withdrawn from the equilibrium system when kinetic modifications are introduced into the equilibrium model.

Figure 5-8 shows the oxygen distribution in the product gas. The majority of the oxygen supplied together with air is consumed in producing CO_2 and water; a smaller portion, about 15-30%, forms CO, and this portion decreases with increasing O/C ratio. However, production of CO_2 and H_2O is a necessary feature of air gasification because both reactions provide the heat needed to maintain the desired operating temperature in the gasifier.

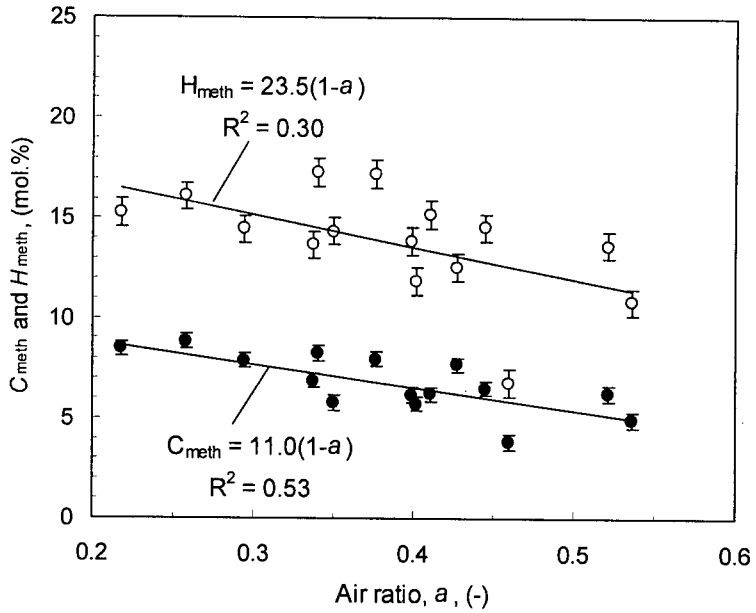

Figure 5-7. Effect of air ratio on the percentages of carbon and hydrogen that remain in methane in the product gas. Data from Runs 1-15. a = 0.21-0.54, T_3 = 970-1090 K, M = 4.2-22.0%.

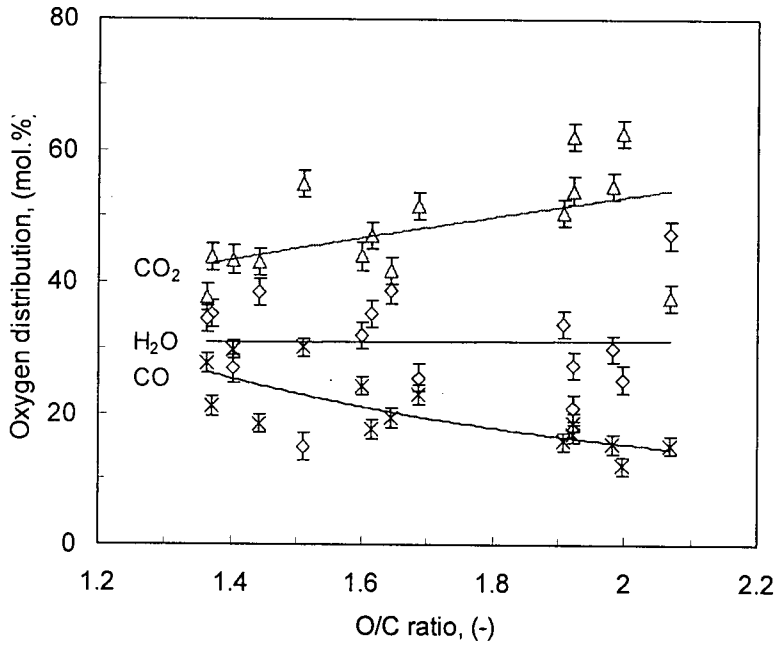

Figure 5-8. Variation of oxygen distribution with the O/C ratio: ∗ – CO, ◇– H_2O, Δ – CO_2. Data from Runs 1-15. a = 0.21-0.54, T_3 = 970-1090 K, M = 4.2-22.0%.

5.4 Gasification Efficiency

There are several ways for evaluating the performance of a gasification system. The *thermal efficiency* is calculated from the total energy input, i.e.

$$\eta_g = \frac{([\mathrm{HHV}]_g + H_g) \times v_g}{[\mathrm{GCV}]_f + \dot{m}_{af}[\mathrm{GCV}]_{af} + H_f + W} \times 100\%, \tag{5-8}$$

where $[\mathrm{HHV}]_g$ (in MJ/Nm^3) is the higher heating value of the product gas, while $[\mathrm{GCV}]_f$ (in MJ/kg) and $[\mathrm{GCV}]_{af}$ (in MJ/kg) denote the gross calorific values of the main fuel and auxiliary fuel, respectively. $\dot{m}_{af}$ is the feed rate of auxiliary fuel relative to that of the main fuel (abbreviated as mf), in kg/kg. v_g is the specific dry gas volume, in Nm^3/kg-mf. H_f and H_g are the sensible heats of the feedstock and product gas, both in MJ/kg-mf, respectively. W is the electrical power used to compress the air supplied to gasify the main fuel, in MJ/kg-mf. In cases where steam is injected, the enthalpy of steam should also be accounted for as an input term. In Eq. (5-8), all the input and output terms should be based on 1 kg of main fuel (as-received basis).

An alternative efficiency, the *cold-gas gasification efficiency*, E_1, excluding the heating value of the condensables (tars), is defined as the percentage of fuel heating value converted into the heating value of the product gas, i.e.

$$E_1 = \frac{[\mathrm{HHV}]_g \times v_g}{[\mathrm{GCV}]_f} \times 100\% \tag{5-9}$$

Since the sensible heat of the feed streams is ignored in this equation, E_1 is called the gasification efficiency, rather than a thermal efficiency which takes into account the sensible heats of all feed and product streams. E_1 is a direct measure of the gasification gains.

A modified cold-gas efficiency, taking account of the heating value of any tars, is defined as

$$E_2 = \frac{[\mathrm{HHV}]_g \times v_g + [\mathrm{HHV}]_t \times y_t}{[\mathrm{GCV}]_f} \times 100\%. \quad (5\text{-}10)$$

Here y_t is the specific tar yield in g/kg-fuel, and $[\mathrm{HHV}]_t$ is the heating value of tar, taken as 30.1 kJ/g-tar (or 30.1 MJ/kg-tar), estimated with Eq. (4-12) from the tar analysis data. E_1 and E_2 have both been extensively widely used in the gasification literature (e.g. Hebden and Stroud, 1981; Probstein and Hicks, 1982).

In the present study, the enthalpy of the product gas and hot water produced by the heat exchangers is not utilized in any downstream equipment. Moreover, the enthalpy of the product gas increases with increasing air ratio, and is maximized under combustion conditions. Hence inclusion of the gas enthalpy term always favours higher air ratios, while the energy converted into the product gas heating value is decreased. Thus, the cold-gas efficiency seems more pertinent than the thermal efficiency in assessing the performance of the process. However, in some cases, external heat is requires to maintain the operating temperature of the system. The cold gas efficiency, being unable to account for the external heat supply, then becomes insufficient. Considering these factors, a modified gasification efficiency is proposed:

$$E = \frac{[\mathrm{HHV}]_g \times v_g}{[\mathrm{GCV}]_f + H_{ext}} \times 100\%, \quad (5\text{-}11)$$

in which H_{ext} is the external heat supplied to the gasifier to maintain the desired operating temperature, in MJ/kg-mf. When there is no external heat source, as in the present study, E is identical to the cold gas efficiency E_1.

The specific gas yield, v_g, can either be based on 1 kg of sawdust feed, or 1 Nm^3 of air supply, designated v_{gs} (Nm^3/kg-sawdust) and v_{ga} (Nm^3/Nm^3-air), respectively. These two parameters were determined based on nitrogen balance and shown in Figure 5-9. It is found that v_{gs} increases with increasing air ratio, while v_{ga} decreases slightly. Both trends are consistent

with first principles. If the air ratio further increases and exceeds 1, the net gas production eventually ceases to increase, as the product gas is then a mixture of air and combustion gas. v_{gs} then becomes proportional to the air ratio, while v_{ga} approaches unity.

A small amount of ethylene and higher hydrocarbons may exist in the gas, contributing up to 5% of the total gas heating value (van der Drift *et al.*, 2001). In this project, the measured C_2H_4 content varied from 0-1.4 %. Unfortunately, the C_2H_4 peak in the gas chromatograph overlaps with the moisture peak for the type of GC column employed and operating conditions used. Therefore, in most gas samples, the ethylene content was taken as zero whenever there was any uncertainty in differentiating it from a moisture peak. With the product gas usually containing 10-20% moisture, the moisture remaining in the gas samples could be as high as 0.5-1%, assuming a moisture removal of 95%. Therefore, what appears to be C_2H_4 content might actually be moisture remaining in the gas. A previous study by van der Drift et al (2001) reports up to 2% ethylene in the gas. It is estimated from their data that the CH_4/C_2H_4 molar ratio is about 2.74 for all the test runs. To make a direct comparison with their data in our mass balance calculations, an estimated C_2H_4 content based on this empirical CH_4/C_2H_4 molar ratio was added to the gas composition to provide a modified gas composition, based on which new gas heating values and thermal efficiencies were determined. This modification could cause up to 3 percent difference in the cold-gas efficiency.

The gasification efficiencies E_1 and E_2 calculated from the mass and energy balance are plotted in Figure 5-10 against the O/C ratio. The gasification efficiencies decrease somewhat with increasing air supply, despite an increase in the carbon conversion. Since the gas heating value diminishes with increasing O/C ratio, the gasification efficiencies will finally decrease to zero under combustion conditions, while the overall carbon conversion approaches unity.

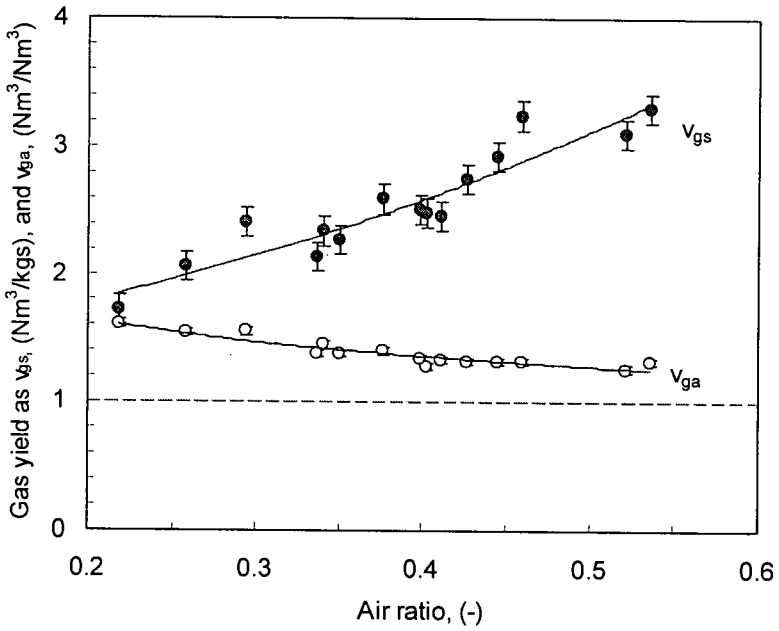

Figure 5-9. Variations of specific gas yield with air ratio. Data from Runs 1-15. a = 0.21-0.54, T_3 = 970-1090 K, M = 4.2-22.0%.

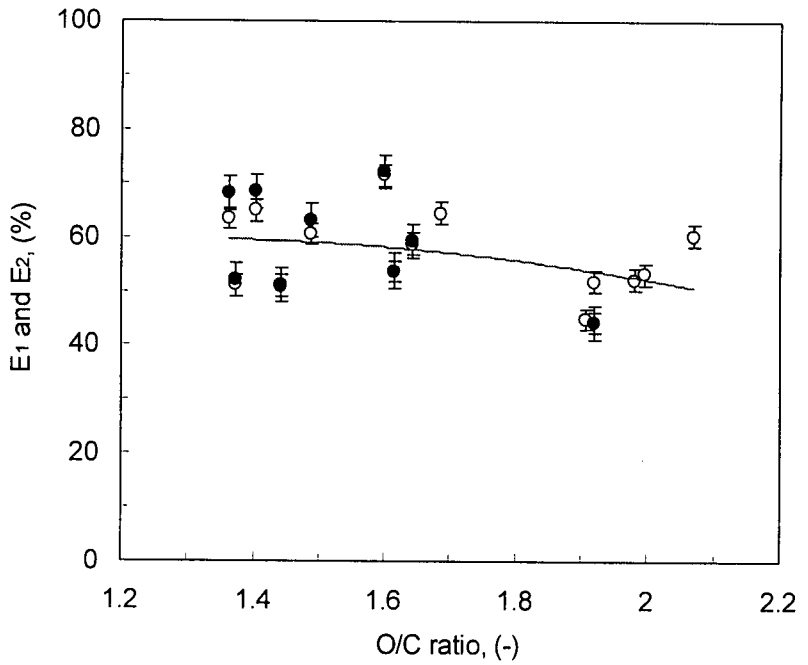

Figure 5-10. Variation of gasification efficiency with O/C ratio. Data from Runs 1-15. a = 0.21-0.54, T_3 = 970-1090 K, M = 4.2-22.0%. ○ – E_1, only product gas considered; ● – E_2, tar also taken into account.

Little is known about how the cold-gas efficiency changes as the air ratio further decreases to zero. From TGA analysis we know that when no oxidant is supplied to the reactor, the pyrolysis of sawdust produces about 20% chars (unconverted carbon) at lower heating rates. However, at very high heating rates, as in a fluidized bed reactor, char is not favoured as a pyrolysis product, and the carbon conversion can be as much as 95% (Probstein and Hicks, 1982). Therefore, at least in theory, the cold-gas efficiency should continue to increase with decreasing air ratio if an external heat source is available to maintain the desired operating temperature, and if the solids residence time is long enough in the gasifier. Surface heat losses decrease as the reactor is scaled up. However, as far as the pilot CFB gasifier was concerned, the operating temperature in the self-heated system decreased with decreasing air ratio. Thus, pyrolysis again favours production of char, CO_2 and water, causing a decrease in efficiency. It is therefore recommended to maintain the O/C ratio within a proper range to maximize the gasification efficiency while keeping the tar yield low.

Figure 5-10 suggests that O/C should be in the range 1.5-1.7 for the species and parameters tested. The declining gasification efficiency with increasing air or O/C ratio also reveals that the carbon conversion does not determine the effectiveness of the gasification process. Instead, the gasification efficiencies defined in Eqs. (5-9) to (5-11) provide more pertinent measures of the performance of a gasifier.

5.5 Summary

This chapter examines the overall carbon conversion and gasification efficiency based on mass and energy balances for each test run. Good mass balance closure is found between the feed and the product streams. The following conclusions can be drawn:

(1) Elemental mass balances indicate that a large fraction of the oxygen, about half of the carbon and a considerable portion of the hydrogen are consumed to produce CO_2 and H_2O. Improving gas quality from gasification requires that the proportion of these two species be decreased.

(2) While carbon conversion increased with increasing O/C ratio, the cold-gas gasification efficiency decreased. Therefore, carbon conversion is not a sufficient criterion for evaluating gasification process. Gasification efficiency can be maximized within an optimum range of air ratio (O/C = 1.5-1.7, or a = 0.30-0.35), while keeping the tar yield relatively low.

(3) Residual carbon content in the bottom ash was less than 2% over the parameter ranges tested. However, the low particle density of char results in a larger cut size of the cyclone and decreased cyclone grade efficiency, leading to the high residual carbon content in the fly ash. Fly ash re-injection, though quite effective in improving the gas heating value, cannot convert all the residual carbon.

CHAPTER 6. EQUILIBRIUM MODELING OF BIOMASS GASIFICATION

6.1 Introduction

There have been several different types of models for gasification systems - kinetic, equilibrium, and other. In this chapter, numerical results from an equilibrium model based on free energy minimization are presented. Unlike a kinetic model that predicts the progress and product composition at different positions along the reacting flow continuum, usually by coupling reaction kinetics with fluid dynamics and mass transfer in a multiphase flow, an equilibrium model considers the gasifier as a system which has attained its maximum possible conversion. The objective of the equilibrium model is, in the first place, to predict the maximum achievable yield of a desired product from a reacting system after infinitely long time for given operating conditions. This assists in obtaining in-depth understanding of the process based on thermodynamic principles. It also provides a very useful design aid in evaluating the limiting possible behaviour of a complex reacting system. The equilibrium model assumes that the system in consideration is in chemical equilibrium. The present study also shows that kinetic modification can be introduced to apply the model to systems do not fully achieve equilibrium.

A chemical reaction system is said to be in chemical equilibrium when there is no further change in the moles of all the species present. At equilibrium the reacting system is at its most stable composition, a condition which is met when the entropy of system is maximized, while its Gibbs free energy is minimized. Without losing generality, consider a constant-temperature, constant-pressure reacting system. Chemical equilibrium is achieved when

$$\left(\frac{\partial G^{tot}}{\partial \varepsilon}\right)_{T,P} = \sum_i n_i \mu_i = 0, \qquad (i = 1, 2, \ldots, N) \qquad (6\text{-}1)$$

subject to the closed-system constraint (i.e. mass conservation) and non-negativity constraints for each of the elements involved. Here G^{tot} is a state function, i.e. the total Gibbs free energy of the system with a total number of moles n; ε refers to the dimensionless reaction coordinate, also called the degree of advancement, degree of reaction, and progress variable. T and P denote the system temperature and pressure, respectively; n_i is the number of moles of the i-th species, while μ_i is its specific chemical potential.

The Gibbs free energy is a thermodynamic function defined as

$$G = H - TS, \tag{6-2}$$

where H is the enthalpy, and S is the entropy. G is a function of temperature, pressure and number of moles.

The chemical potential of the i-th species is defined as

$$\mu_i = \left(\frac{\partial G^{tot}}{\partial n_i} \right)_{T,P,n_j} \tag{6-3}$$

with n_j being the moles of any species other than the species concerned ($j \neq i$).

For a single-phase system, the total free energy can be written as

$$G^{tot}_{T,P} = G(n_1, n_2, \cdots n_N) \tag{6-4}$$

where subscripts T, P denote the temperature and pressure. The number of moles of each species present in the system, $n_i > 0$ ($i = 1, 2, \ldots N$), is determined by assuming simultaneous equilibrium of all relevant chemical reactions.

The mathematical theory of chemical equilibrium was formulated by Gibbs (1876) and van't Hoff (1898). However, it was not until fifty years later when Brinkley (1947) first laid the foundation for general-purpose algorithms for the computation of chemical equilibrium. The solution of chemical equilibrium problems is to find a set of species moles n_i to minimize the

total free energy. There are two formulations of the equilibrium conditions, stoichiometric and non-stoichiometric, leading to two approaches to equilibrium modeling (Smith and Missen, 1982):

(1) The classical, stoichiometric formulation, in which the closed-system constraint is treated by means of stoichiometric equations so as to result in an essentially unconstrained minimization problem, and

(2) The non-stoichiometric formulation (Smith and Missen, 1968; Zeleznik, 1968; Van Zegeren and Storey, 1970), in which stoichiometric equations are not used but, the closed-system constraint is treated by means of Lagrange multipliers for constrained optimization.

The concept of direct free energy minimization was attributed to White *et al.* (1958), who proposed a method for numerical solution of chemical equilibrium without using any stoichiometric equations or reactions. Despite a decade-long controversy between the stoichiometric and non-stoichiometric (i.e. direct free energy minimization) formulations, they are essentially equivalent, as shown in Smith and Missen (1982). However, in practice, the two formulations differ in many ways. The widely used stoichiometric formulation requires a clearly defined reaction mechanism, expressed by a set of simultaneous reversible chemical reactions. The outcome of a general chemical reaction in the reaction mechanism,

$$\nu_1 A_1 + \nu_2 A_2 + \cdots \Leftrightarrow \nu_3 A_3 + \nu_4 A_4 + \cdots, \tag{6-5}$$

can be characterized by its equilibrium constant K:

$$K = \exp\left(\frac{-\Delta G_T^0}{RT}\right) = \frac{\prod(a_i^{\nu_i})_{\text{products}}}{\prod(a_i^{\nu_i})_{\text{reactants}}}, \tag{6-6}$$

where K is a dimensionless number whose value is only dependent on the temperature. ΔG_T^0 is the standard free energy change for the reaction proceeding to completion. It can be determined from the standard free energies of formation of the species involved in the reaction.

However, not all chemical reaction systems have clearly understood reaction mechanisms; many are simplified into lumped mechanisms with a small number of reactions involving a limited number of species. Dealt with by the stoichiometric approach, the quality of the solution depends on the appropriateness of the lumping mechanism. The Gibbs free energy of the system found by the stoichiometric approach might be a local minimum, rather than a global minimum, if the mechanism is inaccurate or oversimplified. In complex reaction systems such as those in combustion or gasification equipment, it is sometimes impossible to write a lumped reaction mechanism. The stoichiometric formulation is unable to tackle such problems.

Moreover, the stoichiometric formulation requires clearly defined species on both sides of each reaction in the reaction mechanism. This is even more difficult in actual applications of the stoichiometric model. In biomass gasification, for example, the chemical formula of the biomass feed is either unknown, or identified as a mixture of a large number of chemical species. In such cases, it would be difficult to choose a few particular compounds in order to calculate the equilibrium constants of the reactions involving them. In stoichiometric modeling, one assumes a composition of pyrolysis products, with a few major species listed, as input for numerical solution. This method is simple and practical, but it deviates from reality, and implies that the numerical solution only commences after the pyrolysis stage.

In a non-stoichiometric formulation, on the other hand, no particular reaction mechanism or species are involved in the numerical solution. The only input data needed to specify the feed is its elemental composition, which can be readily obtained from ultimate analysis data. Since there is no need to reduce a complex reaction system to a simplified mechanism with a few reactions,

it is free of the disadvantage of the stoichiometric formulation. The Gibbs free energy found by the numerical model is guaranteed to be a global minimum value if the convergence tester is good enough. This method is particularly suitable for problems with unclear reaction mechanisms and feed streams whose precise chemical compositions are unknown. Given these advantages, the non-stoichiometric formulation was employed in the present study.

6.2 Overall Description of the Process

The actual gasifier, as shown in Figure 3-1, is a continuous flowing and reacting system intended for steady-state operation at constant pressure. In the equilibrium model, however, the reactor is seen as zero-dimensional, which means that no spatial distribution of parameters will be considered, nor will there be any change effected with time because all forward and reverse reactions have reached chemical equilibrium. Figure 6-1 shows all feed and product streams. Tars are not included in the product stream because of low yield under gasification conditions.

The materials fed to the system may include biomass, air as the fluidizing agent, steam for carbon-steam reaction and re-injected fly ash. The chemical compositions of all feed streams, including the main fuel (sawdust), the auxiliary fuel (Highvale coal) and the oxidizing agent (air and steam), are given in the database established for the equilibrium model (Appendix X). The molar inflow for any individual element involved in the chemical reactions can be written as the sum of moles of that element in different feed streams.

Five elements are considered here, these being the most common elements in biomass and coal: C, H, O, N and S. From steady state molar balances, the total molar flow of each element in the product streams equals that in the feed streams. Some elements may be completely converted into the constituent compounds of the product gas, some are almost inert during the process, and

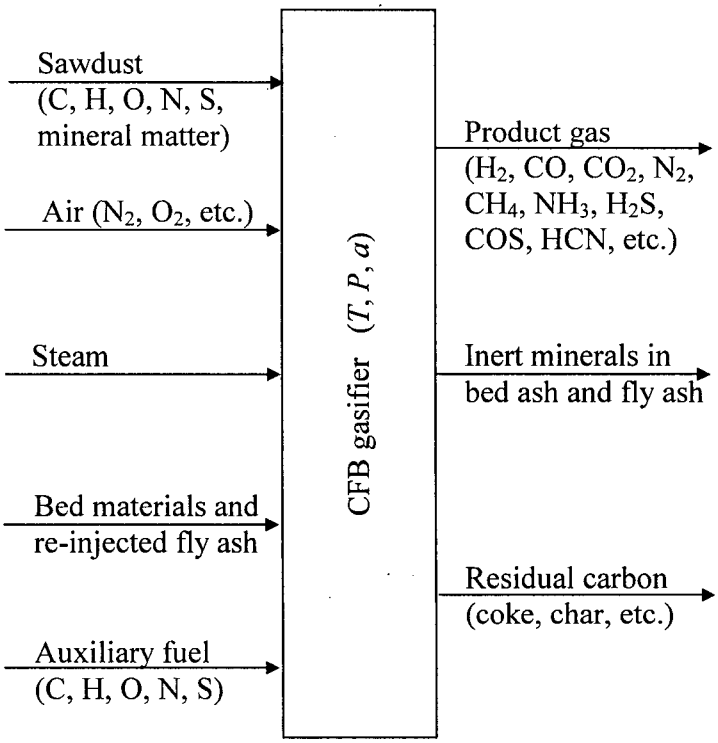

Figure 6-1. Feed and product streams entering and leaving the gasifier.

others are partially converted, and present in both the gaseous products and in the condensed phase, i.e. solid species as single-species phases and possibly an ideal solution of liquid species. All sulfur and nitrogen contents in the biomass are considered to be reactive.

Fixed carbon is considered as only partially gasified in the process because the relatively low reactivity of the solid phase makes the residence time inadequate to reach equilibrium conversion. This means that a conversion efficiency may be imposed on carbon in a kinetically-modified equilibrium model. There are certainly other elements present in the fuel and air supply (e.g. Si entering as SiO_2, and mineral matter in the biomass), but they are considered as inert or independent of the reaction system, and are therefore excluded in the element-species matrix. Although carbon, oxygen and sulfur may be present in mineral matter (e.g. as carbonates and sulfates), and may be converted during gasification, inorganic C, O and S contribute only a very

small fraction in the elemental abundance of the system. Little error therefore results when they are ignored in equilibrium modeling. Other elements in the mineral matter (Si, Ca, Cl, Na, etc.) are grouped as the non-process elements (NPE) in a previous study of black liquor gasification in which a greater proportion of mineral matter is involved than in sawdust gasification, and dealt with separately from the main process and major elements (Ulmgren *et al.*, 1999).

North American standard air composition (Lide, 1994) is used for determining the element abundance in air. Where no such standard information is available, it will not generate large error to assume that air consists of 21 vol.% oxygen and 79 vol.% nitrogen. Since the amount of air is often recorded as the volumetric flow rate under standard-state (i.e. in Nm^3/h), the numbers of moles of oxygen and nitrogen can be easily calculated from the volumetric flow rate data. The stoichiometric air for the fuel used is computed from its elemental analysis, as listed in Chapter 3, Table 3-1.

6.3 The Model

To simplify the problem, only 42 gaseous species and 2 solid species are considered in the present work, as listed in Table 6-1, with these species involving only C, H, O, N and S. The gaseous species form a homogeneous phase, while the two solid species are considered single-species phases. In order to predict emissions, key species involved in nitrogen and sulfur chemistry are included. The ash is considered to be inert, adding only to the thermal capacity in the reactor.

Table 6-1. Species considered in the equilibrium model.

Group	Chemical Formula
(1)	C(g), CH, CH_2, CH_3, CH_4, C_2H_2, C_2H_4, C_2H_6, C_3H_8
(2)	H, H_2, O, O_2, CO, CO_2, OH, H_2O, H_2O_2, HCO, HO_2
(3)	N, N_2, NCO, NH, NH_2, NH_3, N_2O, NO, NO_2, CN, HCN, HCNO
(4)	S(g), S_2(g), SO, SO_2, SO_3, COS, CS, CS_2, HS, H_2S
(5)	C(s), S(s)

6.3.1 RAND algorithm

The RAND algorithm proposed by White *et al.* (1958) can reduce the working matrix of the problem to $(K+\pi)$ by $(K+\pi)$, where K and π represent the number of elements and phases, respectively. The mathematical aspects of this algorithm are well-documented in previous literature (White *et al.*, 1958; Zeleznik, 1968; Smith and Missen, 1982). The algorithm allows the change in moles of a species in the m-th iteration to be expressed explicitly as a function of its current chemical potential, the phase distribution of the species at a given system temperature and pressure, and the Lagrange multiplier:

$$\delta n_i^{(m)} = n_i^{(m)}\left(\sum_{k=1}^{K} a_{ik}\psi_k + u_\alpha - \frac{\mu_i^{(m)}}{RT}\right) \quad \text{for multispecies phases;}$$
$$= u_\alpha n_i^{(m)} \quad \text{for single-species phases.} \tag{6-7}$$

$$(i = 1, 2, \ldots N;\ k = 1, 2, \ldots K;\ \alpha = 1, 2, \ldots \pi)$$

These $\delta n_i^{(m)}$ constitute a vector $\delta \boldsymbol{n}^{(m)}$, which is the change of number of moles for all species upon the current iteration. N designates the total number of species. $n_i^{(m)}$ denotes the moles of species i in the m-th iteration; a_{ik} is the coefficient in the species-element matrix. ψ_k is a function related to the Lagrange multiplier, λ_k, i.e.

$$\psi_k = \frac{\lambda_k}{RT}. \tag{6-8}$$

u_α is the phase split of δn_i, defined as

$$u_\alpha = \sum_{i=1}^{N} \delta n_{i\alpha}^{(m)} / n_t^{(m)} = \delta n_{t\alpha}^{(m)} / n_t^{(m)}, \tag{6-9}$$

where the subscript t means total; α refers to the phase to which a species belongs.

The set of $(K+\pi)$ simultaneous algebraic equations that are to be solved iteratively by the RAND algorithm includes K linear equations regarding element abundance:

$$\sum_{k=1}^{K}\sum_{i=1}^{N} a_{ik}a_{ij}n_i^{(m)}\psi_k + \sum_{\alpha=1}^{\pi} b_{j\alpha}^{(m)}u_\alpha = \sum_{i=1}^{N} a_{ij}n_k^{(m)}\frac{\mu_i^{(m)}}{RT} + b_k - b_k^{(m)}. \quad (j = 1, 2, \ldots, K) \tag{6-10}$$

The π supplementary equations for different phases are:

$$\sum_{k=1}^{K} b_{k\alpha}^{(m)}\psi_k - n_{z\alpha}u_\alpha = \sum_{i=1}^{N} n_{i\alpha}^{(m)}\frac{\mu_{i\alpha}^{(m)}}{RT}. \qquad (\alpha = 1, 2, \ldots, \pi) \tag{6-11}$$

The initial element abundance vector b is calculated from the feedstock. The k-th element of the b-vector at the m-th iteration is

$$b_k^{(m)} = \sum_{i=1}^{N} a_{ik}n_i^{(m)}. \tag{6-12}$$

Mass balance constraints are imposed at every iteration during solution of Eqs. (6-7) to (6-12), while the algorithm iteratively minimizes the Gibbs free energy. As suggested by Smith and Missen (1982), the difference between the initial elemental abundance vector and its current iteration value, $(b_k - b_k^{(m)})$, is added to the right-hand side of Eq. (6-10) to eliminate error accumulation during the iteration process.

Finally, the new numbers of moles vector, $\mathbf{n}^{(m+1)}$, is determined by:

$$\mathbf{n}^{(m+1)} = \mathbf{n}^{(m)} + \omega^{(m)} \delta \mathbf{n}^{(m)} \tag{6-13}$$

where $\omega^{(m)}$ is the step size parameter, $0 < \omega^{(m)} < 1$, chosen such that all new moles generated from the current iteration remain positive. The new molar fractions of all species are then determined by

$$x_i = n_i / n_t \tag{6-14}$$

Note that all molar fractions are subject to the non-negativity constraint. Other quantities, such as elemental distributions, carbon conversion, water coversion, are all derived from the variables in Eq. (6-14).

6.3.2 Chemical potentials

The equilibrium system is assumed to consist of a major ideal gas mixture and some single-species phases (to consider liquid and solid species). The chemical potential of a species in an ideal solution is calculated by the Raoult convention (for the case when the standard state is a pure substance) expression:

$$\mu_i(T, P, x_i) = \mu_i^*(T, P) + RT \ln x_i \tag{6-15}$$

where T, P and x_i stand for operating temperature, system pressure, and molar fraction of a given species, respectively. $\mu_i^*(T, P)$ is the chemical potential of species i as a function of T and P, i.e. the chemical potential of pure species i at (T, P) of the system in the same physical state.

For an ideal gas mixture Eq. (6-15) becomes

$$\mu(T,P,x_i) = \mu_i^o(T) + RT\ln P + RT\ln x_i, \tag{6-16}$$

where the first term on the right-hand side, $\mu^o(T)$, denotes the standard chemical potential at 1 bar. The most convenient way to determine $\mu^o(T)$ is to identify it with the free energy of formation of a species, i.e.:

$$\mu_i^o(T) = \Delta G_{fi}^o(T). \tag{6-17}$$

The chemical potential of a species in an ideal solution depends only on its own concentration and not on the concentrations of the other species present in the system. The chemical potentials of the solid and liquid species are estimated by Eq. (6-15) together with:

$$\mu_i^*(T,p) \approx \mu_i^o(T) + RT\ln P_i^*, \tag{6-18}$$

where P_i^* is the vapor pressure of the liquid or solid (Smith and Missen, 1982).

6.3.3 Energy balance

The energy balance of the process can be written:

$$\sum_l^L m_l \Delta H^{\circ}_{f,298,\text{feed}} + \sum_l^L m_l H_{\text{feed}}(T_{\text{feed},l}) = \sum_i^N n_i \Delta H^{\circ}_{f,298,\text{prod}} + \sum_i^N n_i H_{\text{prod}}(T) + \Delta H(T)$$

$$(l = 1, 2, \ldots, L) \tag{6-19}$$

for any temperature T. The two terms on the left-hand side are the total heat of formation and the total enthalpy of all feed streams, respectively. The first two terms on the right-hand side represent the total heat of formation and total enthalpy of all product species, respectively. The final term, $\Delta H(T)$, denotes the system net energy excess production as a function of temperature. This term can also be extended to account for any heat removed from the reactor or provided by an external heat source. If $\Delta H(T)$ is positive the system adjusts its equilibrium temperature to a higher level. The equilibrium temperature of the system is the temperature at which $\Delta H(T) = 0$.

Eq. (6-19) is based on 1 kg of fuel (dry basis). Note that although different units are involved for m and n, with the ultimate analysis of fuel, all the terms on both sides of the equation are converted into MJ by multiplying by enthalpies expressed in MJ/Nm^3, MJ/kg or kJ/mol as needed.

The heats of formation of the oxidant and steam can be determined from standard thermodynamic data (Pankratz, 1982; Chase *et al.*, 1985). The heat of formation of fuel, in kJ/kg fuel as received, is calculated from the following equation (Li *et al.*, 2001):

$$\Delta H^{\circ}_{f,298,fuel} = \mathrm{HHV} - (327.63C_{ar} + 1417.94H_{ar} + 92.57S_{ar} + 158.67M_{ar}), \qquad (6\text{-}20)$$

where HHV denotes the higher heating value of the fuel (kJ/kg, as-received basis). C_{ar}, H_{ar}, S_{ar} and M_{ar} represent the carbon, hydrogen, sulfur and moisture contents of the fuel (wt.%, as-received basis), respectively. This equation assumes that CO_2, H_2O and SO_2 are the only combustion products.

6.3.4 Thermodynamic properties and standard state

The following conventions are widely accepted for determining the standard states of gases, liquids and solids:

(1) For solid element: The most stable form at 1 bar and standard temperature;

(2) For liquid element: The most stable form at 1 bar and standard temperature;

(3) For gaseous species: Atmospheric pressure and the specified temperature;

(4) For carbon: Graphitic carbon;

(5) Standard temperature: 298 K (25°C).

The availability of thermodynamic data varies from species to species. In some sources thermodynamic properties are given by polynominal correlations, but tabulated data are more common. Standard-state conventions are used for all species considered. Here JANAF

thermodynamic data (Chase *et al.*, 1985), with 1 bar as the standard-state pressure, were chosen as the basic set, while some data were obtained from other sources (Holub and Vonka, 1976; Pankratz, 1982, 1984, 1987; Pankratz *et al.*, 1984; Gurvich *et al.*, 1990; Barin and Plazki, 1995). All free energy data are correlated by least-square linear regressions of the form:

$$\Delta G_f^o(T) = a_1 + b_1 T \ln T + c_1 T^2 + d_1 T^{-1} + e_1 T . \tag{6-21}$$

If the free energy of formation is not tabulated in the data source, it can be calculated from

$$\Delta G_f^o(T) = \Delta H_f^o(T) - T[S^o(T)_{comp} - \sum S^o(T)_{ele}] , \tag{6-22}$$

where subscripts *comp* and *ele* denote compound and elemental states, respectively. The entropy of the species, $S^o(T)$, is related to $C_p^o(T)$ by

$$S^o(T) = \int_0^T C_p^o(T) dT . \tag{6-23}$$

In most thermodynamic reference data books $S^o(T)$ is provided as tabulated data instead of correlations as for other functions. Sometimes the free energy is given as $\log K_f^o(T)$ in the tabulated data. When correlating them, the following equation is used:

$$\Delta G_f^o(T) = -2.30258 RT \log K_f^o(T) , \qquad \text{(kJ/mol)} \tag{6-24}$$

where 2.30258 is the conversion factor between natural and common logarithms.

The correlations for species enthalpy provided by Pankratz (1982, 1984, 1987) and Pankratz *et al.* (1984) assume the form:

$$H^\circ(T) - H_{298}^o = a_2 T + b_2 T^2 + c_2 T^{-1} + d_2 . \tag{6-25}$$

Although the underlying data of these correlations are based on 1 atm rather than 1 bar, the results from Eq. (6-25) are well within the practical measurement accuracy. Therefore, the correlation factors are used here without modification. A database was established which can be called and updated whenever needed. Each call to the database generates:

(a) Correlation factors for free energies of formation and enthalpy of each species,

(b) Species-element matrix and molar weights,

(c) Proximate and ultimate analyses of fuel, and composition of other feed streams.

6.3.5 Numerical solution procedure

The Matlab source code is listed in Appendix X. It consists of three parts: (1) a thermodynamic database and species-element matrix, (2) fuel properties database, and (3) numerical code for free energy minimization and energy balance. The flow chart for the RAND algorithm for both chemical equilibrium and energy balance calculations appears in Figure 6-2.

The convergence criterion is given as the maximum absolute value of the increases in the molar fractions for all species is less than an upper limit, i.e.,

$$\max\left|x_i^{(m+1)} - x_i^{(m)}\right| \le \varepsilon, \qquad i = 1, 2, \ldots, N. \tag{6-26}$$

The upper limit ε is usually set at 1×10^{-6} mole to ensure good accuracy as well as a true global minimum of the Gibbs free energy.

Smith and Missen (1982) reported that convergence in numerical solution of the RAND algorithm is almost assured by the use of a convergence forcer if a successful, non-negative initial guess is made. To ensure that the non-negativity constraint holds, linear programming (Press *et al.*, 1988) is often employed to provide the initial guesses. In our case, a small functional block was devised that examines the stoichiometry of the three major elements (C, H and O), finds the limiting element, and then generates an excess abundance vector, which tells how many moles of the other two elements should be subtracted as stable elemental species such as C(s), H_2(g) or O_2(g), with at least one of them zero. For all other species, a small positive value is initially specified. Numerical solution of the present equilibrium model indicates that an initial guess made in this manner suffices to guarantee quick convergence.

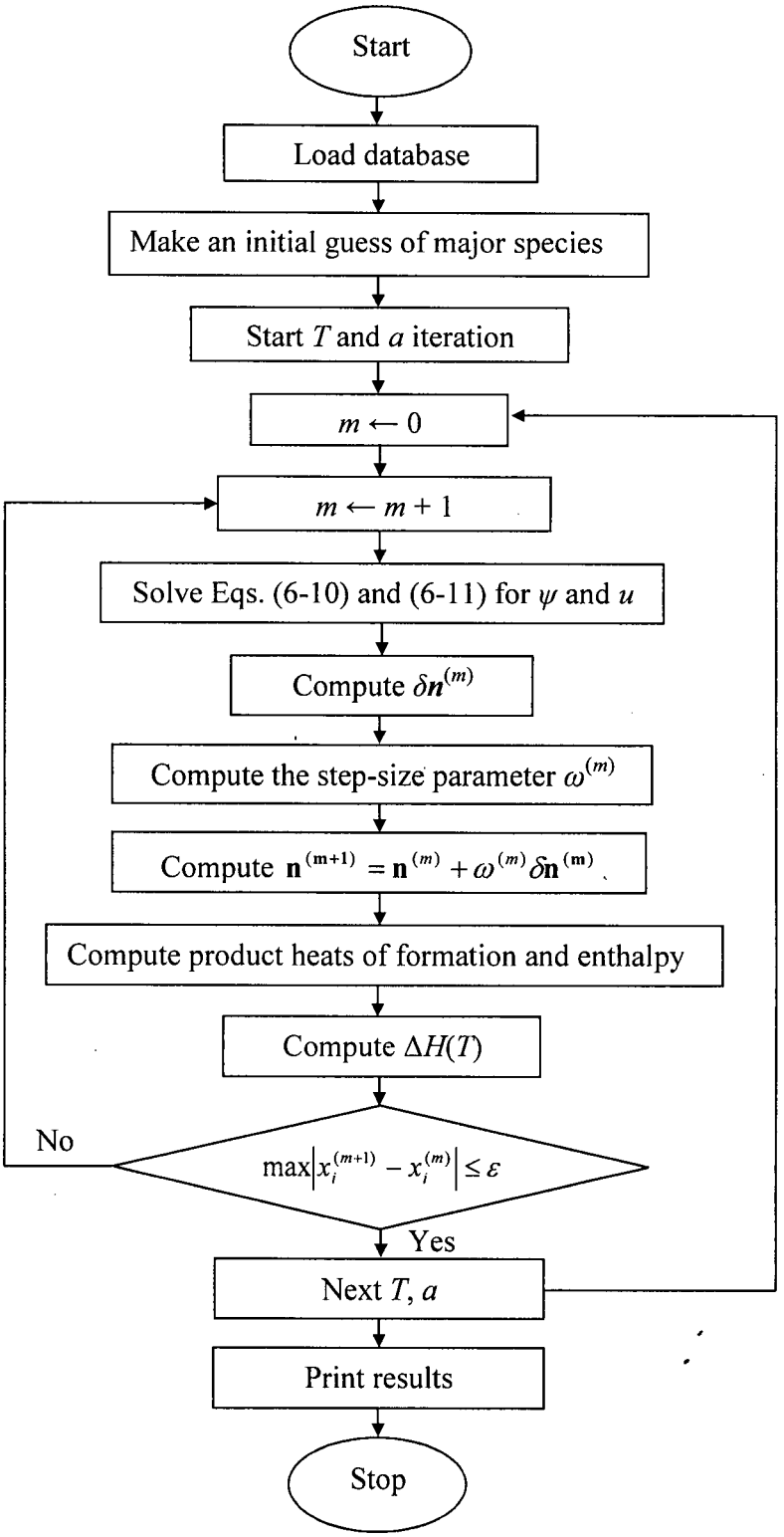

Figure 6-2. Flow chart for the RAND algorithm and energy balance calculations.

6.4 Validation of Model

The method used in the present work was validated in three steps. First, the equilibrium constants of major reactions in biomass gasification, calculated from free energy correlations, were compared with previous literature. All the thermodynamic data correlations were first compared with the original tabulated data. In one or two cases, mistakes in the original tabulated data (e.g. those for NH_2 in Pankratz et al. (1984), p. 224), were detected and corrected. The equilibrium constants, shown in Figure 6-3 in semi-logarithmic coordinates, are in very good agreement with tabulated data (Hougen *et al.*, 1964; Pankratz, 1987). Then predictions for a simple C-H-O system, the H_2O + C(s) reaction, were compared with those reported by Massey (1979) computed from an earlier version of the JANAF thermodynamic tables. As shown in Table 6-2, the mole fractions of carbon and gaseous species evaluated by the two models agree within 1%.

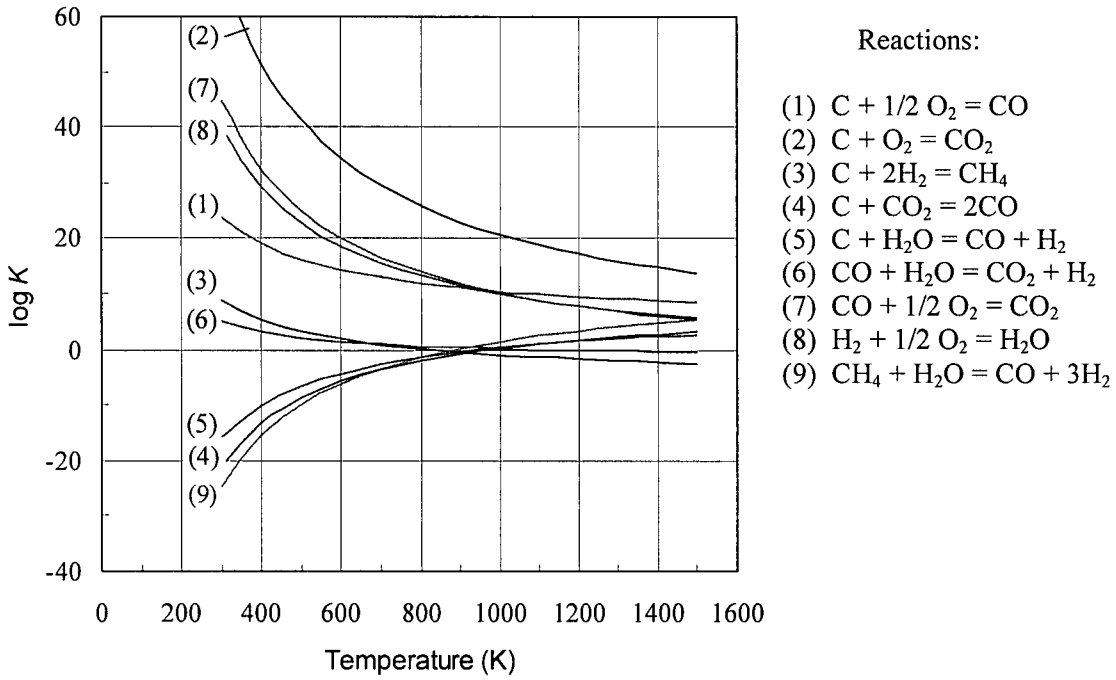

Figure 6-3. Equilibrium constants for major reactions in biomass gasification, calculated from the thermodynamic data correlations in the present study.

Table 6-2. Predicted equilibrium mole fractions in the system H_2O + C(s) at a pressure of 34 atm compared with previous literature (Massey, 1979).

Component	923 K		1023 K		1123 K		1223 K	
	Massey (1979)	This work	Massey (1979)	This work	Massey (1979)	This work	Massey (1979)	This work
C(s)	0.300	0.301	0.254	0.255	0.179	0.180	0.093	0.094
CH_4	0.131	0.130	0.110	0.109	0.085	0.085	0.060	0.061
CO	0.033	0.033	0.095	0.095	0.210	0.209	0.345	0.344
CO_2	0.167	0.167	0.151	0.150	0.112	0.112	0.062	0.063
H_2	0.106	0.106	0.178	0.177	0.263	0.262	0.348	0.347
H_2O	0.263	0.264	0.213	0.214	0.152	0.153	0.091	0.092

In addition, the present method was compared with the stoichiometric equilibrium model of Alemasov *et al.* (1974) for combustion of a rocket propellant, $(CH_3)_2NNH_2$, over a pressure range of 0.01-500 bar, temperatures from 725 to 3900 K, and air ratios from 0.3 to 2.0. The relative differences in species mole fractions were usually well within 1%, and the absolute difference seldom exceeded 0.2%. These comparisons validate the method used in this study.

The results of the equilibrium model are presented in four successive sections below. Section 6.5 presents pure equilibrium predictions by assuming complete conversion of all elements present in the reactor. Section 6.6 discusses how far the actual pilot CFB gasifier is from chemical equilibrium. Section 6.7 provides a theoretical account of carbon formation (also called coke formation) in the reaction system with C, H, and O being the dominant elements. Lastly, Section 6.8 presents results from the kinetically-modified equilibrium model and compares them with experimental data.

6.5 Pure Equilibrium Scenario

6.5.1 Species concentrations

Figure 6-4 shows predictions of the dependence of the molar contents of 7 major species on air ratio when the representative sawdust is gasified at 1.013 bar. The ultimate analysis of the standard sawdust used for equilibrium model calculations, listed in Table 6-3, is averaged from the six species used in the pilot study, and differs little from each of them. Five species (H_2, N_2, CO, CO_2 and CH_4) are given by their molar fractions in the dry product gas, $H_2O(g)$ is shown by its wet gas content, while unconverted carbon C(s) is represented by its molar fraction in the overall equilibrium system. All the numerical predictions are for a temperature range of 600-1600 K. However, to keep the figure from being too cluttered, predictions are presented for only two temperatures, 1000 and 1100 K. Most of the pilot plant test runs were between these two temperatures.

Table 6-3. Ultimate analysis of the typical sawdust for equilibrium model predictions. Values are averaged from the species used in the experiments.

Items	Units	Values
Carbon	wt. % (dry base)	50.88
Hydrogen	wt. % (dry base)	6.60
Oxygen	wt. % (dry base)	40.53
Nitrogen	wt. % (dry base)	0.51
Sulfur	wt. % (dry base)	0.34
Ash	wt. % (dry base)	1.14
Moisture	wt.% (as-received basis)	10.00
Higher heating value	MJ/kg (dry base)	20.55
Stoichiometric air	Nm^3/kg (dry base)	5.39

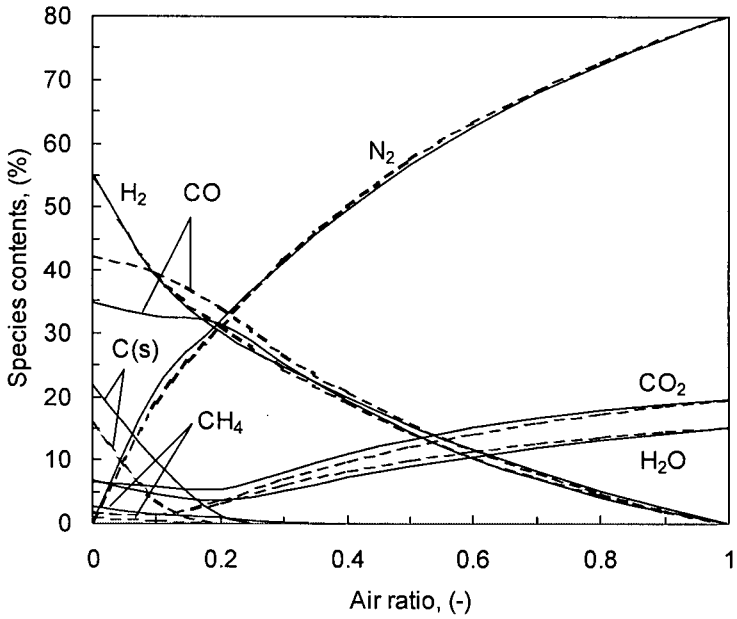

Figure 6-4. Variation of equilibrium gas composition with air ratio for representative sawdust composition at a pressure of 1.013 bar. Solid lines – 1000 K, dashed lines – 1100 K. Initial biomass composition as given in Table 6-3. No steam added.

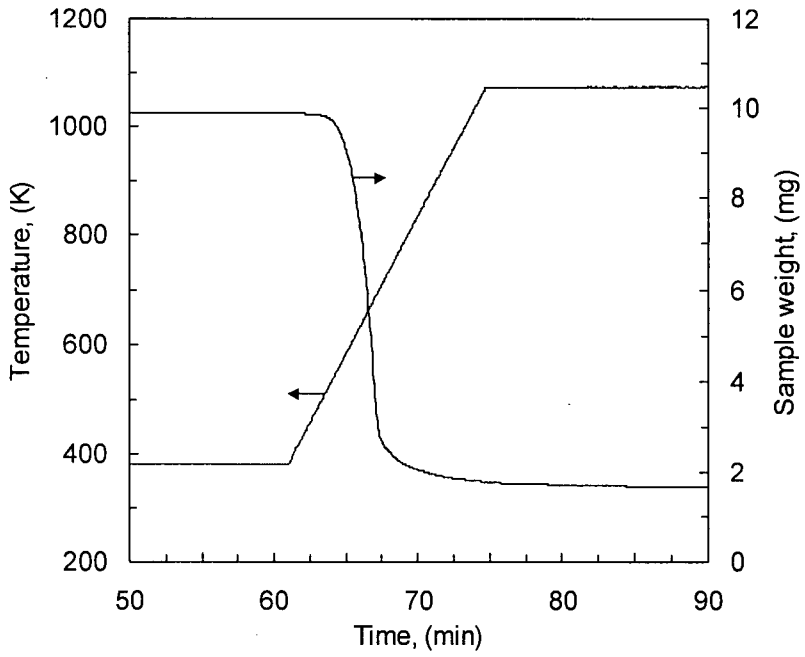

Figure 6-5. Thermogravimetric analysis of sawdust in N_2 at 1073 K. Time range 50-90 min shown; heating rate = 50 K/min.

As expected, major oxidizing species increase with increasing air ratio, while reducing species decrease. It is predicted that the equilibrium content of methane should not exceed 3% at temperatures above 1000 K, even with no air supplied. At typical gasification conditions (a = 0.3), the equilibrium CH_4 concentration is predicted to decrease from 0.25 to 0.02% as the system temperature increases from 1000 to 1100 K. This implies that methane contents significantly higher than this level are not due to equilibrium, but due to partial approach to equilibrium of the pyrolysis products. The CO_2 and H_2O concentrations slightly decrease with increasing air ratio below 1000 K for an air ratio less than 0.2. This is due to the rapid disappearance of unconverted carbon C(s) with increasing air ratio, which causes a rapid growth of the total moles in the gas phase, as well as a rapid decrease in the O/C molar ratio available to the gas phase that favours production of CO instead of CO_2. Likewise, the H_2O concentration decreases slightly. At 1100 K, the initial fraction of unconverted carbon is smaller, and the decreasing trend at low air ratios nearly disappears. For pyrolysis conditions (a = 0), about 15-23% of the total product is predicted to remain in the solid phase as char for the temperature range 1000-1100 K. This is in good agreement with TGA analysis results at 1073 K (800°C), shown in Figure 6-5, in which we found that about 17% of the sawdust sample mass remained as char. The sample started to lose weight at about 450 K after the initial evaporation stage. Maximum weight loss rate was found to occur at ~670 K. The predicted N_2 molar fraction rises to about 80% at stoichiometric combustion, before it begins to decrease with a further increase in the air ratio.

Concentrations of minor species closely related to emissions of nitrogen- and sulfur-containing pollutants are plotted in Figure 6-6 against the air ratio. NH_3, COS and H_2S are predicted to remain the dominant N and S products until the air ratio approaches 1, whereupon the overall atmosphere undergoes a substantial change towards NO and SO_2, together with a

small amount of SO_3. The equilibrium concentration of HCN rarely exceeds 1 ppm, usually an order of magnitude lower than the equilibrium concentration of NH_3. The low concentrations of both HCN and NH_3 show that N_2 is generally inert, only a small proportion of the nitrogen in the system being converted to NH_3 and HCN at temperatures below 1600 K. SO_2 is usually the dominant sulfur-containing product under combustion conditions, with a concentration an order of magnitude higher than that of SO_3. Both compounds decrease in concentration with further increasing air ratio in the combustion regime ($a > 1$) as a result of air dilution. Under gasification conditions H_2S prevails, as is shown in Figure 6-6.

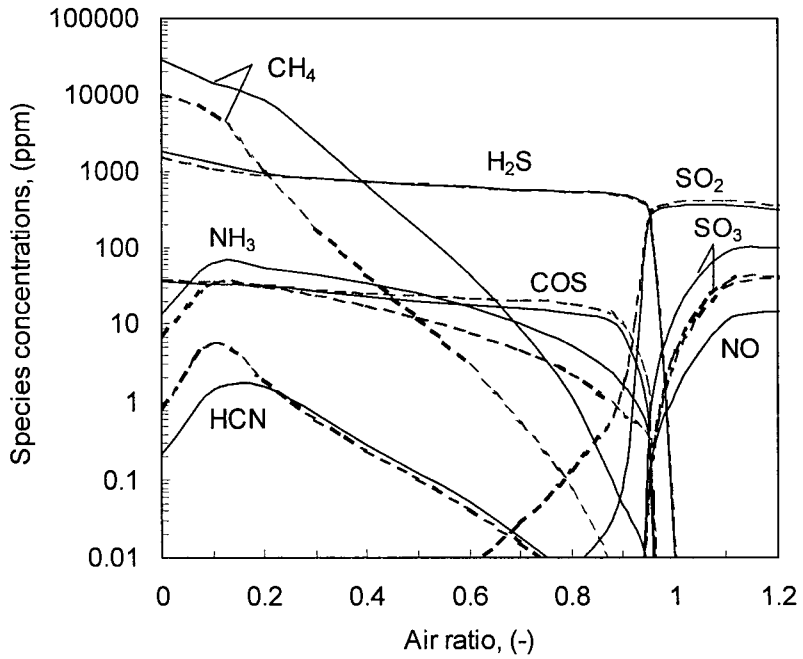

Figure 6-6. Equilibrium concentrations of some nitrogen- and sulfur containing species in sawdust gasification at 1.013 bar. Solid lines – 1000 K, dashed lines – 1100 K.

The molar fractions of HCN and NH_3 are helpful in tracing the two most important reaction pathways for nitrogen chemistry in coal combustion and gasification. These two species are important final products under reducing conditions, as well as key intermediate species for NO and N_2O formation in combustion processes (Miller and Bowman, 1989; Mann *et al.*, 1992).

Unfortunately, the equilibrium method provides no information regarding the selectivity of fuel nitrogen towards HCN or NH_3, nor on the relation between product selectivity and how nitrogen is chemically bound in the fuel. Equilibrium predictions indicate that the concentrations of both HCN and NH_3 reach maxima at moderate temperatures (850-1000 K).

6.5.2 Fate of elements under gasification conditions

The fate of elements in the feedstock can be interpreted in terms of the distribution of fractions converted to different species in the spectrum of final products. These fractions must sum to unity. For the sake of comparison with earlier work, the element distributions have been plotted versus air ratio and temperature.

Figure 6-7 shows the fate of carbon for gasification at 1.013 bar. The height under the lowest curve for each value of *a* represents the molar fraction of unconverted solid carbon, C(s). The narrow band between this curve and the next higher one for the same gives the mole fraction of hydrocarbons, mostly CH_4. The interval to the next curve for the same *a* signifies CO, while the region above the highest corresponding curve is occupied by CO_2. The mole fractions of unconverted carbon, hydrocarbons and CO_2 all decrease with temperature for all air ratios, while that of CO grows monotonically with temperature. At both temperatures plotted, and at air ratios lower than 0.2, a considerable portion of the carbon may remain as solid carbon. A crossover between the portions occupied by CO and CO_2 occurs for an air ratio of about 0.5, when CO_2 first exceeds CO as the major product. For an air ratio between 0.2 and 0.3, there is little change in the CO content due to the gradual disappearance of solid carbon, suggesting that this is a desired range of operation for producing CO-rich gas.

The effects of temperature and pressure on carbon distribution are shown in Figure 6-8, for an air ratio of 0.3, a typical value for the pilot tests in the present study. It is evident for both very low temperatures and very high temperatures, that pressure has little effect on the equilibrium

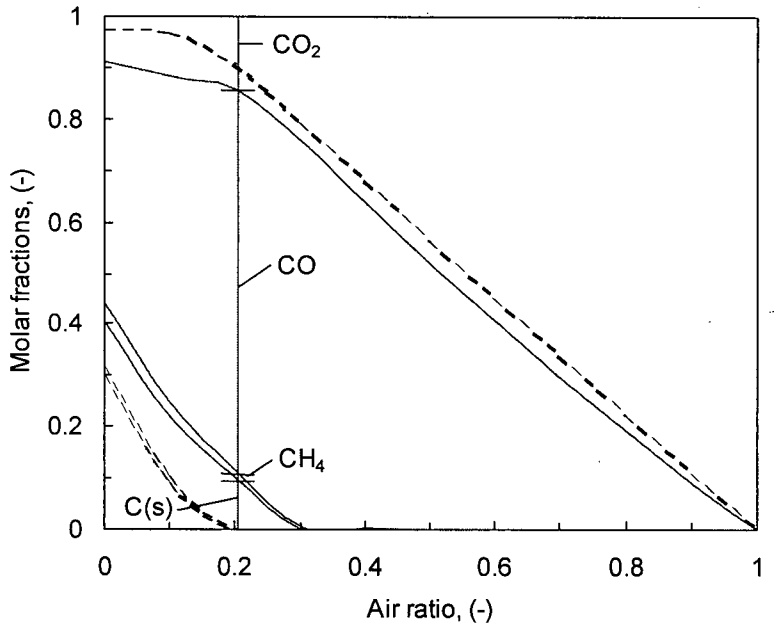

Figure 6-7. Predicted carbon distribution for sawdust gasification at atmospheric pressure: Solid lines: 1000 K, dashed lines: 1100 K.

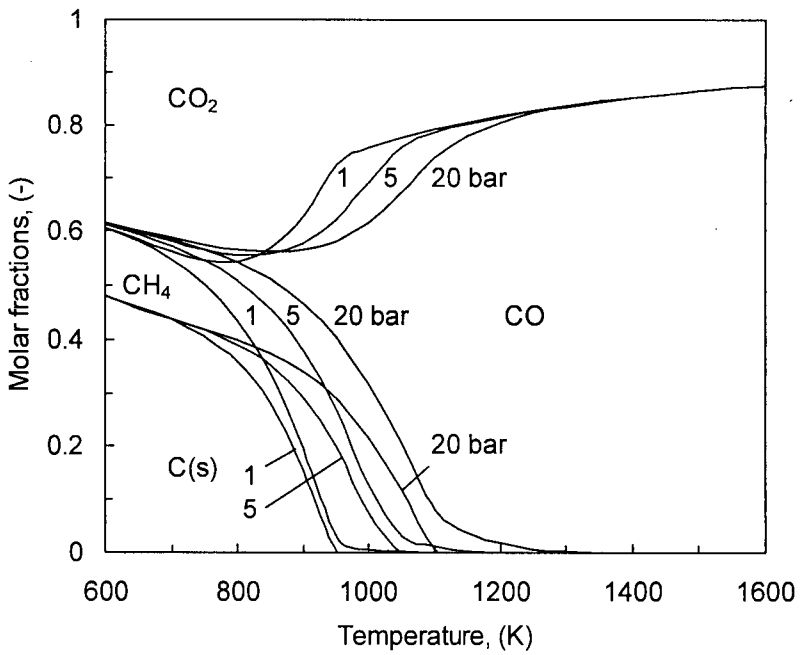

Figure 6-8. Predicted effects of temperature and pressure on carbon distribution for $a = 0.3$.

product distributions. The effect of pressure is only observed for intermediate temperatures from ~700 to 1250 K. For a given reactor temperature in this range, the proportions of C(s), hydrocarbons and CO_2 grow as pressure increases, as expected from Le Chatelier's principle, while that of CO decreases with increasing pressure, i.e. the equilibrium shifts to favour larger molecules so that the total number of moles decreases. The temperature range of noticeable pressure influence for sawdust gasification is almost the same as that for coal gasification (Li *et al.*, 2001). Beyond this range, the system pressure again becomes a secondary factor, while the relative abundance of elements continues to exert a strong influence.

Hydrogen distributions are plotted in Figures 6-9 and 6-10, showing the effects of air ratio, temperature and pressure. CH_4 occupies a significant part of the product spectrum at low air ratios and temperatures below 1000 K. For a = 0.3 at 1 bar, the H_2 mole fraction grows with temperature until 1100 K, where production of H_2O gradually reduces the proportion of H_2. This suggests that an equilibrium-controlled sawdust-based gasification process intended to produce hydrogen-rich gas should operate in the temperature range from 1100 to 1300 K and at an air ratio from 0.15 to 0.25 in order to maximum hydrogen production. For larger air ratios, H_2O starts to dominate the hydrogen distribution as a net product of hydrogen oxidation.

The oxygen distribution in the system is shown in Figures 6-11 and 6-12. In addition to confirming that an air ratio about 0.2 would be optimum for CO production, Figure 6-11 shows that more than half of the oxygen supply is used to produce CO_2 and water for an air ratio larger than 0.33. Operation below this air ratio would be favourable. Unfortunately, due to the usually high moisture content and low energy density, without an external heat source woody biomass such as sawdust may not be able to maintain the high temperature desired for gasification at such low air ratios. In addition to drying and good reactor insulation to help maintain an elevated system temperature, natural gas augmentation and co-gasification of biomass and other fuels may be worth considering.

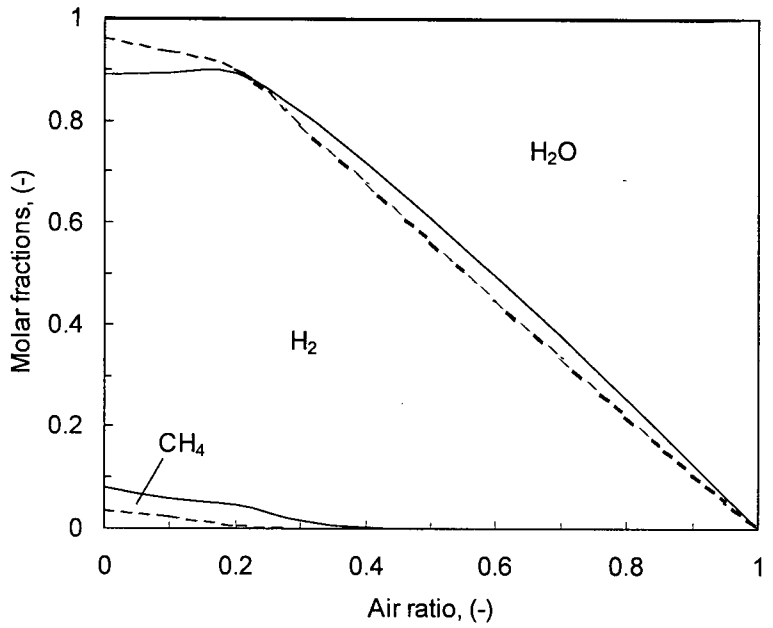

Figure 6-9. Predicted hydrogen distribution for sawdust gasification at atmospheric pressure: Solid lines: 1000 K, dashed lines: 1100 K.

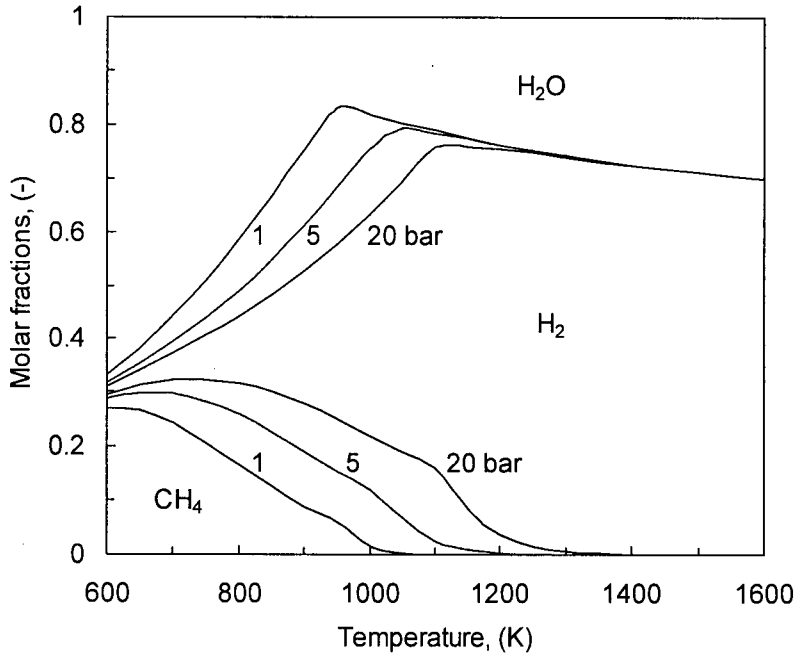

Figure 6-10. Predicted effects of temperature and pressure on hydrogen distribution for $a = 0.3$.

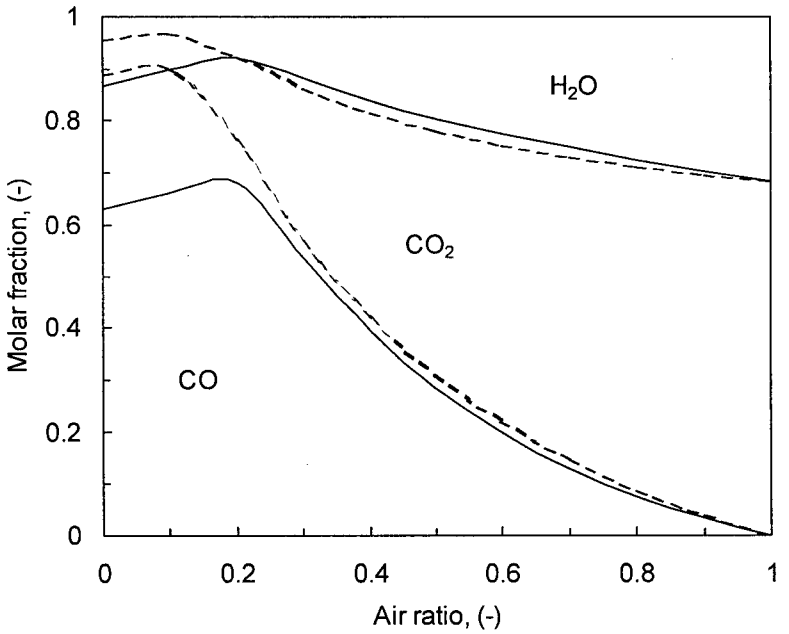

Figure 6-11. Predicted oxygen distribution for sawdust gasification at atmospheric pressure: Solid lines:1000 K, dashed lines: 1100 K.

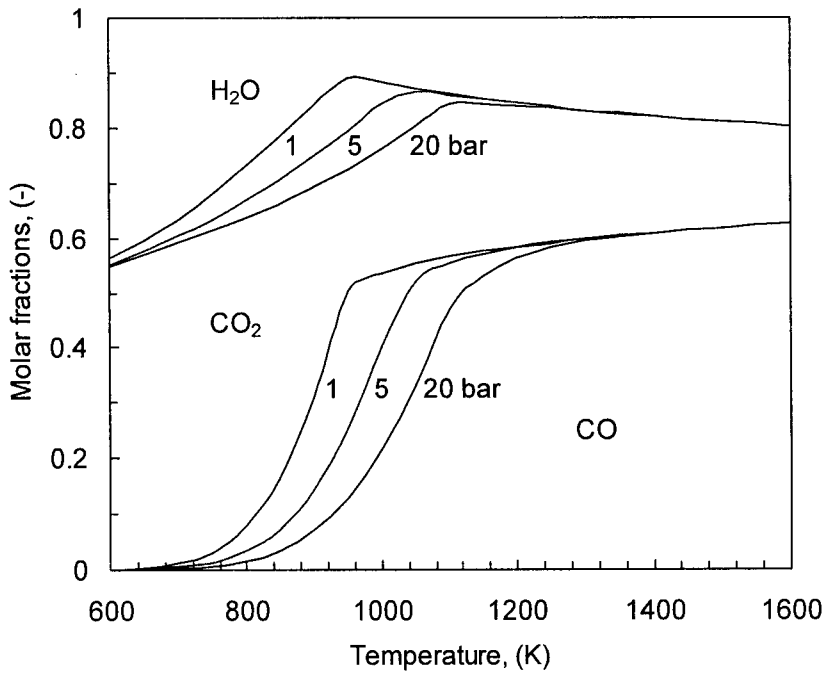

Figure 6-12. Predicted effects of temperature and pressure on oxygen distribution for $a = 0.3$.

Co-gasification can be realized by adding a small portion (e.g. 10-15% by weight) of coal to biomass in order to increase the heating value of the mixed fuel. In this way, the effectiveness of biomass gasification can be significantly improved, while not significantly reducing its advantage with respect to greenhouse gas emissions.

The limited range of pressure influence shown in the product distributions of the three most abundant elements (C, H, and O) implies that high-temperature gasification processes ($T > 1200$ K) need not be pressurized because increasing pressure in such processes only increases the energy consumption with little gain in the equilibrium product quality. The same holds for very low-temperature processes ($T < 700$ K) such as those using supercritical water, hot water as oxidizing agents, or anaerobic processes. However, high pressure does concentrate the gas phase, accelerate reactions and reduce reactor volume and the reaction time required to achieve equilibrium.

The sulfur distribution is shown in Figures 6-13 and 6-14. H_2S always dominates the sulfur distribution at temperatures lower than 1200 K, as long as the air ratio is significantly sub-stoichiometric, but COS may be important in understanding the sulfur chemistry in biomass gasification. At higher temperatures, HS emerges as a major species in the sulfur-containing product spectrum, as shown in Figure 6-14. The sulfur removal efficiency for high-temperature processes may be significantly influenced by HS removal from the gas phase. However, little is reported in previous literature regarding the role of HS in sulfur removal during gasification. Further experimental studies with respect to the kinetics and chemical equilibrium aspects of the HS-sorbent reaction at high temperatures are required.

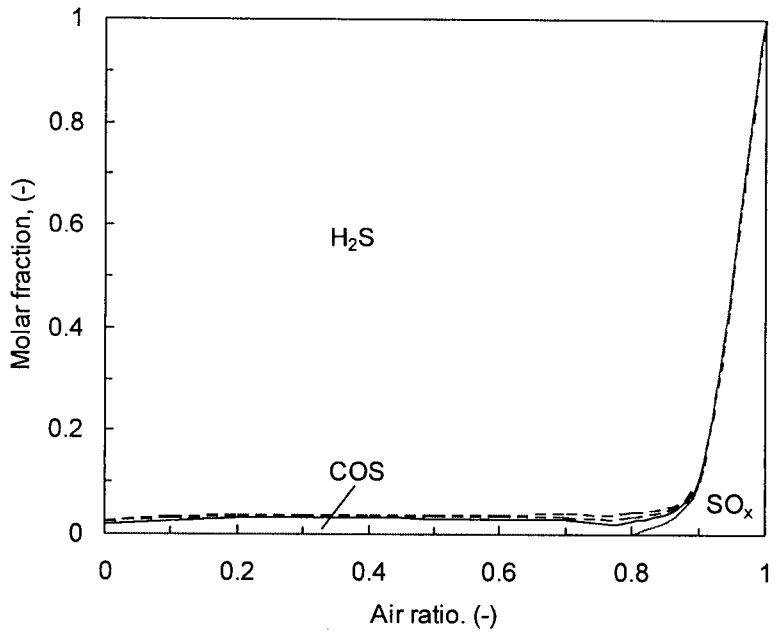

Figure 6-13. Predicted sulfur distribution for sawdust gasification at atmospheric pressure: Solid lines: 1000 K, dashed lines: 1100 K.

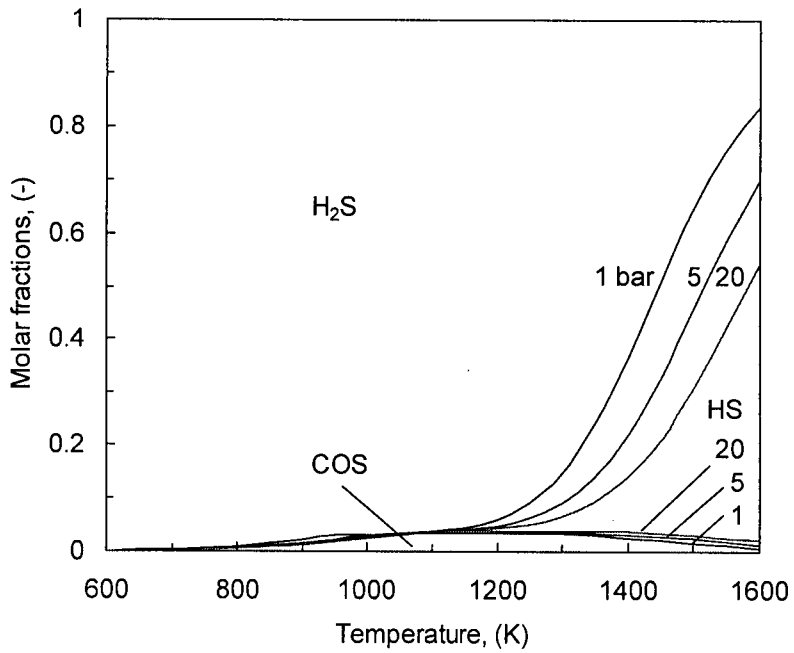

Figure 6-14. Predicted effects of temperature and pressure on sulfur distribution for $a = 0.3$.

6.5.3 Equilibrium carbon conversion

Figure 6-15 shows that the predicted maximum carbon conversion increases monotonously with increasing air ratio and temperature. To improve the equilibrium carbon conversion, the reactor temperature should be above ~1000 K. The curves demarcate the maximum performance of a gasification system achievable from the thermodynamic point of view; higher carbon conversion is thermodynamically impossible. The rest of the carbon simply leaves the system unconverted, causing an efficiency loss. In the literature this equilibrium converted fraction is often mixed up with the incomplete carbon conversion due to kinetic reasons, i.e. due to inadequate solids residence time in the reactor. The equilibrium unconverted carbon cannot be reduced by extending gas and solids residence time, increasing suspension density, re-injecting fly ash, or pressurizing the system. Gasification reactors should avoid conditions which lead to equilibrium unconverted carbon. This problem is further examined in Section 6.7.

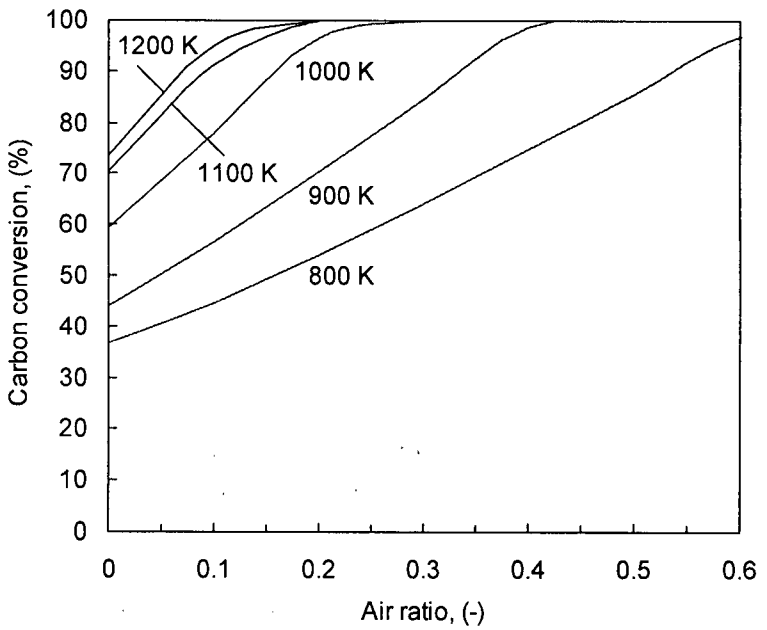

Figure 6-15. Predicted carbon conversion as a function of air ratio and temperature in biomass gasification.

6.5.4 Water conversion

A ratio is defined to evaluate the water demand of the sawdust gasification system:

$$\gamma = \frac{\text{moles of H in product as } H_2O}{\text{moles of H in feed}} \times 100\%. \qquad (6\text{-}27)$$

Figure 6-16 shows that as the air ratio increases, γ first remains low and largely constant, and then starts to grow towards unity as stoichiometric combustion is approached. The level of the initial flat stage depends on temperature, decreasing as system temperature increases. At higher temperatures, a larger fraction of the hydrogen element stays in H_2, so that a demand for steam injection may arise. Note that the standard sawdust contains 10% moisture (as-received basis), contributing about 14% to the total hydrogen in the feedstock. If γ exceeds 14%, water is a net product in the system. In such cases, there is no need for external steam injection because the system is a net producer of water. Figure 6-16 indicates that steam injection is helpful only for temperatures above 1000 K and air ratios less than 0.3.

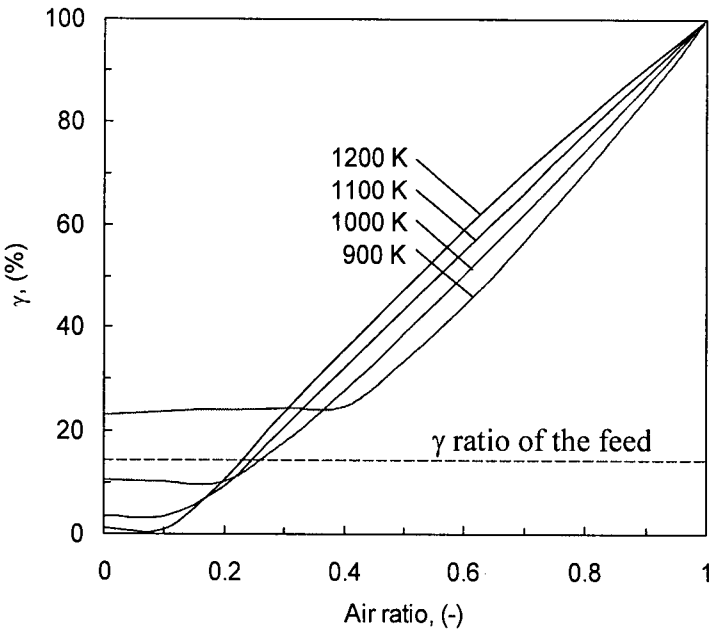

Figure 6-16. Effects of air ratio and temperature on the γ ratio: System pressure = 1.013 bar.

6.5.5 H_2/CO molar ratio

Figure 6-17 shows the variation of the predicted H_2/CO molar ratio in the product gas with increasing air ratio and system temperature. The H_2/CO molar ratio decreases with increasing temperature. At a temperature of 1100 K it becomes almost constant for air ratios greater than 0.2. At higher temperatures, the H_2/CO ratio decrease monotonously with increase air ratio, while at lower temperatures, it passes through a minimum value at a certain air ratio that increases with decreasing temperature. The decreasing H_2/CO molar ratio at temperatures above 1100 K suggests that CO production is favoured at higher temperatures, while H_2 is favoured at lower temperatures. This figure shows that relatively low H_2/CO molar ratios (less than 1) result for woody biomass gasification for the typical air ratio range if the system temperature is higher than 1100 K. This is in qualitative agreement with the experimental observations of van der Drift *et al.* (2001) and the present study.

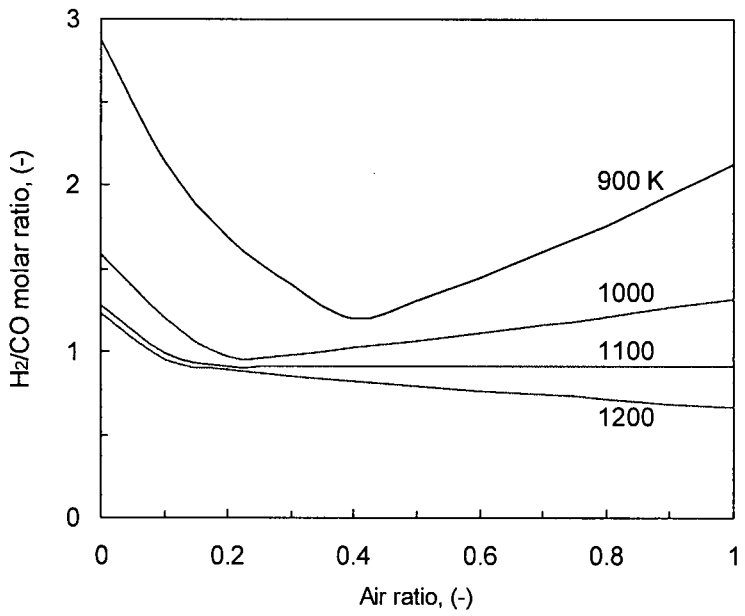

Figure 6-17. Effects of air ratio and temperature on the predicted H_2/CO molar ratio: System pressure = 1.013 bar.

6.5.6 Gas heating value and yield

Figure 6-18 plots the variation of the predicted gas heating value with air ratio for different reactor temperatures. The relationship between the dry gas heating value and the air ratio becomes approximately exponential as the reactor temperature increases, with significant deviation only when the air ratio exceeds 0.55, i.e.

$$\mathrm{HHV} = 11.6\exp(-2.35a), \qquad (a \le 0.55). \tag{6-28}$$

This equation is in qualitative agreement with the experimental fit line in Figure 4-20 despite small differences in the pre-exponential factor and the slope. Moreover, there is a very similar trend for $a > 0.5$ with the experimental data points falling below the exponential line. Since the air ratio in gasification processes rarely exceeds 0.5, an exponential correlation of gas heating value with air ratio is quite reasonable for fitting experimental data.

Figure 6-19 shows the variation of dry gas yield with air ratio. The gas yield can be defined in two ways, (i) the dry gas volume per unit feed (Nm^3/kg-fuel), and (ii) the dry gas volume per unit air supply (Nm^3/Nm^3-air). Both definitions are plotted in the figure. The gas yield based on fuel feed rate increases with increasing air ratio, while that based on air supply decreases with increasing air ratio. The gas yield based on air supply diverges at pyrolysis conditions (a = 0), but converges to a baseline value of 1 for large air ratios. This gas yield can fall slightly below unity in the vicinity of stoichiometric combustion, as the total number of moles of the product stream is slightly smaller than that of the feed streams. This is also why the predicted N_2 content in the gas, as shown in Figure 6-4, can be as high as 80% (slightly higher than its content in air) at stoichiometric combustion before it starts to fall again. Temperature is found to have a noticeable effect only for air ratios less than about 0.4.

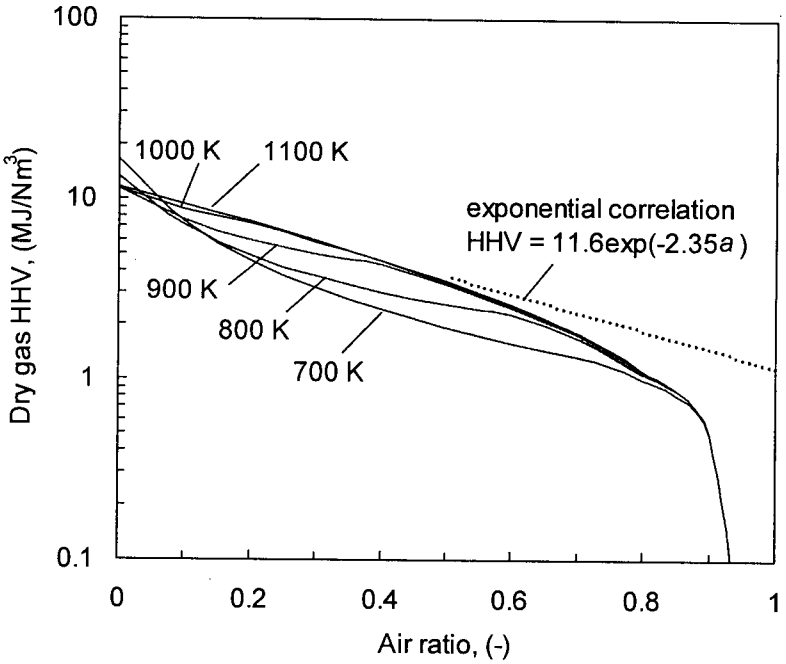

Figure 6-18. Equilibrium predicted variation of dry gas heating value with the air ratio and reactor temperature for a system pressure of 1.013 bar.

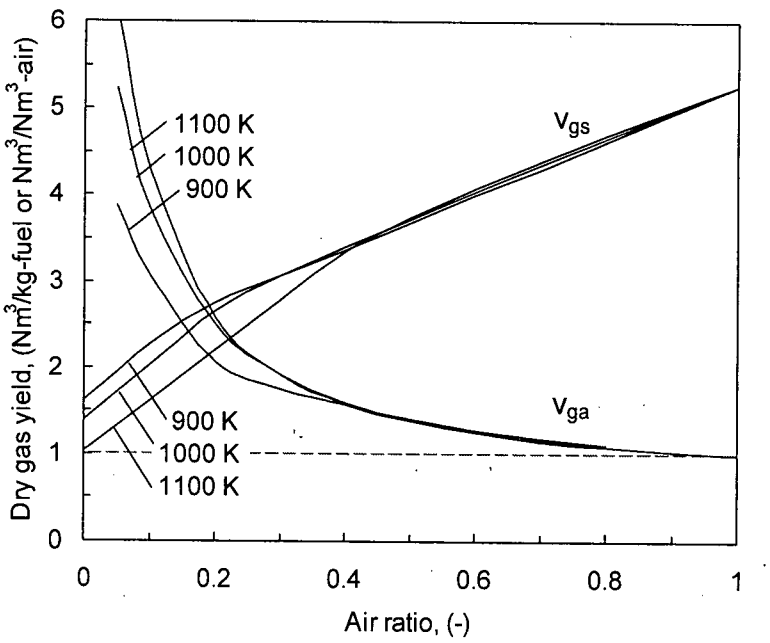

Figure 6-19. Gas yield vs. air ratio: V_{gs} lines represent gas yields per unit feed mass, V_{ga} represent gas yield per unit air supply. System pressure = 1.013 bar.

6.5.7 Cold gas efficiency

The cold gas efficiency predicted by the equilibrium model is plotted in Figure 6-20. This efficiency corresponds to E_1 defined by Eq. (5-9) because tars are not considered in the equilibrium model. On the one hand, the exclusion of tar in the equilibrium prediction of gasification efficiency is due to difficulties in collecting data for the thermodynamic properties of tar species. On the other hand, this is also because the equilibrium tar loading in the product gas should be very low, except for low air ratios or pyrolysis conditions, which is outside the scope of our present gasification study.

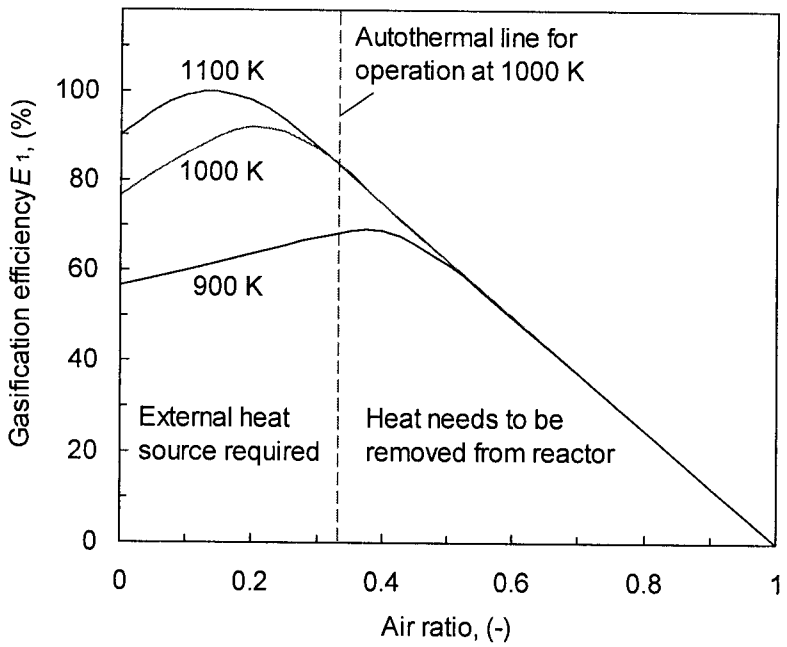

Figure 6-20. Predicted cold gas efficiency vs. air ratio when biomass is gasified at atmospheric pressure.

A striking feature of the curves is the existence of a maximum cold gas efficiency at a non-zero air ratio corresponding to a particular reaction temperature. As temperature further increases above 1100 K, the efficiency curves flatten and approach 100%. Cold gas efficiency decreases linearly with increasing air ratio and approaches 0 for stoichiometric combustion ($a = 1$)

conditions. The operating temperatures in our pilot study varied from ~1000 K to 1100 K. Therefore, maximum gasification efficiency could only be expected at air ratios below 0.3. However, as illustrated by the autothermal line in the figure, the reactor cannot maintain its temperature above 1000 K if the air ratio is less than 0.33. This implies that, due to the relatively low heating value of woody biomass, the theoretical maximum cold-gas efficiency cannot be achieved without external heat input or auxiliary fuel, even at adiabatic conditions for almost any moisture content in the fuel, if the gasifier is to operate at 1000 K or higher.

However, the actual temperature in our pilot study was higher than predicted by the equilibrium model. The reason was that the incomplete conversion of carbon due to kinetic limitations made the effective air ratio (or O/C molar ratio) in the gasifier higher than predicted for the pure equilibrium scenario. The operating temperature in a typical gasifier increases with decreasing fuel feed rate. The effect of the kinetic limitation in carbon conversion was to remove part of the fuel from the system. Therefore, it caused the reactor temperature to exceed its equilibrium level, allowing the system to reach the desired temperature. However, the partial conversion of carbon also caused a considerable decrease in the gas heating value. As a result the cold gas efficiency in a real system is always lower than the theoretical maximum.

6.6 Approach to Chemical Equilibrium

A real gasification system differs from an ideal reactor at chemical equilibrium. The fractional achievement of equilibrium and the carbon conversion in a real process depends on many factors: thermodynamics, chemical kinetics, hydrodynamics, heat and mass transfer, residence time and even particle size distribution. In this section, we present two parameters as measures of how closely a real system approaches chemical equilibrium.

Watkinson *et al.* (1991) reported deviations in gas composition from equilibrium predictions for seven entrained bed gasifiers, six fluidized bed gasifiers and six moving bed units. The best-fit equilibrium temperature, T_{eq}^{0}, based on a stoichiometric equilibrium model, tends to deviate from the reported operating temperature. As in Watkinson *et al.* (1991), the best-fit temperature is defined as the temperature which minimizes the sum of squares of the deviations in five principal gas species (H_2, CO, CO_2, CH_4, N_2) contents for the reactor:

$$T_{eq}^{0} = T \text{ at } \min\left|\sum (y_{eq} - y_{meas})^2\right| \tag{6-29}$$

The same criterion is used in the present study. Typical curves for locating the best-fit equilibrium temperature are shown in Figure 6-21. Typically, the best-fit temperature was about 210°C lower than the time-mean reactor temperature at the exit of the hot cyclone. The root mean square differences in molar contents of the five major species between experimental data and the best fit equilibrium predictions were 3-5 mol.%, depending on air ratio, riser temperature, feed rate and moisture content of the fuel.

When a system actually reaches chemical equilibrium, the deviation between the actual temperature and T_{eq}^{0} disappears. The larger the temperature deviation, the farther the system is from chemical equilibrium. Therefore, the difference between the best-fit T_{eq}^{0} value and the

representative operating temperature (e.g. cyclone exit temperature) can be used as a measure of the approach to equilibrium.

In addition to kinetic limitations, there may be a number of possible reasons for failure to reach equilibrium, one being temperature variation along the high-temperature flow path. If chemical equilibrium was achieved in the cyclone, the corresponding gas composition should reflect chemical equilibrium at the cyclone exit. However, temperature records during the pilot plant tests showed that the temperature difference between the middle of riser (T_3) and cyclone exit (T_6) was usually less than 10°C, the latter being higher. Therefore, the deviation due to temperature variations cannot be the sole factor, because gas composition would shift toward the high-temperature side if chemical equilibrium were achieved in the cyclone. The gas temperature was quenched to 570-670 K in the horizontal duct downstream of the cyclone, after a further residence time of less than 0.2 s while traveling a length of 1500 mm. From the high CH_4 content in the off-gas it is evident that the reacting gas-solid flow did not reach chemical equilibrium after 1-2 s at 970-1120 K. The same reacting stream cannot adjust itself to a new equilibrium in a much shorter time at a much lower temperature (where reaction rates are much lower). Therefore, the gas samples extracted from the inlet of the first heat exchanger must be very close to the gas composition at the cyclone exit; the possible deviation due to self-conditioning of the gas in the horizontal duct can also be ruled out. The deviation in gas composition can, therefore, be attributed to partial approach to equilibrium.

Table 6-4 listed the best-fit equilibrium temperatures and the corresponding minimum deviation from the reported reactor temperature (T_3) from our pilot plant tests. The temperature deviation was on average 275 K based on the time-mean gas compositions, and 190 K based on the "best cases" of the instantaneous gas composition measured from the present experimental study. The best-case gas compositions, listed in Table 6-5, were usually those samples with the

highest H_2 contents in individual test runs; they represent situations nearest the model predictions. All the best-fit temperatures were lower than the actual riser temperature. This is not always true for other reactor types. Watkinson *et al.* (1991) reported that the best-fit temperatures were about 120-180 K lower than operating temperatures for entrained-bed gasifiers, 300 K lower to 100 K higher for fluidized-bed gasifiers, but could be 50-200 K higher than reported operating temperature for moving-bed gasifiers. The reason for the positive shifts in the best-fit temperature is unclear, but may well be due to different ways of reporting the most representative temperature in various reaction systems.

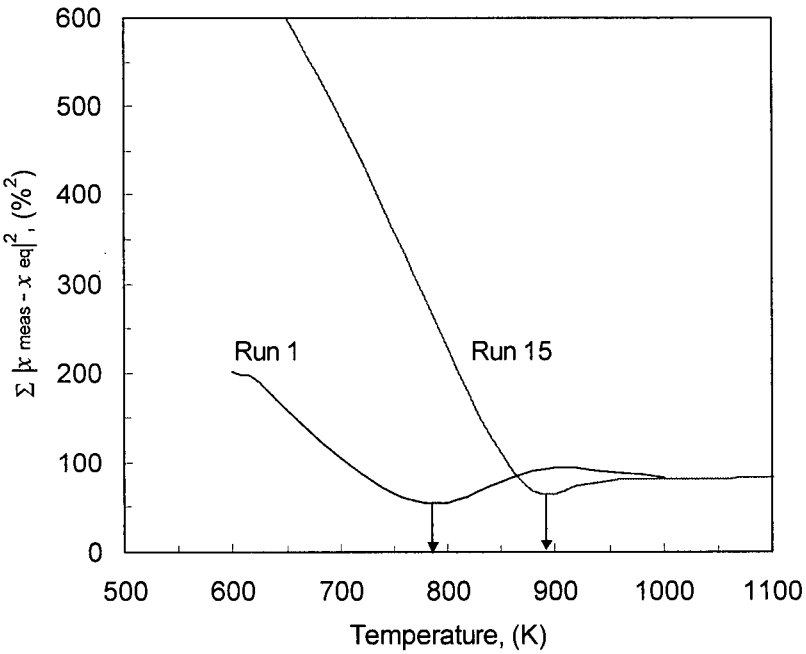

Figure 6-21. Typical curves for the sum of squares of deviation in gas composition versus assumed reactor temperature at atmospheric pressure. Run 1: a = 0.54, M = 22.0 wt.%, T_3 = 1013 K; Run 15: a = 0.46, M = 4.2 wt.%, T_3 = 1078 K.

Table 6-4. Deviations of best-fit equilibrium temperature from experimental reactor temperature in pilot study.

Run	T_3	T_{eq}^0 (mean)	T_{eq}^0 (best case)	ΔT (mean)	ΔT (best case)
	(K)	(K)	(K)	(K)	(K)
1	1013	700	790	313	223
2	991	770	810	221	181
3	1038	670	760	368	278
4	1088	750	830	338	258
5	1045	770	850	275	195
6	1060	740	850	320	210
7	990	800	780	190	210
8	1003	720	870	283	133
9	1025	800	870	225	155
10	1088	720	870	368	218
11	1062	700	780	362	282
12	974	740	820	234	154
13	1001	810	870	191	131
14	1012	840	900	172	112
15	1078	790	890	288	188

Comparing the experimental carbon conversion data with equilibrium predictions, one can find a similar shift towards the low-temperature side, as shown in Figure 6-22. The experimental points dwell in a lower temperature range from 850 to 950K, while the reactor operated at 970-1090 K, in substantial agreement with the best-fit equilibrium temperature data. The deviation from equilibrium conditions indicates that a higher operating temperature is required to reach a given solid conversion than is thermodynamically necessary, whereas this is a necessary feature of most gas-solid reaction systems, such as those in combustion and gasification equipment.

Table 6-5. Best-case dry gas compositions from pilot plant tests.

Run	H_2	N_2	CO	CH_4	CO_2
	(mol %)	(mol %)	(mol %)	(mol %)	(mol %)
1	8.78	63.07	8.80	2.05	17.3
2	3.81	62.73	15.18	2.89	15.39
3	3.69	62.76	14.03	2.73	16.79
4	4.91	58.92	15.06	3.12	17.09
5	5.71	57.36	16.48	3.68	16.59
6	4.82	59.62	16.03	3.43	15.83
7	7.13	61.04	13.8	2.55	15.41
8	5.02	55.70	20.18	4.09	15.02
9	4.84	57.50	19.42	4.01	14.22
10	6.07	56.78	18.03	4.06	15.07
11	4.91	58.92	17.57	3.79	14.81
12	6.95	51.42	21.52	5.18	14.93
13	5.83	52.94	21.78	4.90	14.55
14	8.97	49.74	21.60	4.35	15.35
15	9.08	55.08	16.88	3.00	15.95

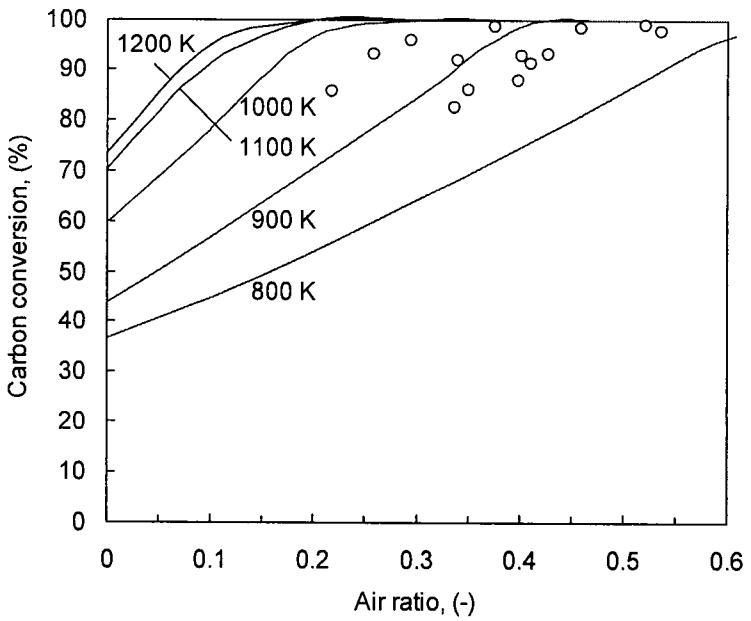

Figure 6-22. Comparison of experimental time-mean carbon conversion with equilibrium predictions. Experimental points: T_3 = 974-1088 K.

6.7 Carbon Formation in Gasification Systems

The inadequate carbon conversion due to kinetic, hydrodynamic and mass transfer reasons must be strictly distinguished from the carbon formation (also called carbon black deposition or coke formation in various contexts) under chemical equilibrium conditions. Carbon formation can occur in equilibrium systems, too. Unfortunately, this has often been ignored or misinterpreted. By examining the carbon formation tendency and the quantity of solid carbon at chemical equilibrium, one can clarify what is the realistic target of conversion that can be achieved by relieving the kinetic rate-limiting factors or by extending the residence time. Since carbon deposition should be avoided in some industrial processes, such as internal combustion equipment and methane steam reforming for hydrogen production, but is desirable in others, such as chemical vapour deposition (CVD) reactors, such a theoretical treatment also helps in evaluating the carbon formation tendency under operating conditions that are difficult to study by experimental means. For these reasons, the method may have wider industrial application beyond the pilot gasification study.

6.7.1 Carbon formation: an interpretation

The presence of residual solid carbon under chemical equilibrium is essentially the saturation of elemental carbon in the gas phase at a given temperature and pressure (Li *et al.*, 2001). Imagine the gas phase as an ideal solution, with solid carbon as the solute, and all gaseous species as the solvent. C(s) in the equilibrium system can then be regarded as an undissolved solute in a saturated solution. When the abundance of the solute is further increased in a saturated solution, the composition of the solution remains unchanged. Hence, for a C-saturated system, the gas composition remains unchanged when solid carbon is added or withdrawn. Table 6-6 provides an example of a C-saturated system with decreasing carbon abundance while

hydrogen and oxygen remain constant. It is found from the first five rows that the gas phase composition does not change so long as undissolved C(s) is still present in the solid phase. Gas composition starts to change when the abundance of carbon in the system decreases to less than 0.64, the saturation point of carbon in the C-H-O system under consideration.

Table 6-6. Gas composition in a C-saturated C-H-O system at 1000 K and 30 bar.

Element abundance (U_C, U_H, U_O), (moles)	CO (%)	CO_2 (%)	H_2 (%)	H_2O (%)	CH_4 (%)	C(s) (%)
(1.0, 1.5, 1.25)	13.6	31.8	17.4	28.3	8.79	23.2
(0.9, 1.5, 1.25)	13.6	31.8	17.4	28.3	8.79	17.9
(0.8, 1.5, 1.25)	13.6	31.8	17.4	28.3	8.79	11.8
(0.7, 1.5, 1.25)	13.6	31.8	17.4	28.3	8.79	4.68
(0.64, 1.5, 1.25)	13.6	31.8	17.4	28.3	8.79	0.01
(0.6, 1.5, 1.25)	12.3	31.4	17.6	31.3	7.41	0.00
(0.5, 1.5, 1.25)	9.18	30.0	17.3	39.3	4.21	0.00

This has a number of important implications. First, if a gasification system in chemical equilibrium is C-saturated, addition of more carbon, e.g. by fly ash re-injection does not improve carbon conversion, because the carbon added in the fly ash simply leaves the reactor unconverted. Secondly, when the system is saturated with carbon, the gas composition becomes completely insensitive to the solids residence time. Thus, the circulating fluidized bed loses one of its advantages over the bubbling fluidized bed in improving coal or biomass conversion. Moreover, if the gasification system is C-saturated for sawdust, adding another fuel with higher C/(H+O) molar ratio (e.g. coal) does not improve the gas quality when they are co-gasified. The carbon in the one fuel simply displaces that in the other when combining with other elements.

6.7.2 Prediction of carbon formation

Since carbon, hydrogen and oxygen are by far the most abundant elements in coal gasification processes, little error in the main gas species results if the system is treated as a ternary C-H-O system and plotted on a ternary diagram. Earlier studies (White *et al.*, 1975; Gruber, 1975) reported the carbon deposition boundary in a methanator with gaseous feeds. The carbon formation boundary given by White *et al.* (1975) is not quantitatively defined, i.e. it is unclear what is the minimum molar fraction of solid carbon in the system that can be considered to represent carbon formation. Gruber (1975) proposed an alternative coordinate system for graphical solution of the carbon formation problem, in which H_2, CO and CO_2 were chosen as the independent species. Transform functions were used to convert gas composition into a Cartesian coordinate system. Probstein and Hicks (1982) proposed a carbon formation envelope in a H/C versus O/C coordinate system for methanators, and obtained similar results.

The problem discussed here differs from that in a methanator. The materials to be gasified are usually solids, subject to incomplete conversion due to kinetic effects. Ternary diagrams are employed for convenience. The carbon formation boundary is depicted as the isotherm corresponding to 99% conversion of carbon into gaseous species at a specific temperature, as shown in Figure 6-23. The three vertices denote C(s)-C(g), H_2-H, and O_2-O. Important binary species are indicated along the edges of the triangle. C-H-O systems above the carbon-formation isotherm at a given temperature are in the carbon-forming regime when at chemical equilibrium, i.e., 1% or more of the carbon remains as unconverted carbon in the ash or solids residue. If a given system is in the carbon-forming regime, C(s) needs to be considered in the equilibrium model. The absence of C(s) in the species menu of an equilibrium model can cause serious errors in equilibrium prediction if the system under consideration lies in the carbon-forming regime.

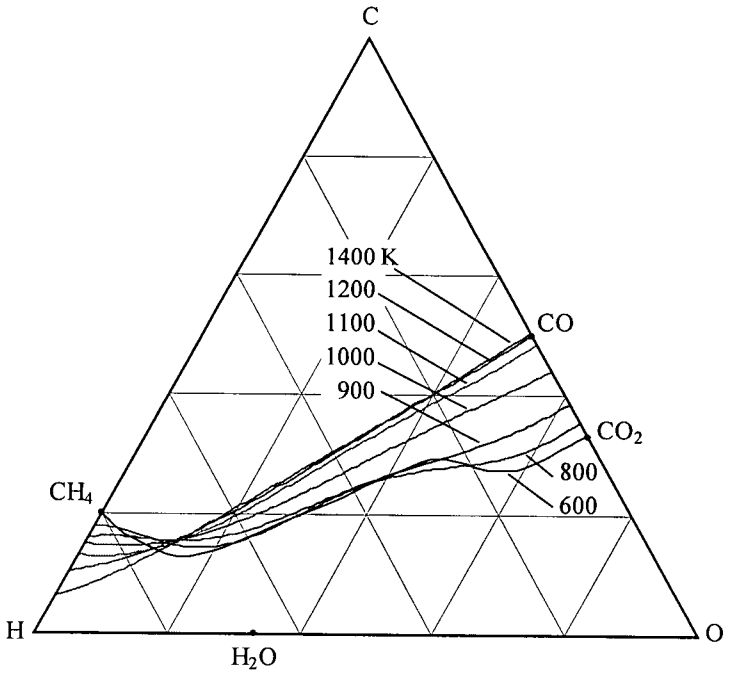

Figure 6-23. Molar ternary diagram showing carbon formation boundary for C-H-O system at a pressure of 1 bar, predicted by non-stoichiometric equilibrium model developed in this work.

Figure 6-23 shows a family of carbon-formation isotherms for C-H-O dominated fuels gasified at 1 bar, predicted by the non-stoichiometric equilibrium model developed in the present study. As a first approximation, these curves can be considered to represent atmospheric pressure. Minor fluctuations caused by light hydrocarbons (C_2H_2 up to C_3H_8) and numerical errors are filtered so that the isotherms generally appear smooth. Each isotherm from the C-H edge to the C-O edge represents a 99% iso-conversion line at a specific temperature. A molar combination that falls above the boundary for a given temperature is considered carbon-forming. At relatively low temperatures in a C-H system, the dominant product is CH_4, so that the curves start from the vicinity of the point representing CH_4.

White *et al.* (1975) base their equilibrium model on a simplified 4-reaction carbon formation mechanism in a methanator:

$$2CO \leftrightarrow CO_2 + C\,(s) \quad (6\text{-}30)$$

$$CO + H_2 \leftrightarrow H_2O + C(s) \quad (6\text{-}31)$$

$$CO_2 + 2H_2 \leftrightarrow 2H_2O + C(s) \quad (6\text{-}32)$$

$$CH_4 \leftrightarrow 2H_2 + C(s) \quad (6\text{-}33)$$

This mechanism considers neither C(g) nor hydrocarbons other than CH_4; nor does it consider the CO shift reaction or carbon combustion reactions.

The isotherms predicted in this study are improved in several respects from those of previous studies (White *et al.*, 1975; Probstein and Hicks, 1982). Due to the introduction of other hydrocarbons in the model developed in the present study, each with a higher C/H molar ratio than CH_4, the left (hydrogen-rich) end of the isotherms are higher than predicted by earlier studies. Therefore, the starting point cannot be predicted only with the equilibrium constant of reaction (6-33). The second difference is with the bends in the curves for high oxygen abundance and modest temperatures. These bends can be attributed to the CO shift reaction and, because they are located in the combustion region, to the transition from low-temperature direct oxidation:

$$C + O_2 = CO_2 \quad (6\text{-}34)$$

to the high-temperature sequential oxidation mechanism, i.e.

$$C + \tfrac{1}{2}\,O_2 = CO \quad (6\text{-}35)$$

$$CO + \tfrac{1}{2}\,O_2 = CO_2 \quad (6\text{-}36)$$

Because CO and CO_2 are the only stable products considered for the C-O binary system, the end point of the isotherms can be successfully predicted by the equilibrium constant of the C-CO_2 reaction (6-30). The point for $CO/CO_2 = 1$ corresponds to a temperature of about 940 K. The high temperature extreme of the carbon formation boundary is a straight line linking H and CO if carbon is considered to be solely C(s). When carbon vapor C(g) is considered, the line may shift slightly toward the C vertex.

In the present study, carbon is represented by graphite, as in most equilibrium studies, but its non-ideality may significantly influence the carbon formation boundary (Gruber, 1975). In real processes, the coke that is laid down is almost never pure carbon, but CH_x where x = 0-0.5, commonly known as Dent carbon, after J. F. Dent (1945) who first reported deposition of a more reactive, non-graphitic carbon in methanators. Since the formation of Dent carbon removes far more carbon than hydrogen from the equilibrium system, it provides an important mechanism for adjusting the C/H molar ratio in order to escape from the carbon-forming regime. The carbon activity is thus problematic for carbonaceous materials where any carbon formed may lie between graphite and active carbon.

The Gibbs free energy of formation for non-ideal carbon may be written:

$$\Delta G^{o}_{f,\text{dent}}(T) = RT \ln a_c \tag{6-37}$$

Here, a_c is the activity of a particular carbon referred to graphite. Values between 1 and 20 have been reported (Johnson, 1981; Kapteijn and Moulijn, 1985). The assumption of graphitic carbon is generally reasonable in thermodynamic calculations since it has been shown (Johnson, 1981) that the non-ideal behavior is due, at least in part, to kinetic effects. A sensibility study of the equilibrium model with respect to the thermodynamic properties of the non-ideal carbon is recommended. The coke is considered as a species with a chemical formula of CH_x (x = 0-0.5) and a free energy of formation of $RT \ln a_c$. Since $RT \ln a_c$ is always greater than zero for non-ideal carbon ($a_c > 1$), less carbon deposition is expected.

Carbon formation boundary isotherms for gasification systems operating at 10 and 20 bar appear in Figures 6-24 and 6-25, respectively. The carbon formation boundaries for different temperatures resemble those for the atmospheric pressure system, but since CH_4 formation is promoted by high pressure, the left terminus of the lines shifts toward the CH_4 point. As the pressure increases, the curves stay closer together, i.e. there is less temperature dependence.

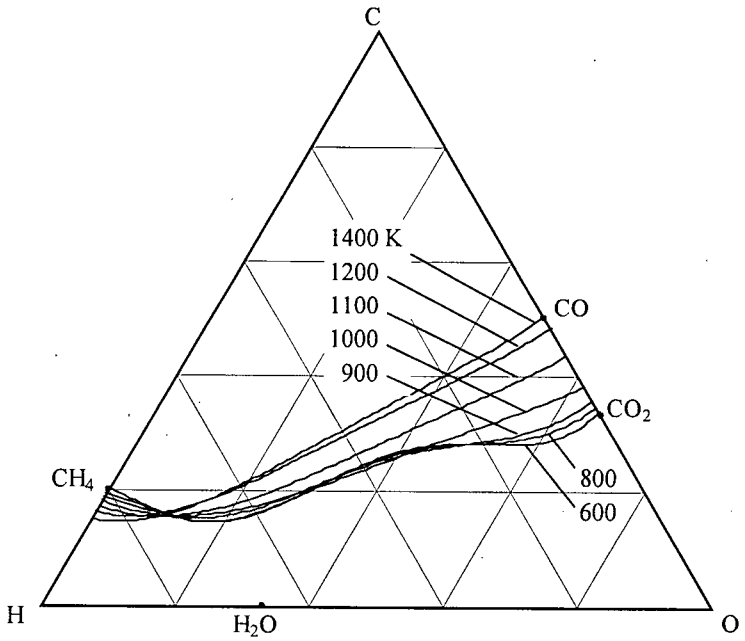

Figure 6-24. Molar ternary diagram showing carbon formation boundary for C-H-O system at a pressure of 10 bar, predicted by non-stoichiometric equilibrium model developed in

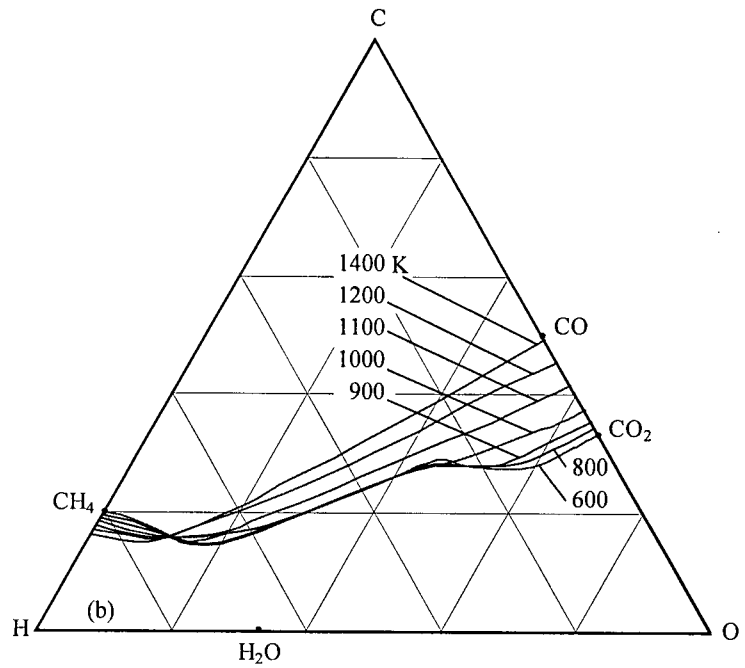

Figure 6-25 Molar ternary diagram showing carbon formation boundary for C-H-O system at a pressure of 20 bar, predicted by non-stoichiometric equilibrium model developed in this work.

6.7.3 Carbon formation tendency in biomass gasification in pilot CFB

The CFB gasifier under consideration can also be represented by a C-H-O ternary diagram since nitrogen is largely inert, and sulfur has such a small molar abundance. In Figure 6-26, the overall elemental abundances from the 15 test runs in the pilot study are represented by solid points in the ternary diagram. Only three points falls in the boundary zone, with none residing in the carbon-forming regime. The operating parameters for the test runs are provided in Table 5-1, with their C-H-O elemental abundance combinations listed in Table 6-7. For these runs, complete carbon conversion may be impossible if the reactor operates at temperatures below 1000 K. For all other test runs, complete carbon conversion can be anticipated if there are no kinetic restrictions.

Table 6-7. Elemental abundance combinations of combined feed streams for biomass gasification tests in pilot CFB gasifier as a C-H-O ternary system.

Run No.	C/(C+H+O)	H/(C+H+O)	O/(C+H+O)
1	0.184	0.421	0.394
2	0.220	0.403	0.377
3	0.223	0.413	0.363
4	0.212	0.389	0.399
5	0.230	0.414	0.356
6	0.224	0.408	0.372
7	0.227	0.430	0.344
8	0.227	0.426	0.347
9	0.247	0.383	0.370
10	0.218	0.420	0.362
11	0.219	0.438	0.342
12	0.246	0.453	0.301
13	0.251	0.434	0.315
14	0.246	0.426	0.328
15	0.232	0.384	0.384

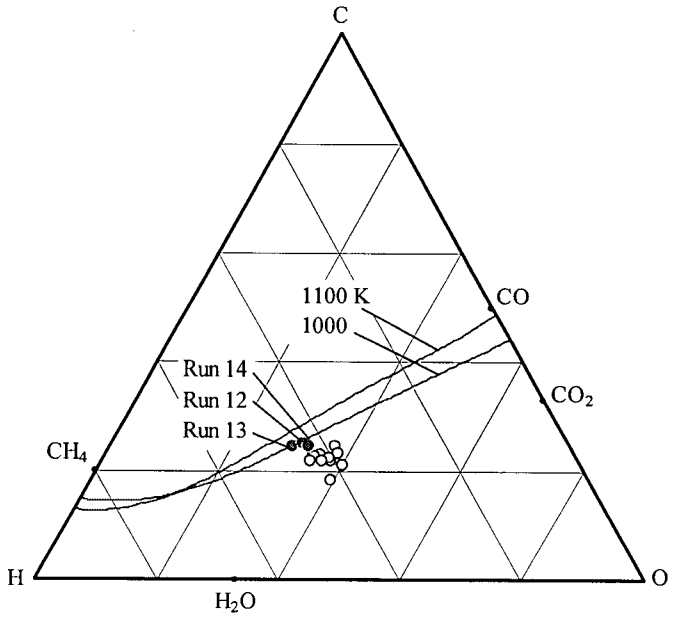

Figure 6-26. Carbon formation tendency in sawdust gasification at atmospheric pressure: Data from CFB pilot test Runs 1-15, gasifying six sawdust species. Open circles for Runs 1-11 and 15, solid circles for Runs 12-14.

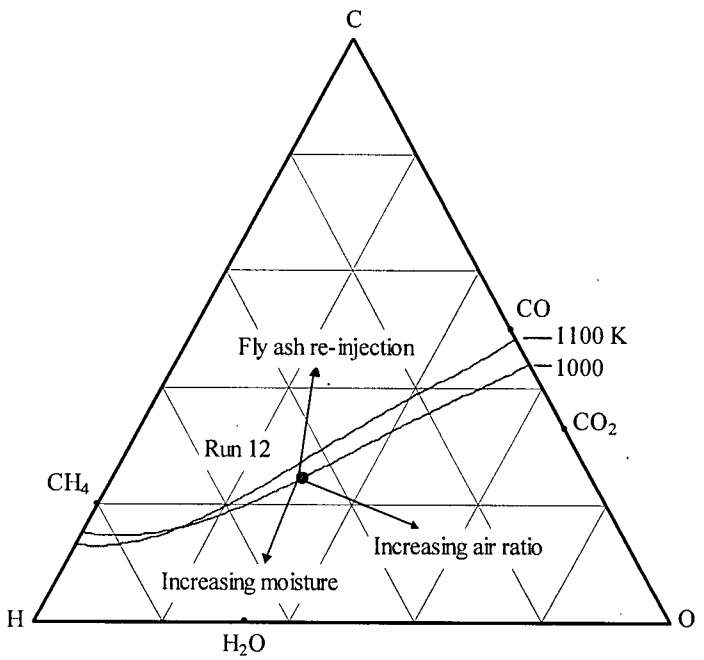

Figure 6-27. Effects of increasing air ratio, moisture in the system and fly ash re-injection on the relative elemental abundance of the C-H-O system as in atmospheric sawdust gasification.

Figure 6-27 illustrates the effect of increasing air ratio, increasing moisture content (either in fuel or by steam injection), and fly ash re-injection on the carbon formation tendency of the system, taking Run 12 as an example. When more air is supplied, the point moves toward the O vertex. When the moisture content of the fuel increases or when steam is injected, the point moves towards the H_2O point. When fly ash is re-injected, the abundance of carbon increases without causing much change in the abundance of H and O since fly ash consists mostly of carbon, so the point migrates toward the C vertex, leading to an increase in the tendency to form carbon.

6.8 Kinetic Modification of Model: Comparison with Experimental Data

6.8.1 Kinetic modification

To correct for kinetic effects, the gasification system can be represented by a C-H-O ternary diagram with part of the carbon and hydrogen removed to account for the non-equilibrium behaviour of carbon and methane. Since none of the operating conditions in our pilot test runs apparently fell in the carbon-forming regime at temperatures above 1000 K, the incomplete carbon conversion can be attributed solely to kinetic effects. In addition, in Figure 5-7, it is shown that up to 9% of the total moles of carbon, and 17% of the hydrogen, stay in methane. Several previous studies (von Fredersdorff, 1963; Coates *et al.*, 1974) have shown that the high measured concentrations of methane from coal gasification result from incomplete conversion of pyrolysis products; equilibrium concentrations of methane in the off-gas are less than 0.1% for the entire parameter range tested. Methane should also be considered in kinetic modification of the equilibrium model in order to better represent the actual process.

If we have the experimental carbon conversion and methane yield, we can correct for the kinetic effects by withdrawing the corresponding carbon and hydrogen from the equilibrium system. The deviations in equilibrium predictions can be substantially reduced. The method has been successfully applied to coal gasification (Li *et al.*, 2001). It was also successful for steam methane reforming (Grace *et al.*, 2001) where hydrogen was preferentially removed through selective palladium membranes. In the present study, it is extended to account for non-equilibrium effects of pyrolysis products like methane and applied to biomass gasification.

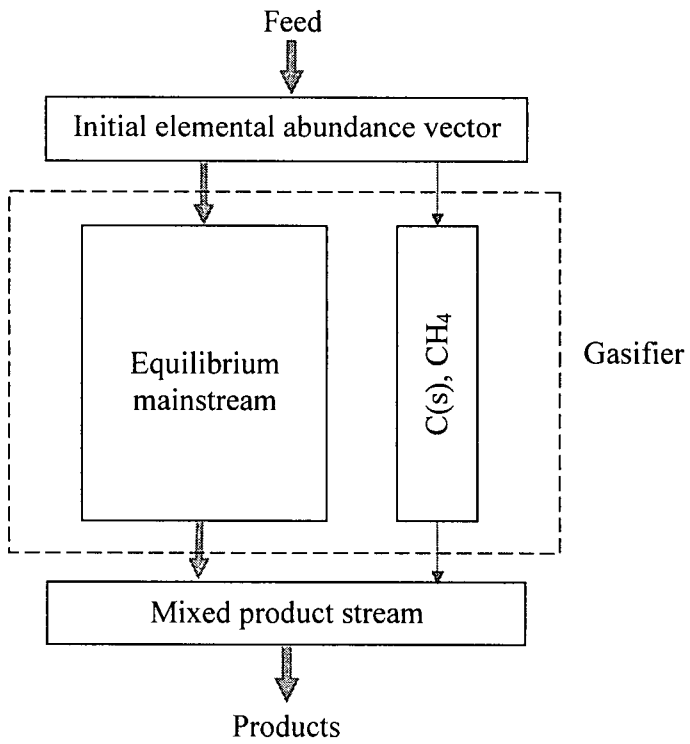

Figure 6-28. Schematic of kinetic modification of equilibrium model.

The kinetically-modified equilibrium model is illustrated schematically in Figure 6-28. The reaction system is assumed to be comprised of a mainstream in chemical equilibrium and a kinetically-controlled short-cut zone producing C(s) and/or methane. The fraction of each part is determined by the operating parameters of the gasifier, such as the air ratio and temperature. The equilibrium mainstream is computed based on the free energy minimization principles, while the

kinetic shortcut is considered by introducing empirical functions to account for the un-converted solid carbon and methane produced during the pyrolysis stage. The whole system is subject to mass balance constraints at every step of the numerical solution.

The element abundance vector of the feed can be written:

$$b_0 = (n_C, n_H, n_O, n_N, n_S). \tag{6-38}$$

It is often taken for granted that the amount of each element participating in the chemical equilibrium is exactly same as in the feed. This can be true when the conditions are such that the reaction kinetics and transfer processes do not impede the achievement of equilibrium. In such cases, the carbon conversion is determined only by thermodynamic constraints. However, the validity of this assumption is questionable for real processes in which reactions (mostly heterogeneous) are controlled or influenced by kinetics and/or diffusion so that some elements never achieve equilibrium. To account for this, the fractional achievement of equilibrium, β, may be imposed, leading to a modified element abundance vector affecting the gas, i.e.:

$$b^* = (\beta_C n_C, \beta_H n_H, \beta_O n_O, \beta_N n_N, \beta_S n_S) \tag{6-39}$$

Base on experimental results from the present study, i.e. Eq. (5-5), the fraction of carbon converted into gas phase is

$$\beta_{C,1} = 0.25 + 0.75\exp(-a/0.23). \tag{6-40}$$

However, a small fraction of carbon entering the gas phase exists as methane, produced during the pyrolysis stage and leaving the system without achieving equilibrium. Mass balance calculations for the pilot runs in this work (Figure 5-7) suggest that this fraction is

$$\beta_{C,2} = 0.11(1-a) \tag{6-41}$$

for the time-mean values, and

$$\beta_{C,2} = 0.15(1-a) \tag{6-42}$$

for the "best cases", i.e. cases which are nearest to the equilibrium predictions. The correlation coefficients for Eqs. (6-41) and (6-42) are 0.53 and 0.59, respectively.

Both $\beta_{C,1}$ and $\beta_{C,2}$ are based on the molar abundance of carbon in the feed. The portion of carbon consumed to produce methane must be deducted from the overall fraction of carbon in the gas phase. The availability of carbon, or the overall fraction of carbon entering chemical equilibrium is therefore

$$\beta_C = \beta_{C,1} - \beta_{C,2}. \tag{6-43}$$

Since one mole of methane contains four moles of hydrogen atoms, the availability of hydrogen at equilibrium is

$$\beta_H = 1 - \frac{4\beta_{C,2} n_C}{n_H}. \tag{6-44}$$

The remaining error in the predictions can be attributed to failure to achieve complete conversion for other elements, as well as measurement errors. Middleton *et al.* (1997) suggested correlating the release of nitrogen and sulfur with the overall conversion. However, since there is no systematic method for handling incomplete conversion of elements other than carbon, the incomplete release of nitrogen and sulfur is not considered. Instead, as a first approximation, we assume complete conversion for all elements other than carbon. Thus, Eq. (6-39) is reduced to:

$$b^* = (\beta_C n_C, \beta_H n_H, n_O, n_N, n_S) \tag{6-45}$$

The effective abundances of carbon and hydrogen in the equilibrium main stream are clearly less than those computed from the feed. Consequently, the effective air ratio exceeds that based on the overall stoichiometry. The modified b^* can reasonably approximate the actual element abundance entering equilibrium, leading to substantially better predictions for the best-fit temperature, as well as the off-gas composition.

6.8.2 Comparison with experimental results

(1) Species molar contents

Figure 6-29 shows the variation of gaseous species contents with air ratio predicted by the kinetically-modified equilibrium model. While N_2 is predicted to be similar to that from the pure equilibrium model, significant changes are found in H_2, CH_4, CO, CO_2 and H_2O. As in Figure 6-4, all species are given as their dry-gas molar contents expect for H_2O, in wet gas content. The modified model predicts much higher CH_4 and H_2O contents than the pure equilibrium model. H_2 and CO go through maxima, not seen in the pure equilibrium predictions.

Figure 6-30 plots the variation of H_2 and CH_4 molar contents with air ratio predicted by the modified equilibrium model. Best cases as listed in Table 6-5 are used for the comparison. The predicted H_2 molar content is still higher than the experimental data except for a few cases. Very little difference is found between predictions for 1000 and 1100 K, so only the latter are plotted. However, CH_4 contents agree very well with experimental data. Similar deviations in H_2 molar contents were also observed in previous work (Ruggiero and Manfrida, 1998).

The likely reason for this deviation is the fractional availability of water to the CO-shift reaction (i.e. $CO + H_2O = CO_2 + H_2$). In a gasification system, the final H_2/CO ratio is affected decisively by the CO-shift reaction (Yan and Zhang, 2000; Hamel and Krumm, 2001). The CO-shift reaction is moderately exothermic (ΔH^0_{298} = 41.1 kJ/mol CO), so that its equilibrium constant decreases with temperature. Therefore, the H_2/CO molar ratio may fall below 1 at high temperatures. Because the shift reaction is among the quickest reactions in the gasification process, it is often assumed to have achieved chemical equilibrium, even in kinetic models (e.g. Vamvuka *et al.*, 1995; Chen *et al.*, 2000; Corella *et al.*, 2000). When all the water in the system is assumed to reach chemical equilibrium, the hydrogen produced by the CO-shift reaction will be over-predicted. However, the water in the fuel is only partially available to the chemical

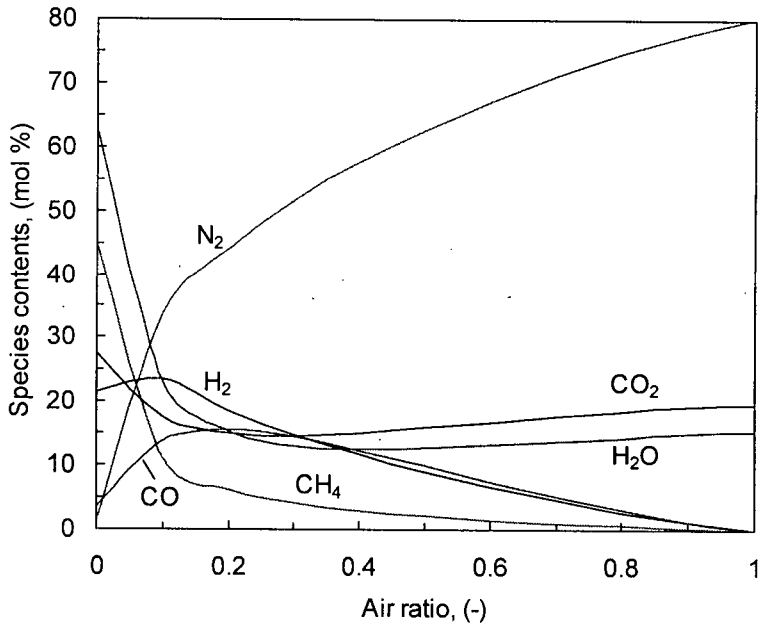

Figure 6-29. Species molar contents vs. air ratio predicted by the kinetically-modified equilibrium model for a temperature of 1100 K.

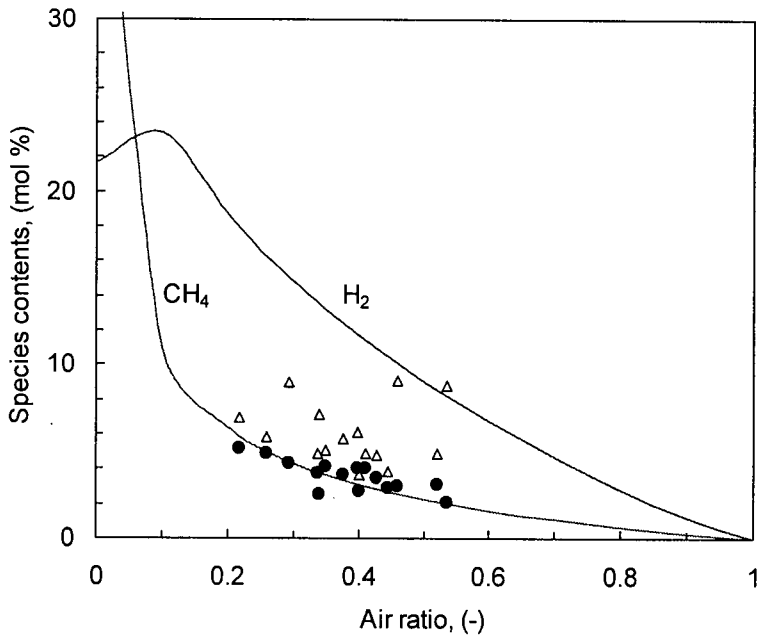

Figure 6-30. Experimental and predicted variation of H_2 and CH_4 molar contents with air ratio for sawdust gasification at 1.013 bar and 1100 K. Experimental data from Runs 1-15: a = 0.22-0.54, M = 4.2-22.0%, T_3 = 970-1090 K. Δ – H_2; • – CH_4.

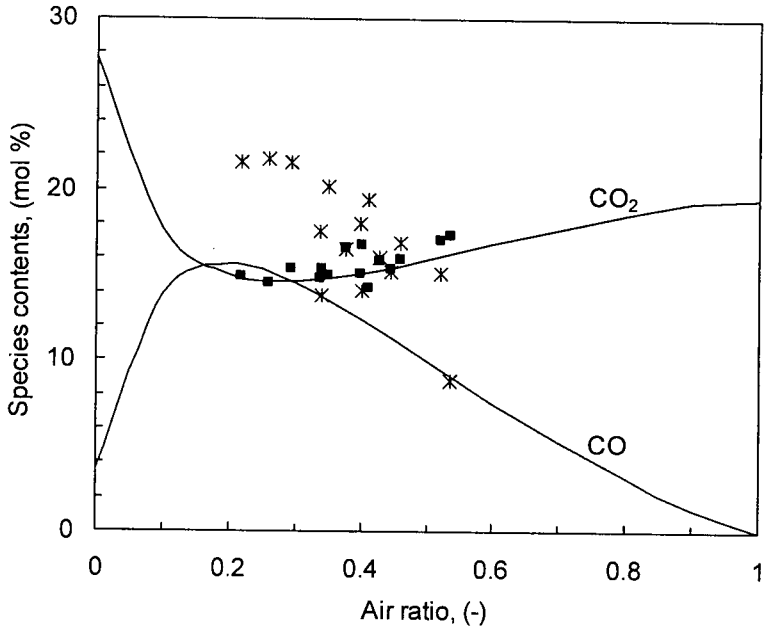

Figure 6-31. Experimental and predicted variation of CO and CO_2 molar contents with air ratio for sawdust gasification at 1.013 bar. Solid lines: predictions for 1100 K. Experimental data from Runs 1-15: a = 0.22-0.54, M = 4.2-22.0%, T_3 = 970-1090 K. ∗ – CO; ■ – CO_2.

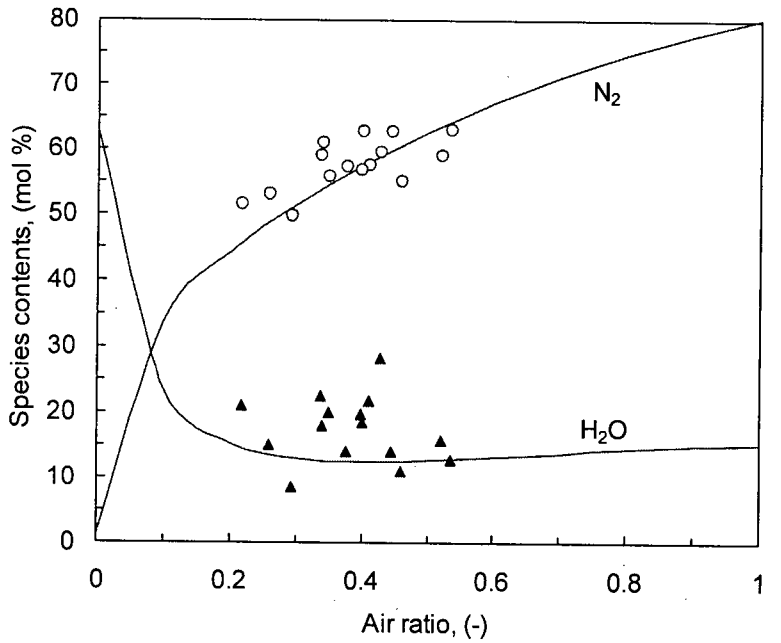

Figure 6-32. Experimental and predicted variation of N_2 and H_2O molar contents with air ratio for sawdust gasification at 1.013 bar: Solid lines: predictions for 1100 K. Experimental data from Runs 1-15: a = 0.22-0.54, M = 4.2-22.0%, T_3 = 970-1090 K. ○ – N_2; ▲ – H_2O.

reactions, as exhibited in the pilot study. This explains why the H_2/CO molar ratio in model predictions is higher than the experimental results (0.25-0.81) from the pilot study. Further improvements in this respect should be sought in future work. However, it is encouraging that the kinetically modified model gives much better predictions than the pure equilibrium model.

Predicted and measured molar contents for CO and CO_2 are compared in Figure 6-31. CO contents are under-predicted by a relative difference of 20-25%. Predicted CO_2 contents are in good agreement with experimental data. Since H_2 contents are over-predicted, while CO contents under-predicted, the resulting H_2/CO molar ratios are about two times higher than the measured data except for Run 1 with particularly high moisture content in the fuel (22.0%).

Figure 6-32 compares predicted and experimental molar contents of N_2 and H_2O in the product gas. The H_2O contents are not directly measured data, but they are obtained from post-test mass balances. Substantial agreement is found for both species.

(2) Gas yield, heating value and gasification efficiency

The specific gas yield predicted with the modified equilibrium model is shown in Figure 6-33 in comparison with both time-mean and best-case experimental data. The kinetically-modified equilibrium model prediction fits the experimental data well. Figure 6-34 compares the experimental data with dry gas higher heating values subjected to kinetic modifications. There is good agreement between the predicted and measured gas heating values, suggesting that changes in the H_2/CO molar ratio due to the CO-shift reaction have little effect on the resulting gas heating value. The heats of combustion of H_2 and CO are very close to each other (285.8 and 283.0 kJ/mol, respectively). Figure 6-35 compares the predicted cold gas efficiency with experimental results. The predicted cold gas efficiency reaches a maximum at an air ratio of about 0.26, in agreement with the prediction of the pure equilibrium version of the model. Despite scatter, the experimental data are in substantial agreement with the model prediction.

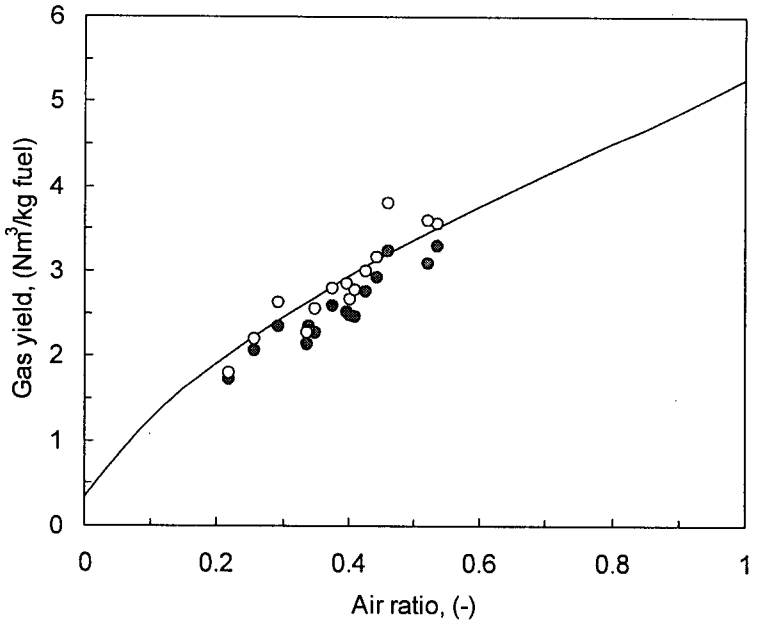

Figure 6-33. Effect of air ratio on predicted and experimental dry gas yields from sawdust gasification at 1.013 bar. Solid line: predictions for 1100 K. Experimental data from Runs 1-15: a = 0.22-0.54, M = 4.2-22.0%, T_3 = 970-1090 K. ○ – best cases; ● – time-mean values.

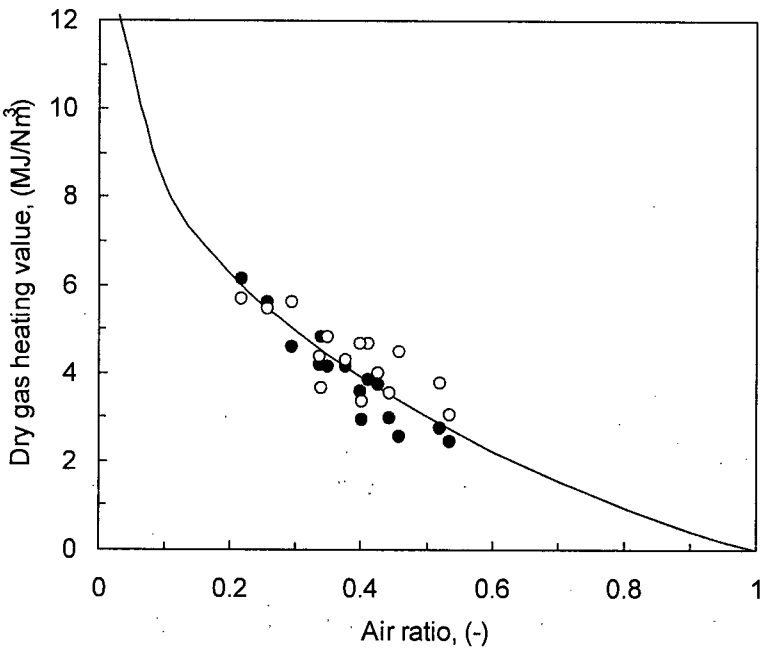

Figure 6-34. Effect of air ratio on predicted and experimental dry gas yields from sawdust gasification at 1.013 bar. Solid line: predictions for 1100 K. Experimental data from Runs 1-15: a = 0.22-0.54, M = 4.2-22.0%, T_3 = 970-1090 K. ○ – best cases; ● – time-mean values.

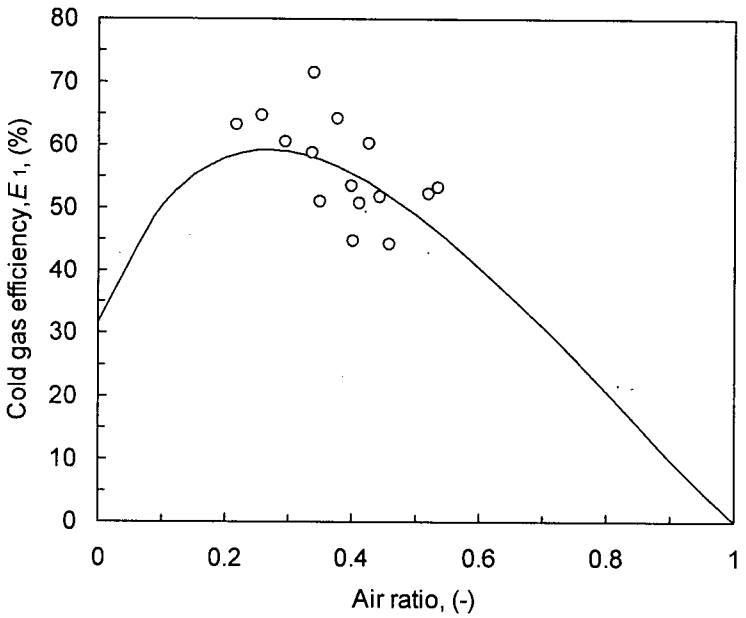

Figure 6-35. Effect of air ratio on predicted and experimental dry gas yields from sawdust gasification at 1.013 bar. Solid line: predictions for 1100 K. Measured data from Runs 1-15: a = 0.22-0.54, M = 4.2-22.0%, T_3 = 970-1090 K. o – time-mean values.

6.9 Summary

This chapter presents two versions of a non-stoichiometric equilibrium model based on free energy minimization, and provides in-depth understanding of the underlying thermodynamic principles governing biomass gasification. The pure equilibrium version predicts that:

(1) The product gas composition from gasification of a typical woody biomass depends primarily on the air ratio. Carbon conversion improves with increasing temperature, but the improvement is less significant when the temperature exceeds 1200 K. The effect of pressure is only observed for temperatures from 700 K to 1250 K.

(2) In the temperature range typical in our pilot study (1000-1100 K), and at air ratios less than 0.2, a considerable portion of the carbon may remain as solid carbon. The equilibrium CH_4

molar content decreases to less than 1% at all air ratios less than 0.2 and temperatures above 1000 K. HS emerges as an important species in the sulfur distribution when the system temperature exceeds 1400 K.

(3) At typical gasification temperatures, an air ratio of 0.2-0.3 is most favourable for producing CO-rich gas. To produce hydrogen-rich gas at atmospheric pressure, the system should operate in the temperature range from 1100 to 1300 K and at an air ratio of 0.15-0.25. Steam injection helps to increase the H_2/CO ratio, but it is practical only for temperatures above 1000 K and air ratios less than 0.3.

(4) Equilibrium predictions suggest that oxygen is mainly used to produce CO_2 and water if the air ratio is larger than 0.33. Operation below this air ratio is favourable. However, woody biomass such as sawdust may not be able to maintain the high temperature desired for gasification at such low air ratios. External heating and co-gasification with other refuse-derived fuels or coal may solve this problem.

(5) The limited range of pressure influence shown in the product distributions of the three most abundant elements (C, H, and O) implies that high-temperature gasification processes ($T > 1200$ K) do not need to be pressurized because increasing pressure only increases the energy consumption with little gain in the equilibrium product quality. The same holds for very low-temperature ($T < 700$ K) processes. However, high pressure does concentrate the gas phase, accelerate reactions and reduce the reaction time and reactor volume required to achieve equilibrium.

(6) The dry gas heating value decreases with increasing air ratio, exhibiting a nearly exponential relationship when reactor temperature exceeds 1000 K, with significant deviation observed only for air ratios larger than 0.55. A maximum cold gas efficiency occurs at a non-

zero air ratio. Cold gas efficiency decreases linearly with a further increase in air ratio and vanishes at stoichiometric combustion conditions.

(7) The model successfully predicts the onset of carbon formation in C-H-O dominated systems. The presence of residual solid carbon is interpreted as saturation of elemental carbon in the gas phase at a given temperature and pressure. When this occurs, increasing air ratio, allowing higher moisture content in the fuel, or injecting steam may help the system to avoid carbon formation. In a C-saturated system, the gas composition becomes insensitive to the elemental abundance of carbon in the feed.

The pure equilibrium version effectively predicts the maximum attainable yield of a given product, and the overall behaviour of the system with changes in different operating parameters. However, carbon conversion in a real process is usually controlled by non-equilibrium factors, and therefore has to be considered by a kinetic model or on an empirical basis.

A kinetically-modified equilibrium model is developed to predict the performance of gasification processes. The modified model, incorporating empirical results from Chapter 5 regarding unconverted carbon and methane, successfully predicts product gas compositions, heating value, gas yield and cold gas efficiency in good agreement with the experimental data, expect for over-predicting the H_2/CO molar ratio. One possible reason that the experimental H_2/CO ratios were less than predicted values is that water was only partially available to the CO-shift reaction, which played a decisive role in determining the final gas composition.

The predicted cold gas efficiency shows a maximum at an air ratio of about 0.26, in agreement with the prediction of the pure equilibrium model. Further work is recommended to examine the role of the CO-shift reaction and partial water conversion in determining the final gas composition in order to improve the H_2/CO molar ratio predictions.

CHAPTER 7. CONCLUSIONS AND SUGGESTIONS FOR FURTHER WORK

7.1 Conclusions

Biomass gasification is a very promising clean energy option for reduction of greenhouse gas emissions. In the present study, six types of sawdust were gasified in a pilot-scale air-blown circulating fluidized bed gasifier to produce low-calorific-value gas. The pilot gasifier employs a riser 6.5 m high and 0.1 m in diameter, a high-temperature cyclone for solids recycle and a ceramic fibre filter unit for gas cleaning. The riser temperature was maintained in the range 970-1120 K while the sawdust feed rate varied from 16-45 kg/h, corresponding to a superficial gas velocity of 4-10 m/s and a throughput of 0.7-2.0 kg/m^2-s. The following conclusions can be drawn from the pilot study:

(1) The product gas composition and heating value depend heavily on the air or O/C ratio and, to a lesser extent, on the operating temperature. The higher heating value of the product gas decreased from 5.6 to 2.1 MJ/Nm^3 as the stoichiometric air ratio increased from 0.22 to 0.54. The gas heating value increased with increasing overall suspension density in the riser. Over the range tested, the feed rate had no significant effect on gas heating value at a fixed air ratio.

(2) Both fly ash re-injection and steam injection caused changes in the product molar ratios. Ash re-injection improved carbon conversion and promoted production of carbon monoxide, while having little effect on the hydrogen balance and hydrogen content of the product gas. Steam injection was effective in promoting steam gasification of char. Though the residual carbon content in the bottom ash was less than 2% for the conditions tested, the low particle density of char resulted in decreased cyclone grade efficiency, leading to high residual carbon

content in the fly ash. Fly ash re-injection, though quite effective in improving the gas heating value, was not able to convert all of the residual carbon.

(3) Tar yield from biomass gasification decreased exponentially with increasing operating temperature. Measured tar yield dropped drastically from 15 to 0.54 g/Nm^3 as the average suspension temperature increased from 970 to 1090 K. Elevating the operating temperature provided the simplest means of decreasing tar in the absence of catalyst. Secondary air had only a very limited effect on tar removal if the total air ratio remains the same. Addition of a nickel-based catalyst significantly affected the product gas composition and species molar ratios as a result of increased H_2 and CO production due to reforming and cracking of higher hydrocarbons. The effectiveness of the catalyst depended on the operating temperature. No deactivation was observed over the limited run time with catalyst addition.

(4) Post-test mass and energy balances were carried out to determine the overall carbon conversion and cold gas efficiency. Good mass balance closure was found between the feed and the product streams. The elemental mass balances indicate that a large fraction of the oxygen, about half of the carbon and a considerable portion of the hydrogen is consumed to produce CO_2 and H_2O. Improving gas quality from gasification requires that the proportion of these two species be decreased.

(5) While carbon conversion increased with increasing O/C ratio, the cold-gas gasification efficiency decreased. Therefore, carbon conversion is not a sufficient criterion for evaluating gasification processes. Gasification efficiency can be maximized within an optimum range of air ratio (a = 0.30-0.35, or O/C = 1.5-1.7), while keeping the tar yield relatively low.

A non-stoichiometric equilibrium model based on free energy minimization was developed to simulate biomass gasification process. Five elements (C, H, O, N and S) and 44 species were considered in the model. The RAND algorithm was used for numerical solution. The model was

coupled with an energy balance equation to evaluate the performance of biomass gasification. Two versions of the model were developed, one accounting for pure equilibrium and the other for real process in which only a partial approach to chemical equilibrium is achieved. The equilibrium model predicts that:

(1) The product gas composition from gasification of woody biomass (e.g. sawdust) depends primarily on the air ratio. Carbon conversion increases with increasing temperature, but the improvement is less significant when the temperature is above 1200 K. In the temperature range of our pilot study (1000-1100 K) and at air ratios below 0.2, a considerable portion of the carbon remains as solid carbon. The equilibrium CH_4 molar content decreases to less than 1% at air ratios greater than 0.2 and temperatures above 1000 K. The high methane content of the product gas observed in the pilot tests does not originate from gasification, but from pyrolysis. HS emerges as an important species in the sulfur distribution when the system temperature exceeds 1400 K.

(2) At typical gasification temperatures, an air ratio of 0.2-0.3 is most favourable for producing CO-rich gas. To produce hydrogen-rich gas at atmospheric pressure, the system should operate at temperatures in the range 1100-1300 K and at air ratios of 0.15-0.25. Steam injection helps to increase the H_2/CO ratio, but it is reasonable only for temperatures above 1000 K and air ratios less than 0.3. Otherwise, steam utilization is low and steam injection may be economically less attractive.

(3) The effect of pressure is only observed for temperatures from 700 to 1250 K. The limited range of pressure influence implies that high-temperature gasification processes ($T > 1200$ K) do not need to be pressurized because elevating pressure only increases the energy consumption with little gain in the equilibrium product quality. The same holds for very low-temperature ($T < 700$ K) processes. However, high pressure does concentrate the gas phase,

accelerate reactions and reduce the reaction time and reactor volume required to achieve equilibrium.

(4) The dry gas heating value decreases with increasing air ratio, while gas yield based on fuel feed rate increases. Both the pure equilibrium model and the kinetically modified model predict that maximum cold gas efficiency occurs at a non-zero air ratio of about 0.25. Cold gas efficiency decreases linearly with a further increase in air ratio and vanishes at stoichiometric combustion conditions.

(5) The model successfully predicts the onset of carbon formation in a C-H-O dominated system when the relative abundance of carbon exceeds a certain level. The presence of residual solid carbon is interpreted as saturation of elemental carbon in the gas phase at a given temperature and pressure. In a C-saturated system, gas composition becomes insensitive to element abundance of carbon in the feed. When carbon formation occurs, increasing air ratio, higher moisture content in the fuel or injected steam help avoid carbon formation.

(6) The pure equilibrium version effectively predicts the maximum attainable yield of a given product and the behaviour of the system with changes in operating parameters. It also provides some understanding of the underlying thermodynamic principles governing biomass gasification. However, carbon conversion in a real process is usually controlled by non-equilibrium factors, and therefore has to be considered by a kinetic model or on an empirical basis. A kinetically-modified equilibrium model was developed for performance prediction of gasification processes. The modified model successfully predicted product gas compositions, heating value, gas yield and cold gas efficiency in good qualitative agreement with the experimental data.

7.2 Recommendations for Further Work

Further research is required to examine a number of factors:

(1) Although the equilibrium model works well in predicting the maximum attainable performance, it cannot predict how long it takes to achieve chemical equilibrium. Kinetic studies of biomass pyrolysis and char gasification for three different physical scales (pore, particle and reactor) are required. Kinetic results are also needed to provide reliable data for the kinetic modification of the equilibrium model. A comprehensive model combining equilibrium insight and kinetic validity will best serve as a research and design tool for the scale-up of biomass gasification systems.

(2) The role of moisture, especially fuel-bound moisture, is not well understood. Little is known about evaporation, diffusion and reaction of moisture in the reaction zone of the gasifier. Most biomass species have relatively high moisture contents, while pre-drying of biomass is both energy- and time-consuming. Deep drying is therefore usually impossible as well as unnecessary. The availability of moisture to the CO-shift reaction has great effect on the final gas composition. Investigation of measures to improve availability of fuel-bound moisture from both equilibrium and kinetic points of view is of theoretical and practical significance.

(3) The kinetics of the CO-shift reaction greatly affects the final gas composition and H_2/CO molar ratio. Though the reaction is often assumed to be in equilibrium, it could be subject to kinetic control at lower temperatures. In addition, equilibrium calculations predict that HS emerges at temperatures above 1400 K as a major species in the sulfur chemistry, assuming a great influence on the sulfur removal from high-temperature biomass gasification processes. Little is known, however, about the reaction kinetics of HS since existing research efforts have been focused on H_2S. The kinetics of reactions involving HS requires further study.

(4) Tar removal and gas conditioning with catalytic addition is another aspect of interest. Catalyst effectiveness and deactivation by carbon deposition or sulfur- or nitrogen-containing species are crucial technical aspects for biomass gasification if catalysts are to be incorporated into integrated gasification combined cycle (IGCC) technology.

(5) CO_2 recycle is believed to improve carbon conversion through the Boudouard reaction ($C + CO_2 = 2CO$). Due to the limited time and equipment, CO_2 recycle was not tested in the present study. This reaction is reported to be effective only at temperatures above 1170 K. However, it may become important at lower temperatures when catalysed by the alkali and transition metals contents in biomass. Kinetic study is therefore recommended. Purchase of a gas pump for CO_2 recycle may be worth considering.

(6) To achieve maximum cold gas efficiency, lower air ratios should be tried. Woody biomass such as sawdust may not be able to maintain the high temperature desired for gasification by itself at air ratios lower than 0.2. External heating and co-gasification with other refuse-derived fuels or coal are two options.

(7) Incorporation of more elements (Ca, Cl, and Na) and species in the equilibrium model is recommended in future work. These species are already included in the thermodynamic database for the equilibrium model. Since introduction of more solid species increases the number of simultaneous equations in the RAND algorithm, it results in much longer time for convergence, and could cause singularities in numerical calculation. However, to understand the ash-related processes during gasification, there is a compelling need for the introduction of more elements and species. Further work on the kinetic modification of equilibrium model is also recommended in order to predict gas composition, in particular the H_2/CO molar ratio, with better accuracy.

NOMENCLATURE

a	air ratio, defined as ratio of actual air supply to stoichiometric air requirement, -
a_{ij}	coefficient in element species matrix representing species i containing element j, -
a_1 - e_1	correlation factors for free energy of formation, -
a_2 - d_2	correlation factors for enthalpy, -
a_c	activity of amorphous carbon, -
b	element abundance vector, -
b_0	initial element abundance vector, -
b^*	element abundance vector modified with kinetic carbon conversion, -
c, c_0	constants in Eq. (2-7)
C	carbon conversion, %;
C_f	free active site on carbon surface, -
C_{far}	carbon content in ash, % of mass
C_{ar}	carbon content in fuel, as-received basis, %
d_i	particle diameter, mm
$\bar{d}$	particle surface mean diameter determined from sieving data, mm
d_{50}	cut size for cyclone separation, mm
E	activation energy, kJ/mol
E_g	gasification efficiency, %
E_1	cold-gas efficiency excluding tars, %
E_2	cold-gas efficiency including tars, %
ER	equivalence ratio, -
F	ratio of carbon in re-injected fly ash to carbon introduced with fuel, -
f_i	mass fraction of particles belonging to i-th size grade in sieving, %
G	Gibbs free energy, kJ/mol
GR	gasifying-agent-to-biomass ratio, -

GCV	gross calorific value of fuel, MJ/kg
ΔG_f°	free energy of formation, kJ/mol
g	acceleration of gravity, 9.81 m/s^2
H	enthalpy, kJ/mol; height, m
H_{ar}	hydrogen content in fuel, as-received basis, %
HHV	higher heating value of product gas, MJ/Nm^3
ΔH	change in system enthalpy, kJ/kg
Δh	height of a section of the riser, m
ΔH_f°	heat of formation, kJ/mol
k	kinetic rate constant, mol, s, or bar
k_0	pre-exponential factor of rate constant, mol, s, bar
K	equilibrium constant, -; total number of elements considered, -
L	total number of feed streams considered, -
M	external moisture addition, kg/kg (dry basis)
M_{ar}	moisture content in fuel, as-received basis, %
(m)	number of iterations, -
m_l	mass of l-th feed stream, kg
$\dot{m}$	feed rate, kg/h
N	total number of species considered, -
N_c	number of revolutions traveled by a particle in cyclone, -
n	moles of a given species or element, mol
n_t	total moles in system, mol
$n_{z\alpha}$	inert moles in phase α, mol
P	system pressure, bar
P_{CO}, P_{CO_2}	partial pressures of CO and CO_2, bar
ΔP	pressure difference, kPa
R	ideal gas constant, 8.314 J/mol K

S	entropy, kJ/mol-K
S_{ar}	sulfur content in fuel, as-received basis, %
S/B	steam-to-biomass ratio, -
t	reaction time, s
T	thermodynamic temperature, K
T_3	riser temperature at T3 level (3946 mm above primary air inlet of gasifier), K
T_{eq}^{o}	equilibrium temperature from best fit to experimental data, K
T_m	mean operating temperature, K
U_i	cyclone inlet gas velocity, m/s
u_a	proportion of phase α in differential change in total moles of system, -
x	molar fraction, -
y	number of moles, mol
y_t	tar yield, g/kg-fuel

Greek letters

β	elemental availability, or fractional achievement of equilibrium conversion, -
β_C	availability of carbon, -
β_H	availability of hydrogen, -
δ	differential increment
γ	fraction of hydrogen atoms present as H_2O in system, -
ε	reaction coordinate, -; maximum allowable error in species moles, mol
$\bar{\varepsilon}$	mean voidage of gas-solid suspension, -
η_i	cyclone grade efficiency, %
λ_k	Lagrange multiplier
μ	viscosity, Pa·s
μ_i	chemical potential of species i, kJ/mol
π	total number of phases considered, -

ρ	density, kg/m^3
ψ_k	function related to Lagrange multiplier

Subscripts

0	initial
50	cut size for cyclone separator
ar	as-received basis
ave	average
C, H, N, O, S	carbon, hydrogen, nitrogen, oxygen, sulfur
daf	dry-ash-free basis
eq	equilibrium model prediction
far	fly ash re-injection
f	feed
i	species index
j, k, l	component, element, feed stream indices
meas	measurement data
p	particle
prod	products
susp	suspension
α	phase index

Superscripts

*	modified value
m	current number of iteration
o	thermodynamic standard state

LITERATURE CITED

Abatzoglou, N., Barker, N., Hasler, P., and Knoef, H. (2000) The development of a draft protocol for the sampling and analysis of particulate and organic contaminants in the gas from small biomass gasifiers. *Biomass Bioenerg.* **18**, 5-17.

Aihara, M., Yu, D., and Antal, M. J. (1993) Wet biomass gasification in supercritical water. *Abstr. Pap. Am. Chem. S.* **205**: 113 – *Cell* Part 1, 28.

Alemasov, V. E., Dregalin, A. F., Tishin, A. P., and Khudyakov, V. A., (1974) Thermodynamic and thermophysical properties of combustion products. Vol. 1: Computation methods. Glushko V. P. ed., Isreal Program for Scientific Translations, Jerusalem.

Alvin M. A. (1998) Impact of char and ash fines on porous ceramic filter life. *Fuel Process. Technol.* **56**, 143-168.

Antal, M. J., Allen, S. G., Schulman, D., Xu, X. D., and Divilio, R. J. (2000) Biomass gasification in supercritical water. *Ind. Eng. Chem. Res.* **39**, 4040-4053.

Arvelakis, S., Sotiriou, C., Moutsatsou, A., and Koukios, E. G. (1999) Prediction of the behaviour of biomass ash in fluidized bed combustors and gasifiers. *J. Therm. Anal. Calorim.* **56**, 1271-1278.

Asadullah, M. Fujimoto, K., and Tomishige, K. (2001) Catalytic performance of Rh/CeO2 in the gasification of cellulose to synthesis gas at low temperature. *Ind. Eng. Chem. Res.* **40**, 5894-5900.

Aznar, M. P., Caballero, M. A., Gil, J., Martin, J. A., and Corella, J. (1998) Commercial steam reforming catalysts to improve biomass gasification with steam-oxygen mixtures. 2. Catalytic tar removal. *Ind. Eng. Chem. Res.* **37**, 2668-2680.

Babu, S. P. (1995) Thermal gasification of biomass technology developments: End of task report for 1992 to 1994. *Biomass Bioenerg.* **9** (1-5): 271-285.

Backman R. and Hupa M. (1990) Gasification of black liquor at elevated pressures: Thermodynamic analysis. Report 90-10, Dept. of Chemical Engineering, Åbo Akademi, Åbo, Finland.

Bain, R. L. (1993) Electricity from biomass in the United States – Status and future direction. *Bioresource Technol.* **46**, 86-93.

Barin I and Plazki G. (1995) *Thermochemical Data for Pure Substances*. VCH Publishers, Weiheim, Germany.

Beenackers, A. A. C. M. (1999) Biomass gasification in moving beds, a review of European technologies. *Renew. Energ.* **16**, 1180-1186.

Berruti, F. and Kalogerakis N. (1989) Modeling the internal flow structure of circulating fluidized beds. *Can. J. Chem. Eng.* **67**, 1010-1014.

Borrelli, S., Giordano, M., and Salatino, P. (1996) Modelling diffusion-limited gasification of carbons by branching pore models. *Chem. Eng. J.* **64**, 77-84.

Brereton, C. M. H. (1987) Fluid mechanics of high velocity fluidized beds. Ph.D. dissertation, the University of British Columbia, Vancouver, BC.

Brereton, C. M. H., Grace, J. R. and Yu J. (1988) Axial gas mixing in a circulating fluidized bed, in *Circulating Fluidized Bed Technology II*, Basu P. and Large, J. F. eds., Pergamon Press, New York, pp. 307-314.

Bridgwater, A. V. (1995) The technical and economic feasibility of biomass gasification for power generation. *Fuel* **74**, 631-653.

Brinkley, S. R. Jr. (1947) Calculation of the equilibrium composition of system of many constituents. *J. Chem. Phys.* **15**, 107-110.

Brown, R. C., Liu, Q., and Norton, G. (2000) Catalytic effects observed during the co-gasification of coal and switchgrass. *Biomass Bioenerg.* **18**, 499-506.

Brunetti, N. (1989) Italian activities in biomass gasification. *Biomass* **18**, 273-285.

Caballero, M. A., Aznar, M. P., Gil, J., Martin, J. A., Frances, E., and Corella, J. (1997) Commercial steam reforming catalysts to improve biomass gasification with steam-oxygen mixtures.1. Hot gas upgrading by the catalytic reactor. *Ind. Eng. Chem. Res.* **36**, 5227-5239.

Caballero, M. A., Corella, J., Aznar, M. P., and Gil, J. (2000) Biomass gasification with air in fluidized bed. Hot gas cleanup with selected commercial and full-size nickel-based catalysts. *Ind. Eng. Chem. Res.* **39**, 1143-1154.

Cahill, P., Rasmussen, G., Tustin, M. and Robertson, D. (1993) Filtration properties of dust from fluidized bed gasification systems, in *Gas Cleaning at High Temperature*, Clift, R. and Seville, J. P. K. eds., Blackie, London, pp. 111-126.

Chase, M. W. Jr., Davies, C. A., Downey, D. J. Jr., Frurip, D. J., McDonald, R. A. and Syverud, A. D. (1985) JANAF thermodynamic tables. 3rd ed. *J. Phys. Chem. Ref. Data.*, **14**, Suppl 1.

Chen, C. X., Horio, M., Kojima, T. (2000) Numerical simulation of entrained flow coal gasifiers. Part I: modeling of coal gasification in an entrained flow gasifier. *Chem. Eng. Sci.* **55**, 3861-3874.

Cheremisinoff, N. P. and Cheremisinoff, P. N. (1985) Particle properties and characterization, in *Encyclopedia of Fluid Mechanics, Vol.* **4**: *Solids and Gas-Solid Flows*. Gulf Publishing Co., Huston, pp. 3-37.

Chern S. M., Walawender W. P. and Fan L. T. (1991) Equilibrium modeling of a downdraft gasifier. 1. Overal gasifier. *Chem. Eng. Commun.* **108,** 243-265.

Coates, R. L., Chen, C. L., and Pope, B. J. (1974) Coal devolatilization in a low pressure, low residence time entrained flow reactor, in *Coal gasification.* Massey, L. G. ed., *Advances in Chemistry Series* **131**. American Chemical Society, Washington D. C, pp. 92-107.

Coll, R., Salvado, J., Farriol, X., and Montane, D. (2001) Steam reforming model compounds of biomass gasification tars: Conversion at different operating conditions and tendency towards coke formation. *Fuel Process. Technol.* **74**, 19-31.

Collot, A. G., Zhuo, Y., Dugwell, D. R., and Kandiyoti, R. (1999) Co-pyrolysis and co-gasification of coal and biomass in bench-scale fixed-bed and fluidised bed reactors. *Fuel* **78**, 667-679.

Corella, J., Herguido, J., Toledo, J. M., and Gomez-Civicos, J. I. (2000) Modeling fluidized bed biomass gasifiers: Part II: Gasification with steam in a bubbling fluidized bed. In *Biomass for energy and industry*, preprint.

Corella, J., Orio, A., and Aznar, P. (1998) Biomass gasification with air in fluidized bed: Reforming of the gas composition with commercial steam reforming catalysts. *Ind. Eng. Chem. Res.* **37**, 4617-4624.

Corella, J., Orio, A., and Toledo, J. M. (1999) Biomass gasification with air in a fluidized bed: Exhaustive tar elimination with commercial steam reforming catalysts. *Energ. Fuel* **13**, 702-709.

Courson, C., Makaga, E., Petit, C., and Kiennemann, A. (2000a) Development of Ni catalysts for gas production from biomass gasification. Reactivity in steam- and dry-reforming. *Catal. Today* **63**, 427-437.

Courson, C., Petit, C., and Kiennemann, A. (2000b) Physico-chemical characterization of a natural olivine and its use in industrial catalysis. *J. Phys. IV* **10**, (P10) 531-540.

De Bari, I., Barisano, D., Cardinale, M., Matera, D., Nanna, F., and Viggiano, D. (2000) Air gasification of biomass in a downdraft fixed bed: A comparative study of the inorganic and organic products distribution. *Energ. Fuel* **14**, 889-898.

Delgado, J., Aznar, M. P., and Corella, J. (1996) Calcined dolomite, magnesite, and calcite for cleaning hot gas from a fluidized bed biomass gasifier with steam: Life and usefulness. *Ind. Eng. Chem. Res.* **35**, 3637-3643.

Delgado, J., Aznar, M. P., and Corella, J. (1997) Biomass gasification with steam in fluidized bed: Effectiveness of CaO, MgO, and CaO-MgO for hot raw gas cleaning. *Ind. Eng. Chem. Res.* **36**, 1535-1543.

Demirbas, A. (2001) Yields of hydrogen-rich gaseous products via pyrolysis from selected biomass samples. *Fuel* **80**, 1885-1891.

Dent, J. F., Moignard, L. A., Blackbraum, W. H., and Herbden, D. (1945) An investigation into the catalytic synthesis of methane by town gas manufacture. 49th Report of the Joint Research Committee of the Gas Research Board and the University of Leeds. GRB20.

Depner, H. and Jess, A. (1999) Kinetics of nickel-catalyzed purification of tarry fuel gases from gasification and pyrolysis of solid fuels. *Fuel* **78**, 1369-1377.

Di Blasi, C. (1993) Analysis of convection and secondary reaction effects within porous solid fuels undergoing pyrolysis. *Combust. Sci. Technol.* **90**, 315-340.

Di Blasi, C., Signorelli, G., and Portoricco, G. (1999) Countercurrent fixed-bed gasification of biomass at laboratory scale. *Ind. Eng. Chem. Res.* **38**, 2571-2581.

Diener, R., Hedden, K., and Schaub, G. (1990) Thermal degradation of volatile pyrolysis products in the crude gaseous products of coal and biomass gasification – Kinetic study on model substances. *Chem-Ing-Tech.* **62**, 572-573.

Dirgo, J. and Leith, D. (1986). Design of Cyclone Separators, in *Encyclopedia of Fluid Mechanics*, ed. Cheremisinoff, N. P., Vol. 4, 1281-1306.

Dong, Y. J. and Steinberg, M. (1997) Hynol - An economical process for methanol production from biomass and natural gas with reduced CO_2 emission. *Int. J. Hydrogen Energ.* **22**, 971-977.

Energy Research Centre of the Netherlands (ECN) (2001) Annual report - 2000. Petten, The Netherlands.

Engstrom F. (1998) Hot gas clean-up bioflow ceramic filter experience. *Biomass Bioenerg.* **15**, 259-262.

Ergudenler, A. (1998) Circulating fluidized bed gasification for pulp and paper applications. Unpublished intermediate report, The University of British Columbia.

Ergudenler, A. and Ghaly, A. E. (1992) Quality of gas produced from wheat straw in a dual-distributor type fluidized bed gasifier. *Biomass Bioenerg.* **3**, 419-430.

Ergudenler, A., Ghaly, A. E., Hamdullahpur, F., and Al-Taweel, A. M. (1997a) Mathematical modeling of a fluidized bed straw gasifier: Part I - Model development. *Energ. Source* **19**, 1065-1084.

Ergudenler, A., Ghaly, A. E., Hamdullahpur, F., and Al-Taweel, A. M. (1997b) Mathematical modeling of a fluidized bed straw gasifier: Part III - Model verification. *Energ. Source* **19**, 1099-1121.

Ergudenler, A., Tang, W. S., Brereton, C. M. H., Lim, C. J., Grace, J. R., and Gennrich, T. J. (1997c) Performance of high-temperature fabric filters under gasification and combustion conditions. *Separat. Purif. Technol.* **11**, 1-16.

FAO (Food and Agricultural Organization of the United Nations) (1986) *Wood gas as engine fuel.* Rome, Italy.

FAO (Food and Agriculture Organization of the United Nations) (2001) *State of the world's forests.* Rome, Italy.

Fiaschi, D. and Michelini, M. (2001) A two-phase one-dimensional biomass gasification kinetics model. *Biomass Bioenerg.* **21**, 121-132.

French, R. J. and Milne, T. A. (1994) Vapor phase release of alkali species in the combustion of biomass pyrolysis oils. *Biomass Bioenerg.* **7**, 315-325.

Garcia, L., French, R., Czernik, S., and Chornet, E. (2000) Catalytic steam reforming of bio-oils for the production of hydrogen: effects of catalyst composition. *Appl. Catal. A – Gen.* **201**, 225-239.

Garcia, L., Salvador, M. L., Arauzo, J., Bilbao, R. (1999) Catalytic steam gasification of pine sawdust. Effect of catalyst weight/biomass flow rate and steam/biomass ratios on gas production and composition. *Energ. Fuel* **13**, 851-859.

Garciabacaicoa, P., Bilbao, R., Arauzo, J., Giordano, N., Antonucci, V. (1994) Scale-up of downdraft moving bed gasifiers (25-300 kg/h) – Design, experimental aspects and results. *Bioresource Technol.* **48**, 229-235.

Gebhard, S. C., Wang, D. N., and Overbend, R. P. (1993) Catalytic conditioning of synthesis gas produced by biomass gasification. *Abstr. Pap. Am. Chem. S.* **205**: 120 – *Cell* Part 1, 28.

Gibbs, J. W. (1876) *Thermodynamics*. In *The Scientific papers of J. Wilard Gibbs*, Vol. I, Dover, New York, 1961.

Gil, J., Aznar, M. P., Caballero, M. A., Frances, E., and Corella, J. (1997) Biomass gasification in fluidized bed at pilot scale with steam-oxygen mixtures. Product distribution for very different operating conditions. *Energ. Fuel* **11**, 1109-1118.

Gil, J., Caballero, M. A., Martin, J. A., Aznar, M. P., and Corella J. (1999) Biomass gasification with air in a fluidized bed: Effect of the in-bed use of dolomite under different operation conditions. *Ind. Eng. Chem. Res.* **38**, 4226-4235.

Grace, J. R., Li, X. T., and Lim, C. J. (2001) Equilibrium modelling of catalytic steam reforming of methane in membrane reactors with oxygen addition. *Catal. Today* **64**, 141-149.

Granatstein, D. L., Talbot, R. E. and Anthony, E. J. (2001) Application of IGCC technology in Canada - Phase IV. CANMET Energy Technology Centre, Report prepared for Environment Canada Oil, Gas and Energy Division.

Gruber G. (1975) Equilibrium considerations in the methane synthesis system, in *Methanation of synthesis gas*, Seglin L. ed., *Advances in Chemistry Series* **146**. American Chemical Society, Washington D. C, pp. 31-46.

Gudenau, H. W., Schauermann, G., and Hahn, W. (1993) Gasification of weidel grass in the circulating fluidized bed. *Brennst-Warme-Kraft* **45**, 491-494.

Guo, B., Li, D. K., Cheng, C. M., Lu, Z. A., and Shen, Y. T. (2001) Simulation of biomass gasification with a hybrid neural network model. *Bioresource Technol.* **76**, 77-83.

Guo, J. W., Song, X. R., and Cui, Y. D. (2002) Catalytic pyrogasification of biomass in a fluidized bed reactor. *Ranliao Huaxue Xuebao* (*J. Fuel Chem.*) (in Chinese) **29**, 319-322.

Gurvich, L. V., Veyts, I. V., and Alcock, C. B. (1990) *Thermochemic Properties of Individual Substances*. Hemisphere, Washington.

Gustavsson, L. (1994) Biomass and district heating systems. *Renew. Energ.* **5**, 838-840.

Hall D. O. and Rosillo-Calle F. (1998) Evaluation environmental effects and carbon sources and sinks resulting from biomass production and use in developing countries, in *Biomass energy: data, analysis and trends*. IEA Conference Proceedings. Paris, France. pp. 267-292.

Hamel, S. and Krumm, W. (2001) Mathematical modelling and simulation of bubbling fluidised bed gasifiers. *Powder Technol.* **120**, 105-112 Sp. Iss.

Hasler, P., Nussbaumer, T. (2000) Sampling and analysis of particles and tars from biomass gasifiers. *Biomass Bioenerg.* **18**, 61-66.

Hebden, D. and Stroud, H. J. F. (1981) Coal gasification processes, in *Chemistry of Coal Utilization*, 2nd Suppl., Elliott, M. A. ed., John Wiley & Sons, New York. pp. 1599-1752.

Henrich, E., Burkle, S., Meza-Renken, Z. I., and Rumpel, S. (1999) Combustion and gasification kinetics of pyrolysis chars from waste and biomass. *J. Anan. Appl. Pyrol.* **49**, 221-241.

Hepola, J., Simell, P., Kurkela, E., and Stahlberg, P. (1994) Sulfur poisoning of nickel catalysts in catalytic hot gas cleaning conditions of biomass gasification. *Stud. Surf. Sci. Catal.* **88**, 499-506.

Hindsgaul, C., Schramm, J., Gratz, L., Henriksen, U., and Bentzen, J. D. (2000) Physical and chemical characterization of particles in producer gas from wood chips. *Bioresource Technol.* **73**, 147-155.

Holub R. and Vonka P. (1976) *The Chemical Equilibrium of Gaseous Systems*. D. Reidel Publishing Company, Dordrecht, The Netherlands.

Hougen O. A., Watson K. M. and Ragatz R. A. (1964) *Chemical process principles. Part II: Thermodynamics*, 2nd ed., John Wiley & Sons, New York.

Howard, J. B. (1981) Fundamentals of coal pyrolysis and hydropyrolysis, in *Chemistry of Coal Utilization*, 2nd Suppl., Elliott, M. A. ed., John Wiley & Sons, New York, pp. 1599-1752.

Ido, T., Mizuno, S., Yosimori, T., Mori, M., and Goto, S. (1999) Gasification of carbonaceous materials by carbon dioxide with molten carbonate catalysts. *Kagaku Kogaku Ronbonshu* **25**, 303-308.

International Panel for Climate Change (IPCC) (2000) Land use, land-use change, and forestry, in *A Special Report of the IPCC. Published for IPCC by the World Meteorological Society and UNEP*, Watson, R. T., Nobel, I. R., Bolin, B., Ravindranath, N. H., Verando, D. J., and D. J. Dokken, eds., Cambridge University Press, Cambridge, UK.

Jacoby, W. A., Gebhard, S. C., Vojdani, R. L., Yilmaz, S., and Cowley, S. (1995) Lifetime testing of catalysts for conditioning of the products of a biomass gasifier. *Abstr. Pap. Am. Chem. S.* **210**: 69 - *Fuel* Part 1, 20.

Jenkins, B. M., Bakker, R. R., and Wei, J. B. (1996) On the properties of washed straw. *Biomass Bioenerg.* **10**, 177-200.

Jensen, P. A., Frandsen, F. J., Dam-Johansen, K., and Sander, B. (2000) Experimental investigation of the transformation and release to gas phase of potassium and chlorine during straw pyrolysis. *Energ. Fuel* **14**, 1280-1285.

Jiang, H. M. and Morey, R. V. (1992) Gasification of corncobs at fluidization. *Biomass Bioenerg.* **3**, 87-92.

Johnson, J. L. (1981) Fundamentals of coal gasification, in *Chemistry of Coal Utilization*, Elliott, M. A. ed., John-Wiley & Sons, New York. pp. 1491-1598.

Kapteijn, F. and Moulijn, J. A. (1985) Kinetics of catalyzed and uncatalyzed coal gasification, in *Carbon and Coal Gasification*, Figueiredo J. T. and Moulijn, J. A. eds., NATO ASI Series 105, Martinus Nijhoff Publishers, Dordrecht, The Netherlands, pp. 291-360.

Kim, Y. J., Lee, J. M., and Kim, S. D. (2000) Modeling of coal gasification in an internally circulating fluidized bed reactor with draught tube. *Fuel* **79**, 69-77.

Knight, R. A. (2000) Experience with raw gas analysis from pressurized gasification of biomass. *Biomass Bioenerg.* **18**, 67-77.

Knoef, H. A. M. (2002a) Gasifier inventory. Website URL: http://www.btgworld.com/gi/

Knoef, H. A. M. (2002b) Private communications on tar sampling.

Kojima, T., Assavadakorn, P., and Furusawa, T. (1993) Measurement and evaluation of gasification kinetics of sawdust char with steam in an experimental fluidized bed. *Fuel Process. Technol.* **36**, 201-207.

Krishnamoorthy, P. R., Seetheramu, S., and Bhatt M. S. (1991) Development of a novel updraft multi-fuel biomass gasifier. *Int. J. Energ. Res.* **15**, 377-390.

Kukerla, E. and Stahlberg, P. (1992) Air gasification of peat, wood and brown coal in a pressurized fluidized-bed reactor. 1. Carbon conversion, gas yield and tar formation. *Fuel Process. Technol.* **31**, 1-21.

Kurkela, E. Stahlberg, P., Simell, P., and Leppalahti, J. (1989) Updraft gasification of peat and biomass. *Biomass* **19**, 37-46.

Laine, N. R., Vastola, F. J. and Walker, P. L. Jr. (1963) The importance of active surface area in the carbon-oxygen reaction. *J. Phys. Chem.* **67**, 2030-2034.

Larson, E. D. and Williams, R. H. (1990) Biomass gasifier steam injected gas turbine cogeneration. *J. Eng. Gas Turb. Power* **112**, 157-163.

Larson, E. D., Kreutz, T. G., and Consonni, S. (1999) Combined biomass and black liquor gasifier/gas turbine cogeneration at pulp and paper mills. *J. Eng. Gas Turb. Power* **121**, 394-400.

Latif, A., Yates, G., and Di Felice R. (1999) Gas mixing and solid circulation in a circulating fluidized bed for the continuous combustion-gasification of biomass. in *Circulating Fluidized Bed Technology VI*, Werther, J. ed., pp. 451-457.

Lau, F. S. (1998) The Hawaiian project. *Biomass Bioenerg.* **15**, 233-238.

Leith, D. and Licht, W. (1972) The collection efficiency of cyclone type particle collectors – A new theoretical approach. *AIChE Symp. Ser.* **68** (26), 196-206.

Li, J. F., Wan, Y. H., and Ohi, J. M. (1997) Renewable energy development in China: Resource assessment, technology status, and greenhouse gas mitigation potential. *Appl. Energ.* **56**, 381-394.

Li, X. T., Grace, J. R., Watkinson, A. P., Lim, C. J., and Ergudenler, A. E. (2001) Equilibrium modeling of gasification: a free energy minimization approach and its application to a circulating fluidized bed coal gasifier. *Fuel* **80**, 195-207.

Li, Y. H. (1999) Kinetic studies of NO and N_2O reduction with coal chars. Ph.D. thesis, Department of Chemical Engineering, the University of Queensland, Brisbane, Queensland, Australia.

Lide, D. R. (1994) *CRC Handbook of Chemistry and Physics*. 74th ed. CRC Press, Boca Raton.

Liu, P., Guo, X. F., Wu, C. Z., Chen, Y., and Arai, N. (2000) Gasification characteristics of biomass wastes in fluidized bed gasifier. *J. Propul. Power* **16**, 606-608.

Lizzio, A. A., Jiang, H. and Radovic, L. R. Jr. (1990) On the kinetics of carbon (char) gasification: Reconciling models with experiments. *Carbon* **28**, 7-19.

Maniatis K, Millich E. (1998) Energy from biomass and waste: The contribution of utility scale biomass gasification plants. *Biomass Bioenerg.* **15** (3) 195-200.

Maniatis, K. and Beenackers, A. A. C. M. (2000) Tar protocol. IEA bioenergy gasification task. *Biomass Bioenerg.* **18**, 1-4.

Mann M. D., Collings M. E. and Botros P. E. (1992) Nitrous oxide emissions in fluidized bed combustion: Fundamental chemistry and combustion testing. *Prog. Energ. Combust. Sci.* **18**, 447-461.

Mansaray, K. G. and Ghaly, A. E. (1999a) Determination of kinetic parameters of rice husks in oxygen using thermogravimetric analysis. *Biomass Bioenerg.* **17**, 19-31.

Mansaray, K. G. and Ghaly, A. E. (1999b) Determination of reaction kinetics of rice husks in air using thermogravimetric analysis. *Energ. Source* **21**, 899-911.

Mansaray, K. G., Ghaly, A. E., Al-Taweel, A. M., Hamdullahpur, F., and Ugursal. V. I. (1999) Air gasification of rice husk in a dual distributor type fluidized bed gasifier. *Biomass Bioenerg.* **17**, 315-332.

Massey, L. G. (1979) Coal gasification for high and low Btu fuels, in *Coal Conversion Technlogy*, Wen C. Y. and Lee, E. S., eds., Addison-Wesley, Reading, Massachussett, pp. 313-427.

McLaughlin, S. B., Samson, R., Bransby, D. and Wiselogel, A. (1996) Evaluating physical, chemical and energetic properties of perennial grasses as biofuels. *Proc., Bioenergy '96 - The Seventh National Bioenergy Conference*, Nashville, Tennessee, pp. 1-8.

Middleton S. P., Patrick J. W. and Walker A. (1997) The release of coal nitrogen and sulfur on pyrolysis and partial gasification in a fluidized bed. *Fuel* **76**, 1195-1200.

Miles, T. R., Miles, T. R. Jr., Baxter, L. L., Jenkins, B. M. and Oden, L. L. (1993) Alkali slagging problems in biomass fuels. *Proc. First Biomass Conf. Amer.*, Burlington, Vermont. pp. 406–421.

Miller J.A. and Bowman C.T., (1989) Mechanism and modeling of nitrogen chemistry in combustion. *Prog. Energ. Combust. Sci.* **15**, 287-338.

Moersch, O., Spliethoff, H., and Hein, K. R. G. (2000) Tar quantification with a new online analyzing method. *Biomass Bioenerg.* **18**, 79-86.

Mory, A. and Zotter, T. (1998) EU-demonstration project BioCoComb for biomass gasification and co-combustion of the product-gas in a coal-fired power plant in Austria. *Biomass Bioenerg.* **15**, 239-244.

Narvaez, I., Corella, J., and Orio, A. (1997) Fresh tar (from a biomass gasifier) elimination over a commercial steam-reformimg catalyst: Kinetics and effect of different variables of operation. *Ind. Eng. Chem. Res.* **36**, 317-327.

Narvaez, I., Orio, A., Aznar, M. P., and Corella, J. (1996) Biomass gasification with air in an atmospheric bubbling fluidized bed. Effect of six operational variables on the quality of the produced raw gas. *Ind. Eng. Chem. Res.* **35**, 2110-2120.

Newby R. A. and Bannister, R. L. (1994) Advanced hot gas cleaning system for coal gasification processes. *J. Eng. Gas Turbines Power* **116**, 338-344.

Nieminen J., Kivela M. R. (1998) Biomass CFB gasifier connected to a 350 MW_{th} steam boiler fired with coal and natural gas - THERMIE demonstration project in Lahti in Finland. *Biomass Bioenerg.* **15** (3): 251-257.

Olivares, A., Aznar, M. P., Caballero, M. A., Gil, J., Frances, E., and Corella, J. (1997) Biomass gasification: Produced gas upgrading by in-bed use of dolomite. *Ind. Eng. Chem. Res.* **36**, 5220-5226.

Olsson, J.G., Pettersson, J. B. C., Padban, N., Bjerle, I. (1998) Alkali metal emission from filter ash and fluidized bed material from PFB gasification of biomass. *Energ. Fuel* **12**, 626-630.

Orio, A., Corella, J., Narvaez, I. (1997) Performance of different dolomites on hot raw gas cleaning from biomass gasification with air. *Ind Eng Chem Res* **36**, 3800-3808.

Padban, N,, Wang, W. Y., Ye, Z. C., Bjerle, I., and Odenbrand, I. (2000) Tar formation in pressurized fluidized bed air gasification of woody biomass. *Energ. Fuel* **14**, 603-611.

Paisley, M. A. and Anson, D. (1998) Biomass gasification for gas turbine-based power generation. *J. Eng. Gas Turb. Power* **120**, 284-288.

Pan, Y. G., Roca, X., Velo, E., and Puigjaner, L. (1999) Removal of tar by secondary air in fluidized bed gasification of residual biomass and coal. *Fuel* **78**, 1703-1709.

Pan, Y. G., Velo, E., Roca, X., Manya, J. J., and Puigjaner, L. (2000) Fluidized-bed co-gasification of residual biomass/poor coal blends for fuel gas production. *Fuel* **79**, 1317-1326.

Pankratz, L.B. (1982) Thermodynamic properties of elements and oxides. *US Bur. Mines Bull.* **672**.

Pankratz, L.B. (1984) Thermodynamic properties of halides. *US Bur. Mines Bull.* **674**.

Pankratz, L.B. (1987) Thermodynamic properties of sulfides. *US Bur. Mines Bull.* **689**.

Pankratz, L.B., Stuve J. M. and Gokcen, N. A. (1984) Thermodynamic data for mineral technology. *US Bur. Mines Bull.* **677**.

Pels J. R., Zeng L. , Van Heiningen A. R. P. (1997) Direct causticization of kraft black liquor with TiO_2 in a fluidized bed - Identification and analysis of sodium titanates. *J. Pulp Pap. Sci.* **23** (12): J549-J554.

Pitcher, K., Hilton, B., and Lundberg, H. (1998) The ARBRE project: Progress achieved. *Biomass Bioenerg.* **15**, 213-218.

Pletka, R., Brown, R. C., Smeenk, J. (2001) Indirectly heated biomass gasification using a latent heat ballast - 1: experimental evaluations. *Biomass Bioenerg.* **20**, 297-305.

Plzak, V. and Wendt, H. (1992) Energetic utilization of biomass – Processes for the production of synthesis gas, hydrogen, and methane, and of synfuel. *Chem-Ing-Tech.* **64**, 1084-1095.

Press, W. H., Flannery, B. P., Teukolsky, S. A., and Vetterling, W. T. (1988) Numerical recipes in C. Cambridge University Press, Cambridge.

Probstein, R. F. and Hicks, R. W. (1982) *Synthetic fuels*. McGraw Hill, New York.

Radovic, L. R., Jiang, H. and Lizzio, A. A. (1991) A transient kinetics study of char gasification in carbon dioxide and oxygen. *Energ. Fuels* **5**, 68-74.

Radovic, L. R., Walker, P. L. Jr., and Jenkins, R. G. (1983) Importance of carbon active sites in the gasification of coal chars. *Fuel* **63**, 849-856.

Rapagna, S., Jand, N., Kiennemann. A., and Foscolo, P. U. (2000) Steam gasification of biomass in a fluidised-bed of olivine particles. *Biomass Bioenerg.* **19**, 187-197.

Ratcliff, M. A., Onischak, M., Gratson, D. A., Patrick, J. A., French, R. J., and Wiant, B. C. (1995) Product analysis from the operation of a 10 ton/day direct, fluidized bed biomass gasifier and HGCU system. *Abstr. Pap. Am. Chem. Soc.* **210**: 55 - *Fuel* Part 1, 20.

Raveendran K., Ganesh A. and Khilar K. C. (1995) Influence of mineral matter on biomass pyrolysis characteristics. *Fuel* **74**, 1812-1822.

Raveendran, K. and Ganesh, A. (1998) Adsorption characteristics and pore-development of biomass-pyrolysis char. *Fuel* **77**, 769-781.

Ravindranath, N. H. (1993) Biomass gasification – Environmentally sound technology for decentralized power generation – A case study from India. *Biomass Bioenerg.* **4**, 49-60.

Roy, C., Pakdel, H., Zhang, H. G., and Elliott, D. C. (1994) Characterization and catalytic gasification of the aqueous by product from vacuum pyrolysis of biomass. *Can. J. Chem. Eng.* **72**, 98-105.

Ruggiero, M. and Manfrida, G. (1999) An equilibrium model for biomass gasification processes. *Renew. Energ.* **16**, 1106-1109.

Sakaki, K., Yamada, K. (1997) CO_2 mitigation by new energy systems. *Energ. Convers. Manage.* **38**, S655-S660 Suppl. S.

Salo, K. and Mojtahedi, W. (1998) Fate of alkali and trace metals in biomass gasification. *Biomass Bioenerg.* **15**, 263-276.

Schenk E. P., van Doorn J. and Kiel J. H. A (1997) Biomass gasification research at ECN in fixed bed and fluidized bed reactors. *Proc. Biomass Gasification and Pyrolysis*, Kaltschmitt, M and Bridgwater, A. V. eds., Stuttgart, Germany, pp. 129-137.

Schmieder, H. and Abeln, J. (1999) Supercritical water oxidation: State of the art. *Chem. Eng. Technol.* **22**, 903-908.

Schuster, G., Löffler, G., Weigl, K. and Hofbauer, H. (2000) Biomass steam gasification – an extensive parametric modeling study. *Biores. Technol.* **77**, 71-79.

Seebauer, V., Petek, J., and Staudinder, G. (1997) Effects of particle size, heating rate and pressure on measurement of pyrolysis kinetics by thermogravimetric analysis. *Fuel* **76**, 1277-1282.

Sheng, G. X. (1989) Biomass gasifiers – From waste to energy production. *Biomass* **20**, 3-12.

Simell, P. , Stahlberg, P., Kurkela, E., Albrecht, J., Deutsch, S., and Sjostrom, K. (2000) Provisional protocol for the sampling and analysis of tar and particulates in the gas from large-scale biomass gasifiers. Version 1998. *Biomass Bioenerg.* **18**, 19-38.

Simell, P., Hepola, J. O., Krause, A. O. I. (1997) Effects of gasification gas components on tar and ammonia decomposition over hot gas cleanup catalysts. *Fuel* **76**, 1117-1127.

Smith, W. R. and Missen, R. W (1982) *Chemical Reaction Equilibrium Analysis: Theory and Algorithms*. John-Wiley and Sons, New York.

Smith, W. R. and Missen, R. W. (1968) Calculating complex chemical equilibria by an improved reaction-adjustment method. *Can. J. Chem. Eng.* **46**, 269-272.

Steinberg, M., Dong, Y., and Borgwardt, R. H. (1993) The co-processing of fossil fuel and biomass for CO_2 emission reduction in the transportation sector. *Energ. Convers. Manage.* **34**, 1015-1022.

Susanto, H. and Beenackers, A. A. C. M. (1996) A moving-bed gasifier with internal recycle of pyrolysis gas. *Fuel* **75**, 1339-1347.

Sutton, D., Kelleher, B., and Ross, J. R. H. (2001) Review of literature on catalysts for biomass gasification. *Fuel Process. Technol.* **73**, 155-173.

Suuberg, E. M. (1977) Rapid pyrolysis and hydropyrolysis of coal. Sc.D. thesis, Dept. of Chemical Engineering, Massachusetts Institute of Technology, Cambridge, MA, USA.

Tillman, D. A. (1991) *The combustion of solid fuels and wastes*. Academic Press, San Diego.

Tomita, A., Mahajan, O. P., and Walker, P. L. (1977) Reactivity of heat-treated coals in hydrogen. *Fuel*, **56**, 137-143.

Turn S. Q., Kinoshita C. M., Ishimura D. M. (1997) Removal of inorganic constituents of biomass feedstocks by mechanical dewatering and leaching. *Biomass Bioenerg.* **12** (4): 241-252.

Turn, S. Q., Kinoshita, C. M., Ishimura, D. M., and Zhou, J. C. (1998) The fate of inorganic constituents of biomass in fluidized bed gasification. *Fuel* **77**, 135-146.

Ulmgren P, Radestrom R, Edblad M, and Wennerstrom, M. (1999) On the chemistry of non-process elements in systems with a pressurized black liquor gasifier. *J. Pulp Pap. Sci.* **25**, 344-350.

Vamvuka, D., Woodburn, E. T. and Senior, P. R. (1995) Modeling of an entrained flow coal gasifier. 1. Development of the model and general predictions. *Fuel* **74**, 1452-1460.

van der Drift, A., van Doorn, J., and Vermeulen, J. W. (2001) Ten residual biomass fuels for circulating fluidized-bed gasification. *Biomass Bioenerg.* **20**, 45-56.

Van Zegeren, F. and Storey, S. H. (1970) *The computation of chemical equilibria.* Cambridge University Press, Cambridge.

van't Hoff, J. H. (1898) *Lectures on Theoretical and Physical Chemistry*, Part I, *Chemical Dynamics*, Lehfeldt, R. A., trans., Edward Arnold, London.

von Fredersdorff C. G. and Elliott M. A. (1963) Coal gasification, in *Chemistry of coal utilization.* Lowry H. H. ed., John Wiley & Sons, Inc., New York.

Waldheim, L. and Carpentieri, E. (2001) Update on the progress of the Brazilian wood BIG-GT demonstration project. *J. Eng. Gas Turb. Power* **123**, 525-536.

Walker, P. L. Jr., Foresti, R. J. Jr., and Wright, C. C. (1953) Surface area studies of carbon-carbon dioxide reaction. *Ind. Engrg. Chem.* **45**, 1703-1710.

Walker, P. L. Jr., Shelef, M., and Anderson, R. T. (1968) Catalysis of carbon gasification, in *Chemistry and Physics of Carbon*, Vol. 4, Marcel Dekker, New York, pp. 287-383.

Walker, P. L. Jr., Taylor, R. L., and Ranish, J. M. (1991) An update on the carbon-oxygen reaction. *Carbon* **29**, 411-421.

Wang, W. Y., Padban, N., Ye, Z. C., Andersson, A., and Bjerle, I. (1999) Kinetics of ammonia decomposition in hot gas cleaning. *Ind. Eng. Chem. Res.* **38**, 4175-4182.

Wang, W. Y., Padban, N., Ye, Z. C., Olofsson, G., Andersson, A., and Bjerle, I. (2000) Catalytic hot gas cleaning of fuel gas from an air-blown pressurized fluidized-bed gasifier. *Ind. Eng. Chem. Res.* **39**, 4075-4081.

Wang, Y. and Kinoshita, C. M. (1992) Experimental analysis of biomass gasification with steam and oxygen. *Sol. Energ.* **49**, 153-158.

Wanzl, W. (1994) Techniques for studying and modeling coal pyrolysis and their relevance to biomass and wastes. *Biomass Bioenerg.* **7**, 131-141.

Warnecke R. (2000) Gasification of biomass: comparison of fixed bed and fluidized bed gasifier. *Biomass Bioenerg.* **18**, 489-497.

Watkinson, A. P., Lucas, J. P., and Lim, C. J. (1991) A prediction of performance of commercial coal gasifiers. *Fuel* **70**, 519-527.

White, G. A., Roszkowski, T. R., and Stanbridge, D. W. (1975) The RMProcess. In *Methanation of synthesis gas.* Len Seglin, L. ed., *Advances in Chemistry Series* 146. American Chemical Society, Washington D. C., pp. 138-148.

White, W. B., Johnson, S. M., and Dantzig, G. B. (1958) Chemical equilibrium in complex mixtures. *J. Chem. Phys.* **28**, 751-755.

Willeboer, W. (1998) The Amer demolition wood gasification project. *Biomass Bioenerg.* **15**, 245-249.

Williams R. H. and Larson E. D. (1996) Biomass gasifier gas turbine power generating technology. *Biomass Bioenerg.* **10** (2-3) 149-166.

Xu, B. Y. (1997) Biomass resources and utilization in China. In *Biomass Energy: Key Issues and Priority Needs*, IEA Conference Proceedings, Paris, pp. 159-163.

Xu, X. D. and Antal, M. J. (1998) Gasification of sewage sludge and other biomass for hydrogen production in supercritical water. *Environ. Prog.* **17,** 215-220.

Yan, H. M and Zhang, D. K. (2000) Modelling of fluidised-bed coal gasifiers: elimination of the combustion product distribution coefficient by considering homogeneous combustion. *Chem. Eng. Process* **39**, 229-237.

Zainal, Z. A., Ali, R., and Lean, C. H. Seetharamu, K. N. (2001) Prediction of performance of a downdraft gasifier using equilibrium modeling for different biomass materials. *Energ. Convers. Manage.* **42**, 1499-1515.

Zeleznik, F. J. (1968) Calculation of complex chemical equilibria. *Ind. Eng. Chem.* **60**, 27-57.

Zeng, L. and van Heiningen, A. R. P. (1997) Pilot fluidized-bed testing of kraft black liquor gasification and its direct causticization with TiO_2. *J. Pulp Pap. Sci.* **23** (11) J511-J516.

Zevenhoven-Onderwater, M. , Backman, R., Skrifvars, B. J., and Hupa, M. (2001a) The ash chemistry in fluidised bed gasification of biomass fuels. Part I: predicting the chemistry of melting ashes and ash-bed material interaction. *Fuel* **80**, 1489-1502.

Zevenhoven-Onderwater, M., Backman, R., Skrifvars, B. J., Hupa, M, Liliendahl, T, Rosen, C, Sjostrom, K, Engvall, K, and Hallgren, A. (2001b) The ash chemistry in fluidised bed gasification of biomass fuels. Part II: Ash behaviour prediction versus bench scale agglomeration tests. *Fuel* **80**, 1503-1512.

Zhao, H. B., Draelants, D. J., Baron, G. V. (2000a) Performance of a nickel-activated candle filter for naphthalene cracking in synthetic biomass gasification gas. *Ind. Eng. Chem. Res.* **39** (9): 3195-3201.

Zhao, H. B., Draelants, D. J., Baron, GV. (2000b) Preparation and characterisation of nickel-modified ceramic filters. *Catal. Today* **56** (1-3): 229-237, 25.

Zhou, J. C., Masutani, S. M., Ishimura, D. M., Turn, S. Q., and Kinoshita, C. M. (2000) Release of fuel-bound nitrogen during biomass gasification. *Ind. Eng. Chem. Res.* **39**, 626-634.

APPENDICES

Appendix I Materials Size Distributions

Table A-1. Size distribution of sawdust and coal (sieve analysis).

(A) Size distribution density

d_p	f_i, (%)						
(mm)	PS mix	Mixed	Cedar	Hemlock	Cypress	SPF	Coal[a]
0.09[b]	1.51	1.29	2.01	0.63	0.41	0.87	3.25
0.25	16.84	13.07	4.92	1.46	0.95	2.02	5.98
0.417	17.22	12.82	1.56	4.60	1.56	5.44	4.85
0.71	27.26	26.07	14.19	8.98	2.84	12.01	9.62
1.4	34.06	38.74	22.57	35.77	12.24	34.37	18.67
1.7	2.69	4.69	10.17	10.57	7.00	10.99	8.32
2	0.24	1.54	3.46	6.51	6.14	7.80	6.67
2.38	0.19	1.79	19.33	13.47	11.42	9.00	9.750
2.8	0	0	9.16	10.81	34.46	12.24	8.75
6.73	0	0	12.63	7.21	22.97	5.25	24.13
mean $\overline{d}$ [c]	0.38	0.43	0.67	0.92	1.49	0.82	0.56

Notes: (a) - Highvale subbituminous coal; (b) – upper limit of a sieve size range;
(c) - See Chapter 3, Eq. (3-1) for definition.

(B) Cumulative size distribution (sieve analysis)

d_p, under	Σf_i, (%)						
(mm)	PS mix	Mixed	Cedar	Hemlock	Cypress	SPF	Coal
0.09	1.51	1.29	2.01	0.63	0.41	0.87	3.25
0.25	18.35	14.36	6.93	2.09	1.36	2.89	9.23
0.417	35.57	27.18	8.49	6.68	2.93	8.33	14.08
0.71	62.83	53.24	22.68	15.66	5.77	20.35	23.70
1.4	96.89	91.98	45.25	51.43	18.01	54.72	42.37
1.7	99.58	96.67	55.42	62.00	25.01	65.70	50.69
2	99.81	98.21	58.88	68.51	31.15	73.51	57.37
2.38	100	100	78.21	81.98	42.57	82.51	67.11
2.8			87.37	92.79	77.03	94.75	75.87
6.73			100	100	100	100	100

Table A-2. Size distribution of bed material and ash.

(A) Size distribution density

d_p	f_i, (%)		
(mm)	Sil. sand	Bed ash	Catalyst
0.09	0.10	0.21	0.87
0.25	3.46	6.19	10.56
0.417	22.61	36.27	20.15
0.71	73.13	55.73	25.39
1.4	0.70	1.06	42.49
1.7	0	0.25	0.53
2	0	0.08	0
2.38	0	0.06	0
2.8	0	0.04	0
6.73	0	0.11	0
mean d_p	0.45	0.40	0.44

d_p	f_i, (%)
(mm)	Fly ash
0.037	16.59
0.075	24.13
0.29	15.28
0.106	9.09
0.15	10.26
0.212	7.26
0.5	17.39
0.71	0
1.4	0
2.0	0
mean dp	0.059

Note: Silica sand is used as bed material. Ni-based Süd-Chemie catalyst is used for tar reduction.

(B) Cumulative size distribution

d_p, under	Σf_i, (%)		
(mm)	Sil. sand	Bed ash	Catalyst
0.09	0.10	0.21	0.87
0.25	3.56	6.40	11.44
0.417	26.17	42.67	31.59
0.71	99.30	98.41	56.98
1.4	100	99.46	99.47
1.7		99.71	100
2		99.79	
2.38		99.85	
2.8		99.89	
6.73		100	

d_p, under	Σf_i, (%)
(mm)	Fly ash
0.075	16.59
0.29	40.72
0.106	56.00
0.15	65.09
0.212	75.35
0.5	82.61
0.71	100
1.4	
2.0	
2.38	

Appendix II Calibration Data for Air Rotameters

Table A-3. Concordance table between rotameter readings and air flow rates.

Primary Air 1		Primary Air 2		Secondary Air		Horizontal		Vertical		Pneumatic	
Read.	Flow	Read.	Flow	Read.	Flow	Read.	Flow	Read.	Flow	Read.	Flow
(scale)	(m^3/h)	(scale)	(m^3/h)	(scale)	(m^3/h)	(scale)	(m^3/h)	(scale)	(m^3/h)	(scale)	(m^3/h)
0	0	0	0	0	0	0	0	0	0	0	0
10	1.69	5	2.12	10	0.71	0.1	0.37	10	0.37	5	1.24
20	3.38	10	4.23	20	1.42	0.2	0.74	20	0.74	10	2.48
30	5.08	15	6.35	30	2.13	0.3	1.12	30	1.12	15	3.72
40	6.77	20	8.46	40	2.84	0.4	1.49	40	1.49	20	4.96
50	8.46	25	10.58	50	3.55	0.5	1.86	50	1.86	25	6.20
60	10.15	30	12.69	60	4.27	0.6	2.23	60	2.23	30	7.44
70	11.85	35	14.81	70	4.98	0.7	2.61	70	2.61	35	8.68
80	13.54	40	16.92	80	5.69	0.8	2.98	80	2.98	40	9.92
90	15.23	45	19.04	90	6.40	0.9	3.35	90	3.35	45	11.16
100	16.92	50	21.16	100	7.11	1	3.72	100	3.72	50	12.40
110	18.61	55	23.27	110	7.82	1.1	4.10	110	4.10	55	13.64
120	20.31	60	25.39	120	8.53	1.2	4.47	120	4.47	60	14.88
130	22.00	65	27.50	130	9.24	1.3	4.84	130	4.84	65	16.12
140	23.69	70	29.62	140	9.95	1.4	5.21	140	5.21	70	17.36
150	25.38	75	31.73	150	10.66	1.5	5.59	150	5.59	75	18.60
160	27.08	80	33.85	160	11.37	1.6	5.96	160	5.96	80	19.84
170	28.77	85	35.96	170	12.08	1.7	6.33	170	6.33	85	21.09
180	30.46	90	38.08	180	12.80	1.8	6.70	180	6.70	90	22.33
190	32.15	95	40.19	190	13.51	1.9	7.08	190	7.08	95	23.57
200	33.84	100	42.31	200	14.22	2	7.45	200	7.45	100	24.81
210	35.54			210	14.93	2.1	7.82	210	7.82		
220	37.23			220	15.64	2.2	8.19	220	8.19		
230	38.92			230	16.35	2.3	8.57	230	8.57		
240	40.61			240	17.06	2.4	8.94	240	8.94		
250	42.31			250	17.77	2.5	9.31	250	9.31		

Appendix III Calibration Data for Steam Meter and Feeders

III-1. Calibration of Steam meter

Type of steam meter: In-line mechanical
Range of steam flow: 0 –250 g-water/min

Steam meter setting (-)	Time interval (min)	Measured water wt. (g)	Actual steam flow (kg/h)
38	6	70	0.7
43	6	85	0.85
66	6	200	2
86	6	370	3.7
100	6	500	5
118	6	785	7.85
130	6	850	8.5

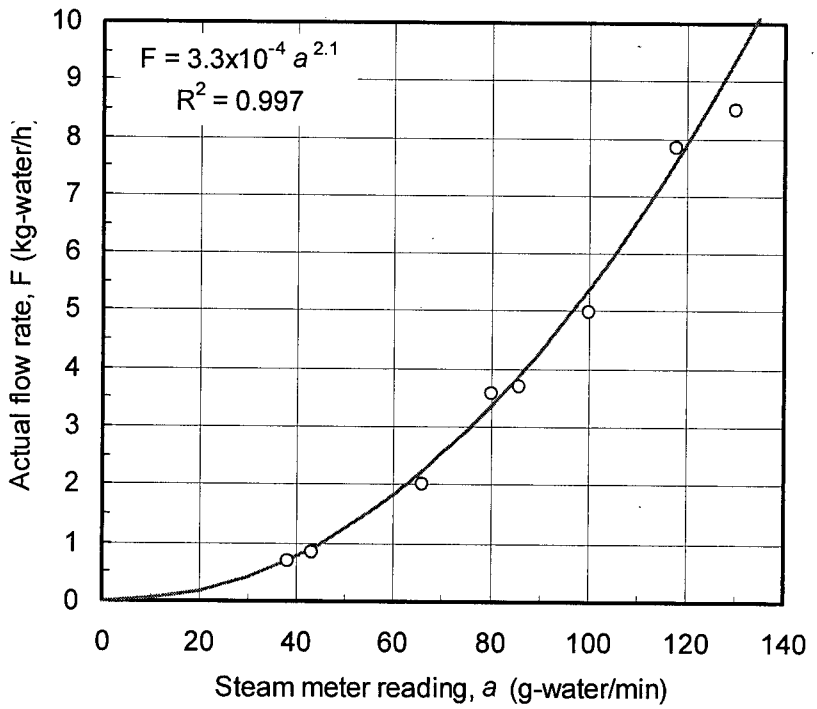

Figure A-1. Steam meter calibration curve.

III-2 Calibration of coal feeder

Type of feeder: Screw feeder with DC-motor driven rotary valve and speed control, assisted by 15 mm pneumatic conveying line and a coal injection jet.
Maximum feed rate: 50 kg/h (as-received)

Calibration data for Highvale coal are listed below:

Feeder setting	Actual feed rate (kg/h)
1	1.02
1.5	7.35
2	10.2
2.3	12.3
2.5	14.3
3	18.7

Properties of Highvale coal are given in Table 3-1 and Table A-1.

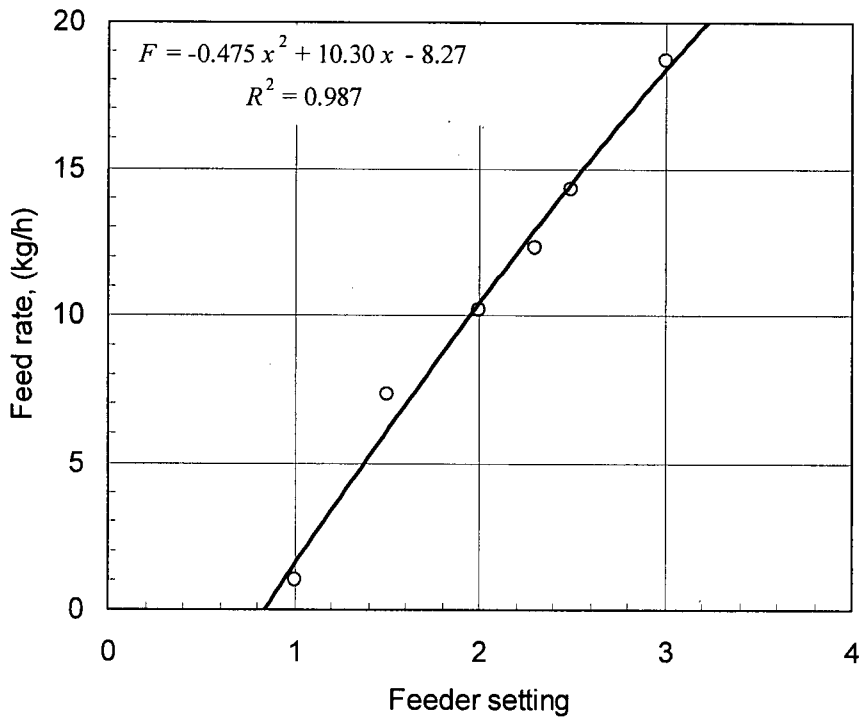

Figure A-2. Calibration curve for coal feeder.

III-3 Calibration of sawdust feeder

Type of feeder: Screw feeder with DC-motor driven rotary valve and speed control.
Maximum feed rate: 50 kg/h (dry basis)

Calibration data for cypress sawdust are listed below:

Feeder seeting (-)	Feed rate (kg/h-dry)	Actual feed rate (m^3/h-dry)
0	3.21	0.023
2.8	10.55	0.074
5	15.79	0.111
5	15.16	0.106
7.5	21.48	0.151
10	23.70	0.167
12.5	29.75	0.209
15	33.15	0.233
20	36.28	0.255
20	40.71	0.286
25	49.68	0.349

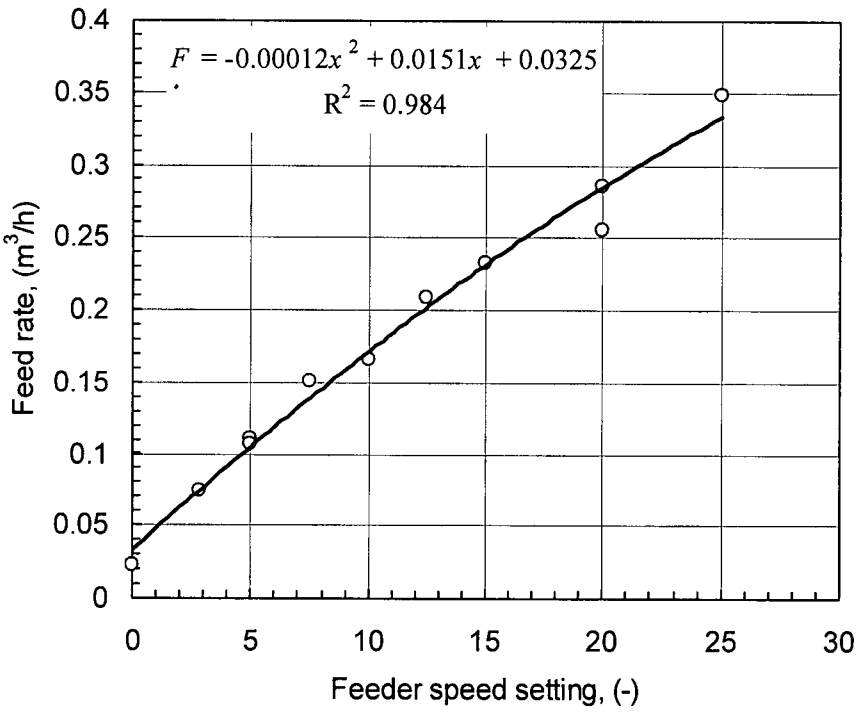

Figure A-3. Calibration curve for sawdust feeder.

Appendix IV. Locations of Thermocouples and Pressure Transducers

Table A-4. Locations and designations of thermocouples.

TC indicator channel	PC designation	Type	Location
C1	T0	K	Exit of start-up burner
C2	T1	K	Riser, 1660 mm above primary air inlet
C3	T2	K	Riser, 2803 mm above primary air inlet
C4	T3	K	Riser, 3946 mm above primary air inlet
C5	T4	K	Riser, 5089 mm above primary air inlet
C6	T5	K	Riser, 6156 mm above primary air inlet
C7	T6	K	Standpipe, top
C8	T7	K	Standpipe, middle
C9	T8	K	Standpipe, bottom
C10	T9	K	Preheated secondary air, bottom of riser
C11	T10	K	Bypass connector
C12	T11	K	Air heater, gas inlet
C13	T12	K	(Removed)
C14	T13	K	Heat exchanger, gas exit
C15	T14	K	Filter, gas inlet
C16	T15	K	Filter, inside
C17	T16	K	Filter, gas exit
C18	TH1	E	Preheated air temperature
C19	TH2	E	Cold air temperature
C20	TH3	E	Cold water temperature
C21	TH4	E	Warm water temperature
C22	TH5	E	Hot water temperature
C23	T_{roof}	K	Roof burner, exit

Table A-5. Location and designation of pressure transducers.

PC designation	Type	Model number	Output	Location
P0	Gauge	PX182-100GI	1-5 V DC	Primary air inlet
P1	Gauge	PX182-100GI	1-5 V DC	T1 level
P2	Gauge	PX182-100GI	1-5 V DC	Loop seal horizontal aeration level
P3	Diff.	PX143-05BD5V	3.5-5 V DC	Across filter unit
P4	Diff.	PX142-005D5V	1-5 V DC	T0-T1 levels
P5	Diff.	PX143-05BD5V	3.5-5 V DC	T1-T2 levels
P6	Diff.	PX142-005D5V	1-5 V DC	T2-T3 levels
P7	Diff.	PX142-005D5V	1-5 V DC	T3-T4 levels
P8	Diff.	PX142-005D5V	1-5 V DC	Standpipe top to loop seal horizontal aeration port
P9	Diff.	PX142-005D5V	1-5 V DC	Loop seal horizontal aeration port to vertical aeration port
P10	Diff.	PX163-005BD5V	3.5-5 V DC	Loop seal vertical aeration port to primary air inlet

Notes:
(1) All pressure transducers are Omega PX140, PX160 or PX182 Series products, employing solid state piezoresistive sensors.
(2) Gauge = gauge pressure type; Diff. = differential pressure type.
(3) Refer to Table A-4 for the location of thermocouples.

Appendix V. Gasifier Operating Procedure for Sawdust

A. CHECKLIST - PRIOR TO STARTUP

It is recommended to go through the following checklist at least 24 hours prior to the scheduled test and also immediately before the test begins.

Make sure that the entire system is complete and sealed. Check/inspect the following:

- ❑ All instrumentation including thermocouples, rotameters, pressure transducers, pressure gauges, TC indicators, etc.,
- ❑ Pressure switches on the natural gas line (total of two) and on the primary air line
- ❑ Air compressor pressure (80-120 psi)
- ❑ Instrument air pressure (30-50 psi)
- ❑ Natural gas pressure (3-5 psi)
- ❑ Nitrogen cylinder pressure (100-2500 psi) for filter purging and emergency riser purging
- ❑ Fully open the cast-iron gate valve to filter unit.
- ❑ Ensure filter by-pass valve on the exhaust duct is wide open.
- ❑ Gas sampling line purged by nitrogen and cleaned
- ❑ All gas analyzers in good working condition. See GAS SAMPLING AND ANALYSIS section for more details.
- ❑ Coal and sawdust hoppers filled-up and sealed properly
- ❑ Rotary valve motor and controller for coal hopper in good condition
- ❑ Sawdust screw feeder and controller in good condition
- ❑ Pneumatic air supply connection to both coal hopper and sawdust hopper ready, and valve closed
- ❑ Sand in the gasifier (record the amount of sand inside the gasifier, about 30 kg)
- ❑ Filter ash hopper in place and bolts tightened properly
- ❑ Knife gate valve of the filter ash hopper wide open
- ❑ Cooling-water supply for fuel injector, second- and third-stage heat exchangers, and bypass connector ready (turn on and check for leaks)
- ❑ Power to main control panel
- ❑ Power to data logging system
- ❑ Power to all analyzers (O_2, CO/CO_2)
- ❑ Power to gas chromatograph
- ❑ Pressure tap purge air on
- ❑ Air purging valves for lower and upper sawdust hoppers must be closed

- Valve on the coal injection nozzle must be closed
- Valve for direct air supply to burner should be open and valve for preheat air supply closed

When ready to start-up:

- Turn on power to main control panel
- Turn on TC indicator switch
- Turn on main-air-supply switch (solenoid valve)
- Turn on switch to the FAN (Rooftop)
- Set the main-air-regulator pressure to **40** psi (or 10-15 psi higher than the intended operating pressure, if pressurized)
- Turn on power to all gas analyzers for warming-up
- Turn on cooling water valve for the coal feed port. Set the rotameter to 20% of maximum.
- Turn on computer/data acquisition system
- Run data logging software (c:\cfbnew.exe)
- Start saving data (C:\testdata\filename.dat)

B. START-UP WITH NATURAL GAS BURNER

Note: All temperatures (T) refer to those displayed on the computer monitor.*

Make sure that the stainless steel plugs on the burner are removed, and both the spark igniter and the ignition rod are installed and wired properly.

- Open the primary air valve P1 and set to **70%** of its maximum range. Let it run for 2 minutes, and then close P1.
- Open the horizontal (aeration) air valve and set the flow rate to **5-10%** of maximum range.
- Open the vertical (circulation) air supply to the loop-seal and set the flow rate to **40-50 %** of maximum range.
- Open the primary air valves (P1 and P2) and set them to **70%** of their maximum range. Let it run for 3 to 5 minutes.
- Reduce the primary air flow to **P1 = 160/250** and **P2 = 30/100** of their maximum ranges.
- Observe the pressures on both the horizontal and vertical air lines (from the pressure gauges right above each rotameter) and ensure flow without any restriction (pressure-drop **<3-5 psi**). If the pressure-drop is high, it means the line is plugged by silica sand and needs to be purged and cleaned. To clean:
- Pull out horizontal aeration tube out and purge with air. Push the tube back in while purging with air. This will avoid sand filling and plugging the tube.
- Open the valve on the 5-psi natural gas line.

- Reset the pressure switches (both on the high pressure and the low pressure sides) by pushing the rod located on the right hand side of each pressure switch.
- Turn on the switch for the burner controller by pushing it up.
- After the solenoid valve (on the natural gas line) opens automatically, adjust the flow rate to read about **0.2** on the natural-gas rotameter (located at far right hand side of the control panel).
- Set the TC indicator selector to position-1 to monitor the temperature at the exit of the burner (bottom of the gasifier) – the thermocouple will respond immediately to the ignition and/or loss of ignition. It is possible to detect whether there is a flame or not by monitoring the TC indicator.
- NEVER EXCEED **1000 °C** IN THE START-UP BURNER COMBUSTION CHAMBER (Set the sound-alarm in the data acquisition and control system – F12 - to go off at **1025 °C**).
- Make sure that the alarm switch is *pressed down.*
- In case of an unstable gas flow (and/or unstable ignition), reduce the auxiliary air flows (H and V) to the loop-seal to reduce (or stop) the solid circulation from the stand-pipe to the riser and to avoid pressure fluctuations resulting from high solids build-up in the riser.

C. HEAT-UP BY BURNING SOLID START-UP FUEL AND NATURAL GAS

- Turn on the roof top burner.
- When heat exchanger exit temperature (T13) reaches **100** °C, close filter bypass valve.
- Start cooling water supply.
- Open cooling water valve to heat exchangers. Set rotameters to 20% of maximum range.
- Open the cooling water valve to the bypass connector cooling coil. (The ball valve is located at the bottom on the back of the control panel).
- Start feeding sawdust when bed temperature (T3) reaches **420**°C.
- Start feeding coal when bed temperature (T3) reaches **450**°C.
- Start roof top burner to incinerate the combustible gases produced.
- Make sure that the power to the **FAN** of the rooftop burner is turned on.
- Turn on the switch for the rooftop-burner on the control panel.
- Confirm that there is a flame by monitoring T_{roof} on the computer screen.
- Keeping the start-up burner **ON**, gradually reduce the natural gas supply to control the combustion chamber temperature, finally to about 0.1/2.5 or 0.12/2.5. After the bed temperature (T3) reaches the desired operating temperature (about **700** °C), shut down the start-up burner.
- Monitor O_2 content at the exit of bypass connector, and adjust air supply and sawdust feed rate to control the riser temperature.
- Open the valve on the N_2 cylinder(s) for filter back-purging, and set the pressure to 50-60 psi.

- Check the pressure inside the surge tank (for filter back pulsing) should read 15-45 psi.
- Make sure that the fuel injection nozzle is not plugged – a quick check is possible by opening the valve on the coal injection nozzle and the pneumatic feed line simultaneously. Check the rotameter to make sure that air is flowing.
- If the flow is restricted, turn off rotary valve on coal hopper and close the valves on both the pneumatic air line and the plant air line (on left-hand side of control panel).
- Disconnect the coal injection nozzle and copper pneumatic line, and remove the blockage.
- Resume coal feeding by switching on the rotary valve and opening the two ball valves along the pneumatic line.
- Open the valves on the fuel injection nozzle and the pneumatic feed line at the same time and set to **45 %** (45/100) of its maximum range.
- Turn on variable speed controller for the rotary valve on the coal hopper-1 and set it to the scale number corresponding to the required feed rate on the calibration curve (**1.2** for Feed Hopper-I).

D. NORMAL OPERATION

- Unload flyash from the filter.
- Inspect the rotary valve and the hose for pneumatic feed; one should be able to observe coal feed both inside the rotary valve and the hose.
- Adjust fuel and air supply rates to operate at desired air ratio. This can be done by changing the sawdust feed rate, while keeping the air flow relatively stable: P1=60% (150/250); P2=30% (30-33/100); S=2% (5/250); Lower hopper purge air = 50%.
- Establish stable solids circulation by adjusting the air flow rates at the loop-seal (H=5-10%; V=25-35% of their respective maximums).
- When sawdust is used, maintain the reactor temperature (i.e. T3 to T8) at 700-850 °C.
- When solids level is low in sawdust lower hopper, refer to FUEL REFILL PROCEDURE.

E. PRESSURIZING THE CFB - OPTIONAL

- Make sure that the filter by-pass valve is closed.
- Set the main-air pressure on the regulator to about 10 to 15 psi above the intended operating pressure (max. 75 psig).
- Set sound alarm to a maximum allowable pressure and temperature (5 psi and 25°C above the intended operating pressure and temperature, respectively).
- To eliminate gas backflux from riser to the hoppers, pressurize the feed hoppers to a pressure slightly (1-5 psi) higher than the intended operating pressure.
- Close the gate valve at the inlet of the filter unit gradually while observing the increase in the system pressure (pressure gauge installed at the bottom of the first heat-exchanger).

- Increase the air and the fuel supply rates gradually while increasing the system pressure to keep the superficial velocity at the required level.

F. FUEL REFILL PROCEDURE

- Make sure that the pinch valve is closed.
- Reduce the pressure in the upper hopper to atmospheric pressure by opening the pressure-relief valve on the second floor.
- Open fuel feeding port (blind flange on the top of the upper hopper).
- Fill up the upper hopper with sawdust.
- Close fuel feed port.
- Open purge valve to elevate the pressure slightly higher (1-5 psi) than operating pressure and then close it.
- Open pinch valve.
- If sawdust is not flowing, supply pulsing air via the purge line.
- Close the pinch valve.

G. NORMAL SHUTDOWN

- Make sure that all sampling tasks have been finished before initiating the shutdown procedure. Refer to GAS SAMPLING AND ANALYSIS section for detailed instructions.
- Shut down fuel feed system by switching off the variable speed motor at the bottom of the lower hopper.
- Shut down air supply by shuting off both plant air and instrument air valves in front of control panel.
- Open the valve on the N_2 cylinder (behind the control panel).
- Open the N_2 valve on front panel (below primary air valve), set N_2 flow rate at P1=5/250.
- Make sure all temperature indications are going down.
- Keep cooling water flowing to heat exchanger until gas temperature (T14) drops to 100°C.
- Make sure knife valve at bottom of the filter drain pipe is closed.
- Shut down rooftop burner.
- Turn off all analyzers.
- Operators may leave after all the above steps have been finished. Keep N_2 purge and cooling water on overnight.

Next morning,

- Stop saving data and copy data from PC hard drive to a floppy disk.

- Shut down data acquisition system (the computer).
- Shut down main power to control panel.
- Shut down cooling water supply to the bypass cooling coil, heat exchangers and feed port.
- Collect fly ash in the drum for further handling.

H. EMERGENCY SHUT DOWN

- Stop fuel feed.
- Shut down Main-Air switch on the control panel.
- Shut down all auxiliary air supplies.
- Open (*counter-clockwise*) the gate valve before the filter to relief system pressure. In doing so, monitor the pressure gage on the right-hand side to make sure that pressure is dropping.
- Make sure that the Start-Up-Burner is switched off and the natural gas Main-Shut-Off-Valve is closed.

Emergency shutdown procedure finished.

Make sure to

- Keep all cooling waters on.
- Keep computer data acquisition on.

Appendix VI. Tar Sampling Procedure

1. Sampling principles

1.1 Tar sampling should only be performed while the gasifier system is operating under normal, steady-state conditions.

1.2 The sampling procedure is only valid for tar and gas sampling, with the temperature at the sampling point higher than 250°C to ensure that tar components are still in vapour state.

1.3 If particulate sampling is performed at the same time, isokinetic conditions must be satisfied.

1.4 Sampling flow rate should be large enough to collect enough tar for gravimetric determination of tar yield, but not too large to cause considerable solvent carryover or tar fog in the impingers.

1.5 System pressure should not exceed 1.5 bar to protect the impingers and other glassware.

1.6 Leak test the sampling system prior to each sampling to ensure that there is no air infiltration or gas leakage.

2. Solvent-temperature combination

Possible solvent-temperature combinations:

Solvent full name	Temperature	Comments
Acetone	-3°C and 35-45°C	Widely used.
Dichloromethane (DCM)	-3°C and 35-45°C	Toxic and having high ozone depletion potential.
Isopropyl glycol	0°C and -30°C	Collection efficiency for some species could be low.

3. Sampling equipment

The tar sampling equipment consists of the following components:

- A sampling nozzle,
- A heating element to maintain gas temperature above 150°C,
- A filter for removing particulates,
- One or two stages of moisture trap to remove moisture content in the gas,
- An empty-bottle condenser working at –3 to -49°C to collect condensate,
- A thermometer to measure the temperature in the small compartments containing the impingers,

- At least three stages of tar impingers, each containing 50 ml of solvent, working at temperatures recommended for the solvent combinations,
- A rotameter to measure sampling flow,
- A ball valve to cut off tar sampling flow,
- A gas bypass for gas sampling or gas discharge or testing the sampling line,
- A vacuum pump if the system works under vacuum conditions (optional if the system pressure is higher than atmospheric).

4 Pre-sampling procedure

- Obtain a 500 ml beaker and a 50 ml one and weigh them to ±0.1 g and ±0.1 mg accuracy, respectively.
- Get 150 ml solvent and weigh the mass of solvent to ±0.1 g accuracy (m_{s1}).
- Using a 50 ml beaker, fill each of the three sampling impingers with 50 ml solvent (For a 250 ml impinger, no more than 100 ml of solvent should be filled to reduce carryover).
- Make sure that filters are newly replaced and filled with fresh or regenerated silica gel.
- Leak test sampling train to make sure that there is no leak.

5 Sampling procedure

- Open ball valve to tar sampling train, close valve to gas sampling device.
- Record date, time, run number and fuel type.
- Make sure that bubbles appear in all the sampling impingers.
- Adjust sampling flow rate reading in the rotameter to 0.09-0.12 Nm^3/h (1.5-2.0±0.1 litres/min).
- Check pressure indications on computer screen, and make sure that pressure at the sampling port does not exceed 1.5 bar (absolute). Otherwise all valve after the impingers must be kept open all the time.
- Monitor gas flow continually, making sure that neither the sampling line nor the gas filter or the impingers are blocked by particulates, condensate water and ice formed in the impingers.
- If blockage occurs, close the ball valve, and record the time when sampling was stopped.
- Troubleshoot sampling equipment and restore tar sampling. Record time. Adjust the sampling flow to the same level as before the blockage happened.
- Stop tar sampling 5 minutes before gasifier is shut down. Record time.
- Shut off all ball valves along sampling line. Turn off heating element.
- Disconnect all sampling impingers and condenser, collect solvent and condensate with a beaker of known weight (or one of the impingers) for post-sampling treatment.

6 Post sampling procedure

6.1 Remove particulates

- Fill a 50 ml beaker with 50 ml solvent. Rinse all impingers one by one and mix solutions together. Weigh solution collected.
- Rinse silicone rubber tubing with 50 ml solvent, and weigh solution collected.
- Mix rinse solutions with impinger solution. Weigh mixed solution.
- Take a piece of dry filter paper, and weigh it to ±0.1 mg accuracy.
- While transferring mixed solution to a 500 ml beaker, filter out particulates using filter paper.
- Weigh the filter paper contaminated with particulates and remnant solvent (m_{p1}).
- Use 50 ml of fresh solvent, and flush filter paper carefully until the dark brown colour disappears.
- Put filter paper in a clean aluminum pan of known weight (pre-weighed to ±0.1 mg precision), and dry it at 105°C for 2 hours to let the solvent evaporate.
- Weigh filter paper again (m_{p2}).
- $m_{sr} = m_{p1} - m_{p2}$ is the mass of *remnant solvent* on the filter paper.
- Put filter paper in a clean aluminum pan, flush both sides of the filter paper gently with tap water until paper turns white.
- Dry filter paper at 105°C for 2 hour and weigh it ($m_{p3} \sim m_{p0}$).
- $m_p = m_{p2} - m_{p3}$ is the mass of *particulates*.

6.2 Solvent evaporation

- Take 20 ml of mixed solution from the well-shaken mixed solution (of volume V) with a shallow glass dish (100 mm dia., 15 mm high) with known weight m_d. (to ±0.001 g)
- Dry small solution sample at 50-60°C for 48 hours.
- Transfer dish to a desiccator and allow it to cool to room temperature.
- Weigh dish to ±0.001 g accuracy (m_{dt}).
- Determine tar amount: $m_t = m_{dt} - m_d$.
- Calculate total tar amount collected: $m_{tot} = (V/20)\, m_t$.

6.3 Correction for solvent loss (container wall loss, etc.)

- Sum the volumes of all solvents consumed for sampling and flushing (V_0).
- Assume that all solution lost during collection and transferring has the same composition as the remaining mixed solution.
- Calculate modified tar amount: $m_{tar} = m_{tot}(V_0)/V$.
- Use the m_{tar} value to determine tar yield, in g/Nm^3 of product gas.

Appendix VII. Operating Parameters and Gas Chromatography Data

Notes: (1) Listed below is a complete set of instantaneous operating parameters and gas chromatography data, based on which time-mean values were obtained. Nickel-based catalyst was added to the reactor during Runs 14 and 15.
(2) Symbols: a = air ratio; O/C = oxygen to carbon molar ratio; T_3 = riser temperature at thermocouple T3 level; M = moisture content of sawdust; HHV_{298} = dry gas higher heating value at 298 K; HHV_{273} = dry gas heating value at 273 K.
(3) All gas chromatography data are in volume (molar) percentages.
(4) Shaded lines represent the first sample of each test run, usually taken during the transition period from combustion to gasification. Remnant coal might still affect the gas composition and heating value for these samples.
(5) Fuel type: SPF = spruce, pine and fir mixture; Ced/hem = cedar and hemlock mixture; P/S = 50 wt.% pine bark and 50 wt.% spruce sawdust mixture; Mixed = mixed sawdust of unknown species composition.

Run No.	Time	a	O/C	T_3	M	Steam inject.	Ash inject.	HHV_{298}	HHV_{273}	H_2	N_2	CO	CH_4	CO_2	C_2H_4	Total	Fuel type
(-)		(-)	(-)	(°C)	(%)	(kg/h)	(kg/h)	(MJ/m^3)	(MJ/m^3)	(v.%)	(v.%)	(v.%)	(v.%)	(v.%)	(v.%)	(v.%)	
1	15:40	0.789	2.319	729	22.0	0	0	0.15	0.17	0.37	79.07	0.96	0.00	19.60	0	100	Cypress
1	17:05	0.573	1.859	817	22.0	0	0	1.05	1.16	3.07	73.56	4.19	0.60	18.58	0	100	Cypress
1	17:25	0.447	1.599	789	22.0	0	0	2.08	2.30	6.58	67.35	7.66	1.25	17.16	0	100	Cypress
1	17:32	0.447	1.600	774	22.0	0	0	2.39	2.64	7.76	65.75	8.53	1.45	16.51	0	100	Cypress
1	17:44	0.365	1.425	755	22.0	0	0	2.26	2.50	7.51	66.18	8.03	1.33	16.95	0	100	Cypress
1	18:08	0.365	1.425	724	22.0	0	0	2.58	2.85	8.63	64.12	8.40	1.74	17.11	0	100	Cypress
1	18:20	0.354	1.508	713	22.0	0	0	2.75	3.05	8.78	63.07	8.80	2.05	17.30	0	100	Cypress
1	19:01	0.437	1.884	682	22.0	0	0	2.97	3.29	7.91	61.05	10.13	2.51	18.40	0	100	Cypress
1	19:01	0.437	1.884	682	22.0	0	0	2.98	3.30	7.91	60.88	10.17	2.52	18.52	0	100	Cypress
1	19:16	0.437	1.884	676	22.0	0	0	2.81	3.11	5.92	62.35	10.76	2.50	18.47	0	100	Cypress
1	19:16	0.437	1.884	676	22.0	0	0	2.82	3.12	5.95	62.22	10.83	2.50	18.50	0	100	Cypress
2	15:20	0.516	1.642	680	9.70	0	0	1.42	1.57	2.83	71.04	6.45	0.99	18.69	0	100	Cypress
2	15:58	0.503	1.615	720	9.70	0	0	1.38	1.52	3.02	71.08	6.01	0.95	18.93	0	100	Cypress
2	16:14	0.434	1.496	748	9.70	0	0	1.61	1.78	3.13	69.63	7.12	1.20	18.92	0	100	Cypress
2	16:33	0.494	1.782	766	9.70	0	0	1.89	2.09	2.79	68.22	8.67	1.60	18.71	0	100	Cypress
2	17:38	0.328	1.428	751	9.70	0	0	2.98	3.30	3.65	62.92	14.19	2.62	16.63	0	100	Cypress
2	17:50	0.328	1.428	751	9.70	0	0	3.21	3.55	3.81	62.73	15.18	2.89	15.39	0	100	Cypress
2	18:06	0.376	1.529	751	9.70	0	0	3.06	3.38	3.62	64.38	14.71	2.67	14.62	0	100	Cypress
2	18:15	0.421	1.626	719	9.70	0	0	1.53	1.70	1.60	88.85	8.49	1.05	0.00	0	100	Cypress

2	18:18	0.421	1.626	710	9.70	0	0	1.94	2.15	2.13	74.95	9.63	1.66	11.63	0	100	Cypress
2	18:27	0.421	1.626	710	9.70	0	0	1.07	1.18	1.08	85.77	5.70	0.81	6.63	0	100	Cypress
2	18:58	0.370	1.517	707	9.70	0	0	2.59	2.87	3.00	66.18	12.84	2.17	15.82	0	100	Cypress
2	19:22	0.370	1.517	707	9.70	0	0	2.96	3.27	3.42	65.38	14.45	2.54	14.22	0	100	Cypress
2	19:30	0.370	1.517	707	9.70	0	0	2.32	2.57	2.58	69.48	11.68	1.93	14.34	0	100	Cypress
3	15:25	0.470	1.588	758	10.48	0	0	1.28	1.41	2.38	72.39	5.86	0.93	18.44	0	100	SPF
3	15:53	0.470	1.588	778	10.48	0	0	1.37	1.52	2.70	72.10	6.18	0.98	18.04	0	100	SPF
3	16:13	0.444	1.533	796	10.48	0	0	1.56	1.72	3.15	70.25	6.92	1.12	18.56	0	100	SPF
3	16:50	0.368	1.556	757	10.48	0	0	2.86	3.16	3.60	63.53	13.60	2.47	16.80	0	100	SPF
3	16:52	0.381	1.585	763	10.48	0	0	2.67	2.95	2.98	73.49	13.49	2.18	8.03	0	100	SPF
3	16:58	0.381	1.585	757	10.48	0	0	3.01	3.33	3.69	62.76	14.03	2.73	16.79	0	100	SPF
3	17:20	0.381	1.585	756	10.48	0	0	1.79	1.98	1.79	70.43	9.41	1.42	16.95	0	100	SPF
3	17:30	0.381	1.585	754	10.48	0	0	2.76	3.05	3.38	65.89	13.13	2.41	15.19	0	100	SPF
3	17:30	0.381	1.585	754	10.48	0	0	2.78	3.08	3.43	65.48	13.21	2.45	15.42	0	100	SPF
3	17:40	0.356	1.532	754	10.48	0	0	2.12	2.35	2.73	67.10	10.61	1.66	17.90	0	100	SPF
3	17:58	0.356	1.532	757	10.48	0	0	3.01	3.33	3.63	62.91	14.16	2.70	16.60	0	100	SPF
4	16:22	0.604	1.905	819	10.00	0	0	0.84	0.93	1.63	74.50	3.92	0.59	19.37	0	100	Hemlock
4	16:43	0.582	2.003	834	10.00	0	0	1.40	1.55	1.84	71.38	7.13	1.04	18.62	0	100	Hemlock
4	17:45	0.582	2.003	828	10.00	0	0	0.50	0.55	0.71	79.82	2.38	0.40	16.70	0	100	Hemlock
4	18:20	0.393	1.601	826	10.00	0	0	2.47	3.53	3.56	64.66	11.23	2.17	17.13	1.26	100	Hemlock
4	18:35	0.401	1.620	826	10.00	0	0	3.11	3.44	4.49	61.55	13.69	2.87	17.39	0	100	Hemlock
4	19:00	0.401	1.620	801	10.00	0	0	2.48	3.48	3.04	64.56	11.75	2.19	17.29	1.17	100	Hemlock
4	19:01	0.401	1.620	800	10.00	0	0	3.47	4.57	3.97	59.33	16.03	3.28	16.23	1.15	100	Hemlock
4	19:02	0.401	1.620	799	10.00	0	0	3.17	3.51	3.89	61.70	14.91	2.83	16.68	0	100	Hemlock
4	19:03	0.401	1.620	798	10.00	0	0	2.65	2.93	3.39	64.13	12.93	2.18	17.38	0	100	Hemlock
4	19:04	0.401	1.620	797	10.00	0	0	2.65	2.93	3.16	64.57	12.81	2.29	17.17	0	100	Hemlock
4	19:05	0.401	1.620	796	10.00	0	0	2.59	2.86	3.08	64.81	12.80	2.14	17.17	0	100	Hemlock
4	19:06	0.401	1.620	795	10.00	0	0	2.45	2.71	3.05	66.06	12.02	2.01	16.86	0	100	Hemlock
4	19:07	0.401	1.620	794	10.00	0	0	2.06	2.28	2.59	68.38	10.46	1.58	16.99	0	100	Hemlock
4	19:08	0.401	1.620	793	10.00	0	0	2.29	2.53	2.79	67.12	11.13	1.94	17.02	0	100	Hemlock
4	19:09	0.401	1.620	792	10.00	0	0	1.24	1.37	2.04	71.73	6.37	0.78	19.09	0	100	Hemlock
4	19:10	0.401	1.620	791	10.00	0	0	3.39	4.16	4.29	59.75	15.62	3.11	16.60	0.63	100	Hemlock
4	19:30	0.371	1.555	783	10.00	0	0	3.41	4.34	4.91	58.92	15.06	3.12	17.09	0.90	100	Hemlock
4	19:48	0.371	1.555	776	10.00	0	0	3.40	3.76	4.47	62.80	15.31	3.16	14.25	0	100	Hemlock

4	20:05	0.365	1.543	776	10.00	0	0	3.39	3.75	4.67	61.67	15.35	3.06	15.26	0	100	Hemlock
5	16:45	0.556	1.731	843	8.80	0	0	2.17	2.45	4.37	66.69	7.91	2.13	18.83	0.07	100	Hemlock
5	17:05	0.432	1.633	842	8.80	0	0	2.66	2.95	3.15	65.44	12.46	2.44	16.50	0	100	Hemlock
5	17:18	0.356	1.472	816	8.80	0	0	3.86	4.39	5.71	57.36	16.48	3.68	16.59	0.18	100	Hemlock
5	17:35	0.356	1.472	816	8.80	0	0	2.10	2.49	2.50	69.76	10.14	1.83	15.52	0.25	100	Hemlock
5	17:35	0.356	1.472	812	8.80	0	0	2.25	2.49	2.80	67.34	10.62	1.99	17.25	0	100	Hemlock
5	17:39	0.356	1.472	809	8.80	0	0	2.34	3.19	2.86	65.42	11.02	2.09	17.66	0.95	100	Hemlock
5	17:43	0.356	1.472	706	8.80	0	0	3.23	4.99	3.99	59.87	14.11	3.23	16.57	2.23	100	Hemlock
5	17:43	0.356	1.472	803	8.80	0	0	2.73	3.02	3.30	64.46	12.93	2.43	16.89	0	100	Hemlock
5	17:45	0.356	1.472	799	8.80	0	0	3.40	4.34	4.97	59.29	15.08	3.07	16.68	0.92	100	Hemlock
5	17:47	0.356	1.472	796	8.80	0	0	2.29	3.05	2.57	66.68	10.75	2.12	17.06	0.81	100	Hemlock
5	17:51	0.356	1.472	793	8.80	0	0	2.86	3.56	3.28	62.87	13.44	2.65	17.15	0.61	100	Hemlock
5	17:55	0.356	1.472	790	8.80	0	0	2.51	3.20	2.91	64.78	12.00	2.23	17.42	0.66	100	Hemlock
5	18:07	0.356	1.472	788	8.80	0	0	2.23	2.89	2.61	67.12	10.81	1.94	16.85	0.67	100	Hemlock
5	18:11	0.356	1.472	785	8.80	0	0	2.58	2.85	4.36	64.17	11.56	2.10	17.80	0	100	Hemlock
5	18:15	0.356	1.472	782	8.80	0	0	2.45	3.36	4.12	64.26	11.12	1.96	17.52	1.03	100	Hemlock
5	18:35	0.356	1.472	753	8.80	0	0	3.43	4.06	4.38	59.76	15.55	3.21	16.69	0.40	100	Hemlock
5	19:52	0.356	1.600	740	8.80	2.72	0	2.53	3.41	2.80	67.59	12.43	2.20	14.03	0.95	100	Hemlock
5	19:58	0.356	1.600	740	8.80	2.72	0	2.75	5.04	3.42	62.01	13.05	2.42	15.97	3.14	100	Hemlock
5	20:10	0.356	1.600	739	8.80	2.72	0	3.78	4.53	4.77	57.99	17.07	3.56	16.06	0.56	100	Hemlock
5	20:28	0.356	1.600	739	8.80	2.72	0	3.76	4.16	4.62	58.67	17.20	3.52	16.00	0	100	Hemlock
6	16:42	0.380	1.528	824	9.19	0	0	3.83	4.24	6.10	61.90	15.56	3.76	12.68	0	100	Hemlock
6	17:00	0.380	1.528	820	9.19	0	0	3.08	3.40	4.45	64.00	13.35	2.89	15.31	0	100	Hemlock
6	17:58	0.477	1.958	811	9.19	3.7	0	2.22	2.46	2.77	69.85	10.01	2.11	15.26	0	100	Hemlock
6	18:16	0.477	1.958	804	9.19	3.7	0	2.68	2.96	3.57	65.08	11.84	2.54	16.96	0	100	Hemlock
6	18:18	0.477	1.958	770	9.19	3.7	0	2.53	2.90	2.74	66.00	11.56	2.50	17.06	0.15	100	Hemlock
6	18:20	0.477	1.958	770	9.19	3.7	0	3.19	3.54	4.10	61.76	13.91	3.16	17.07	0	100	Hemlock
6	18:22	0.477	1.958	770	9.19	3.7	0	2.10	2.33	2.25	68.77	9.84	2.00	17.14	0	100	Hemlock
6	18:24	0.477	1.958	770	9.19	3.7	0	2.27	2.51	2.20	68.08	10.52	2.27	16.93	0	100	Hemlock
6	18:26	0.477	1.958	770	9.19	3.7	0	2.05	2.27	2.16	70.24	9.49	2.01	16.10	0	100	Hemlock
6	18:28	0.477	1.958	770	9.19	3.7	0	1.52	1.68	1.38	73.11	7.49	1.40	16.62	0	100	Hemlock
6	18:30	0.477	1.958	770	9.19	3.7	0	1.30	1.44	1.39	75.04	6.15	1.21	16.21	0	100	Hemlock
6	18:32	0.477	1.958	770	9.19	3.7	0	1.40	1.55	1.40	73.95	6.99	1.22	16.43	0	100	Hemlock
6	18:34	0.477	1.958	770	9.19	3.7	0	1.52	1.69	1.56	73.76	7.30	1.42	15.96	0	100	Hemlock

6	18:36	0.477	1.958	770	9.19	3.7	0	0.85	0.94	0.96	78.13	4.93	0.50	15.48	0	100	Hemlock
6	18:38	0.477	1.958	770	9.19	3.7	0	1.23	1.36	1.34	74.75	6.02	1.08	16.81	0	100	Hemlock
6	18:40	0.477	1.958	770	9.19	3.7	0	1.03	1.14	1.06	75.83	4.56	1.07	17.48	0	100	Hemlock
6	19:02	0.474	1.949	790	9.19	3.51	0	2.43	2.69	3.32	66.85	10.76	2.29	16.87	0	100	Hemlock
6	19:23	0.474	1.949	782	9.19	3.51	0	2.71	3.00	3.53	66.65	12.05	2.58	15.20	0	100	Hemlock
6	19:35	0.474	2.392	778	9.19	10.52	0	2.76	3.06	3.67	66.23	12.26	2.61	15.23	0	100	Hemlock
6	20:10	0.339	1.711	765	9.19	5.99	0	3.58	3.96	4.75	59.88	15.79	3.41	16.17	0	100	Hemlock
6	20:40	0.339	1.916	745	9.19	10.52	0	3.48	3.85	4.22	62.21	15.36	3.44	14.77	0	100	Hemlock
6	20:45	0.339	1.916	743	9.19	10.52	0	3.62	4.17	4.82	59.62	16.03	3.43	15.83	0.26	100	Hemlock
7	15:45	0.307	1.413	752	11.70	0	0	4.23	4.68	6.10	56.74	17.87	4.12	15.16	0	100	Hemlock
7	16:13	0.346	1.496	728	11.70	0	0	3.87	4.28	5.03	58.80	17.27	3.67	15.23	0	100	Hemlock
7	16:45	0.336	1.474	711	11.70	0	0	3.76	4.16	4.91	59.88	16.88	3.53	14.80	0	100	Hemlock
7	17:10	0.336	1.474	699	11.70	0	0	3.73	4.13	4.71	59.85	17.62	3.28	14.54	0	100	Hemlock
7	17:15	0.336	1.474	700	11.70	0	0	3.13	3.46	3.94	63.83	15.01	2.67	14.55	0	100	Hemlock
7	17:32	0.336	1.474	793	11.70	0	0	3.40	3.80	6.29	60.89	15.18	2.61	14.97	0.06	100	Hemlock
7	17:48	0.336	1.474	828	11.70	0	0	3.32	3.71	7.13	61.04	13.80	2.55	15.41	0.06	100	Hemlock
7	17:48	0.336	1.474	830	11.70	0	0	3.41	3.91	7.02	59.92	14.24	2.72	15.89	0.21	100	Hemlock
8	16:22	0.388	1.596	811	11.26	0	0	3.08	3.41	4.85	62.45	13.19	2.83	16.69	0	100	SPF/cyp
8	16:44	0.443	1.713	787	11.26	0	32.69	3.12	3.46	4.36	62.51	14.49	2.69	15.95	0	100	SPF/cyp
8	16:50	0.443	1.713	770	11.26	0	32.69	3.35	3.71	4.62	61.56	15.53	2.92	15.37	0	100	SPF/cyp
8	17:12	0.293	1.393	742	11.26	0	0	4.35	4.82	5.02	55.70	20.18	4.09	15.02	0	100	SPF/cyp
8	17:30	0.316	1.442	697	11.26	0	0	3.19	3.53	3.43	62.96	15.73	2.78	15.11	0	100	SPF/cyp
8	17:52	0.316	1.442	697	11.26	0	0	3.41	3.78	3.67	61.58	16.56	3.06	15.13	0	100	SPF/cyp
8	18:34	0.305	1.420	698	11.26	0	0	3.54	3.92	3.83	60.91	17.04	3.20	15.02	0	100	SPF/cyp
8	18:52	0.305	1.420	700	11.26	0	0	2.51	2.78	3.30	66.35	12.12	2.08	16.15	0	100	SPF/cyp
8	18:57	0.410	1.643	700	11.26	0	12.32	2.30	2.54	2.97	67.79	11.31	1.85	16.08	0	100	SPF/cyp
8	19:16	0.410	1.643	722	11.26	0	12.32	2.86	3.17	3.65	64.18	13.80	2.42	15.95	0	100	SPF/cyp
8	19:23	0.410	1.643	740	11.26	0	12.32	2.83	3.13	3.59	64.23	13.39	2.47	16.32	0	100	SPF/cyp
8	19:40	0.406	1.635	765	11.26	0	0	2.37	2.62	3.05	66.97	10.93	2.15	16.91	0	100	SPF/cyp
9	17:55	0.500	1.899	765	14.95	0	0	2.54	2.81	2.55	69.01	9.12	3.34	15.98	0	100	Hemlock
9	18:37	0.370	1.621	772	14.95	0	0	2.62	2.91	3.32	65.59	12.35	2.32	16.43	0	100	Hemlock
9	18:50	0.370	1.621	772	14.95	0	0	3.33	3.69	4.09	61.63	15.36	3.08	15.84	0	100	Hemlock
9	18:59	0.370	1.621	772	14.95	0	0	2.74	3.03	3.53	65.37	12.82	2.42	15.85	0	100	Hemlock
9	19:05	0.415	1.718	760	14.95	0	12.49	3.09	3.42	3.87	63.58	15.03	2.59	14.93	0	100	Hemlock

9	19:12	0.415	1.718	765	14.95	0	12.49	3.51	3.89	4.17	61.14	16.60	3.17	14.92	0	100	Hemlock
9	19:15	0.415	1.718	750	14.95	0	12.49	3.59	3.98	4.23	60.98	16.98	3.25	14.56	0	100	Hemlock
9	19:34	0.348	1.575	735	14.95	0	12.49	2.83	3.13	3.32	64.79	14.09	2.33	15.47	0	100	Hemlock
9	19:50	0.348	1.575	730	14.95	0	12.49	4.22	4.67	4.84	57.50	19.42	4.01	14.22	0	100	Hemlock
9	20:03	0.430	1.749	731	14.95	0	16.70	3.38	3.74	3.91	62.37	16.45	2.92	14.36	0	100	Hemlock
9	20:13	0.378	1.640	731	14.95	0	16.70	2.66	2.95	3.21	66.33	13.17	2.19	15.09	0	100	Hemlock
9	20:37	0.377	1.636	731	14.95	0	16.70	3.13	3.47	3.80	63.06	15.19	2.68	15.28	0	100	Hemlock
9	20:42	0.370	1.622	739	14.95	0	0	2.67	2.95	3.19	65.61	13.31	2.18	15.72	0	100	Hemlock
10	17:32	0.380	1.573	866	12.55	0	0	2.46	2.73	4.64	65.50	10.77	1.95	17.14	0	100	Ced/ham
10	17:49	0.380	1.573	851	12.55	0	0	2.68	2.96	4.42	65.09	11.52	2.38	16.59	0	100	Ced/ham
10	18:45	0.380	1.573	825	12.55	0	0	4.22	4.67	6.07	56.78	18.03	4.06	15.07	0	100	Ced/ham
10	19:00	0.424	1.667	817	12.55	0	5.73	2.65	2.93	3.99	65.64	12.13	2.23	16.01	0	100	Ced/ham
10	19:05	0.424	1.667	814	12.55	0	5.73	2.47	2.73	3.36	65.94	11.90	2.00	16.80	0	100	Ced/ham
10	19:17	0.380	1.573	810	12.55	0	0	2.69	2.98	3.79	65.19	11.86	2.51	16.65	0	100	Ced/ham
10	19:35	0.372	1.556	809	12.55	0	0	1.99	2.20	2.89	69.27	9.13	1.70	17.00	0	100	Ced/ham
10	19:52	0.372	1.556	809	12.55	0	0	1.21	1.34	1.59	73.39	5.96	0.96	18.10	0	100	Ced/ham
10	20:27	0.468	1.762	769	12.55	0	0	2.33	2.58	3.10	67.79	10.77	2.07	16.27	0	100	Ced/ham
10	20:33	0.351	1.512	769	12.55	0	0	3.17	3.51	4.27	62.34	14.40	2.88	16.12	0	100	Ced/ham
10	20:40	0.361	1.534	769	12.55	0	0	3.46	3.83	4.48	61.02	15.68	3.21	15.60	0	100	Ced/ham
11	17:25	0.467	1.805	845	14.71	0	0	2.83	3.14	4.32	64.35	12.01	2.68	16.64	0	100	Hemlock
11	18:32	0.334	1.522	777	14.71	0	0	3.15	3.49	4.07	62.99	14.13	2.98	15.83	0	100	Hemlock
11	19:07	0.334	1.522	778	14.71	0	0	3.93	4.35	4.91	58.92	17.57	3.79	14.81	0	100	Hemlock
11	19:11	0.334	1.522	772	14.71	0	0	3.88	4.29	4.78	58.59	17.65	3.65	15.20	0	100	Hemlock
11	19:21	0.334	1.522	764	14.71	0	0	3.58	3.96	4.45	60.75	16.38	3.33	15.08	0	100	Hemlock
11	19:30	0.334	1.522	761	14.71	0	0	3.82	4.23	4.65	59.18	17.68	3.54	14.95	0	100	Hemlock
11	19:41	0.334	1.522	758	14.71	0	0	3.16	3.50	3.91	63.18	14.75	2.87	15.30	0	100	Hemlock
11	20:21	0.334	1.522	739	14.71	0	0	3.38	3.74	3.89	61.39	16.26	2.99	15.48	0	100	Hemlock
11	20:31	0.334	1.522	725	14.71	0	0	3.27	3.62	3.61	62.17	16.32	2.75	15.15	0	100	Hemlock
11	20:38	0.334	1.522	715	14.71	0	0	3.37	3.73	3.77	62.21	16.67	2.87	14.48	0	100	Hemlock
12	16:50	0.157	1.113	730	10.05	0	0	3.73	4.13	7.23	60.95	15.01	3.29	13.53	0	100	P/S
12	17:24	0.157	1.113	727	10.05	0	0	5.25	5.81	6.00	51.15	23.75	5.14	13.96	0	100	P/S
12	18:54	0.218	1.253	730	10.05	0	0	5.12	5.67	6.95	51.42	21.52	5.18	14.93	0	100	P/S
12	19:01	0.218	1.253	735	10.05	0	0	4.94	5.47	6.51	52.92	21.08	4.97	14.53	0	100	P/S
12	19:32	0.218	1.253	690	10.05	0	0	4.44	4.91	4.67	55.40	20.62	4.30	15.02	0	100	P/S

12	19:37	0.218	1.253	684	10.05	0	0	4.90	5.42	4.38	52.37	23.45	4.78	15.02	0	100	P/S
12	19:51	0.218	1.253	676	10.05	0	0	4.19	4.64	4.32	56.95	20.21	3.87	14.66	0	100	P/S
12	19:58	0.218	1.253	669	10.05	0	0	4.11	4.55	4.06	57.26	20.12	3.73	14.83	0	100	P/S
12	20:16	0.218	1.253	673	10.05	0	0	4.00	4.43	4.23	57.96	19.52	3.57	14.72	0	100	P/S
12	20:20	0.218	1.253	676	10.05	0	0	2.97	3.28	3.14	63.77	14.94	2.50	15.66	0	100	P/S
13	16:36	0.259	1.320	809	6.55	0	0	3.29	3.64	4.87	63.02	14.27	3.05	14.79	0	100	Mixed
13	17:03	0.259	1.320	790	6.55	0	0	4.45	4.93	5.80	55.81	19.67	4.27	14.44	0	100	Mixed
13	17:19	0.259	1.320	754	6.55	0	0	4.92	5.45	5.83	52.94	21.78	4.90	14.55	0	100	Mixed
13	17:32	0.259	1.320	723	6.55	0	0	4.95	5.48	5.41	52.98	22.48	4.90	14.23	0	100	Mixed
13	18:05	0.259	1.320	726	6.55	0	0	4.06	4.49	4.54	58.28	18.74	3.89	14.55	0	100	Mixed
13	18:09	0.259	1.320	725	6.55	0	0	4.62	5.11	5.00	54.45	21.35	4.46	14.73	0	100	Mixed
13	18:34	0.259	1.320	720	6.55	0	0	4.25	4.71	4.83	56.49	19.95	3.95	14.79	0	100	Mixed
13	18:41	0.259	1.320	716	6.55	0	0	4.27	4.72	4.76	56.68	20.22	3.92	14.42	0	100	Mixed
13	18:58	0.259	1.320	706	6.55	0	0	4.32	4.78	5.31	56.24	20.32	3.86	14.26	0	100	Mixed
13	19:04	0.259	1.320	703	6.55	0	0	3.63	4.02	4.73	60.46	16.85	3.24	14.72	0	100	Mixed
13	19:09	0.254	1.309	702	6.55	0	0	4.18	4.62	5.14	57.00	19.63	3.74	14.49	0	100	Mixed
13	19:15	0.254	1.309	700	6.55	0	0	4.34	4.80	5.04	56.00	20.53	3.94	14.50	0	100	Mixed
13	19:22	0.257	1.316	698	6.55	0	0	4.42	4.89	4.94	55.01	21.15	3.98	14.92	0	100	Mixed
13	19:29	0.261	1.325	697	6.55	0	0	4.43	4.91	4.94	55.42	21.14	4.03	14.47	0	100	Mixed
14	16:55	0.544	1.990	785	6.70	0	0	3.32	3.67	10.42	54.52	13.68	1.55	19.83	0	100	Mixed
14	17:14	0.291	1.398	747	6.70	0	0	4.18	4.63	8.44	53.97	18.16	3.15	16.27	0	100	Mixed
14	17:23	0.291	1.398	721	6.70	0	0	5.21	5.77	9.48	47.99	22.51	4.31	15.72	0	100	Mixed
14	17:34	0.290	1.396	702	6.70	0	0	4.82	5.33	8.54	50.26	21.33	3.89	15.98	0	100	Mixed
14	17:41	0.290	1.396	698	6.70	0	0	4.75	5.25	7.53	51.17	21.70	3.90	15.70	0	100	Mixed
14	17:50	0.290	1.396	699	6.70	0	0	3.53	3.91	3.93	61.51	17.27	3.08	14.22	0	100	Mixed
14	18:14	0.293	1.402	706	6.70	0	0	3.95	4.37	6.49	56.10	18.13	3.16	16.12	0	100	Mixed
14	18:22	0.306	1.434	708	6.70	0	0	4.38	4.84	6.90	53.54	19.97	3.62	15.97	0	100	Mixed
14	18:43	0.306	1.434	712	6.70	0	0	3.89	4.31	6.58	56.69	17.57	3.13	16.03	0	100	Mixed
14	19:05	0.316	1.457	729	6.70	0	0	4.23	4.68	7.05	54.83	19.23	3.40	15.49	0	100	Mixed
14	19:29	0.316	1.457	763	6.70	0	0	3.99	4.42	7.63	55.03	17.69	3.03	16.62	0	100	Mixed
14	19:53	0.325	1.479	774	6.70	0	0	4.33	4.79	8.31	53.40	18.29	3.58	16.43	0	100	Mixed
14	19:57	0.283	1.378	771	6.70	0	0	3.79	4.19	7.29	56.14	16.43	2.98	17.16	0	100	Mixed
14	20:10	0.283	1.378	771	6.70	0	0	3.16	3.50	5.89	61.09	13.69	2.57	16.76	0	100	Mixed
14	20:13	0.283	1.378	770	6.70	0	0	3.26	3.61	6.15	60.21	14.21	2.59	16.87	0	100	Mixed

14	20:24	0.283	1.378	771	6.70	0	0	3.93	4.34	7.67	55.52	16.74	3.14	16.92	0	100	Mixed
14	20:27	0.283	1.378	765	6.70	0	0	5.06	5.60	8.97	49.74	21.60	4.35	15.35	0	100	Mixed
14	20:35	0.282	1.376	767	6.70	0	0	4.11	4.55	7.60	55.02	17.57	3.42	16.39	0	100	Mixed
14	20:39	0.282	1.376	766	6.70	0	0	3.50	3.87	6.57	58.50	15.02	2.85	17.06	0	100	Mixed
14	20:47	0.282	1.376	763	6.70	0	0	3.43	3.79	6.54	58.59	15.03	2.67	17.18	0	100	Mixed
14	20:50	0.282	1.376	760	6.70	0	0	3.83	4.24	7.20	56.35	16.89	2.99	16.56	0	100	Mixed
15	19:50	0.290	1.697	789	4.18	0	0	2.40	2.65	4.83	66.94	10.16	1.89	16.18	0	100	Mixed
15	20:10	0.283	1.697	772	4.18	0	0	2.91	3.22	5.04	60.34	12.49	2.51	19.61	0	100	Mixed, T1
15	20:30	0.283	1.697	780	4.18	0	0	1.42	1.57	3.38	72.50	9.00	0.00	15.12	0	100	Mixed, T2
15	21:34	0.306	1.697	768	4.18	0	0	2.01	2.23	6.08	67.74	11.51	0.00	14.68	0	100	Mixed, T3
15	18:36	0.544	1.870	831	4.18	0	0	1.64	1.81	5.18	67.52	6.47	0.84	19.99	0	100	Mixed, T4
15	19:30	0.306	1.870	814	4.18	0	0	2.45	2.70	7.42	61.91	13.92	0.00	16.74	0	100	Mixed
15	19:58	0.291	1.697	775	4.18	0	0	1.47	1.63	4.17	70.72	5.63	0.98	18.51	0	100	Mixed
15	20:02	0.290	1.697	773	4.18	0	0	4.05	4.49	9.08	55.08	16.88	3.00	15.95	0	100	Mixed
15	20:32	0.325	1.697	782	4.18	0	0	1.05	1.16	2.62	72.80	6.53	0.00	18.05	0	100	Mixed
15	20:57	0.316	1.774	782	4.18	0	0	2.67	2.96	6.16	62.49	11.48	1.81	18.07	0	100	Mixed

Appendix VIII. Mass and Energy Balance Calculation: Sample Calculation Sheet

A sample calculation sheet is provided here.

Input test data				
Run number	-	-	Sawdust Run -	SD-11
Date of test	-	-	dd/mmm/yy	1-Nov-01
Fuel species	-	-	Name of the sawdust species	Hemlock
Total gasification run time	t	h	From test data sheets	3.80
Total SD consumed over gasif stage	Wsd	kg	= F*t, or as weighed	120.77
Moisture content in sawdust	Ms	%	From fuel data, as-received basis	14.71
Total coal consumption	Wc	kg	= F*t, or as weighed	60.98
Co-gasified coal weight	Wcog	kg	From test data sheets	0
Moisture content in coal	Mc	%	From coal analysis, as-received basis	9.00
Total amount of air supplied	Vair	Nm^3	From test data sheets	185.98
Additional cooling nitrogen	Vnitro	Nm^3	From test data sheets	0
Total weight of initial bed materials	Wbm	kg	From test data sheets	29.96
Bed ash added as initial b.m.	Wba	kg	From test data sheets	18.61
Fly ash reinjection	Wfa	kg	From test data sheets	0
Total steam injection	Wst	kg	See below	0
Time-mean operating temperature	T	C	From test data sheets	788.54
Time-mean operating temperature	Ta	K	= T + 273.15	1061.69
Operating pressure (bottom of bed)	P	bar	actual pressure at rotameter exit	1.19
Time mean air ratio	a	-	From test data sheets	0.337
Mean gas composition				
Hydrogen	$[H_2]$	%	From test data sheets	4.18
Nitrogen	$[N_2]$	%	Same as above	62.57
Carbon monoxide	[CO]	%	Same as above	14.57
Methane	$[CH_4]$	%	Same as above	2.97
Carbon dioxide	$[CO_2]$	%	Same as above	15.70
Total bed ash collected	Wbao	kg	From test data sheets	23.15
Carbon content in dry bed ash	[C]	%	Measured, previous run	0.24
Moisture content in bed ash	Mbao	%	Measured, current run	0.00
Total fly ash collected	Wfao	kg	From test data sheets	8.17
Carbon content in dry fly ash	[C*]	%	Measured, previous run	36.02
Moisture content in fly ash	Mfao	%	Measured, current run	4.59
Weight of tar collected from stack	Wt	kg	As weighed	0
Moisture content in tar	Mt	%	From tar analysis, as-received basis	10.00

Part 1 - Incoming streams

1. Fuel - Dry basis				
Carbon	C	%	Ultimate analysis, dry basis	51.80
Hydrogen	H	%	Same as above	6.20
Oxygen	O	%	Same as above	40.62
Nitrogen	N	%	Same as above	0.60
Sulfur	S	%	Same as above	0.38
Ash	A	%	Same as above	0.40

Total	Tot	%	= Sum of above items	100.00
Moisture content in sawdust	Ms	%	From fuel data, as-received basis	14.71
Sawdust heating value (dry basis)	HHV0	MJ/kg	= 327.8*C+1419.3*H+193.9*S-128.9*O-334.9	20.28
SD higher heating value (as fired)	HHVsd	MJ/kg	= HHV0*(100-Ms)/100	17.30
SD lower heating value (as fired)	LHVsd	MJ/kg	= HHV-2.984*(92.7*H+11.1*M)/1000	15.10
Stoichiometric air	V0	Nm^3/kg	See fuel data, as received basis	4.57
Total weight of sawdust loaded	Wsdtot	kg	See test data sheets	120.31
Total gasification run time	t	h	From transition to shutdown	3.80
SD consumed in gasif. (as fired)	Wsd	kg	= F*t, or as weighed	120.77
Mean fuel feed rate	F	kg/h	Over the gasification period, as fired	31.78
Total dry fuel consumed	W1	kg	= Wsd*(100-M)/100	103.00
Carbon	C1	kg	= W1*C/100	53.36
Hydrogen	H1	kg	= W1*(H/100 + M/100*2.01588/18.0153)	6.39
Oxygen	O1	kg	= W1*(O/100 + M/100*15.9994/18.0153)	41.84
Nitrogen	N1	kg	= W1*N/100	0.62
Sulfur	S1	kg	= W1*S/100	0.39
Ash - mineral matter	A1	kg	= W1*A/100	0.41
Check total weight	Wtot	kg	= Sum of above six items	103.00
Lower heating value of main fuel	E1	MJ	= LHVsd*Wsd	1823.17

2. Auxiliary fuel – Ash in the coal is also considered in the mass balance

Name of auxiliary fuel	-	-	Name of coal	Highvale
Carbon	C	%	Ultimate analysis, dry basis	62.86
Hydrogen	H	%	Same as above	3.63
Oxygen	O	%	Same as above	17.80
Nitrogen	N	%	Same as above	0.22
Sulfur	S	%	Same as above	0.77
Ash	A	%	Same as above	14.73
Total	Tot	%	= Sum of above items	100.00
Moisture content in coal	Mc	%	From coal analysis, as-received base	9.00
Coal heating value (dry basis)	HHVcd	MJ/kg	= 327.8*C+1419.3*H+193.9*S-128.9*O-334.9	23.27
Coal heating value (as fired)	HHVcog	MJ/kg	= HHVcd*(100-Mc)/100	21.18
Coal lower heating value (as fired)	LHVc	MJ/kg	= HHV-2.984*(92.7*H+11.1*M)/1000	19.88
Stoichiometric air of coal	V0c	Nm^3/kg	See fuel data	5.93
Total coal consumption	Wc	kg	= F*t, or as weighed	60.98
Co-gasified coal weight	Wcog	kg	From test data sheet	0.00
Total dry coal consumption	W2	kg	= Wc*(100-Mc)/100	55.49
Co-gasified dry coal weight	W2cog	kg	= Wcog*(100-Mc)/100	0
Carbon	C2	kg	= W2cog*C/100	0
Hydrogen	H2	kg	= W2cog*H/100	0
Oxygen	O2	kg	= W2cog*O/100	0
Nitrogen	N2	kg	= W2cog*N/100	0
Sulfur	S2	kg	= W2cog*S/100	0
Ash - mineral matter	A2	kg	= W2*A/100 (Note: Not W2cog)	8.17

Check total weight	Wtot	kg	= Sum of above six items	8.17
Heat from co-gasified coal	E2	MJ	= LHVcog*Wcog	0.00
3. Oxidant - Air				
Total amount of air supplied	Vair	Nm^3	From test data sheet	185.98
Mean air flow	Fair	Nm^3/h	= Vair / t	48.94
Carbon weight percent in air	Ca	%	North American standard air	0.05
Hydrogen weight percent in air	Ha	%	Same as above	0.05
Oxygen weight percent in air	Oa	%	Same as above	23.14
Nitrogen weight percent in air	Na	%	Same as above	75.52
Sulfur weight percent in air	Sa	%	Same as above	0.00
Other elements	Xa	%	Same as above	1.24
Total	Tot	%	= Sum of above five items	100.00
Additional cooling nitrogen	Vnitro	Nm^3	From test data sheet	0.00
Total weight of air	Wa	kg	= 1.293*Vair, (at 273 K, 1.013 bar)	240.47
Carbon	C3	kg	= Wa*Ca/100	0.11
Hydrogen	H3	kg	= Wa*Ha/100	0.12
Oxygen	O3	kg	= Wa*Oa/100	55.65
Nitrogen	N3	kg	= Wa*Na/100 + Vnitro*1.2506	181.61
Nominal fuel stoichiometric air	V0m	Nm^3/kg	= (V0*Wsd+V0c*Wcog)/ (Wsd+Wcog)	4.57
Overall air ratio	a	-	= [Vair/(Wsd+Wcog)]/V0m	0.337
4. Water carried in by steam injection and moisture in sawdust and coal				
Mean steam injection rate	Fst	kg/h	From test data sheet	0.00
Duration of steam injection	tst	h	From test data sheet	0.00
Total steam injected	Wwst	kg	= Fst*tst, or as metered	0.00
Moisture content in sawdust	Msd	%	From fuel analysis	14.71
Weight of water in sawdust	Wwsd	kg	= Wsd*Msd/100	17.76
Moisture content in coal	Mc	%	From fuel analysis	9.00
Weight of water in coal	Wwc	kg	= Wc*Mc/100	5.49
Total weight of water in feed	Wwtot4	kg	= Wwst + Wwsd + Wwc	23.25
Hydrogen	H4	kg	= Wwtot4*2.01588/18.0153	2.60
Oxygen	O4	kg	= Wwtot4*15.9994/18.0153	20.65
Enthalpy of steam	E4	MJ	= Wwst * 2706.3/1000	0.00
5. Sand and ash				
Total weight of bed materials	Wbm	kg	From test data sheets	29.96
Bed ash added as bed material	Wba	kg	From test data sheets	18.61
Carbon content in dry bed ash	[C]	%	Measured, previous run	0.63
Inert content in dry bed ash	[A]	%	= 100 - [C]	99.37
Moisture content in as-it-is bed ash	Mba	%	Measured, previous run	0.05
Carbon in bed ash	Cba	kg	= Wba*(100-Mba)/100*[C]/100	0.12
Inert in bed ash	Aba	kg	= Wba*(100-Mba)/100*[A]/100	18.49
Water in bed ash	Wwba	kg	= Wba*Mba/100	0.01
Sand added as bed material	As	kg	= Wbm - Wba	11.35
Fly ash reinjection	Wfa	kg	From test data sheets	0.00
Carbon content in dry fly ash	[C*]	%	Measured, previous run	55.61

Inert content in dry fly ash	[A*]	%	= 100 - [C*]	44.39
Moisture content in as-it-is fly ash	Mfa	%	Measured, previous run	0.87
Carbon in fly ash	Cfa	kg	= Wfa*(100-Mba)/100*[C*]/100	0.00
Inert in fly ash	Afa	kg	= Wfa*(100-Mba)/100*[A*]/100	0.00
Water in fly ash	Wwfa	kg	= Wfa*Mfa/100	0.00
Total weight of water in ash	Wwtot5	kg	= Wwba + Wwfa	0.01
Hydrogen as ash moisture	H5	kg	= Wwtot5*2.01588/18.0153	0.00
Oxygen as ash moisture	O5	kg	= Wwtot5*15.9994/18.0153	0.01
Total carbon in ash	C5	kg	= Cba + Cfa	0.12
Total inert material in sand and ash	A5	kg	= Aba + As + Afa	29.84
Heating value of residual C in ash	E5	MJ	= C5*32.783	3.84

6. Summary of feed streams

Carbon	Cin0	kg	= C1 + C2 + C3 + C5	53.59
Carbon content in residual *coal* ash	Cash	%	Measured	5
Carbon, modified	Cin	kg	= Cin0 + A2*Cash/100	54.00
Hydrogen	Hin	kg	= H1 + H2 + H3 + H4 + H5	9.11
Oxygen	Oin	kg	= O1 + O2 + O3 + O4 + O5	118.15
Nitrogen	Nin	kg	= N1 + N2 + N3	182.23
Sulfur	Sin	kg	= S1 + S2	0.39
Ash - mineral matter	Ain	kg	= A1 + A2 + A5	38.42
Total weight in	Win	kg	= Cin + Hin + Oin + Nin + Sin + Ain	402.29
Total energy in	Ein	GJ	= E1 + E2 + E4 + E5	1827.0
Overall O/C ratio	O/C	-	= (Oin/15.9994)/(Cin/12.011)	1.643

Part 2 - Output streams

1. Product gas

Time-mean dry gas composition				
Hydrogen	[H_2]	%	From test data sheets	4.18
Nitrogen	[N_2]	%	Same as above	62.57
Carbon monoxide	[CO]	%	Same as above	14.57
Methane	[CH_4]	%	Same as above	2.97
Carbon dioxide	[CO_2]	%	Same as above	15.70
Dry gas HHV	HHV0	MJ/Nm^3	= (285.8[H_2]+283*[CO]+890.8*[CH_4])/0.027887	3.53
Ethylene estimated	[C_2H_4]	%	Estimated, van der Drift (2001)	1.09
Total	Tot	%	= Sum of above five	101.09
Normalized gas composition				
Hydrogen	[H_2]	%		4.14
Nitrogen	[N_2]	%		61.90
Carbon monoxide	[CO]	%		14.42
Methane	[CH_4]	%		2.94
Carbon dioxide	[CO_2]	%		15.53
Ethylene, estimated	[C_2H_4]	%		1.07
Total	Tot	%		100.00
Modified dry gas heating value	HHVg	MJ/Nm^3	= (286[H_2]+283*[CO]+891*[CH_4] +1411*[C_2H_4])/0.0279	4.17
CO/CO_2 molar ratio	[CO/CO_2]	-	= [CO]/[CO_2]	0.928
H_2/CO molar ratio	[H_2/CO]	-	= [H_2]/[CO]	0.287

CH_4/H_2 molar ratio	$[CH_4/H_2]$	-	$= [CH_4]/[H_2]$	0.711
For every 1 Nm^3 (298 K, 1.013 bar) of product gas				
Gas constant	R	J/mol-K	Known	8.31448
Standard temperature	T0	K	Standard state	298
Standard pressure	P	bar	Standard state	1.013
Number of moles in 1 Nm^3 of gas	Y	-	= P/RT (assuming ideal gas)	40.88
Moles of H_2	n1	mol	$= Y*[H_2]/100$	1.69
Moles of N_2	n2	mol	$= Y*[N_2]/100$	25.31
Moles of CO	n3	mol	$= Y*[CO]/100$	5.89
Moles of CH_4	n4	mol	$= Y*[CH_4]/100$	1.20
Moles of CO_2	n5	mol	$= Y*[CO_2]/100$	6.35
Moles of C_2H_4	n6	mol	$= Y*[C_2H_4]/100$	0.44
Moles of C	N1	mol	= n3 + n4 + n5 + 2*n6	14.33
Moles of H	N2	mol	= n1*2 + 4*n4 + 4*n6	9.95
Moles of O	N3	mol	= n3 + 2*n5	18.60
Moles of N	N4	mol	= 2*n2	50.61
Calculate total gas volume based on dry gas composition and nitrogen balance				
Total moles of N_2 in feed	NN2	mol	= Nin*1000/28.0135	6504.95
Moles of N_2 in 1 Nm^3 of gas	n2	mol	Same as above	25.31
Total volume of dry product gas	Vg	Nm^3	= NN2/n2	257.03
Dry gas yield per 1 kg of sawdust	vgas	Nm^3/kg	= Vg/(Wsd+Wcog)	2.13
Dry gas yield per 1 Nm^3 of air supp.	vga	Nm^3/Nm^3	= Vg/Vair	1.38
Moles of each element in product gas				
Carbon	C6	kg	= Vg*N1*12.011/1000	44.23
Hydrogen	H6	kg	= Vg*N2*1.00794/1000	2.58
Oxygen	O6	kg	= Vg*N3*15.9994/1000	76.47
Nitrogen	N6	kg	= Vg*N4*14.0067/1000	182.22
Total heating value in product gas	E6	MJ	= Vg*HHVg	1072.31
Moles of C and H in CH_4				
Carbon in CH_4	C6meth	kg	= n4*Vg*12.011/1000	3.71
Hydrogen in CH_4	H6meth	kg	= 4*n4*Vg*1.00794/1000	1.25
Fraction of carbon staying as CH_4	Cmeth	%	= C6met/Cin * 100%	6.875
Fraction of H residing in CH_4	Hmeth	%	= Hmet/Hin * 100%	13.679
2. Ash				
Total bed ash collected	Wbao	kg	From test data sheets	23.74
Carbon content in dry bed ash	[Co]	%	Measured, current run	0.71
Inert content in dry bed ash	[Ao]	%	= 100 - [Co]	99.29
Moisture content in bed ash	Mbao	%	Measured, current run	0.20
Carbon in bed ash	Cbao	kg	= Wbao*(100-Mbao)/100*[Co]/100	0.17
Inert in bed ash	Abao	kg	= Wbao*(100-Mbao)/100*[Ao]/100	23.52
Water in bed ash	Wwba	kg	= Wbao*Mbao/100	0.05
Total fly ash collected	Wfao	kg	From test data sheets	24.52
Total ashing loss of dry fly ash	[L*]	%	Measured, current run, (900 °C, 2 h)	55.15
Carbon content in dry fly ash	[Cfa]	%	= 86% of ashing loss	47.43
Hydrogen content in dry fly ash	[Hfa]	%	= 4% of ashing loss	2.21

Oxygen content in dry fly ash	[Ofa]		= [L*] – [Cfa] – [Hfa]	5.52
Inert content in dry fly ash	[Ao*]	%	= 100 - [L*]	44.85
Moisture content in as-it-is fly ash	Mfao	%	Measured, current run	16.83
Carbon in fly ash	Cfao	kg	= Wfao*(100-Mbao)/100*[Cfa]/100	9.67
Hydrogen in fly ash	Hfao	kg	= Wfao*(100-Mbao)/100*[Hfa]/100	0.45
Oxygen in fly ash	Ofao	kg	= Wfao*(100-Mbao)/100*[Ofa]/100	1.12
Inert in fly ash	Afao	kg	= Wfao*(100-Mbao)/100*[Ao*]/100	9.15
Moisture in fly ash	Wwfao	kg	= Wfao*Mfao/100	4.13
Total weight of water in ash	Wwtot7	kg	= Wwbao + Wwfao	4.17
Hydrogen as ash moisture	H7	kg	= Wwtot7*2.01588/18.0153 + Hfa	0.92
Oxygen as ash moisture	O7	kg	= Wwtot7*15.9994/18.0153 + Ofa	4.83
Total carbon in ash	C7	kg	= Cbao + Cfao	9.84
Total inert in sand and ash	A7	kg	= Abao + Afao	32.77

3. Tars

Tar composition				
Carbon	C	%	Ultimate analysis, dry base	72.90
Hydrogen	H	%	Same as above	5.40
Oxygen	O	%	Same as above	9.00
Nitrogen	N	%	Same as above	2.65
Sulfur	S	%	Same as above	0.05
Ash	A	%	Same as above	10.00
Total	Tot	%	= Sum of above items	100.00
Tar collected from vertical pipe	Wt1	kg	= F*t, or as weighed	0.114
Tar collected from rooftop	Wt2	kg	Totally 5.221 kg dry tar	0.240
Total dry tar	W8	kg	= Wc*(100-Mc)/100	0.353
Moisture content in rooftop tar	Mt	%	From coal analysis, as-received base	14.82
Tar heating value (dry basis)	HHVt0	MJ/kg	= 328*C+1419*H+194*S-129*O-335	30.1
Tar yield, dry tar	Tar	g/Nm^3	= W8*1000/Vgas	1.37
Carbon	C8	kg	= W3*C/100	0.26
Hydrogen	H8	kg	= W3*H/100	0.02
Oxygen	O8	kg	= W3*O/100	0.03
Nitrogen	N8	kg	= W3*N/100	0.01
Sulfur	S8	kg	= W3*S/100	0.00
Ash - mineral matter	A8	kg	= W3*A/100	0.04
Check total weight	Wtot	kg	= Sum of above six items	0.35
Heating value of tar	E8	MJ	= Wt*HHVt	10.63

4. Water and H_2S in product gas - Measured or predicted

For every 1 Nm^3 of product gas				
Time mean bed temperature	T	C	From test data sheets	788.54
Operating pressure (bottom of bed)	P	bar	From test data sheets	1.19
Time mean air ratio	a	-	Same as above	0.337
Total volume of product gas	Vg	Nm^3	Same as above	257.03
Gas yield per kg of sawdust	vg	Nm^3/kg	Same as above	2.13
Constant	Y	-	Same as above	40.88
H_2S content in gas, predicted	[H_2S]	%	Predicted from equilibrium model	0.1045
Moles of H_2S	n6	mol/Nm^3	= Y*[H_2S]/100	0.04
Moles of H	N6	mol/Nm^3	= 2*n6	0.09

Moles of S	N8	mol/Nm^3	= n7	0.04
Hydrogen	H9	kg	= Vg*N6*1.00794/1000	0.022
Sulfur	S9	kg	= Vg*N8*32.066/1000	0.352
Total oxygen out, excluding water	Ocum	kg	= O6 + O7 + O8	80.212
Oxygen in water	Owat	kg	= Oin - Ocum	37.938
Moisture content in gas, assumed	[H2O]	%	= Owat*1000/(15.9994)/(Vg*Y)*100	22.564
Moles of H_2O	n7	mol/Nm^3	= Y*[H_2O]/100	9.23
Moles of H	N9	mol/Nm^3	= 2*n7	18.45
Moles of O	N10	mol/Nm^3	= n7	9.23
Hydrogen	H10	kg	= Vg*N9*1.00794/1000	4.780
Oxygen	O10	kg	= Vg*N10*15.9994/1000	37.938
5. Summary of product streams				
Carbon	Cout	kg	= C6 + C7 + C8	54.33
Hydrogen	Hout	kg	= H6 + H7 + H8 + H9 + H10	8.17
Oxygen	Oout	kg	= O6 + O7 + O8 + O9 + O10	118.15
Nitrogen	Nout	kg	= N6 + N8	182.23
Sulfur	Sout	kg	= S8 + S9	0.35
Ash - mineral matter	Aout	kg	= A7 + A8	32.81
Total weight out	Wout	kg	= Cin + Hin + Oin + Nin + Sin + Ain	396.03
Total energy out	Eout	MJ	= E6 + E8	1082.94
Energy out as heating value of gas	E6	MJ	Same as above	1072.31
6. Summary				
Operating temperature	T	C	Same as above	788.5
Operating pressure	P	bar	Same as above	1.19
Representing air ratio	a	-	Same as above	0.337
Mean gas heating value	HHVg	MJ/Nm^3	Same as above	4.17
Gas yield	vgas	Nm^3/kg	Same as above	2.13
Carbon closure	RC	%	= Cout/Cin*100	100.61
Hydrogen	RH	%	= Hout/Hin*100	89.74
Oxygen	RO	%	= Oout/Oin*100	100.00
Nitrogen	RN	%	= Nout/Nin*100	100.00
Sulfur	RS	%	= Sout/Sin*100	90.01
Ash – inert species	RA	%	= Aout/Ain*100	85.38
Overall mass balance closure	RT	%	= Wout/Win*100	98.44
Carbon conversion, gas	[CC]	%	= C6/Cin*100	81.91
Overall carbon conversion, + tars	[CC+]	%	= (C6+C8)/Cin*100	82.39
Cold gas thermal efficiency, gas	E	%	= E6/Ein*100	58.69
Overall thermal efficiency, + tars	E+	%	= Eout/Ein*100	59.27

Appendix IX. Ash Composition

Table A-6. Composition of fly ash.

(a) Group 4A analysis

Item	Units	FA-2 (Run 2)	FA-6 (Run 6)	FA-7 (Run 7)	FA-14 (Run 14)
SiO_2	%	79.80	27.99	18.45	17.08
Al_2O_3	%	0.99	8.58	7.38	18.73
Fe_2O_3	%	0.33	2.41	2.18	1.59
MgO	%	0.11	0.74	0.49	0.73
CaO	%	0.93	8.40	6.82	5.78
Na_2O	%	0.29	1.41	1.33	0.69
K_2O	%	0.29	0.51	0.32	0.76
TiO_2	%	0.06	0.26	0.23	0.14
P_2O_5	%	0.02	0.13	0.08	0.22
MnO	%	0.02	0.08	0.04	0.16
Cr_2O_3	%	0.008	0.028	0.018	0.016
Ba	ppm	217	1787	1736	963
Ni	ppm	87	410	206	26822
Sc	ppm	1	6	5	4
LOI	%	17.1	49.0	62.4	50.5
Total C	%	9.10	34.89	49.15	43.58
Total S	%	0.01	0.28	0.44	0.12
Sum	%	99.99	99.79	99.96	99.91

Method: 0.200 gram sample by $LiBO_2$ fusion, analysis by ICP-ES. LOI by loss on ignition. Total C and S by LECO (Not included in the sum).

(b) Group 4B analysis

Item	Units	FA-2 (Run 2)	FA-6 (Run 6)	FA-7 (Run 7)	FA-14 (Run 14)
Co	ppm	1.9	7.2	7.9	27.6
Cs	ppm	0.3	0.6	0.5	0.5
Ga	ppm	10.1	14.8	13.0	18.1
Hf	ppm	1.6	3.4	3.4	2.0
Nb	ppm	2.8	12.6	11.0	6.3
Rb	ppm	5.4	9.9	6.7	12.6
Sn	ppm	6	5	4	6
Sr	ppm	83.1	585.6	597.4	349.5
Ta	ppm	0.1	0.5	0.5	0.3
Th	ppm	2.1	11.1	10.9	5.2
U	ppm	0.8	4.2	3.8	2.0
V	ppm	22	44	42	36
W	ppm	<0.1	2.4	9.8	9.0
Zr	ppm	55.5	117.2	124.1	64.6
Y	ppm	5.9	24.1	25.7	12.3
La	ppm	12.5	48.5	43.6	24.3
Ce	ppm	19.0	71.0	70.1	34.3
Pr	ppm	2.09	7.91	7.47	4.01
Nd	ppm	7.4	30.2	29.8	15.1
Sm	ppm	1.2	4.4	5.0	2.5
Eu	ppm	0.21	0.57	0.64	0.25
Gd	ppm	1.03	3.67	3.89	1.88
Tb	ppm	0.17	0.61	0.65	0.30
Dy	ppm	0.82	3.58	3.68	1.97
Ho	ppm	0.18	0.73	0.77	0.38
Er	ppm	0.51	2.00	2.32	0.99
Tm	ppm	0.10	0.32	0.33	0.15
Yb	ppm	0.50	2.19	2.37	0.98
Lu	ppm	0.10	0.31	0.36	0.18

Method: REE – $LiBO_2$ fusion, ICP/MS finished.

(c) Group 1DX – Leaching test

Item	Units	FA-2 (Run 2)	FA-6 (Run 6)	FA-7 (Run 7)	FA-14 (Run 14)
Mo	ppm	2.0	6.7	4.8	3.7
Cu	ppm	8.1	17.4	18.1	27.9
Pb	ppm	3.6	13.5	16.9	8.8
Zn	ppm	18	31	26	107
Ni	ppm	112.7	298.6	180.8	24661.1
As	ppm	1.1	4.3	4.3	2.8
Cd	ppm	0.1	0.2	0.2	1.1
Sb	ppm	0.8	1.5	1.0	0.7
Bi	ppm	0.1	0.3	0.3	0.2
Ag	ppm	0.1	0.4	0.5	0.3
Au	ppm	2.0	1.3	0.7	0.8
Hg	ppm	0.01	0.01	0.02	< 0.01
Ti	ppm	< 0.1	0.1	0.1	0.1

Method: 0.50 gram sample leached with 3 ml 2-2-2 HCl-HNO3-H2O at 95°C for one hour, diluted to 10 ml, analysed by ICP-MS. Upper limits – Ag, Au, Hg, W = 100 ppm; Mo, Co, Cd, Sb, Bi, Th, U and B = 2000 ppm; Cu, Pb, Zn, Ni, Mn, As, V, La and Cr = 10000 ppm.

Appendix X. Program listings of the equilibrium model

1. Load thermodynamic database

File name: coaldata.m
Function: To load thermodynamic database
Source code: See below.

```
%  This program loads the thermodynamic database for the FEM model

NE      = 5;                    % Specify number of elements
[Dat1, Dat11, Dat2, Dat3, Dath, Dath1] = coaldat(NE);

format short e
```

2. *Thermodynamic database*

File name: coaldat.m
Function: Thermodynamic, chemical and fuel property database for the equilibrium model
The database is designed for a maximum of 8 elements, 77 species.
Source code: See below.

```
function [Dat1, Dat11, Dat2, Dat3, Dath, Dath1] = coaldat(NE)
%  COALDAT chooses species and generates data for FEM algorithm based on the
number of elements.

disp('  ')
disp('    DATA FOR COAL AND BIOMASS COMBUSTION / GASIFICATION MODEL  ')
disp('  ')
disp('    Version 3.0                    Xuantian Li (June 15, 1999)  ')
disp('  ')

%  (1) Tmermodynamic data

%  Dat1 - Thermodynamic data. Source: JANAF (1985). Unit: kJ/mol, P = 1 bar

%  col 1   = species index
%  col 2   = phase index (1 = gas, 2 = liquid, 3 = solid)
%  col 3~7 = 5 correlation factors of DGfo(T)
%  col 8   = cut-off temperature above which alternative correlations are used
%  col 9   = species identification

%  Form of correlations
%  dGfo(T,i) = Dat1(i,3) + Dat1(i,4)*T*log(T) + Dat1(i,5)*T^2 + Dat1(i,6)/T
               + Dat1(i,7)*T;

data1 =[

%  Gaseous species - the first ideal solution

%  NP       a           b           c           d          e        T  Species

1  1   718.7355   -0.0031881   1.9694E-06   -349.8554  -0.137650  3000  % C-g
2  1   598.0953    0.0043862  -1.9285E-07   -343.7758  -0.146320  3000  % CH
3  1   389.5788    0.0077494  -6.6767E-07   -144.1515  -0.110660  3000  % CH2
4  1   149.0231    0.014182   -2.9054E-06     41.6868  -0.084363  3000  % CH3
5  1   -71.8931    0.02432    -6.5597E-06    362.4270  -0.070448  3000  % CH4
6  1   237.5202    0.033256    1.0033E-06   -100.2833  -0.152990  3000  % C2H2
7  1    54.1895    0.021684   -5.6205E-06    449.8686  -0.079724  3000  % C2H4
8  1   -81.0970    0.043877   -1.7094E-05   1355.4000  -0.095520  3000  % C2H6
9  1   350.4716    0.66056    -2.6670E-04 -46636.1389  -4.40930   1600  % C3H8
10 1   215.7586   -0.0073886   9.1095E-07     10.6162  -0.000162  3000  % H
11 1     0          0           0              0         0         3000  % H2
12 1   248.3877   -0.0052751   8.6902E-07    -86.4689  -0.025042  3000  % O
13 1     0          0           0              0         0         3000  % O2
14 1  -106.8226    0.0033849   1.2143E-06   -326.6449  -0.117690  3000  % CO
15 1  -392.9600    0.0012695   3.3456E-07    -11.6092  -0.012005  3000  % CO2
16 1    40.3471    0.0020491  -1.2972E-07    -99.8727  -0.030869  3000  % OH
17 1  -239.0906    0.010852   -2.2307E-06     18.3029  -0.026247  3000  % H2O
```

```
18 1  -123.5618     0.033093    -1.6006E-05    -333.1775   -0.117240   3000  % H2O2
19 1    45.1098     0.0055998    1.4897E-07      34.6607   -0.088745   3000  % HCO
20 1     2.4359     0.0054918   -1.5372E-06     135.5294    0.007803   3000  % HO2
21 1   471.1519    -0.0062291    8.7182E-07     -24.5552   -0.016799   3000  % N
22 1     0           0            0              0          0         3000  % N2
23 1   158.6539    -0.0028993    1.1294E-06       6.8426   -0.009485   3000  % NCO
24 1   376.9439     0.00071778  -2.6308E-07     -27.3018   -0.025106   3000  % NH
25 1   190.2236     0.0071296   -1.8680E-06     302.7894   -0.011408   3000  % NH2
26 1   -44.8484     0.01514     -4.8125E-06     333.6023    0.006629   3000  % NH3
27 1    78.2427    -0.0042333   -3.3034E-07     327.3182    0.107480   3000  % N2O
28 1    90.1960    -0.0004493    1.5852E-07      -9.4708   -0.009467   3000  % NO
29 1    30.8041    -0.00073718  -9.3478E-08     255.6206    0.069885   3000  % NO2
30 1   435.7871    -0.0052945    3.2164E-05      97.4931   -0.050972   1300  % CN
31 1   136.4484     0.0032993   -3.0523E-07     -42.9127   -0.057570   3000  % HCN
32 1  -101.6731     0.0035636   -4.1540E-07     135.7470    0.009485   3000  % HCNO
33 1   289.7121     0.034221    -1.2994E-05    -591.9209   -0.363310    882  % S-g
34 1   160.9443     0.094171    -4.0715E-05   -1257.4685   -0.783600    882  % S2
35 1     8.5516     0.0041034    2.1502E-05    -115.6319   -0.127750    882  % SO
36 1  -292.1318     0.010504     1.6770E-05     -64.8202   -0.090967    882  % SO2
37 1  -391.3302     0.013933     1.1711E-05      62.5729   -0.015461    882  % SO3
38 1  -137.0166    -0.0030409    2.6447E-05     -46.3667   -0.085981    882  % COS
39 1   348.7762     0.13911     -3.3397E-05   -3564.5543   -1.145700   3000  % CS
40 1   121.0552    -0.0025409    4.9600E-05    -177.7956   -0.180370    882  % CS2
41 1   170.4059     0.061514    -1.7989E-05   -1712.5844   -0.544870   3000  % HS
42 1   -11.1102     0.023046     1.3079E-05     -244.5911   -0.207000    882  % H2S
43 1   120.0283    -0.0050448    7.4745E-07      -18.0719   -0.020620   3000  % Cl
44 1     0           0            0              0          0         3000  % Cl2
45 1   -91.0771     0.0039131   -7.9513E-07      -34.6297   -0.035919   3000  % HCl
46 1   117.6082     0.033919    -1.5573E-05     -331.9480   -0.321700   1171  % Na
47 1  -187.8035     0.035312    -1.8113E-05     -242.8665   -0.235570   1171  % NaOH
48 1 -1072.0630    -0.11214      1.4202E-04    2227.5049    0.900530   1171  % Na2SO4
49 1  -169.6071     0.038915    -1.8283E-05     -363.5927   -0.318660   1171  % NaCl-g
50 1   180.2741     0.00016753   1.2421E-05     -123.7122   -0.124680   1773  % Ca-g
51 1    40.7320    -0.011558     1.9722E-05      224.1673   -0.007229   1773  % CaO-g
52 1  -618.3319    -0.018033     1.9297E-05      574.4943    0.207910   1773  %Ca(OH)2
53 1   185.7102     0.11895     -8.1082E-06    -3158.4494   -1.006700   1773  % CaS-g

%  Liquid species - the second ideal solution

54 2     0           0            0              0          0         1171  % Na-l
55 2  -445.9895    -0.11189      3.6991E-05     6703.4883    0.910340   1171  % Na2O-l
56 2  -459.3828    -0.074551     2.3967E-05     3491.8695    0.664410   1171  % NaOH-l
57 2 -1512.0850    -0.65586      3.1344E-04    36973.2297    4.841900   1171  % Na2CO3
58 2  -770.5716    -0.83388      5.2169E-04    37800.9203    5.676300   1171  % Na2S-l
59 2 -1805.6090    -0.83986      5.0615E-04    37729.5329    6.081200   1171  % Na2SO4
60 2  -397.4964     0.0027913   -1.6935E-05     1717.7270    0.076591   1171  % NaCl-l
61 2  -195.1217    -0.03771      5.8557E-06    -2560.3111    0.382540   2500  % Ca-l
62 2  -566.7801    -0.027185     1.9285E-05      418.3720    0.257940   1773  % CaO-l

%  Solids - single-species phases

63 3     0           0            0              0          0         3000  % C-s
64 3     0           0            0              0          0         3000  % S-s
65 3  -436.2111    -0.038132     2.9169E-05     1030.1304    0.389390   1171  % Na2O-s
66 3  -435.1112    -0.0062054   -2.2299E-05      595.9177    0.221760   1171  % NaOH-s
67 3 -1156.8340    -0.053051     2.3470E-05     1404.1967    0.645620   1171  % Na2CO3
68 3  -811.0560    -0.8308       5.1991E-04    37657.5045    5.686700   1171  % Na2S-s
69 3 -1799.7500    -0.78703      4.7835E-04    35304.4574    5.737200   1171  % Na2SO4
```

```
70 3  -402.2163    0.02726    -2.2745E-05   -443.3801  -0.081660  1171  % NaCl-s
71 3     0          0           0              0          0        1773  % Ca-s
72 3  -644.5782   -0.026871    1.9067E-05    466.1628   0.280090  1773  % CaO-s
73 3  -996.2730   -0.022354    4.4400E-06    596.7389   0.447650  1000  %Ca(OH)2
74 3 -1241.8400   -0.071011    3.4234E-05   2447.3300   0.745000  1200  % CaCO3
75 3  -417.4180    0.10164    -7.0773E-06  -2991.0648  -0.713070  1773  % CaS-s
76 3 -1412.6200    0.050125   -1.1297E-06   -312.6500   0.024180  2000  % CaSO4
77 3  -818.1100   -0.0857846   2.8497E-05   -178.0300   0.741505  1112  % CaCl2
];

data11 = [

%  Gaseous species - the first ideal solution

%  NP     a            b           c            d          e         T    Species

1  1   718.7355   -0.0031881   1.9694E-06   -349.8554  -0.137650  3000  % C-g
2  1   598.0953    0.0043862  -1.9285E-07   -343.7758  -0.146320  3000  % CH
3  1   389.5788    0.0077494  -6.6767E-07   -144.1515  -0.110660  3000  % CH2
4  1   149.0231    0.0141820  -2.9054E-06     41.6868  -0.084363  3000  % CH3
5  1   -71.8931    0.0243200  -6.5597E-06    362.4270  -0.070448  3000  % CH4
6  1   237.5202    0.0332560   1.0033E-06   -100.2833  -0.152990  3000  % C2H2
7  1    54.1895    0.0216840  -5.6205E-06    449.8686  -0.079724  3000  % C2H4
8  1   -81.0970    0.0438770  -1.7094E-05   1355.4000  -0.095520  3000  % C2H6
9  1   350.4716    0.66056    -2.6670E-04 -46636.1389  -4.40930   1600  % C3H8
10 1   215.7586   -0.0073886   9.1095E-07     10.6162  -0.000162  3000  % H
11 1     0          0           0              0          0        3000  % H2
12 1   248.3877   -0.0052751   8.6902E-07    -86.4689  -0.025042  3000  % O
13 1     0          0           0              0          0        3000  % O2
14 1  -106.8226    0.0033849   1.2143E-06   -326.6449  -0.117690  3000  % CO
15 1  -392.9600    0.0012695   3.3456E-07    -11.6092  -0.012005  3000  % CO2
16 1    40.3471    0.0020491  -1.2972E-07    -99.8727  -0.030869  3000  % OH
17 1  -239.0906    0.0108520  -2.2307E-06     18.3029  -0.026247  3000  % H2O
18 1  -123.5618    0.0330930  -1.6006E-05   -333.1775  -0.117240  3000  % H2O2
19 1    45.1098    0.0055998   1.4897E-07     34.6607  -0.088745  3000  % HCO
20 1     2.4359    0.0054918  -1.5372E-06    135.5294   0.007803  3000  % HO2
21 1   471.1519   -0.0062291   8.7182E-07    -24.5552  -0.016799  3000  % N
22 1     0          0           0              0          0        3000  % N2
23 1   158.6539   -0.0028993   1.1294E-06      6.8426  -0.009485  3000  % NCO
24 1   376.9439    0.00071778 -2.6308E-07    -27.3018  -0.025106  3000  % NH
25 1   190.2236    0.0071296  -1.8680E-06    302.7894  -0.011408  3000  % NH2
26 1   -44.8484    0.0151400  -4.8125E-06    333.6023   0.006629  3000  % NH3
27 1    78.2427   -0.0042333  -3.3034E-07    327.3182   0.107480  3000  % N2O
28 1    90.1960   -0.0004493   1.5852E-07     -9.4708  -0.009467  3000  % NO
29 1    30.8041   -0.00073718 -9.3478E-08    255.6206   0.069885  3000  % NO2
30 1   164.8626    0.0531160  -1.7015E-05 115377.2750  -0.267280  3000  % CN
31 1   136.4484    0.0032993  -3.0523E-07    -42.9127  -0.057570  3000  % HCN
32 1  -101.6731    0.0035636  -4.1540E-07    135.7470   0.009485  3000  % HCNO
33 1   216.5859   -0.0012033   9.4057E-08   -920.1499  -0.051352  3000  % S-g
34 1     0          0           0              0          0        3000  % S2-g
35 1   -58.3392    0.00071189 -1.0075E-07   -230.9811  -0.010629  3000  % SO
36 1  -366.2515   -0.0040415   8.4388E-07    546.8531   0.104060  3000  % SO2
37 1  -472.4207   -0.0114260   1.5682E-06   1474.2158   0.254670  3000  % SO3
38 1  -203.0049   -0.0012573   8.5715E-07    128.0412  -0.001837  3000  % COS
39 1   348.7762    0.1391100  -3.3397E-05  -3564.5543  -1.145700  3000  % CS
40 1    -9.9250   -0.0017091   1.0910E-06   -455.0825   0.003789  3000  % CS2
41 1   170.4059    0.0615140  -1.7989E-05  -1712.5844  -0.544870  3000  % HS
42 1   -95.1612   -0.0016036   1.2867E-07   1797.0360   0.063333  3000  % H2S
```

```
43 1   120.0283   -0.0050448   7.4745E-07    -18.0719  -0.020620  3000  % Cl
44 1     0          0           0              0         0         3000  % Cl2
45 1   -91.0771    0.0039131  -7.9513E-07    -34.6297  -0.035919  3000  % HCl
46 1     0          0           0              0         0         3000  % Na-g
47 1  -307.5971   -0.0028573   2.4583E-07    162.7579   0.114810  3000  % NaOH-g
48 1 -1979.1620   -0.2721400   3.0537E-05 264780.0380   2.748800  3000  % Na2SO4
49 1  -288.8874    0.0012026   2.3460E-08     56.2872   0.028103  3000  % NaCl-g
50 1     0          0           0              0         0         3000  % Ca-g
51 1  -120.2318    0.0171030  -6.8175E-06   -566.2313  -0.082174  3000  % CaO-g
52 1  -779.1250   -0.0138330   1.6886E-06   -263.4823   0.309010  3000  %Ca(OH)2
53 1  -135.1063   -0.0052293  -2.6241E-06   -380.4109   0.091046  3000  % CaS-g

%  Liquid species - the second ideal solution

54 2  -102.0722    0.00027844 -3.8827E-06     31.9057   0.089756  1600  % Na-l
55 2  -603.1522   -0.0483350   9.7810E-07    641.5320   0.642100  3000  % Na2O-l
56 2  -532.4731   -0.0368850   3.8832E-06   -307.9617   0.486990  2500  % NaOH-l
57 2 -1357.4400   -0.0777160   2.8704E-06   -126.2168   1.012900  2500  % Na2CO3
58 2  -615.2298   -0.0331660   7.0543E-07    -50.4397   0.521040  3000  % Na2S-l
59 2 -1664.5100   -0.0717650   2.9858E-06   -181.8829   1.147800  3000  % Na2SO4
60 2  -505.1877   -0.0281640   3.1939E-07    -70.9886   0.368450  2500  % NaCl-l
61 2  -195.1217   -0.0377100   5.8557E-06  -2560.3111   0.382540  2500  % Ca-l
62 2  -725.6541   -0.0173170  -5.6041E-07   -991.9894   0.318130  3000  % CaO-l

%  Solids - single-species phases

63 3     0          0           0              0         0         3000  % C-s
64 3     0          0           0              0         0         3000  % S-s
65 3  -713.7362   -0.1176400   2.1687E-05   4547.5904   1.192000  2000  % Na2O-s
66 3  2469.6893    4.8916000  -1.8881E-03 125735.7140 -34.769600  1500  % NaOH-s
67 3 -1387.7580   -0.0645030  -9.0077E-06   -198.6146   0.960480  2000  % Na2CO3
68 3  -769.4582   -0.1608900   2.5916E-05   1662.5306   1.519800  2000  % Na2S-s
69 3 -1590.6950    0.0073529  -4.5470E-05      0        0.632690  1500  % Na2SO4
70 3  2490.9921    4.9294000  -1.9042E-03 126100.0000 -35.077000  1500  % NaCl-s
71 3     0          0           0              0         0         1773  % Ca-s
72 3  -799.9182   -0.0168030  -3.0821E-07   -309.0810   0.337110  3000  % CaO-s
73 3  -996.2730   -0.0223540   4.4400E-06    596.7389   0.447650  1000  %Ca(OH)2
74 3 -1241.8400   -0.0710110   3.4234E-05   2447.3300   0.745000  1200  % CaCO3
75 3  -700.9383   -0.0146900  -4.0703E-07   -158.3563   0.313420  3000  % CaS-s
76 3 -1412.6200    0.0501250  -1.1297E-06   -312.6500   0.024180  2000  % CaSO4
77 3  -818.1100   -0.0857846   2.8497E-05   -178.0300   0.741505  1112  % CaCl2
];


%  Dath - Heat of formation and correlation factors for enthalpy.
%  Data from Pankratz (1982, 1984, 1987) Unit: kJ/mol.
%  Ref. pressure: 1 atm (1.013 bar) for 38 species given in Pankratz's books,
%                 1 bar for all other species (JANAF data).
%  Water occurs as H2O (g), otherwise wrong.

%  col 1    = species index
%  col 2    = phase index
%  col 3~6  = correlation factors for enthalpy
%  col 7    = heat of formation of the species (kJ/mol)
%  col 8    = temperature range of application
%  col 9    = species identification

%  Ho(T)-Ho(298) = aT/1000 + bT^2/1000000 + cT^-1 + d
```

```
datah = [

%  Gaseous species

%  NP      a        b           c           d          DHfo(298)   T     Species

1   1    20.7192    0.037656     -8.7864    -6.15048    716.670   2000  % C-g
2   1    27.6313    2.7448       41.0016    -8.8832     594.128   3000  % CH
3   1    38.6452    3.7555      408.7690   -14.0607     386.392   3000  % CH2
4   1    47.3888    6.2452      784.6346   -18.7179     145.687   3000  % CH3
5   1    52.9240    9.9567     1405.2934   -24.1768     -74.873   3000  % CH4
6   1    57.6040    5.8194     1046.3957   -22.4273     226.731   3000  % C2H2
7   1    73.3320   10.869      2132.0253   -33.4348      52.467   3000  % C2H4
8   1    70.7250   27.312      4372.6784   -37.9474     -84.000   3000  % C2H6
9   1   103.2600   43.4030      878.3933   -19.1280    -103.847   3000  % C3H8
10  1    20.7861    0              0        -6.19650    217.999   3000  % H
11  1    27.0119    1.753096     -69.0360    -7.97889      0       3000  % H2
12  1    20.8656   -0.012552     -93.7216    -5.90362    249.173   3000  % O
13  1    30.2503    2.104552     189.1168    -9.84077      0       2000  % O2
14  1    28.0663    2.3138        25.9408   -8.6609     -110.527   2000  % CO
15  1    45.3671    4.342992     961.9016   -17.13766    -393.522   2000  % CO2
16  1    26.5977    1.991584    -195.8112    -7.45170     38.987   3000  % OH
17  1    28.8487    6.029144    -100.4160    -8.79895    -241.826   2000  % H2O(g)
18  1    42.7186    9.547888     541.4096   -15.4013     -136.106   1500  % H2O2
19  1    42.0411    3.1052       554.7696   -15.7137      43.514   3000  % HCO
20  1    37.1539    5.054272     467.7712   -13.09592      2.092   3000  % HO2
21  1    20.7861    0              0        -6.19650    472.683   3000  % N
22  1    27.2671    2.464376     -33.0536    -8.23830      0       2000  % N2
23  1    51.8911    2.0775       770.5358   -19.2298     159.410   3000  % NCO
24  1    27.8197    1.8458        12.6111    -8.6206     376.560   3000  % NH
25  1    34.0257    4.4683       214.1698   -11.8113     190.372   3000  % NH2
26  1    43.1447    7.1278       724.6100   -17.3521     -45.898   3000  % NH3
27  1    44.2918    5.045904     771.5296   -16.24229     82.048   3000  % N2O
28  1    28.1541    2.615        -11.2968    -8.58975     90.291   2000  % NO
29  1    41.4174    4.966408     658.1432   -14.99546     33.095   2000  % NO2
30  1    28.8052    2.2265        58.6635    -9.1533     435.136   1300  % CN
31  1    43.7801    3.4977       615.5683   -16.264      135.143   3000  % HCN
32  1    59.8200    4.1845      1030.9512   -22.9877    -101.671   3000  % HCNO
33  1    22.5810   -0.472792    -122.1728    -6.28018    276.980   2000  % S-g
34  1    34.9071    1.33888      285.7672   -11.48508    128.600   2000  % S2-g
35  1    32.8737    1.577368     323.4232   -11.02484      5.007   2000  % SO
36  1    47.3796    3.330464     843.9128   -17.25482    -296.842   2000  % SO2
37  1    67.0109    4.389016    1685.7336   -26.02448    -395.765    882  % SO3
38  1    49.4884    3.652632     899.5600   -18.0958     -138.407   2000  % COS
39  1    33.4302    0.995792     375.7232   -11.31772     280.328   3000  % CS
40  1    56.3815    1.5756       714.1594   -20.0176      116.943   3000  % CS2
41  1    28.6646    1.916272    -234.7224    -7.92868     139.327   2500  % HS
42  1    31.5515    6.71532      121.3360   -10.40979     -20.502   2000  % H2S
43  1    23.9450   -0.719648     149.3688    -7.57722     121.302   2000  % Cl
44  1    36.9322    0.368192     285.7672   -12.0039       0       3000  % Cl2
45  1    26.7190    2.359776     -89.9560    -7.87429     -92.312   2000  % HCl
46  1    20.7652    0.016736      -1.2552    -6.18814     107.300   3000  % Na-g
47  1    51.9505    1.6391       346.7762   -16.9438     -197.757   3000  % NaOH-g
48  1    14.4120    2.915       2366.9623   -53.1502    -1033.620   3000  % Na2SO4
49  1    37.2358    0.3858       118.9968   -11.5661     -181.418   3000  % NaCl-g
50  1    19.8067    0.3758      -571.4430    -5.6241     177.800   3000  % Ca-g
51  1    23.0042    6.5738      -410.8451    -5.0186      43.932   3000  % CaO-g
```

```
52  1   85.9217    3.571       991.8630   -29.7821   -610.764  3000  %Ca(OH)2
53  1   24.3673    7.2837     -331.7881    -6.0861    123.595  3000  % CaS-g

%  Liquid species - the second ideal solution

54  2   29.3047   -0.38493    -380.3256    -5.03754     0      1171  % Na-l
55  2  104.6000    0             0        -31.186    -372.843  3000  % Na2O-l
56  2   88.5501   -2.5713     -180.4221   -25.6167   -416.878  2500  % NaOH-l
57  2  209.0100   -4.1645    12222.2540  -102.5933  -1108.520  2500  % Na2CO3
58  2  932.3960 -284.8718        0       -626.9640   -323.940  1445  % Na2S-l
59  2   21.1740   -3.3885     8801.9448    90.8069  -1356.390  3000  % Na2SO4
60  2   42.0032   11.19638    -161.9208   -12.97458  -385.923  1171  % NaCl-l
61  2   18.2956   11.2672      -24.5763    -6.4483     0      1171  % Ca-l
62  2   48.9970    2.514       573.2851   -16.8339   -557.335  2100  % CaO-l

%  Solids - single-species phases

63  3   14.7193    3.204944    720.9032    -7.09188     0      2000  % C-s
64  3   31.8890   -2.1803    -1884.7120    -3.0467     0       882  % S-s
65  3   55.9694   20.572728    -78.2408   -18.25479  -417.982  1300  % Na2O-s
66  3  108.4800   -8.7382     1892.2624   -38.4824   -425.931  1500  % NaOH-s
67  3  126.2500   28.23       1673.3871   -46.939   -1130.770  2000  % Na2CO3
68  3   74.8308    9.9286     -182.4224   -22.5810   -366.100  1100  % Na2S-s
69  3   87.4047   58.426     -4393.8200   -16.7088  -1379.290  1500  % Na2SO4
70  3   42.0032   11.196384   -161.9208   -12.97458  -411.120  1074  % NaCl-s
71  3   30.8253    6.845       560.9676   -12.8472     0      1773  % Ca-s
72  3   48.9970    2.514       573.2851   -16.8339   -635.089  2100  % CaO-s
73  3   91.6459   14.7372      941.6648   -31.6522   -986.085  1000  %Ca(OH)2
74  3   97.9350   14.198      1855.4379   -36.8346  -1207.600  1200  % CaCO3
75  3   49.9402    2.117104    334.3016   -16.20045  -473.210  2000  % CaS-s
76  3   32.8630   61.278     -6316.0380     4.5425  -1434.110  2000  % CaSO4
77  3   69.8393    7.694376    159.4104   -22.04131  -795.400  1045  % CaCl2
];


datah1 = [

%  Gaseous species

%  NP      a        b           c           d        DHfo(298)     T    Species
1   1   18.4891    0.48116   -2158.9440    -2.38906   716.670  3000  % C-g
2   1   27.6313    2.7448       41.0016    -8.8832    594.128  3000  % CH
3   1   38.6452    3.7555      408.7690   -14.0607    386.392  3000  % CH2
4   1   47.3888    6.2452      784.6346   -18.7179    145.687  3000  % CH3
5   1   52.9240    9.9567     1405.2934   -24.1768    -74.873  3000  % CH4
6   1   57.6040    5.8194     1046.3957   -22.4273    226.731  3000  % C2H2
7   1   73.3320   10.869      2132.0253   -33.4348     52.467  3000  % C2H4
8   1   70.7250   27.312      4372.6784   -37.9474    -84.000  3000  % C2H6
9   1  103.2600   43.4030      878.3933   -19.1280   -103.847  3000  % C3H8
10  1   20.7861    0             0         -6.19650   217.999  3000  % H
11  1   27.0119    1.753096    -69.0360    -7.97889     0      3000  % H2
12  1   20.8656   -0.012552    -93.7216    -5.90362   249.173  3000  % O
13  1   34.8946    0.874456   2635.9200   -15.43059     0      3000  % O2
14  1   34.2084    0.5188        0        -13.7528   -110.527  3000  % CO
15  1   61.3835    0.309616   9056.6864   -37.08279  -393.522  3000  % CO2
16  1   26.5977    1.991584   -195.8112    -7.45170    38.987  3000  % OH
17  1   28.8487    6.029144   -100.4160    -8.79895  -241.826  2000  % H2O(g)
18  1   42.7186    9.547888    541.4096   -15.4013   -136.106  1500  % H2O2
```

```
19  1    42.0411     3.1052      554.7696   -15.7137     43.514  3000  % HCO
20  1    37.1539     5.054272    467.7712   -13.09592     2.092  3000  % HO2
21  1    20.7861     0             0         -6.19650   472.683  3000  % N
22  1    36.1707     0.234304   4568.9280   -19.42631     0      3000  % N2
23  1    51.8911     2.0775      770.5358   -19.2298    159.410  3000  % NCO
24  1    27.8197     1.8458       12.6111    -8.6206    376.560  3000  % NH
25  1    34.0257     4.4683      214.1698   -11.8113    190.372  3000  % NH2
26  1    43.1447     7.1278      724.6100   -17.3521    -45.898  3000  % NH3
27  1    44.2918     5.045904    771.5296   -16.24229    82.048  3000  % N2O
28  1    28.1541     2.615       -11.2968    -8.58975    90.291  2000  % NO
29  1    41.4174     4.966408    658.1432   -14.99546    33.095  2000  % NO2
30  1    28.8052     2.2265       58.6635    -9.1533    435.136  1300  % CN
31  1    43.7801     3.4977      615.5683   -16.264     135.143  3000  % HCN
32  1    59.8200     4.1845     1030.9512   -22.9877   -101.671  3000  % HCNO
33  1    17.3887     0.702912  -4331.2770     1.50624   276.980  3000  % S-g
34  1    39.7898     0.4184     5271.8400   -20.06228   128.600  3000  % S2-g
35  1    37.3087     0.665256   4993.6040   -18.58114     5.007  3000  % SO
36  1    58.3333     0.288696   5014.9424   -29.0788   -296.842  3000  % SO2
37  1    79.1404     0.573208   1163.9888   -34.76067  -395.765  3000  % SO3
38  1    49.4884     3.652632    899.5600   -18.0958   -138.407  2000  % COS
39  1    33.4302     0.995792    375.7232   -11.31772   280.328  3000  % CS
40  1    56.3815     1.5756      714.1594   -20.0176    116.943  3000  % CS2
41  1    28.6646     1.916272   -234.7224    -7.92868   139.327  2500  % HS
42  1    31.5515     6.71532     121.3360   -10.40979   -20.502  2000  % H2S
43  1    23.0915    -0.326352   1771.9240    -8.25503   121.302  3000  % Cl
44  1    36.9322     0.368192    285.7672   -12.0039      0      3000  % Cl2
45  1    34.2460     0.598312   4134.6288   -17.99538   -92.312  3000  % HCl
46  1    20.7652     0.016736     -1.2552    -6.18814   107.300  3000  % Na-g
47  1    51.9505     1.6391      346.7762   -16.9438   -197.757  3000  % NaOH-g
48  1    14.4120     2.915      2366.9623   -53.1502  -1033.620  3000  % Na2SO4
49  1    37.2358     0.3858      118.9968   -11.5661   -181.418  3000  % NaCl-g
50  1    19.8067     0.3758     -571.4430    -5.6241    177.800  3000  % Ca-g
51  1    23.0042     6.5738     -410.8451    -5.0186     43.932  3000  % CaO-g
52  1    85.9217     3.571       991.8630   -29.7821   -610.764  3000  %Ca(OH)2
53  1    24.3673     7.2837     -331.7881    -6.0861    123.595  3000  % CaS-g

%  Liquid species - the second ideal solution

54  2    29.3047    -0.38493    -380.3256    -5.03754     0      1171  % Na-l
55  2   104.6000     0             0        -31.186    -372.843  3000  % Na2O-l
56  2    88.5501    -2.5713     -180.4221   -25.6167   -416.878  2500  % NaOH-l
57  2   209.0100    -4.1645    12222.2540  -102.5933  -1108.520  2500  % Na2CO3
58  2    92.0480     0             0         11.7989   -323.940  2000  % Na2S-l
59  2    21.1740    -3.3885     8801.9448    90.8069  -1356.390  3000  % Na2SO4
60  2    68.4502     0             0         -0.33054  -385.923  1800  % NaCl-l
61  2    35.0000     0             0         -2.648       0      2500  % Ca-l
62  2    62.7600     0             0        -28.193    -557.335  3000  % CaO-l

%  Solids - single-species phases

63  3    23.6019     0.560656   3012.4800   -15.42641     0      3000  % C-s
64  3    31.8890    -2.1803    -1884.7120    -3.0467      0       882  % S-s
65  3    55.9694    20.572728    -78.2408   -18.25479   -417.982  1300  % Na2O-s
66  3   108.4800    -8.7382     1892.2624   -38.4824    -425.931  1500  % NaOH-s
67  3   126.2500    28.23       1673.3871   -46.939   -1130.770  2000  % Na2CO3
68  3  -582.2747   310.5239        0        336.3476    -366.100  1276  % Na2S-s
69  3    87.4047    58.426     -4393.8200   -16.7088  -1379.290  1500  % Na2SO4
70  3    68.4502     0             0         -0.33054  -411.120  1800  % NaCl-s
```

```
71  3    5.2567     3.407     -27056.4100    212.0632       0       3000  % Ca-s
72  3   51.2990     1.9775      1301.8968    -13.8306    -635.089   3000  % CaO-s
73  3   91.6459    14.7372       941.6648    -31.6522    -986.085   1000  %Ca(OH)2

74  3   97.9350    14.198       1855.4379    -36.8346   -1207.600   1200  % CaCO3
75  3   49.9402     2.117104     334.3016    -16.20045   -473.210   2000  % CaS-s
76  3   32.8630    61.278      -6316.0380      4.5425   -1434.110   2000  % CaSO4
77  3  122.2690    -7.451704     -70.2912    -31.91137   -795.400   1600  % CaCl2
];

%  (2) Species-element matrix (SEM)
%  ---------------------------------------------------------------------

%  Data2 - Basic chemical data
%  col 1    = species index
%  col 2~9  = species-element matrix
%  col 10   = molecular weight of a species

data2 = [

%  Group 1 - gases

%  C  H  O  N  S  Cl Na Ca  M. wt     Species

1  1  0  0  0  0  0  0  0  12.011     % C-g
2  1  1  0  0  0  0  0  0  13.0189    % CH
3  1  2  0  0  0  0  0  0  14.0269    % CH2
4  1  3  0  0  0  0  0  0  15.0348    % CH3
5  1  4  0  0  0  0  0  0  16.0428    % CH4
6  2  2  0  0  0  0  0  0  26.0379    % C2H2
7  2  4  0  0  0  0  0  0  28.0538    % C2H4
8  2  6  0  0  0  0  0  0  30.0696    % C2H6
9  3  8  0  0  0  0  0  0  44.6565    % C3H8
10 0  1  0  0  0  0  0  0  1.00794    % H
11 0  2  0  0  0  0  0  0  2.01588    % H2
12 0  0  1  0  0  0  0  0  15.9994    % O
13 0  0  2  0  0  0  0  0  31.9988    % O2
14 1  0  1  0  0  0  0  0  28.0104    % CO
15 1  0  2  0  0  0  0  0  44.0098    % CO2
16 0  1  1  0  0  0  0  0  17.0073    % OH
17 0  2  1  0  0  0  0  0  18.0153    % H2O
18 0  2  2  0  0  0  0  0  34.0147    % H2O2
19 1  1  1  0  0  0  0  0  29.0183    % HCO
20 0  1  2  0  0  0  0  0  33.0067    % HO2
21 0  0  0  1  0  0  0  0  14.0067    % N
22 0  0  0  2  0  0  0  0  28.0135    % N2
23 1  0  1  1  0  0  0  0  42.0171    % NCO
24 0  1  0  1  0  0  0  0  15.0147    % NH
25 0  2  0  1  0  0  0  0  16.0226    % NH2
26 0  3  0  1  0  0  0  0  17.0306    % NH3
27 0  0  1  2  0  0  0  0  44.0129    % N2O
28 0  0  1  1  0  0  0  0  30.0061    % NO
29 0  0  2  1  0  0  0  0  46.0055    % NO2
30 1  0  0  1  0  0  0  0  26.0177    % CN
31 1  1  0  1  0  0  0  0  27.0257    % HCN
32 1  1  1  1  0  0  0  0  43.0251    % HCNO
33 0  0  0  0  1  0  0  0  32.066     % S-g
34 0  0  0  0  2  0  0  0  64.132     % S2-G
```

```
35 0  0  1  0  1  0  0  0   48.0654   % SO
36 0  0  2  0  1  0  0  0   64.0648   % SO2
37 0  0  3  0  1  0  0  0   80.0642   % SO3
38 1  0  1  0  1  0  0  0   60.0764   % COS
39 1  0  0  0  1  0  0  0   44.077    % CS
40 1  0  0  0  2  0  0  0   76.143    % CS2
41 0  1  0  0  1  0  0  0   33.0739   % HS
42 0  2  0  0  1  0  0  0   34.0819   % H2S
43 0  0  0  0  0  1  0  0   35.4527   % Cl
44 0  0  0  0  0  2  0  0   70.9054   % Cl2
45 0  1  0  0  0  1  0  0   36.4606   % HCl
46 0  0  0  0  0  0  1  0   22.9898   % Na-g
47 0  1  1  0  0  0  1  0   39.9971   % NaOH-g
48 0  0  4  0  1  0  2  0   142.043   % NaSO4-g
49 0  0  0  0  0  1  1  0   58.4425   % NaCl-g
50 0  0  0  0  0  0  0  1   40.078    % Ca-g
51 0  0  1  0  0  0  0  1   56.0774   % CaO-g
52 0  2  2  0  0  0  0  1   74.0927   % Ca(OH)2-g
53 0  0  0  0  1  0  0  1   72.144    % CaS-g

%  Group 2 - liquids

54 0  0  0  0  0  0  1  0   22.9898   % Na-l
55 0  0  1  0  0  0  2  0   61.9789   % Na2O-l
56 0  1  1  0  0  0  1  0   39.9971   % NaOH-l
57 1  0  3  0  0  0  2  0   105.989   % Na2CO3-l
58 0  0  0  0  1  0  2  0   78.0455   % Na2S-l
59 0  0  4  0  1  0  2  0   142.043   % NaSO4-l
60 0  0  0  0  0  1  1  0   58.4425   % NaCl-l
61 0  0  0  0  0  0  0  1   40.078    % Ca-l
62 0  0  1  0  0  0  0  1   56.0774   % CaO-l

%  Group 3 - solids

63 1  0  0  0  0  0  0  0   12.011    % C-s
64 0  0  0  0  1  0  0  0   32.066    % S-s
65 0  0  1  0  0  0  2  0   61.9789   % Na2O-s
66 0  1  1  0  0  0  1  0   39.9971   % NaOH-s
67 1  0  3  0  0  0  2  0   105.989   % Na2CO3-s
68 0  0  0  0  1  0  2  0   78.0455   % Na2S-s
69 0  0  4  0  1  0  2  0   142.043   % NaSO4-s
70 0  0  0  0  0  1  1  0   58.4425   % NaCl-s
71 0  0  0  0  0  0  0  1   40.078    % Ca-s
72 0  0  1  0  0  0  0  1   56.0774   % CaO-s
73 0  2  2  0  0  0  0  1   74.0927   % Ca(OH)2-s
74 1  0  3  0  0  0  0  1   100.087   % CaCO3-s
75 0  0  0  0  1  0  0  1   72.144    % CaS-s
76 0  0  4  0  1  0  0  1   136.142   % CaSO4-s
77 0  0  0  0  0  2  0  1   110.983   % CaCl2-s
];

% (3) Fuel analyses
%  ------------------------------------------------------------------------

%  Data3 - Fuel data

data3 = [
```

```
%  Sawdust species
%  Proximate analysis (as received basis, wt %)  -  10 species maximum.

%  1      2      3      4      5      6      7      8      9
%  Highv  Cypr   SPF    Heml   SPF    Ced/H  PBS    Mix-1  Mix-2

   43.4   59.9   59.5   59.5   59.5   59.5   59.5   59.5   59.5   % Volatile matter
   30.2   40.0   40.0   40.0   40.0   40.0   40.0   40.0   40.0   % Fixed carbon
   13.4    0.5    0.5    0.5    0.5    0.5    0.5    0.5    0.5   % Ash
    9.0    0.0    0.0    0.0    0.0    0.0    0.0    0.0    0.0   % Moisture

%  Ultimate analysis (dry base, wt %)

%  1      2      3      4      5      6      7      8      9
%  Highv  Cypr   SPF    Heml   SPF    Ced/H  PBS    Mix-1  Mix-2

   57.2   51.60  50.40  51.80  51.00  52.05  49.14  48.87  50.88  % C
    3.3    6.20   6.25   6.20   6.23   6.16   7.26   7.86   6.60  % H
   16.2   40.39  41.69  40.62  41.04  40.25  39.51  40.31  40.53  % O
    0.7    0.65   0.62   0.60   0.64   0.56   0.25   0.21   0.51  % N
    0.2    0.46   0.34   0.38   0.40   0.39   0.50   0.07   0.34  % S
    0.0    0.0    0.0    0.0    0.0    0.0    0.0    0.0    0.0   % Cl
    0.0    0.0    0.0    0.0    0.0    0.0    0.0    0.0    0.0   % Na
    0.0    0.0    0.0    0.0    0.0    0.0    0.0    0.0    0.0   % Ca
   13.4    0.70   0.70   0.40   0.70   0.60   3.34   2.69   1.14  % Ash
    9.0    0.0    0.0    0.0    0.0    0.0    0.0    0.0    0.0   % Moisture
   25.5   20.26  19.75  20.28  20.01  20.35  18.96  20.23  20.55  % HHV (MJ/kg)
];

%  Select species to be considered in the sub-set with NE elements

Dat1   = [ ];     % Initialization
Dat11  = [ ];
Dat2   = [ ];
Dat3   = [ ];
Dath   = [ ];
Dath1  = [ ];

if NE == 1           % C
   Dat1   = [ data1(1,:);  data1(63,:)];
   Dat11  = [data11(1,:); data11(63,:)];
   Dat2   = [ data2(1,:);  data2(63,:)];
   Dath   = [ datah(1,:);  datah(63,:)];
   Dath1  = [datah1(1,:); datah1(63,:)];
elseif NE == 2       % C-H
   Dat1   = [ data1(1:11,:);  data1(63,:)];
   Dat11  = [data11(1:11,:); data11(63,:)];
   Dat2   = [ data2(1:11,:);  data2(63,:)];
   Dath   = [ datah(1:11,:);  datah(63,:)];
   Dath1  = [datah1(1:11,:); datah1(63,:)];
elseif NE == 3       % C-H-O
   Dat1   = [ data1(1:20,:);  data1(63,:)];
   Dat11  = [data11(1:20,:); data11(63,:)];
   Dat2   = [ data2(1:20,:);  data2(63,:)];
   Dath   = [ datah(1:20,:);  datah(63,:)];
   Dath1  = [datah1(1:20,:); datah1(63,:)];
elseif NE == 4       % C-H-O-N
   Dat1   = [ data1(1:32,:);  data1(63,:)];
```

```
   Dat11  = [data11(1:32,:); data11(63,:)];
   Dat2   = [ data2(1:32,:);  data2(63,:)];
   Dath   = [ datah(1:32,:);  datah(63,:)];
   Dath1  = [datah1(1:32,:); datah1(63,:)];
elseif NE == 5        % C-H-O-N-S
   Dat1   = [ data1(1:42,:);  data1(63:64,:)];
   Dat11  = [data11(1:42,:); data11(63:64,:)];
   Dat2   = [ data2(1:42,:);  data2(63:64,:)];
   Dath   = [ datah(1:42,:);  datah(63:64,:)];
   Dath1  = [datah1(1:42,:); datah1(63:64,:)];
elseif NE == 6       % C-H-O-N-S-Cl
   Dat1   = [ data1(1:45,:);  data1(63:64,:)];
   Dat11  = [data11(1:45,:); data11(63:64,:)];
   Dat2   = [ data2(1:45,:);  data2(63:64,:)];
   Dath   = [ datah(1:45,:);  datah(63:64,:)];
   Dath1  = [datah1(1:45,:); datah1(63:64,:)];
elseif NE == 7       % C-H-O-N-S-Cl-Na
   Dat1   = [ data1(1:49,:);  data1(54:60,:);  data1(63:70,:)];
   Dat11  = [data11(1:49,:); data11(54:60,:); data11(63:70,:)];
   Dat2   = [ data2(1:49,:);  data2(54:60,:);  data2(63:70,:)];
   Dath   = [ datah(1:49,:);  datah(54:60,:);  datah(63:70,:)];
   Dath1  = [datah1(1:49,:); datah1(54:60,:); datah1(63:70,:)];
elseif NE == 8
   Dat1   = data1;
   Dat11  = data11;
   Dat2   = data2;
   Dath   = datah;
   Dath1  = datah1;
end

Dat3    = data3;

disp(' Chemical, thermodynamic and fuel analysis data')
disp(' for coal and biomass combustion/gasification is successfully loaded.')
disp('  ')
```

3. *Main program for free energy minimization (FEM) model RAND algorithm*

File name: sdgas2.m
Function: Main program of equilibrium model
Source code: See below.

```
disp('                    EQUILIBRIUM MODEL FOR SAWDUST GASIFICATION ')
disp('              - NON-STOICHIOMETRIC FREE ENERGY MINIMIZATION METHOD')

%  Version 6.0          [ Standard Version for C-H-O-N-S Systems ]
%                          (C) Xuantian Li (May 29, 2002)

%  (1) Input Model Parameters

%  Coal and sawdust gasification share the same database: coaldat.m
%  All calculations are made based on 1 kg of biomass (dry basis)

prompt = {'Enter minimum temperature, deg C',
          'Enter number of T intervals', 'Enter T increment, K',
          'Enter system pressure, bar', 'Enter initial air ratio',
          'Enter Ca/S molar ratio', 'Enter fuel type index',
          'Enter number of air ratio changes','Steam injection rate,
         mol/mol','moisture content in as-fired sawdust, %'};
def      = {327, 21, 50, 1.013, 0.4, 0, 9, 1, 0, 10}
title    = 'Inputs for equilibrium model'
lineNo   = 1;
answer   = inputdlg(prompt, title, lineNo, def);

[S1, S2, S3, S4, S5, S6, S7, S8, S9, S10] = deal(answer{:});

Ti       = str2num(S1);          % Munimum operating temperature (C)
T0       = Ti + 273;             % Operating temperature (K)
NT       = str2num(S2);          % Number of T intervals (-)
DT       = str2num(S3);          % Temperature increment (K)
p        = str2num(S4);          % System pressure (bar)
alpha    = str2num(S5);          % Initial air ratio (-)
Ca       = str2num(S6);          % Ca/S molar ratio (-)
NF       = str2num(S7);          % Fuel type: 1 = Highv.; 2 = Cypress, etc.
IZ       = str2num(S8);          % Number of outer-layer iteration times
rsteam   = str2num(S9);          % Steam injection (kg steam/kg dry fuel)
moist    = str2num(S10);         % Moisture content in as-rec'd sawdust (%)

%  The total weight (kg) of moisture added to 1 kg of dry-basis sawdust:
totmoist = rsteam + moist/(100-moist);

dalfa    = 0.1;                  % The increment of air ratio
rfuel    = 1;                    % Fuel feed rate (kg/hr): dry base
NFIT     = 0;                    % 0 = Assume 100% Cconv,  1 = Fit Cconv.
NREV     = 1;                    % EA0: 0 = Direct input,  1 = From database
NE       = 5;                    % Number of elements
NANA     = 2;                    % Base, fuel analysis: 1: ar, 2: ad, 3: daf
NO       = 1;                    % Oxidant: 1 = air, 2 = pure oxygen
NREP     = 3;                    % Print: 1 = short, 2 = 6 species, 3 = long
dissip   = 0;                    % Dissipation from the reactor surface
```

```
err       = 0.000001;          % Maximum error for convergence test
NCP       = 1;                 % Calculate fuel Cp(T) and enthalpy using:
                    1 = Coimbra and Queiroz (1995);  2 = Richardson (1993)
Iguess    = 0;                 % 0: simple method,  1: linear programming

%  ------------------------------------------------------------------------

disp(' ')
disp(['      Current Date:    ' date  '  ' ])
disp(' ')

previous_flops = flops;


%  (2) Calculate number of independent reactions in the system.

SEM       = Dat2(:, [2:(1+NE)]);  % Load species-element matrix (SEM)
[N,M]     = size(SEM);            % Size of species-element matrix
NC        = M;                    % Number of components
nr        = rank(SEM);            % Rank of SEM
mr        = N - rank(SEM);        % Model parameter
T         = T0;                   % Initial temperature (K)
R         = 8.31448;              % Thermodynamic constant, J/mol-K

for i=1:N
   SI(i)=Dat1(i,2);
end

%  Count the respective numbers of gas, liquid and solid species

ngas      = 0;                    % Initialization
nliq      = 0;
nsol      = 0;
for i = 1:N
   if SI(i) == 1
      ngas = ngas + 1;
   elseif SI(i) == 2
      nliq = nliq + 1;
   elseif SI(i) == 3
      nsol = nsol + 1;
   end
end

%  Count the number of phases

NP        = 1;                    % Gas phase as an ideal solution
if nliq >= 1
   NP = NP + 1;                   % Liquid species form another ideal solution
end
NP        = NP + nsol;            % Each solid species is an individual phase

NZ        = 0;                    % Number of inert species
N1        = N - NZ;               % Number of reactive species
N2        = M + 1;                % An index that will be used later
N3        = M + NP;               % An index that will be used later

disp(' ')
disp(['      Number of elements considered    =  ' num2str(M)  ])
```

```
disp(['      Number of species considered     =  ' num2str(N)   ])
disp(['      Number of gaseous species        =  ' num2str(ngas)  ])
disp(['      Number of liquid species         =  ' num2str(nliq)  ])
disp(['      Number of solid species          =  ' num2str(nsol)  ])
disp(['      Number of components             =  ' num2str(NC)   ])
disp(['      Number of phases involved        =  ' num2str(NP)   ])
disp(' ')


%  (3) Calculate initial element abundance (moles)

alfa = alpha;                    % Initialization of z

if NREP == 1
   report = zeros(NT,1+IZ);
end

%  -------------------  Start outer-layer iteration  ----------------------

for iz = 1:IZ                     % outer-layer iteration of AR or P
EA0      = zeros(M,1);            % Clear memory and re-initialize EA0
alfa     = alpha + (iz-1)*dalfa; % Current air ratio

%  Call abundsd2.m to calculate an element abundance vector (EAV):
[EA0,CEA,V0,Vair,mair,Uwat,Hfeed,HHV,hff,Conv,DUCmeth] =
abundsd2(NE,Dat3,rfuel,totmoist,NF,NO,NANA,NFIT,alfa,Ca);

UC       = EA0(1);
UH       = EA0(2);
UO       = EA0(3);
if M >= 4
   UN    = EA0(4);
end
if M >= 5
   US    = EA0(5);
end

%  Characterize the AEV and locate it in a ternary diagram:
rc       = EA0(1)/(EA0(1)+EA0(2)+EA0(3));
rh       = EA0(2)/(EA0(1)+EA0(2)+EA0(3));
ro       = EA0(3)/(EA0(1)+EA0(2)+EA0(3));

rrr      = [rc, rh, ro]
ea0      = [UC, UH, UO];

if M == 3
   mfeed = UC*12.011 + UH*1.00794 + UO*15.994;
elseif M == 4
   mfeed = UC*12.011 + UH*1.00794 + UO*15.994 + UN*14.0067;
elseif M >= 5
   mfeed = UC*12.011 + UH*1.00794 + UO*15.994 + UN*14.0067 + US*32.066;
end

totmol   = 0.0;                  % The total moles of all feed elements
for j = 1:M
   totmol = totmol + EA0(j);
end
```

```
CEA       = EA0;

%  (4) Estimate the initial guess of gas composition (y and x vectors)

A0 = [                              % Components
   1 0 1 0 0 0 0 0                  % CO      = 14 (Species ID number)
   0 2 0 0 0 0 0 0                  % H2      = 11
   1 0 2 0 0 0 0 0                  % CO2     = 15
   0 0 0 2 0 0 0 0                  % N2      = 22
   0 0 0 0 1 0 0 0                  % S(g)    = 33
   0 0 0 0 0 1 0 0                  % Cl(g)   = 43
   0 0 0 0 0 0 1 0                  % Na(g)   = 46
   0 0 0 0 0 0 0 1 ];               % Ca(g)   = 50

%  (4.1) a0 is the coefficient matrix to estimate the moles of components.
%  Row = species; Col = element

a0        = A0(1:M,1:M);

if M == 3
   anonc = [SEM(1:10,:); SEM(12:13,:); SEM(16:21,:)];
elseif M == 4
   anonc = [SEM(1:10,:); SEM(12:13,:); SEM(16:21,:); SEM(23:33,:)];
elseif M == 5
   anonc = [SEM(1:10,:); SEM(12:13,:); SEM(16:21,:); SEM(23:32,:);
            SEM(34:44,:)];
elseif M == 6
   anonc = [SEM(1:10,:); SEM(12:13,:); SEM(16:21,:); SEM(23:32,:);
            SEM(34:42,:); SEM(44:47,:)];
elseif M == 7
   anonc = [SEM(1:10,:); SEM(12:13,:); SEM(16:21,:); SEM(23:32,:);
            SEM(34:42,:); SEM(44:45,:); SEM(47:64,:)];
elseif M == 8
   anonc = [SEM(1:10,:); SEM(12:13,:); SEM(16:21,:); SEM(23:32,:);
            SEM(34:42,:); SEM(44:45,:); SEM(47:49,:); SEM(51:77,:)];
end


% ------------------------------------------------------------------------

if Iguess == 0

%  (4.2) Make an initial guess by a hand-estimation device

small     = min(EA0);               % Smallest component in EA0
stoi      = [UC, UH, UO/1.5];       % A device to evaluate C-H-O stoichiometry
smaller   = min(stoi);              % Smallest element in UC, UH and UO/1.5
ynonc     = small * ones(N-M, 1)/10000;

%  This logical variable modifies the initial guess for H2O to keep all
component moles positive.

%  The following block is valid only for M >= 3:

   if smaller == stoi(1)            % C-lean
      ynonc(10) = UH - UC;          % Deduce H as H(g)
      ynonc(11) = UO - 1.5 * UC;    % Deduce O as O(g)
   elseif smaller == stoi(2)        % H-lean
```

```
      ynonc(1)  = UC - UH;          % Deduce C as C(g)
      ynonc(11) = UO - 1.5 * UH;    % Deduce O as O(g)
   elseif smaller == stoi(3)        % O-lean
      ynonc(1)  = UC - UO/1.5;      % Deduce C as C(g)
      ynonc(10) = UH - UO/1.5;      % Deduce H as H(g)
   end

%  End of the block.

   lens = length(ynonc);
   if lens ~= (N-NC)
      disp('     Length of the non-component vector is wrong.')
      pause
   end

%  Calculate b0 the right-hand side vector
   db0 = zeros(M,1);     b0 = zeros(M,1);
   for k = 1:M
      for i = 1:(N-M)
         db0(k) = db0(k) + anonc(i,k)*ynonc(i);
      end
      b0(k) = EA0(k) - db0(k);
   end

%  Solve for initial guess

   yc0   = a0\b0;                % Use transpose of b0.

   if M == 3
      y0    = [ynonc(1:10); yc0(2); ynonc(11:12); yc0(1); yc0(3);
               ynonc(13:18) ];
   elseif M == 4
      y0    = [ynonc(1:10); yc0(2); ynonc(11:12); yc0(1); yc0(3);
               ynonc(13:18); yc0(4); ynonc(19:29)];
   elseif M == 5
      y0    = [ynonc(1:10); yc0(2); ynonc(11:12); yc0(1); yc0(3);
               ynonc(13:18); yc0(4); ynonc(19:28); yc0(5); ynonc(29:39)];
   elseif M == 6    % Must check carefully before use
      y0    = [ynonc(1:10); yc0(2); ynonc(11:12); yc0(1); yc0(3);
               ynonc(13:18); yc0(4); ynonc(19:28); yc0(5); ynonc(29:37);
               yc0(6); ynonc(38:47)];
   elseif M == 7    % Must check carefully before use
      y0    = [ynonc(1:10); yc0(2); ynonc(11:12); yc0(1); yc0(3);
               ynonc(13:18); yc0(4); ynonc(19:28); yc0(5); ynonc(29:37);
               yc0(6); ynonc(38:41); yc0(7); ynonc(42:57)];
   elseif M == 8    % Must check carefully before use
      y0    = [ynonc(1:10); yc0(2); ynonc(11:12); yc0(1); yc0(3);
               ynonc(13:18); yc0(4); ynonc(19:28); yc0(5); ynonc(29:37);
               yc0(6); ynonc(38:41); yc0(7); ynonc(42:43); yc0(8);
               ynonc(44:69)];
   end

   [h,H] = enth(Dath,Dath1,T,y0);  % Calculate enthalpy
   [cy0,ys0,x0,xg0,xs0,EA,CEA0] = calcc(SI, SEM, y0, EA0);

%  (4.3) Check the non-negativity contraint

   ymin = min(yc0);
```

```
   if ymin < 0
      NT = 1;
      NIT = 1;
      disp('  ')
      disp(' Non-negativity requirements not met.')
      disp(' Use linear programming to make another initial guess.')
      disp('  ')
   end

end  % End initial guess


%  (5) Update CEA and cy to serve as the basis for iteration

[cy,ys,x,xg,xs,EA,CEA] = calcc(SI,SEM,y0,EA0);


%  (6) Solve for a new set of y(i) by iteration using RAND algorithm

m       = 1;                    % Mark the first iteration
Ind     = 0;                    % If Ind = 0, go ahead to next iteration.

%  The following sentences are for initialization
a1      = zeros(N3, N3) + eps;
y       = y0;                   summit   = zeros(NT,1);
xt      = zeros(NT,N);          yt       = zeros(NT,N);
xtdry   = zeros(NT,N);          dqt      = zeros(NT,1);
Cwat    = zeros(NT,1);          hhvgas   = zeros(NT,1);
HHVgas  = zeros(NT,1);          hhvdry   = zeros(NT,1);
vgdry   = zeros(NT,1);          vgwet    = zeros(NT,1);
E1      = zeros(NT,1);          E2       = zeros(NT,1);
spc     = zeros(NT,2);          sph      = zeros(NT,2);
spo     = zeros(NT,2);          spn      = zeros(NT,2);
sps     = zeros(NT,2);          gama     = zeros(NT,1);
methane = zeros(NT,1);
%  End of matrix initialization.

if NREP ~= 1
   report = [ ];   report1 = [ ];   report2 = [ ];
end

%  (6.1)  Start temperature iteration

for it = 1:NT                   % Starts temperature iteration

   if it == 1
      NIT = 100;
   else
      NIT = 40;                 % Maximum number of iterations
      for i = 1:N
         y(i) = yt(it-1,i);
      end
   end

   TT(it) = T0 + (it-1)*DT;
   T      = TT(it);

%  Initialization for each T iteration:
```

```
   [cy,ys,x,xg,xs,EA,CEA] = calcc(SI,SEM,y,EA0);
   [smu,smustar] = chempot(T,p,Dat1,Dat11);
   [h,H] = enth(Dath,Dath1,T,y);
%  End of initialization.

%  Calculate chemical potential of each species

   for i = 1:N
      if SI(i) == 1
         smutp(i) = smustar(i) + R*T*log(xg(i)+1e-200)/1000.0;  % Gases
      elseif SI(i) == 2
         smutp(i) = smustar(i);                                 % Liquids
      elseif SI(i) == 3
         smutp(i) = smustar(i);                                 % Solids
      end
   end

%  Calculate the total enthalpy and total free energy
   toth = 0.0;
   totg = 0.0;

   for i = 1:N
      toth = toth + H(i);        % Total enthalpy of reaction system
      totg = totg + smutp(i);    % Total Gibbs free energy of system
   end

   Ind = 0;

%  Continue iteration until a new value is given to Ind.

   while Ind == 0


%  (7) Calculate the chemical potential of species i at T and p.

   itm = mod(it,30);
   imm = mod(m,30);

   [a1,b1] = abzuc(SI,SEM,EA,CEA,EA0,smutp,T,p,y,imm);

   x1 = a1\b1;


%  (7.1) Calculate new species mole numbers.

   bir   = zeros(N,1);
   f     = zeros(N,1);
   dy    = zeros(N,1);

%  Calculate dy(i)
   for i = 1:N
      for j = 1:M
%  Important intermediate argument.
         bir(i) = bir(i) + SEM(i,j)* x1(j);
%  Do not alter anything in this line.
      end

      if SI(i) == 1
```

```
      f(i) = bir(i) + x1(N2) - smutp(i)*1000/(R*T);
   end

   if M == 3
      f(21) = x1(N2+1);       % C(s)
   elseif M == 4
      f(33) = x1(N2+1);       % C(s)
   elseif M == 5
      f(43) = x1(N2+1);       % C(s)
      f(44) = x1(N2+2);       % S(s)
   elseif M == 6
      f(46) = x1(N2+1);       % C(s)
      f(47) = x1(N2+2);       % S(s)
   end
%  Add other single-species phases HERE in future versions.
   end

   for i = 1:N
      dy(i)  = f(i)*y(i);        % Increase in each species moles
   end

   [ynew]    = forcer(dy,y);        % Call the convergence forcer
   y = ynew;
   maxdy     = max(abs(dy));

%  (7.2) Update system data, prepare for next temperature iteration.

   [cy,ys,x,xg,xs,EA,CEA] = calcc(SI,SEM,y,EA0);
   [dq,totdh,toth,totph,totgh,totsh] =
      heatcoal(T,alfa,Dath,Dat3,NF,H,y,Uwat,Ca,dissip,Hfeed,hff);
   Ttoth(it) = toth;
   dqt(it)   = dq;
   totdht(it)= totdh;
   totht(it) = toth;
   totpht(it)= totph;
   totght(it)= totgh;
   totsht(it)= totsh;
   Ttoth(it) = toth;
%  disp([' Net heat output to maintain current T  = ' num2str(dq) ' kJ/hr' ])

   for i = 1:N
      if SI(i) == 1
         smutp(i) = smustar(i) + R*T * log(xg(i)+1e-200)/1000.0;
      elseif SI(i) == 3
         smutp(i) = smustar(i);
      end
   end

%  (7.3) Calculate the species split of each element

   for i = 1:N
      Cy(it,i) = cy(i,1);
      Hy(it,i) = cy(i,2);
      Oy(it,i) = cy(i,3);
      if M >= 4
         Ny(it,i) = cy(i,4);
      end
   end
```

```
%  (7.4) Set condition for termination of iteration

   if m > NIT
      Ind = 2;
   elseif max(abs(dy)) <= err    % Never write it as: abs(max(dy)) !!
      Ind = 1;
   else
      Ind = 0;
   end

   m = m + 1;

end                              % Terminate temperature iteration
%  Record the Ind value

if itm == 1
   if Ind == 1
      disp('  ')
      disp([' Convergence is attained at the ' num2str(m) '-th iteration.'])
      disp('  ')
   elseif Ind == 2
      disp('  ')
      disp([' Convergence not attained after ' num2str(NIT) ' iterations.'])
      disp('  ')
   end
end

Ind     = 0;                     % Reset Ind. Very important sentence.
m       = 1;                     % Reset m.

for i = 1:N
   yt(it,i) = y(i);
   xt(it,i) = x(i);
   xtg(it,i)= xg(i);
   dqt(it)  = dq;
end

for i = 1:N
   xtdry(it,i) = xtg(it,i)/(1 - xtg(it,17));  % Species content in dry gas
   summit(it)  = summit(it) + yt(it,i);
end

%  ------------------------------------------------------------------------
methane = zeros(NT,1) + DUCmeth;
%  Adjust pre-ducted CH4 back to the main stream:
yt(it,5) = yt(it,5) + DUCmeth;
%  Add CH4 to gas phase:
summit(it) = summit(it) + DUCmeth;
%  ------------------------------------------------------------------------

%  (7.5) Calculate equilibrium composition to be reported

if M == 5                        % This function designed for sawdust
   for i = 1:N
%  Overall molar composition
      xt(it,i)    = yt(it,i)/summit(it);
%  Wet gas composition, excluding C(s) and S(s)
```

```
      xtg(it,i)  = yt(it,i)/(summit(it) - yt(it,43) - yt(it,44));
%  Dry gas composition, excluding water, C(s) and S(s)
      xtdry(it,i)= yt(it,i)/(summit(it)-yt(it,17) - yt(it,43) - yt(it,44));
   end

   xtg(it,43) = 0;
   xtg(it,44) = 0;
   xtdry(it,17) = 0;
   xtdry(it,43) = 0;
   xtdry(it,44) = 0;
end

% Water conversion
Cwat(it) = 100* (Uwat - yt(it,17)) / Uwat;      % Units in (%)

% Calculate wet gas HHV:
if M <= 4
   hhvgas(it) = 100/(8.31448*298.15)* ( xtg(it,5)*890.8 + xtg(it,6)*1301.1
                + xtg(it,7)*1411.2 + xtg(it,8)*1560.7 + xtg(it,9)*2220.1
                + xtg(it,11)*285.8 + xtg(it,14)*283.0 );  % MJ/Nm3
elseif M >= 5
   hhvgas(it) = 100/(8.31448*298.15)* ( xtg(it,5)*890.8 + xtg(it,6)*1301.1
                + xtg(it,7)*1411.2 + xtg(it,8)*1560.7 + xtg(it,9)*2220.1
                + xtg(it,11)*285.8 + xtg(it,14)*283.0  + xtg(it,42)*562.6
                + xtg(it,38)*553.2 + xtg(it,40)*684.2 );  % MJ/Nm3
end

%  Calculate dry gas heating value:
hhvdry(it) = hhvgas(it)/(1-xtg(it,17));

end % Normally end temperature iteration


%  (8) Preparing output report

if M == 3
   Cconv = 100.0*(1 - yt(:,21)/UC);     % Carbon conversion
   vgdry  = (summit-yt(:,17)-yt(:,9)-yt(:,N))*8.31448*298.15/(1.013*100000);
%  vgdry = Dry gas yield (Nm3/kg fuel)
   vgwet  = ( summit-yt(:,N) )*8.31448*298.15/(1.01325*100000);
%  vgwet = Wet gas yield (Nm3/kg fuel)
   E1 = 100*(vgdry(:).*hhvdry(:)*1000 + (dqt(:) <= 0) .* dqt(:))/(HHV*rfuel);
%  E1 = Gasif. Eff. E1 (%) excluding condensables
   E2 = 100*(vgwet(:).*hhvgas(:)*1000 + (dqt(:) <= 0) .* dqt(:))/(HHV*rfuel);
%  E2 = Gasif. Eff. E1 (%) including condensables

elseif M == 4
   Cconv  = 100.0*(1 - yt(:,33)/UC);
   vgwet  = (summit-yt(:,N))*8.31448*298.15/(1.01325*100000);
   vgdry  = (summit-yt(:,17)-yt(:,9)-yt(:,N))*8.31448*298.15/(1.013*100000);
   E1 = 100*(vgdry(:).*hhvdry(:)*1000 + (dqt(:) <= 0) .* dqt(:))/(HHV*rfuel);
   E2 = 100*(vgwet(:).*hhvgas(:)*1000 + (dqt(:) <= 0) .* dqt(:))/(HHV*rfuel);

elseif M == 5
   Cconv  = 100.0*(1 - yt(:,43)/UC);
   vgwet  = (summit-yt(:,43) )*8.31448*298.15/(1.01325*100000);
   vgdry  = (summit-yt(:,17)-yt(:,9)-yt(:,43))*8.31448*298.15/(1.013*100000);
   E1 = 100*(vgdry(:).*hhvdry(:)*1000 + (dqt(:) <= 0) .* dqt(:))/(HHV*rfuel);
```

```
   E2 = 100*(vgwet(:).*hhvgas(:)*1000 + (dqt(:) <= 0) .* dqt(:))/(HHV*rfuel);
end

%  (8.1) Major species statistics

if M == 3
   report(:,1) = TT(:);
   report(:,(1+iz)) = 100*xt(:,21);

elseif M == 4
   ytc = [yt(:,5),yt(:,7),yt(:,14:15),yt(:,11),yt(:,17),yt(:,23),yt(:,22),
         yt(:,26),yt(:,33)];
%        CH4, C2H4, CO, CO2, H2, H2O, HCN, N2, NH3, C(s)
   if NREP == 1
      report(:,1) = TT(:);
      report(:,(1+iz)) = 100*xt(:,33);
   elseif NREP == 2
      report = 100*[TT(:)/100, xtdry(:,14:15), xtdry(:,11), xtdry(:,5),
               yt(:,17)*2/(100*UH)];
   elseif NREP == 3

elseif M == 5
   if NREP == 1
      report = 100*[TT(:)/100, xt(:,43)];
   elseif NREP == 2
      report1  = 100*[TT(:)/100, xtdry(:,14:15), xtdry(:,11), xtdry(:,5)];
   elseif NREP == 3

%  (8.2) Fate of elements - Elemental split

   spc(:,1) =             yt(:,43)*1/EA0(1);     % C(s)
   spc(:,2) = spc(:,1) + yt(:,5) /EA0(1);        % CH4
   spc(:,3) = spc(:,2) + yt(:,14)*1/EA0(1);      % CO
   spc(:,4) = spc(:,3) + yt(:,15)*1/EA0(1);      % CO2
   spc(:,5) = spc(:,4) + yt(:,30)*1/EA0(1);      % HCN

   sph(:,1) =             yt(:,5)*4/EA0(2);      % CH4
   sph(:,1) = sph(:,1) + ( yt(:,7)*4)/EA0(2);    % C2H4
   sph(:,2) = sph(:,1) + yt(:,11)*2/EA0(2);      % H2
   sph(:,3) = sph(:,2) + yt(:,17)*2/EA0(2);      % H2O
   sph(:,4) = sph(:,3) + yt(:,10)*1/EA0(2);      % H
   sph(:,4) = sph(:,4) + (yt(:,31))/EA0(2);      % HCN
   sph(:,4) = sph(:,4) + (yt(:,26)*3)/EA0(2);    % NH3

   spo(:,1) =             yt(:,14)*1/EA0(3);     % CO
   spo(:,2) = spo(:,1) + yt(:,15)*2/EA0(3);      % CO2
   spo(:,3) = spo(:,2) + yt(:,17)*1/EA0(3);      % H2O
   spo(:,4) = spo(:,3) + yt(:,13)*2/EA0(3);      % O2

   spn(:,1) = (yt(:,30)+ yt(:,31))*1/EA0(4);     % HCN
   spn(:,2) = spn(:,1) + yt(:,22)*2/EA0(4);      % N2
   spn(:,3) = spn(:,2) + yt(:,26)*1/EA0(4);      % NH3

   sps(:,1) = (yt(:,36)+ yt(:,37))*1/EA0(5);     % SO2 + SO3
   sps(:,2) = sps(:,1) + yt(:,38)*1/EA0(5);      % COS
   sps(:,3) = sps(:,2) + yt(:,41)*1/EA0(5);      % HS
   sps(:,4) = sps(:,3) + yt(:,42)*1/EA0(5);      % H2S
```

```
%  Molar fraction of hydrogen that stays in H2O in the product.
   gama(:) = 100*yt(:,17)*2/UH;

%  ------------------------------------------------------------------------

%  Major species
   report1  = 100*[TT(:)/100,  xtdry(:,11), xtdry(:,22), xtdry(:,14),
              xtdry(:,5), xtdry(:,15), xtdry(:,6)+xtdry(:,7)+xtdry(:,8)
              + xtdry(:,9), xtdry(:,42), xtg(:,17), xt(:,43)];
%  T, H2, N2, CO, CH4, CO2, C2+, H2S, H2O, C(s)

%  Conversion and efficiency
   report2  = [xtdry(:,26), xtdry(:,40), Cconv(:), gama(:), hhvdry(:),
              vgdry(:), 100000*hhvdry(:).*vgdry(:)/HHV, dqt(:) ];

%  Minor species
   report3  = 1000000*[ xtdry(:,5:9), xtdry(:,26:31), xtdry(:,36:38),
              xtdry(:,42) ];
%  (ppm)       CH4-C3H8    NH3-HCN    SO2,SO3,COS    H2S

%  The smallest species is not reported, but calculated by difference.
   report4  = [TT(:), spc(:,1:4), sph(:, 1:3), spo(:, 1:3), spn(:, 1:2),
              sps(:, 1:3)];
%             C split    H split    O split    N split    S split

   current_alfa = alfa;
   current_alfa
   % EA0'
   % Uwat
   report1
   report2
   end

end

%  ------------------------------------------------------------------------

end                    % End of outer-layer pressure/alpha/iz iteration

%  End of the FEM equilibrium model program.
```

4. Elemental abundance

File name: adundsd2.m
Function: To calculate the abundance of each element present in the system
Source code: See below.

```
function [EA0,CEA,V0,Vair,mair,Uwat,Hfeed,HHV,hff,Conv,DUCmeth] =
abundsd2(NE,Dat3,rfuel,totmoist,NF,NO,NANA,NFIT,aleph,Ca)

%  ABUNDSD2 calculates element adundance from sawdust, oxidant, and steam data
%  Last update: January 6, 2002
*  Carbon and methane modified version 1.0

%  The total abundance of an element is the sum of its abundances in main fuel,
%  auxiliary fuel, air, steam and sorbent.
%  All calculations are based on 1 kg of sawdust feed (dry basis).

% Make sure that all ultimate analyses of sawdust are on dry basis
Car   = Dat3(5,NF);
Har   = Dat3(6,NF);
Oar   = Dat3(7,NF);
Nar   = Dat3(8,NF);
Sar   = Dat3(9,NF);
Clar  = Dat3(10,NF);
Naar  = Dat3(11,NF);
Caar  = Dat3(12,NF);

%  (1) Calculate moles of each element

Conv1 = 100;       Conv2 = 0;   % Initialization
UCint  = Car*rfuel*1000/(12.011*100);

if NFIT == 0
   Conv = 100;
elseif NFIT == 1
%  An experimental carbon conversion, (%)
   Conv1 = 25.0 + 75.0*(1 - exp(-aleph/0.23));
   Conv2 = 1.34*(11.0*(1-aleph));   % Carbon conversion over tested range
   Conv = Conv1 - Conv2;
end

UC       = UCint*(Conv1-Conv2)/100;  % Moles of C entering equilibrium
DUCmeth  = UCint*Conv2/100;          % Moles of carbon deducted as CH4
UHint    = Har*rfuel*1000/(1.00794*100);
UHext    = 2*totmoist*1000/18.0153;  % Each mol H2O contains 2 mol H
UH0      = UHint + UHext;

if NFIT == 1
%  The actual moles of H that enters the equilibrium system
   UH         = UH0 - 4*DUCmeth;
else
   UH      = UH0;
end
```

```
Uwat     = totmoist*1000/18.0153;
%  Uwat denotes external moisture added to the dry base, mol/kg_dry fuel
if Uwat <= 0.000001
   Uwat = 0.000001;
end

UOint  = Oar*rfuel*1000/(15.9994*100);
%  UOint does not include O from the ash-bound oxygen.

if NE < 5
   Tm0     = Car/12.011 + (Har/1.00794)/4.0 - (Oar/15.9994)/2.0;
else
   Tm0     = Car/12.011 + (Har/1.00794)/4.0 - (Oar/15.9994)/2.0 + Sar/32.066;
end
%  Tm0 is the total moles of O2 (not O) required to burn 100 g of fuel

if NO == 1
%  Stoichiometic air @ 298 K, 1.013 bar (Nm3/kg_dry sawdust):
   V0      = (Tm0)*22.7116*(298.16/273.16)/(1.01325027*20.9476);
else
%  Stoichiometic pure oxygen (Nm3/kg_dry fuel):
   V0      = (Tm0)*22.7116*(298.16/273.16)/(1.01325027*99.992);
end
Vair     = V0*rfuel*aleph;        % Nm3/hr @ 1 atm, 298 K

%  mair    = (Tm0/0.209476) * 28.964 * 10 * rfuel * aleph;       % gram/hr
%  mair includes the weight of minor species (Ar, Ne, etc.) in air.
%  So mair can be calculated with another formula:
mair     = (Tm0*31.9988 + Tm0*(0.78084/0.209476)*28.0135
           + Tm0*(0.000314/0.209476)*44.0098)*rfuel*10*aleph;    % (gram/hr)

if NO == 1
   UOair   = 2* Tm0 * aleph *(10* rfuel) * ( 1 + 0.000314/0.209476);
%  One mole of O2 contains 2 moles of O atoms
%  One mole of air also contains 0.000314 mole of CO2
else
   UOair   = 2* Tm0*(rfuel*1000/100)*aleph;
%  One mole of O2 contains 2 moles of O atoms
end

UOext    = UHext/2.0;             % Oxygen that comes from total moisture
UOsor    = 0.0;
UO       = UOint + UOair + UOext + UOsor;
%  UOint must be added because it has been subtracted from UOair.

%  If the oxidant is air, modify the C abundance due to CO2 in air.
if NO == 1
   UC      = UC + 0.000314*Tm0*(rfuel*1000/100)*aleph;
end

UNint   = Nar*rfuel*1000/(14.0067*100);
if NO == 1
   UNair   = (78.084/20.9476)*UOair;     % The N/O molar ratio in air
else
   UNair   = UOair*0.008/99.992;         % Ind. grade oxygen has 0.008% N2
end
UN      = UNint + UNair;
```

```
if NE >= 5
   US     = Sar* rfuel*1000/(32.066*100);
   UCasor = Ca*US;                    % Sorbent for sulfur retention
end

if NE >= 6
   UCl    = Clar * rfuel*1000/(35.4527*100);
end

if NE >= 7
   UNa    = Naar * rfuel*1000/(22.9898*100);
end

if NE >= 8
   UCaint = Caar * rfuel*1000/(40.078*100);
   UCatot = Ca*(US + UCl);       % Moles of Ca needed to remove S and Cl
   UCasor = UCatot - UCaint;     % Total externally added Ca (sorbent)
   purity = 96.5/100;            % Purity of sorbent
   rsorb  = UCasor* 56.0774/(purity*1000);  % Sorbent feed rate (kg/hr)
   Caconv = 1.0/Ca;              % Ca conversion
   UCa    = UCatot * Caconv;     % The actual mol of Ca entering equilibrium
end

% ------------------------------------------------------------------------

EA0 = zeros(NE,1);               % Initialization of EAV

if NE == 2
   EA0 = [UC; UH];
elseif NE == 3
   EA0 = [UC; UH; UO];
elseif NE == 4
   EA0    = [UC; UH; UO; UN];
elseif NE == 5
   EA0    = [UC; UH; UO; UN; US];
elseif NE == 6
   EA0    = [UC; UH; UO; UN; US; UCl];
elseif NE == 7
   EA0    = [UC; UH; UO; UN; US; UCl; UNa];
elseif NE == 8
   EA0    = [UC; UH; UO; UN; US; UCl; UNa; UCa];
end

% ------------------------------------------------------------------------

if NF >= 10
   EA0 = zeros(NE,1);
end

CEA     = EA0;

%  (2) Calculate enthalpy of feedstock

tfuel   = 25;                    % (deg C)
tmoist  = tfuel;
tstm    = 130;
tsorb   = 25;
toxy    = 150;
```

```
tsurr    = 25;
hstm     = 0;
hsorb    = 0;
rair     = mair/(Vair+0.000001); % Air density at 1 atm, 298 K (kg/m3)

%  (3) The heat of formation of fuel

%  Assume the molecular weight of the fuel is 100.
%  The chemical formula of the fuel is C_a1 H_a2 O_a3 N_a4 S_a5

af       = zeros(8,1);
ar2db    = 100/(100-totmoist);   % ar2db > 1
ar2daf   = 100/(100-Dat3(13,NF)-totmoist);
%  ar2daf > 1. Conversion factor from ar base to daf base

af(1)    = Dat3(5,NF)/12.011;     % C
af(2)    = Dat3(6,NF)/1.00794;    % H
af(3)    = Dat3(7,NF)/15.9994;    % O
af(4)    = Dat3(8,NF)/14.0067;    % N
af(5)    = Dat3(9,NF)/32.066;     % S
af(6)    = Dat3(10,NF)/35.453;    % Cl
af(7)    = Dat3(11,NF)/22.9898;   % Na
af(8)    = Dat3(12,NF)/40.078;    % Ca

HHVdaf   = 2.3252*(144.4* Dat3(5,NF)*ar2daf + 610.2* Dat3(6,NF)*ar2daf
           - 65.9* Dat3(7,NF)*ar2daf + 0.39* (Dat3(7,NF)*ar2daf)^2 );
%  HHVdat in kJ/kg, dry ash free base
HHVdb    = 327.83*Dat3(5,NF)*ar2db  + 1419.3*Dat3(6,NF)*ar2db
           + 193.85*Dat3(9,NF)*ar2db - 43.96* Dat3(11,NF)*ar2db
           - 128.95* Dat3(7,NF)*ar2db - 334.9;  % kJ/kg_dry
HHV1     = HHVdaf/ar2daf;          % Dulong formula
HHV2     = HHVdb/ar2db;            % BL dry solids formula
HHV      = 0.1*HHV1 + 0.9*HHV2;    % As-received base HHV (kJ/kg)
hhvdaf   = HHV * ar2daf;           % Don't remove this line! Daf base (kJ/kg)
Tfuel    = tfuel + 273.15;

%  Now calculate the heat of formation of the fuel (H2O in liq. state)
%  a1   C   + a1   O2  = a1   CO2          a1 *   (-393.522) kJ/mol
%  a2/2 H2  + a2/4 O2  = a2/2 H2O          a2/2 * (-285.840) kJ/mol
%  a5   S   + a5   O2  = a5   SO2          a5 *   (-296.842) kJ/mol
%  a1   CO2 + a2/2 H2O + a4/2 N2 + ... = Fuel + Tm0 O2 + 79/21* Tm0 N2
%  The heat of formation of the fuel is:

hff      = HHV - 10*( af(1)*393.522 + af(2)/2*285.840 + af(5)*296.842
           + (totmoist/18.0153)*285.84 );  % kJ/kg_coal (ar basis)

hfuel    = 1.15e-4*Tfuel^2 + 0.82709*Tfuel - 239.38;  % (kJ/kg); Tfuel in K

if NO == 1     % air
   cpoxy  = 8.31448*(3.355 + 0.575*(toxy +273.15)/1000
            - 0.016 * (1/(toxy  + 273.15)^2) *100000 )/1000;  % kJ/mol.K
else           % oxygen
   cpoxy  = 8.31448*(3.639 + 0.506*(toxy +273.15)/1000
            - 0.227 * (1/(toxy  + 273.15)^2) *100000 )/1000;  % kJ/mol.K
end

cpsorb   = 8.31448*(6.104 + 0.443*(tsorb+273.15)/1000
           - 1.047 * (1/(tsorb + 273.15)^2) *100000 )/1000;  % kJ/mol.K
```

```
cpstm    = 8.31448*(3.470 + 1.450*(tstm +273.15)/1000
           + 0.121 * (1/(tstm  + 273.15)^2) *100000 )/1000;  % kJ/mol.K

if NO == 1
   moxy    = (Tm0/0.209476)*aleph*rfuel;       % moles of air
else
   moxy    = (Tm0/0.99992) *aleph*rfuel;
end

hoxy     = cpoxy * moxy  *(toxy-25);           % kJ
hsorb    = cpsorb* UCasor*(tsorb-25);          % kJ
hstm     = cpstm * UOext *(tstm-25);           % kJ
%  This line implies that water and steam are added at the same T.

Hfeed    = hfuel + hoxy + hstm + hsorb;

disp(' ')
disp([' Stoichiometric moles of O2    =  ' num2str(Tm0)    ' (mole/100g dry
fuel) ']) 
disp([' Stoichiometric air of fuel    =  ' num2str(V0)     ' (Nm3/kg_dry
fuel) ']) 
disp([' Total air supply              =  ' num2str(Vair)   ' (Nm3/hr)']) 
disp([' Higher heating value of fuel =  ' num2str(HHV)    ' (kJ/kg dry
fuel) ']) 
disp([' Enthalpy of feed              =  ' num2str(Hfeed)  ' (kJ/kgfuel)
']) 
disp(' ')
```

5. Standard chemical potential

File name: mut.m
Function: To compute the standard chemical potential of each species
Source code: See below.

```
function [smu,smustar] = mut(T,p,Dat1,Dat11)
%  MUT calculates the standard chemical potential mu* at (T,p)

[N,NN]  = size(Dat1);              % NN is useless but recorded here.
R       = 8.31448;

for i = 1:N
   Tcut(i) = Dat1(i,8);

   if T > 1177.0
      Dat1(44,2) = 2;              % Na becomes vapor at this temperature
   end
   smu(i) = Dat1(i,3) + Dat1(i,4)*0.001 * T*log(T)
            + Dat1(i,5)*T^2 /1000000.0 + Dat1(i,6)/T + Dat1(i,7)*T;

   if T > Tcut(i)                  % Alternative correlations for DGfo(T)
      smu(i) = Dat11(i,3) + Dat11(i,4)*0.001 * T*log(T)
               + Dat11(i,5)*T^2 /1000000.0 + Dat11(i,6)/T + Dat11(i,7)*T;
   end

   if Dat1(i,2) == 1               % For condensed phase
      smustar(i) = smu(i);         % mu* = DGfo(T), ignoring vapor term
   elseif Dat1(i,2) == 2           % For gas phase
      smustar(i) = smu(i) + R * T * log(p) /1000;
   end
end
```

6. Species enthalpy

File name: enth.m
Function: To compute the enthalpy of each species
Source code: See below.

```
function [h,H] = enth(Dath,Dath1,T,y)
%  ENTH computes the enthalpy of each species, unit in kJ/mol

[N,M]    = size(Dath);
H        = zeros(N,1);

for i = 1:N
   if T <= Dath(i,8)
      h(i) = Dath(i,3)*T/1000 + Dath(i,4)*T^2/1000000 + Dath(i,5)/T
             + Dath(i,6);
   else
      h(i) = Dath1(i,3)*T/1000 + Dath1(i,4)*T^2/1000000 + Dath1(i,5)/T +
Dath1(i,6);
   end
   H(i) = h(i).*y(i);
end
```

7. Elements in the RAND matrix

File name: abzuc.m
Function: To compute the RAND matrix A and vector B
Source code: See below.

```
function [a1,b1] = abzuc(SI,SEM,EA,CEA,EA0,smutp,T,p,y,imm)
%  ABZUC calculates the RAND matrix elements a1(N3,N3)
%  In RAND algorithm, the Lagrange multipliers are solved from a1.x = b1

[N,M]    = size(SEM);

%  (1) Count the number of gas, liquid and solid species

ngas     = 0;    nliq = 0;    nsol = 0;
for i = 1:N
   if SI(i) == 1
      ngas = ngas + 1;
   elseif SI(i) == 2
      nliq = nliq + 1;
   elseif SI(i) == 3
      nsol = nsol + 1;
   end
end

%  Count the number of phases

NP       = 1;                    % Gas phase as an ideal solution
if nliq > 0
   NP    = NP + 1;               % Liquid phase as another ideal solution
end
NP       = NP + nsol;            % Each solid as a single-species phase

if nliq > 0
   NP     = nsol + 2;
else
   NP     = nsol + 1;
end

NZ       = 0;                    % Number of inert species
N1       = N - NZ;               % Number of reactive species
N2       = M + 1;
N3       = M + NP;
R        = 8.31448;

if min(EA0) > 0.0001
   yz      = 0.005*min(EA0);
else
   yz      = 0.0000005;
end

a1      = zeros(N3,N3);
b1      = zeros(N3,1);
```

```
% (2) Compute a1 matrix

%  Zone I - [j <= M, k <= M]
for j=1:M
   for k=j:M
      for i=1:N1
         a1(j,k) = a1(j,k)+SEM(i,j)*SEM(i,k)*y(i);
      end
      a1(k,j) = a1(j,k);
   end
end

%  Zone II - [j <= M, k > M]
   for j = 1:M
      for k = N2:N3
         a1(j,k) = CEA(j,(k-M));
      end
   end

%  Zone III - [j > M, k <= M]
   for j = N2:N3
      for k = 1:M
         a1(j,k) = CEA(k,(j-M));
      end
   end

%  Zone IV - [j > M, k > M]
   for j = N2:N3
      for k = N2:N3     % Note that for k > M, k = M + phase index 1.
         %if j == N2 & k == N2
         if j == k
            if j == N2
               a1(j,k) = - yz; % Moles of inert species in gas phase.
            else
               a1(j,k) = - yz/100;
            end
         else
            a1(j,k) = 0;
         end
      end
   end

ra1 = rank(a1);
ra2 = cond(a1);

%  (3) Compute b1 vector

%  Zone I - [j <= M]

   for j = 1:M
   b1(j) = b1(j) + EA0(j) - EA(j);    % Checked correct
      for i = 1:N1
         b1(j) = b1(j) + SEM(i,j)*y(i)*smutp(i)*1000/(R*T);
      end
   end

%  EA0(j): the initial element abundance vector estimated from feed data.
```

```
%  EA(j): the element abundance of the current iteration.
%  The incorporation of EA0(j)-EA(j) on the right side is believed to help
prevent error accumulation.

%  Zone II - [j > M]
for j = N2:N3

   if j == N2                    % Gas phase
      for i = 1:N
         b1(N2) = b1(j) + y(i) * (SI(i) == 1) * smutp(i)*1000/(R*T);
         % RT is timed by 1000 because the unit of smutp is kJ/mol
      end

   elseif j >= N2 + 1
      if nliq > 0                % or M >= 7
         for i = 1:N
            b1(N2+1) = b1(j) + y(i)* (SI(i) == 2) * smutp(i)*1000/(R*T);
            % RT is timed by 1000 because the unit of smutp is kJ/mol
         end
      else
         if M == 3
            b1(N2+1) = y(N)*smutp(N)*1000/(R*T);     % SSP-1: C(s)
         elseif M == 4
            b1(N2+1) = y(N)*smutp(N)*1000/(R*T);     % SSP-1: C(s)
         elseif M == 5
            b1(N2+1) = y(43)*smutp(43)*1000/(R*T);   % SSP-1: C(s)
            b1(N2+2) = y(44)*smutp(44)*1000/(R*T);   % SSP-1: S(s)
         end
         % Add other single-species phases here:
         % b1(N2+2) = ...
      end
   end
end

if imm == 1

   if ra1 ~= M + NP
      disp(' ')
      disp(['      Rank of RAND coefficient matrix  =  ' num2str(ra1)  ])
      disp(['      Condition number of RAND matrix  =  ' num2str(ra2)  ])
      disp(' ')
   elseif ra2 > 50000000
      disp(' ')
      disp(['      Condition number of RAND matrix  =  ' num2str(ra2)  ])
      disp(' ')
   end

end
```

8. Convergence forcer

File name: forcer.m
Function: To speed up convergence by ensuring non-negativity of each species
Source code: See below.

```
function [ynew] = forcer(dy,y)
%  FORCER computes new mole numbers and qurantee their non-negativity.
%  Do not modify anything in this function.

n       = length(dy);
par     = 0.5;
ynew    = zeros(n,1);

for i=1:n
   if par < -dy(i)/y(i)
      par = -dy(i)/y(i);
   end
end

par     = 1/par;
if par > 0 & par <=1
   if par < 0.1
      par = par*0.999;
   else
      par = par*0.99;
   end
else
   par=1.0;
end

for i = 1:n
   ynew(i) = y(i) + dy(i) * par;
   if ynew(i) <= 1e-200              % Minimum value control
      ynew(i) = 1e-200;
   end
end
```

9. *Molar fraction of each species*

File name: calcc.m
Function: To calculate the current molar fraction of each species
Source code: See below.

```
function [cy,ys,x,xg,xs,EA,CEA] = calcc(SI,SEM,y,EA0)

%  CALCC updates the current molar fractions and element abundance vector
%  with new y results.
%  Version 2.0                    Xuantian Li (Feb. 18, 1999)

[N,M]    = size(SEM);
NP       = 1;                     % One homogeneous phase.
ytot     = 0;     ytot1  = 0;      ytot2  = 0;
x        = zeros(N,1);            % Overall molar fraction of species i.
xg       = zeros(N,1);            % Molar fraction of species i in gas phase.
cy       = zeros(N,M);            % Element distribution in each species.
EA       = zeros(M,1);            % Overall element abundance.
ns       = zeros(N,1);

%  Count the number of single-species phases

m = 0;   nliq = 0;
for i = 1:N
   if SI(i) ~= 1
      if SI(i) == 2
         nliq = nliq + 1;
      end
      m = m + 1;
      ns(i) = m;
   end
end
ys      = zeros(m,1);    xs      = ones(m,1);
NP      = NP + m;
CEA     = zeros(M,NP);            % Phase distribution of each element.
for k = 1:m
   for i = 1:N
      if ns(i) == k
         ys(k) = y(i);
      end
   end
end

%  Compute the species split of each element, cy

for i = 1:N
   for j = 1:M
      cy(i,j) = y(i)*SEM(i,j)/EA0(j);
   end
end
for i = 1:N
   ytot  = ytot  +  y(i);
   ytot1 = ytot1 +  (SI(i) == 1) * y(i);    % Gas phase
```

```
   ytot2 = ytot2 +  (SI(i) == 2) * y(i);    % liquid phase
end

x       = y/ytot;                % Overall rduced molar fraction
for i = 1:N
   if SI(i) == 1
      xg(i) = y(i)/ytot1;       % Reduced molar fraction in gas phase.
   elseif SI(i) == 2
      xl(i) = y(i)/ytot2;       % Reduced molar fraction in liquid phase.
   end
end

%  Calculate a new EA and CEA for iteration

for j = 1:M
   for i = 1:N
      EA(j) = EA(j) + y(i)*SEM(i,j);

      if SI(i) == 1
         dirac = 1.0;
      else
         dirac = 0.0;
      end

      CEA(j,1) = CEA(j,1) + y(i)*dirac*SEM(i,j);  % Gas

      if nliq >= 1
         CEA(j,2) = CEA(j,2) + y(i)*(SI(i) == 2)*SEM(i,j); % Liquid phase
         % M == 7 or 8
         % CEA(j,3) = C(s)
         % CEA*j,4) = S(s), ...
      else
         if M == 3
            CEA(j,2) = y(N)*SEM(N,j);              % Solid phases 1 = C(s)
         elseif M == 4
            CEA(j,2) = y(N)*SEM(N,j);              % Solid phases 1 = C(s)
         elseif M == 5
            CEA(j,2) = y(43)*SEM(43,j);            % Solid phases 1 = C(s)
            CEA(j,3) = y(44)*SEM(44,j);            % Solid phases 2 = S(s)
         elseif M == 6
            CEA(j,2) = y(46)*SEM(46,j);            % Solid phases 1 = C(s)
            CEA(j,3) = y(47)*SEM(47,j);            % Solid phases 2 = S(s)
         end
      end
   end
end
```

10. Energy balance

File name: heatcoal.m
Function: Energy balance modulus
Source code: See below.

```
function [dq,totdh,toth,totph,totgh,totsh] =
heatcoal(T,alfa,Dath,Dat3,NF,H,y,Uwat,Ca,dissip,Hfeed,hff);

%  HEATCOAL does energy balance for coal and biomass gasification.
%  All results are per 1 kg of biomass (dry basis)

%  Version 4.0                          Xuantian Li (Nov. 21, 2000)

%  Initialization
[N,M]   = size(Dath);
toth    = 0;  totdh   = 0;  totph   = 0;  totgh    = 0;  totsh    = 0;
htrans  = 0;  dq      = 0;  calcin  = 0;  sure     = 0;  sure0    = 0;
tfactor = 0;  afactor = 0;  uncal   = 0;  sulfate  = 0;  spentlime= 0;
ttt     = 0;  hcal    = 0;  huncal  = 0;  hsulfate = 0;  hsptlime = 0;
%  End of initialization

%  (1) Enthalpy of feedstock: Hfeed

hfeed  = Hfeed;                % kJ

%  (2) Total product heat of formation @298K and enthalpy at T

for i = 1:N
   totdh = totdh + Dath(i,7)*y(i);      % Total heat of formation, kJ
   toth  = toth  + H(i);                % System total enthalpy, kJ
end

%  Calculate fractional calcination and sulfur retention

if Ca >= 0.1                      % If sorbent is added for sulfur removal
   [sure,calcin] = sulfre(T,alfa,Ca);

% Sulfur retention products (basis: 1 kg of fuel)
   sulfur  = (Dat3(9,NF)/100)*1000/32.066; % Moles of sulfur in 1 kg fuel
   calcium = sulfur*Ca;                    % Moles of Ca added
   hcal    = calcium*calcin*(-178.989);    % Heat effect of calcination
   uncal   = calcium*(1-calcin);           % Moles of uncalcined CaCO3
   sulfate = sulfur*sure;                  % Moles of CaSO4 formed
   hsulf   = sulfate*502.179;              % Heat effct of sulfation
   spentlime = (calcium - uncal)-sulfate;  % Moles of spent lime
   dhsure  = hcal + hsulf;                 % Net heat effect of sulf-re

%  Sensible heat (enthalpy) of sulfur retention products
   huncal    = uncal*    (97.935*T/1000 + 14.198*T^2/1000000 + 1855.4379/T
               - 36.8346);          % CaCO3
   hsulfate  = sulfate*  (32.863*T/1000 + 61.278*T^2/1000000 - 6316.038 /T
               +  4.5425);          % CaSO4
   hsptlime  = spentlime*(48.997*T/1000 + 2.5140*T^2/1000000 +  573.2851/T
```

```
                - 16.8339);          % CaO
end

%  Old ash in fuel
oldash  = Dat3(3,NF)/100;            % kg/kg_fuel (Note: not mol/kg_fuel)
holdash = oldash*(1.15e-4*T^2 + 0.82709*T - 239.38);   % kJ/kg_fuel

%  New ash from sulfur retention
newash  = uncal + sulfate + spentlime;  % mol/kg_fuel
hnewash = huncal + hsulfate + hsptlime; % kJ/kg_fuel
htotash = holdash + hnewash;            % kJ/kg_fuel

%  Modification of gas and solid enthalpy
totgh   = toth - H(43) - H(44);     % Total gas enthalpy, kJ/kg_fuel
totsh   = H(43) + H(44) + htotash; % Total solid enthalpy, kJ/kg_fuel
totph   = totgh + totsh;            % Total product enthalpy, kJ/kg_fuel
%  Reduction of SO2 moles due to sulfur retention is already considered in
elelemtal abundance

%  (3) Heat of formation of the feed: From Dath

hf1     = hff;                  % Fuel, kJ/kg_fuel
hf2     = Uwat*Dath(17,7);      % DHfo(298) for H2O (vapor), kJ/kg_fuel
hf3     = -1207.6*calcium;      % Heat of formation of limestone
hffeed  = hf1 + hf2 + hf3;      % kJ/kg_fuel

%  (4) Reactor surface heat transfer in this time interval (preset as 1 hr)

htrans   = dissip;

%  (5) Heat required to maintain the current temperature (kJ/kg_fuel)

dq       = hffeed + hfeed + (dhsure - totdh) - totgh - totsh - htrans;
%  HHV already considerd in hff, kJ/kg_fuel (as received)
```